

**Energy Budget- and Temperature Index- based Calculations
of Seasonal Mass Balances and Discharge in the Tropical
Glacier Artesonraju and Artesoncocha Basin in the
Cordillera Blanca, Peru**

Dissertation zur
Erlangung des akademischen Grades
Doktor der Ingenieurwissenschaften (Dr.-Ing.)

vorgelegt im Fachbereich
Bauingenieurwesen und Umweltingenieurwesen
der Universität Kassel

von:

María Fernanda Lozano Gacha
Department of Geohydraulics and Engineering Hydrology
University of Kassel, Germany

Kassel, June 6, 2020

This work has been accepted by the Faculty of Civil and Environmental Engineering of the University of Kassel as dissertation for acquiring the academic degree of Doktor der Ingenieurwissenschaften (Dr.-Ing.).

1. Advisor: Prof. Dr. rer. nat. Manfred Koch, University of Kassel, Germany
2. Co-advisor: Dr. Pierre Chevallier, Institute of Research for Development, Montpellier, France
3. Committee: Prof. Dr.-Ing. Matthias Gaßmann, University of Kassel, Germany
4. Committee: Dr.-Ing. Mohammed Zare, Leibniz Institute for Agricultural Engineering and Bioeconomy Department of Technology, Assessment and Substance Cycles, Postdam, Germany

Date of the disputation: November 19, 2019

Dissertation zur Erlangung des akademischen Grades eines Doktors der Ingenieurwissenschaften (Dr.-Ing.) an der Universität Kassel, Fachgebiet Geohydraulik und Ingenieurhydrologie, Institut für Geotechnik und Geohydraulik, Fachbereich Bauingenieur- und Umweltingenieurwesen.

Tag der mündlichen Prüfung: 19. November 2019

To my beloved late father Fernando Lozano Delgado.

A la memoria de mi amado padre Fernando Lozano Delgado

Acknowledgements

I express my honest gratitude to God for giving me the strengths to reach the goals of this important work in my life.

My sincere thanks to my Supervisor Prof. Dr. rer. nat. Manfred Koch for his invaluable contribution which led me to focus my research, for his patience, motivation and his knowledge, I really appreciate his support in this challenging process. I would like also to acknowledge with gratitude the support of Dr. Pierre Chevallier with his important remarks and advice that help me to improve this thesis.

I would like to thank my late father, Fernando Lozano Delgado, with all my heart, who taught me the importance of persistence. Without any doubt, his efforts, his immense love and his wise words of motivation inspired me to reach the end of this research. I would also thank my mother Yolanda Gacha Herrera, who supported me with her care in the exhausting hours of this work and thanks to my son, Immanuel who is my inspiration in life.

I would like also to express my gratitude to my colleagues from the Universität Kassel for their conviviality which made my research life more enjoyable.

Thanks to Paulina Avilez, the Autoridad Nacional del Agua del Perú (ANA), Instituto Nacional de Recursos Naturales (INRENA), the Servicio Nacional de Meteorología e Hidrología (SENAMHI) del Peru and the World Glacier Monitoring Service (WGMS) for the data provided for this research. Finally my thankfulness to Dr. Regina Hock, who developed and provided the models applied in this research.

Abstract

The core of the present Doctoral study deals with glacier simulations for calculating mass balance and discharge in the Artesonraju glacier and Artesoncocha basin, in the Cordillera Blanca (CB), Peru. For this purpose, two different models are used. One is an energy-model (EBM) which is physically based and uses energy fluxes measurements on the glaciers, whereas the other one is a temperature index model (TIM) which is empirical and uses mainly temperature and precipitation as its main input data.

An analysis of the climatic time series data and the mass balance measurements in the CB is firstly undertaken. A high correlation of the daily temperatures, in the horizontal plane (especially above the 4500 m.a.s.l.) is found. Correlation of precipitation, in contrast, responds more to local geographical patterns, with the highest correlations found for stations located in the same catchment. Trends of annual mean temperature are revealed in 27% of the climate stations, out of which 90% show a positive and 10% a negative one. Trends of annual precipitation are seen in only 14% of the stations, out of which 66% are positive and 44% negative. A strong influence of the ENSO phenomenon on temperature and precipitation is observed where, however, the intensities of the ENSO anomalies do not always respond proportionally to the temperature and precipitation anomalies. Unfortunately, most time series, particularly, those with short records which are mostly in the glacier areas, exhibit many gaps and were filled in using several time series methods. Seasonal mass balances measurements are scant and only available between September 2003 and May 2008. Previously reported annual mass balance estimations indicated negative values, affected primarily by the ENSO phenomenon. Energy fluxes are only available for the Artesonraju glacier at 4838 m.a.s.l. between March 2004 and December 2007. The data analysis shows a clear seasonality in the longwave radiation fluxes and less in the shortwave fluxes. Correlation calculations among measured energy fluxes and other climatic variables reveal a statistically significant association of daily net radiation with daily temperature and of longwave incoming radiation with precipitation.

The energy balance model (EBM) calibrations show that by using seasonal albedos reasonable results for mass balances and discharge can be obtained, as witnessed by annually aggregated Nash Sutcliffe coefficients (E) of 0.57-0.85 in the period 2004-2007. Mass losses between -1.9 and -0.64 m.w.e. are calculated for that time period. A high influence of ENSO on the mass balance of the glacier is observed. The Elevation Line Altitudes (ELAs) are also well simulated in comparison with the UGRH- observed ones and lie between 5000 and 5050 m.a.s.l. It is demonstrated that the net radiation which drives the energy balance and melting processes is mainly affected by the amount of reflected shortwave radiation of the different surfaces. The longwave radiation has an important role as a sink of radiative energy in the dry season. The mean turbulent fluxes counteract themselves in the dry season, while their role in the accumulation zone, especially in the wet season, could be significant due to their counteracting effect of net radiation in this zone. A sensitivity analysis shows that the threshold temperature snow/rain T_0 is a very sensitive parameter in the model, as it determines the extension of areas with different albedos. An optimal threshold temperature between 2.8 and 4°C is deduced from the model simulations.

Despite the low seasonality of temperature which leads to undervaluing the use of temperature index in tropical glaciers, the application of this (second) (TIM) model in the present study proves otherwise, particularly when using seasonal degree-day melt factors (DDF). Thus, for the calibration- (2004-2007) and validation period (2001-2004), an annually aggregated E of 0.75-0.89 and of 0.7-0.82, respectively, are obtained. The calculated annual mass balances range between -1.2-(-1.7) m.w.e. over the whole time period and agree somewhat better with the UGRH- measured ones than those of the energy model above. Calibrated seasonal $DDFs$ for snow of 5.4, 4.8 and 2.8 $\text{mmd}^{-1}\text{C}^{-1}$ for the three seasons, SO, NDJFM and AMJJA, respectively, fit the model best, whereas those for ice are determined as 9, 16 and 6.5 $\text{mmd}^{-1}\text{C}^{-1}$, respectively. Likewise to the EBM above, the temperature threshold snow/rain T_0 , turns out to be a very sensitive parameter in TIM as well, and optimal values between 2.5 and 3.5°C are found with this model. Moreover, for both TIM and EBM, concurrently calibrated storage constants of the cascade runoff routine indicate seasonal trends for all three glacier surfaces (ice, snow, firn).

From the comparison of the various EBM- and TMI- simulation results, it is concluded that those for discharge and mass balances are better for the latter than for the former model. The limited performance of EBM against TMI is most likely due to the sometimes low quality of the data available which precludes the possibility of using the most accurate parameterization in that model. Regarding the success of the TIM model, this is mainly due to the use of seasonal $DDFs$ in the model, not done heretofore in tropical glacier modelling.

Zusammenfassung

Der Kern der vorliegenden Doktor Studie befasst sich mit Gletschersimulationen des Massengleichgewichts und des Abflusses im Artesonraju-Gletscher und im Artesoncocha-Becken in der Cordillera Blanca (CB), Peru. Zu diesem Zweck werden zwei verschiedene Modelle verwendet. Eines ist ein physikalisch basiertes Energiemodell (EBM), das Energieflussmessungen an den Gletschern verwendet und das andere ein empirisches Temperaturindexmodell (TIM), das nur Temperatur und Niederschlag als Eingabe braucht.

Zunächst erfolgt eine Analyse der klimatischen Zeitreihen und der Massenbilanzmessungen in der CB. Eine hohe Korrelation der Tagestemperaturen in der horizontalen Ebene (insbesondere oberhalb der 4500 m.a.s.l.) wird gefunden, während die Korrelation der Niederschläge eher auf lokale geografische Muster reagiert, mit der höchsten Korrelation für Stationen im selben Einzugsgebiet. Temperaturtrends zeigen sich bei 27% der Klimastationen, von denen 90% positiv und 10% negativ sind. Niederschlagstrends sind nur in 14% der Stationen zu beobachten, mit 66% positiv und 44% negativ. Ein starker, aber nicht immer proportionaler Einfluss des ENSO- Phänomens auf Temperatur und Niederschlag wird beobachtet. Da die meisten Zeitreihen, insbesondere solche mit kurzen Aufzeichnungen viele Lücken aufweisen, mussten sie mit verschiedenen Zeitreihenmethoden ausgefüllt werden. Messungen von Massenbilanzen sind spärlich und nur zwischen September 2003 und Mai 2008 verfügbar. Zuvor vermeldete Schätzungen dazu ergaben negative Werte, hauptsächlich zufolge des ENSO-Phänomens. Energieflüsse sind nur für den Artesonraju-Gletscher auf 4838 m.a.s.l zwischen März 2004 und Dezember 2007 verfügbar und zeigen eine deutliche Saisonalität bei den langwelligen Strahlungsflüssen und weniger bei den kurzwelligen. Signifikante Korrelationen zwischen der täglichen Nettostrahlung mit der Temperatur und der langwelligen einfallenden Strahlung mit dem Niederschlag werden ermittelt.

Die Kalibrierungen des Energiebilanzmodells (EBM) zeigen, dass durch die Verwendung von saisonalen Albedos vernünftige Ergebnisse für Massenbilanzen und Abflüsse erzielt werden können, mit jährlich aggregierten Nash Sutcliffe-Koeffizienten (E) von 0,57-0,85 im Zeitraum 2004-2007. Massenverluste zwischen -1,9 und -0,64 m.w.e. werden für diesen Zeitraum berechnet. Es wird ein hoher Einfluss von ENSO auf die Massenbilanz des Gletschers beobachtet. Die Elevation Line Altitudes (ELAs) sind auch im Vergleich zu den UGRH-beobachteten gut simuliert und liegen zwischen 5000 und 5050 m.a.s.l. Es zeigt sich, dass die Nettostrahlung, die die Energiebilanz und die Schmelzprozesse antreibt, hauptsächlich von der Menge der reflektierten kurzwelligen Strahlung der verschiedenen Oberflächen beeinflusst wird. Die langwellige Strahlung spielt eine wichtige Rolle als Strahlungsenergiesenke in der Trockenzeit. Die mittleren turbulenten Flüsse heben sich in dieser Zeit auf, spielen aber in der Akkumulationszone, insbesondere in der Regenzeit, aufgrund ihres entgegenwirkenden Effekts in der Nettostrahlung wieder ein Rolle. Eine Sensitivitätsanalyse zeigt, dass die Schwellentemperatur Schnee/Regen (T_0) ein sehr sensibler Modellparameter ist, da sie die Ausdehnung von Gebieten mit unterschiedlichen Albedos bestimmt. Aus den Modellsimulationen wird eine optimale Schwellentemperatur von 2,8-4 ° C abgeleitet.

Trotz der geringen Saisonalität der Temperatur, die die Verwendung des (zweiten) Temperaturindex- Modells (TIM) in tropischen Gletschern zunächst in Frage stellt, zeigt diese Studie etwas anderes, insbesondere wenn saisonale Grad-Tag-Schmelzfaktoren (DDF) verwendet werden. So werden mit TIM für den Kalibrierungs- (2004-2007) und Validierungszeitraum (2001-2004) jährlich aggregierter E von 0,75-0,89, respektive 0,7-0,82 erhalten. Die berechneten jährlichen Massenbilanzen liegen zwischen -1,2 und -(- 1,7) m.w.e. und stimmen etwas besser als die des EBM mit den UGRH-gemessenen überein. Die kalibrierten saisonalen $DDFs$ für Schnee betragen 5,4, 4,8 und 2,8 $\text{mmd}^{-1}\text{C}^{-1}$ für die drei Jahreszeiten SO, NDJFM und AMJJA, während die für Eis zu 9, 16 und 6,5 $\text{mmd}^{-1}\text{C}^{-1}$ bestimmt werden. Ähnlich wie beim EBM stellt sich die Temperaturschwelle T_0 auch in TIM als sehr empfindlicher Parameter heraus, mit optimalen Werten zwischen 2,5-3,5 ° C. Darüber hinaus zeigen die für TIM, als auch für EBM gleichzeitig kalibrierten Speicherkonstanten der Kaskadenabflussroutine saisonale Trends für alle drei Gletscheroberflächen (Eis, Schnee, Firn) an.

Der endgültige Vergleich der Simulationsergebnisse für EBM- und TMI- zeigt, dass die simulierten Abflüsse und Massenbilanzen für das letztere Model besser sind. Dieses erstaunliche Ergebnis ist wohl auf die teilweise schlechterer Qualität der für die Aufstellung des (im Prinzip besser parametrisierten) EBM- Modells verfügbaren Daten zurückzuführen, Andererseits ist der Erfolg des TIM-Modells auch in der Verwendung von saisonalen $DDFs$ im Modell begründet, was bisher bei der Modellierung tropischer Gletscher noch nicht durchgeführt wurde.

Table of Content

Abstract	iv
List of Figures	xi
List of Tables	xiv
1 Introduction	16
1.1 Aim of the Research Project	18
1.2 Structure of the Thesis	18
2 Study Area and Data	20
2.1 Study Area	20
2.2 Data	23
2.2.1 Climate data	23
2.2.1.1 Temperature	23
2.2.1.2 Precipitation	25
2.2.1.3 Relative Humidity and Wind	25
2.2.1.4 Energy Fluxes	25
2.2.2 Discharge	25
2.2.3 Mass balance measurements	29
2.2.4 Grid data	30
3 Analysis of Climate Setting in the Tropical Glaciers of La Cordillera Blanca	31
3.1 The Climate of the High Mountains in La Cordillera Blanca	31
3.1.1 General climate characteristics of Andean tropical glaciers	31
3.1.2 Air temperature	31
3.1.2.1 General statistics analysis and mutual station correlations	31
3.1.2.2 Seasonal patterns of temperature	33
3.1.2.3 Interannual variability of temperature and correlations with Niño SSTs	35
3.1.2.4 Temperature Trends	41
3.1.3 Precipitation	45
3.1.3.1 General statistical analysis and mutual station correlations	45

3.1.3.2	Seasonal patterns of precipitation	47
3.1.3.3	Interannual variability of precipitation and correlations with Niño.....	48
3.1.3.4	Precipitation Trends	54
3.1.4	Relative humidity	54
3.1.5	Wind.....	57
3.2	Concluding Remarks	59
4	Analysis of Current Data of Mass Balances in the Glaciers in La Cordillera Blanca	61
4.1	General Concepts and Notations.....	61
4.1.1	Accumulation.....	61
4.1.2	Ablation.....	62
4.1.3	Surface mass balance.....	62
4.1.4	Equilibrium Line Altitude (ELA)	63
4.2	Seasonal Variations of Mass Balance	63
4.3	Measurements of Glaciers Mass Balance.....	64
4.4	Concluding Remarks	66
5	Review and Analysis of Measured Energy Fluxes Data in the Artesonraju Glacier	67
5.1	General Concepts and Notations.....	67
5.2	Field Data of Energy Fluxes at the Artesonraju Glacier	72
5.3	Daily Measured Energy Fluxes.....	73
5.3.1	Shortwave incoming radiation.....	74
5.3.2	Shortwave reflected radiation.....	74
5.3.3	Longwave incoming radiation (from the atmosphere).....	75
5.3.4	Longwave emitted radiation (longwave radiation by the surface).....	75
5.4	Analysis of Seasonality and Trends of the Energy Fluxes.....	76
5.5	Correlations of Energy Fluxes, Temperature and Precipitation	78
5.6	Concluding Remarks	80
6	Filling of Data Gaps in the Climate Data Series	81
6.1	Rational and Overview.....	81

6.2	Gap Filling by Multiple Linear Regression.....	81
6.2.1	Theoretical basis of multilinear regression	81
6.2.2	Results.....	82
6.2.2.1	Temperature data.....	82
6.2.2.2	Energy Fluxes	83
6.3	Interpolation of Energy Fluxes by Seasonal Decomposition of Time Series by Loess (STL), Harmonic Analysis and Fitted Optimal Autoregression (AR) Models	87
6.3.1	Basis of STL, harmonic analysis and AR	88
6.3.2	Results.....	90
6.3.2.1	Shortwave incoming radiation.....	90
6.3.2.2	Reflected shortwave radiation.....	92
6.3.2.3	Longwave incoming radiation.....	94
6.3.2.4	Longwave emitted by the surface.....	96
6.4	Concluding Remarks	98
7	Energy Balance in Tropical Glaciers.....	99
7.1	Review on Climactic Factors Influencing Mass Balance Changes in Andean Tropical Glaciers (Energy Fluxes Current Results).....	99
7.1.1	Approaching energy balance studies on Andean tropical glaciers.....	100
7.1.1.1	Radiative fluxes	104
7.1.1.2	Turbulent fluxes of heat:	105
7.1.1.3	Conductive heat flux from/into the ground and rain fluxes	107
7.1.2	The drivers of melting processes on tropical glaciers	107
7.1.3	The effect of ENSO on tropical glaciers	109
7.2	Modelling Mass Balances and Discharge with Energy Balance Fluxes in the Artesonraju glacier and the Basin of Artesoncocha	111
7.2.1	General overview and approach	111
7.2.2	Methodology and parameterization	111
7.2.2.1	Net radiation	112
7.2.2.2	Turbulent Fluxes of Latent and Sensible Heat.....	118
7.2.2.3	Ground heat flux and rain energy	119
7.2.2.4	Accumulation.....	119

7.2.2.5	Ablation	119
7.2.2.6	Discharge	120
7.2.3	Model application and evaluation	121
7.2.3.1	Overview of modelling approach.....	121
7.2.3.2	Input data	121
7.2.3.3	Main calibration parameters.....	121
7.2.4	Results and discussion	122
7.2.4.1	Simulated Discharge.....	123
7.2.4.2	Mass balance, mass balance profiles and ELAs	124
7.2.4.3	Evaluation of energy fluxes.....	130
7.2.4.4	Sensitivity analysis of calibration parameters	140
7.2.4.5	Uncertainties in the simulation	145
7.2.5	Concluding remarks	146
8	Temperature Index Modelling in Tropical Glaciers	148
8.1	Review on Empirical Temperature Index Models for Modelling Mass Balance and Discharge in Glaciers.....	148
8.1.1	Basis of the temperature index model	148
8.1.2	Advantages and disadvantages of temperature index models	149
8.1.3	Spatial and temporal differences of the degree-day factors.....	149
8.1.4	Physical fundamentals of temperature index models	150
8.1.5	Temperature index model in tropical glaciers	151
8.2	Use of Seasonal Degree Factors for Modelling Discharge and Mass Balance of the Artesoncocha Basin	152
8.2.1	General remarks on the applicability of <i>DDFs</i> in La Cordillera Blanca.....	152
8.2.2	Methodology	152
8.2.2.1	Parameterization.....	152
8.2.2.2	Simulation period and input data.....	152
8.2.2.3	Main calibration parameters.....	153
8.2.3	Results and discussion	154
8.2.3.1	Simulated discharge	154
8.2.3.1	Mass Balance and ELAs for the calibration period.....	154

- 8.2.3.2 Parameters' sensitivity 158
- 8.2.3.1 Validation of discharge 164
- 8.2.3.2 Mass balance profiles, ELAs and total mass balance for the validation period 166
- 8.2.3.3 Uncertainties in the simulation 169
- 8.2.4 Concluding remarks 169
- 9 Comparison of Energy Balance Model (EBM) - and Temperature Index Model (TIM) - Simulation Results 171
 - 9.1 Comparison of Simulated Discharge 171
 - 9.2 Comparison of Mass Balance Profiles and ELAs..... 172
 - 9.3 Comparison of EBM- and TIM- Calibration Parameters..... 174
 - 9.3.1 Energy fluxes and *DDFs*..... 174
 - 9.3.2 Seasonal storage constants (mean residence times) 175
 - 9.3.3 Threshold temperature *rain/snow* T_0 175
 - 9.4 Concluding Remarks 177
- References..... 178

List of Figures

Figure 2.1. Location Cordillera Blanca, Artesonraju glacier and Artesoncocha Basin	21
Figure 2.2. Artesoncocha basin, Artesonraju glacier and Artesoncocha lake.....	22
Figure 2.3. Satellitel image of the Artesonraju Glacier. Taken from Google Earth 2019	22
Figure 2.4. Temperature gauge stations in the Cordillera Blanca.....	26
Figure 2.5. Location of precipitation stations in the Santa basin and the Cordillera Blanca	28
Figure 2.6. Net of stakes (red points) and pits (yellow points) in the Artesonraju Glacier	29
Figure 3.1. Mean, minimum and maximum daily temperature (between 1970 and 2010) as a function of altitude for stations above 3000 m.a.s.l.....	32
Figure 3.2. Kendall correlation of the temperature of stations above 3000 m.a.s.l.....	33
Figure 3.3. Seasonal pattern (box whisker plots) of temperature for each month of a year in the glacier stations and the stations Parón, Querococha and Recuay.....	34
Figure 3.4. Annual mean temperatures of the reanalysis data (NCEP) and of various CB- stations	36
Figure 3.5. Ocean Niño Index (ONI), 3-month running mean SST anomaly.....	37
Figure 3.6. Niño SST Regions (SST).....	37
Figure 3.7. Correlations for lag=0 of El Niño 1.2, 3, and 3.4 with time series of daily temperature at stations of the study area	38
Figure 3.8. Lagged cross correlations of monthly SSTs of Niño 1.2, 3 and 3.4 regions with the monthly temperature in the glacier stations Artesonraju, Yanamarey, Uruashraju and Huarapasca and the Artesoncocha station.....	40
Figure 3.9. Mean daily precipitation in the CB as a function of elevation	45
Figure 3.10. Correlation coefficients of daily precipitation data above 3000 m.a.s.l.....	47
Figure 3.11. Seasonal pattern (box whisker plots) of daily precipitation for each month of the year for stations located in the glaciers, Artesonraju, Yanamarey, Uruashraju, Huarapasca and in their basins, Parón and Querococha.....	48
Figure 3.12. Annual precipitation (mm year ⁻¹) at stations with largest records of precipitation. 49	
Figure 3.13. Correlation coefficients of Niño 1.2, 3.and 3.4 with daily precipitation in the glaciers stations and Parón, Aguascocha, Llanganuco and Lag. Querococha.....	51
Figure 3.14. Lagged cross correlations of monthly SSTs of Niño 1.2,3 and 3.4 region with monthly precipitation.....	53
Figure 3.15. Cross-correlations of the time series of relative humidity	56
Figure 3.16. Seasonal pattern of relative humidity	57
Figure 3.17. Correlation coefficients for daily wind speed.....	58
Figure 3.18. Seasonal pattern of daily wind speed.....	59
Figure 4.1. Accumulation and ablation scheme	61
Figure 4.2. Annual mass balance profiles MB (left panel) and ELA (right panel) of the glaciers Artesonraju, Uruashraju and Yanamarey from 2003-2007	65
Figure 5.1. Absorption capacity of the gases in the atmosphere for shortwaves and longwaves. 68	
Figure 5.2. Energy budget in the Earth and Atmosphere System, Kiehl and Trenberth (1997) ...	69
Figure 5.3. Daily time series of shortwave incoming and reflected radiation at glacier Artesonraju.....	75
Figure 5.4. Daily longwave incoming radiation and longwave emitted radiation at glacier Artesonrajuat.....	76
Figure 5.5. Daily averages (2004-2008) of various energy fluxes for different months of a year	77

Figure 5.6. Correlation coefficients among the energy fluxes variables, Shortwave radiation Incoming (SW_{inc}), Shortwave radiation reflected (SW_{ref}), Longwave radiation incoming (LW_{inc}), Longwave radiation emitted by the surface (LW_{surf}), Net Radiation (Q_N), Temperature ($T_{glacier}$'s name), Precipitation, Relative Humidity (R_h), Wind Speed (U) and discharge in Artesoncocha and the closest reanalysis data NCEP in the north and in the south..... 79

Figure 6.1. Results of multiple linear regression model for filling in and extrapolating daily temperature at Artesonraju station..... 83

Figure 6.2. Results of multiple linear regression model for filling in and extrapolating daily shortwave incoming radiation at Artesonraju station 84

Figure 6.3. Results of the multiple linear regression model for filling in and extrapolating daily shortwave reflected at Artesonraju station 85

Figure 6.4. Results of the multiple linear regression model for filling in and extrapolating daily longwave incoming radiation at Artesonraju station 86

Figure 6.5. Results of the multiple linear regression model for filling in and extrapolating daily longwave emitted radiation by the surface at Artesonraju station..... 87

Figure 6.6. Plots showing various results of the different steps of the gap-filling procedure for the shortwave incoming radiation 92

Figure 6.7. Plots showing various results of the different steps of the gap-filling procedure for the shortwave reflected radiation 94

Figure 6.8. Plots showing various results of the different steps of the gap-filling procedure for the longwave incoming radiation 96

Figure 6.9. Plots showing various results of the different steps of the gap-filling procedure for the longwave emitted radiation by the surface 98

Figure 7.1. Inner (upper panel) and outer (middle panel) tropics glaciers-regime and the seasonal differences of the location of the ITCZ (right panel), mid latitude glacier-regime (lower panel)..... 102

Figure 7.2. Simulated and measured discharge at the outlet of Artesoncocha lake..... 124

Figure 7.3. Measured and simulated mass balance profiles for the Artesonraju glacier area 125

Figure 7.4. Spatial variations of annual measured and simulated (EBM) mass balances in the Artesonraju basin for three hydrological years, with RMSE of each simulation year as indicated 127

Figure 7.5 Measured and simulated annual mass balance 128

Figure 7.6. Mean daily of simulated mass balances (upper panel), temperature (middle panel) and precipitation (lower panel) for each season of the years studied 129

Figure 7.7. Measured and simulated net shortwave radiation at Artesonraju glacier station..... 131

Figure 7.8. Measured and simulated net longwave radiation at Artesonraju glacier station 132

Figure 7.9. Measured and simulated net radiation at the Artesonraju glacier gauge station 133

Figure 7.10. Simulated daily net radiation and turbulent fluxes 134

Figure 7.11. Mean seasonal net radiation and turbulent fluxes at the Artesonraju glacier 135

Figure 7.12. Mean seasonal contribution of radiative fluxes terms 135

Figure 7.13. Average energy profiles for melting/sublimation-, net radiation- and turbulent fluxes for September-October (SO), November –March (NDJFM) and April-August (AMJJA) 137

Figure 7.14. Turbulent fluxes profiles for months September-October (SO), November –March (NDJFM) and April-August (AMJJA)..... 138

Figure 7.15. Shortwave and longwave balance profiles from September-October (SO), November-March (NDJFM) and April-August (AMJJA)..... 139

Figure 7.16. Snow and ice albedo sensitivity in terms of the Nash-Sutcliffe parameter E 141

Figure 7.17. Threshold temperature rain/snow T_0 sensitivity in terms of E . Red point shows the points located above 3.5°C 143

Figure 8.1. TMI-simulated (calibrated) and measured discharge at Artesoncocha lake outlet .. 155

Figure 8.2. Measured and TMI- simulated mass balance profiles for the years of calibration 156

Figure 8.3. TMI- simulated and measured mass balances for the different years of calibration 157

Figure 8.4. Degree-Day Factor sensitivity plots in terms of the Nash-Sutcliffe parameter E for the three seasons considered, with optimal values for ice and snow as indicated 159

Figure 8.5. TMI-sensitivity of three storage constants (snow, ice and firn) in each season 162

Figure 8.6. Threshold temperature rain/snow T_0 - sensitivity in terms of E . Red point shows the points located above 3.5°C 165

Figure 8.7. TMI-simulated and measured discharge for the validation period..... 166

Figure 8.8. TMI-simulated mass balance profiles of the validation period 167

Figure 8.9. Seasonal mass balance profiles 168

Figure 9.1. Daily measured-, EBM- and TIM- simulated discharge for the different years..... 172

Figure 9.2. Measured-, EMB-, and TIM- simulated mass balance profiles for the different years 173

Figure 9.3. Yearly EMB-, and TIM- mass balance and calculated with measured data by UGRH 174

Figure 9.4. EBM- and TIM- simulated seasonal threshold temperature rain/snow T_0 sensitivities in terms of E for the different years..... 176

List of Tables

Table 2.1. Gaps in the temperature series for different climate stations	24
Table 2.2 Length and gaps of the longest daily precipitation time series.....	27
Table 3.1. Statistics (mean, median, standard deviation (SD), minimum (Min) and maximum (Max), and lower (1stQ) and upper (3rdQ) quartile and variance (VAR)) of daily temperature at the stations of CB.....	33
Table 3.2. Trends of monthly and annual temperatures using the SMK and MK test, respectively. Stations with significant trends (reject H0) for both monthly and yearly data are marked in yellow and ones with different results in white	44
Table 3.3. Statistic (mean, median, standard deviation (SD), minimum (Min) and maximum (Max), and lower (1stQ) and upper (3rdQ) quartile and variance (VAR)) of the daily precipitation for stations located above 3.500 m.a.s.l.	46
Table 3.4. Annual mean precipitation trend using the Mann-Kendall test.....	55
Table 3.5. Statistical of mean, median, standard deviation (SD), minimum (Min) and maximum (Max), and lower (1stQ) and upper (3rdQ) quartile and variance (VAR) of daily relative humidity	56
Table 3.6. Statistical of mean, median, standard deviation (SD), minimum (Min) and maximum (Max), and lower (1stQ) and upper (3rdQ) quartile and variance (VAR) of daily wind speed	58
Table 4.1. 2002-2008 annual mass balances (MB) and ELAs in Artesonraju, Yanamarey and Uruashraju glaciers (data taken by Gallaire <i>et al.</i> , 2007 and WGMS, 2015)	65
Table 5.1. Statistical of mean, median, standard deviation (SD), minimum (Min) and maximum (Max), and lower (1stQ) and upper (3rdQ) quartile and variance (VAR) of daily energy fluxes at Artesonraju glacier between 2004-2007	73
Table 5.2. Results of normality tests on time series of daily energy fluxes.....	73
Table 7.1. Energy balance studies made in the tropical Andean glaciers	101
Table 7.2. Some reported energy fluxes in the Andean tropical glaciers	103
Table 7.3. Reported ENSOs and mass balance signals in the Andean glaciers.....	110
Table 7.4. Conditions for calculating diffuse radiation in the Energy Balance Model (Hock and Tijm-Reijmer, 2012).....	115
Table 7.5. Typical albedo ranges for glacier surfaces.	116
Table 7.6. Input data for energy balance fluxes model.....	122
Table 7.7. Studied simulation periods	122
Table 7.8. Statistical measures of the simulated discharge.....	123
Table 7.9. Annual simulated and measured mass balances and ELAs and calculated accumulation-area ratio from simulated data	126
Table 7.10. Simulated annually averaged daily energy flux terms in the Artesonraju glacier	136
Table 7.11. Optimal seasonal storage constants for the three kinds of glacier surfaces	144
Table 8.1. Input data for the temperature index model (TMI)	153
Table 8.2. TMI- obtained Nash Sutcliffe Coefficients for discharge in the calibration period.....	154
Table 8.3. Correlation of daily means of energy fluxes and degree-day factors, for various seasons.....	160
Table 8.4. Reservoir storage constants for various tropical glaciers compared with the seasonal ones determined by the TMI- model in the present study.	163
Table 8.5. TMI- simulated Nash Sutcliffe Coefficients E and $RMSE$ for the validation period	164

Table 8.6. Simulated and measured mass balance, ELA, snow line and AAR (accumulation area ratio) for the whole simulation time (validation and calibration periods)..... 167

Table 9.1. Comparison of Nash-Sutcliffe Coefficient (E) of EBM- and TIM- discharge simulations 171

Table 9.2. EBM- and TIM- optimized seasonal storage constants for firn, ice and snow..... 175

1 Introduction

Climate alterations that have occurred in the past or may occur in the future in the tropics are a major matter of research, due to the importance of the tropics in the atmospheric circulation. In this context, the glaciers located in tropical areas are significant indicators of climate variations. Any change in climate parameters alters the energy exchange between the glacier surface and the atmosphere. Consequently, there is a close relationship between climatic variables and the gain or losses in mass, i.e. accumulation or ablation of glaciers. The rate of melting, sublimation and accumulation could change in the wake of climate variability, producing a readjustment in the glaciers' extension and, consequently, a change in their capacity to release water. One of the most important signs of climate change is glacier retreat (IPCC, 2008). Oerlemans (2005) has documented glacier retreats around the world of 169 glacier records from 1800 to 2000, as discussed in more detail further below.

It is important to consider that climate change affects glaciers in the tropics in different ways than it does to those located in the mid- or high latitudes of the earth. Energy fluxes, thermal homogeneity in time and space (Kaser and Osmaston, 2002), as well as different seasonal patterns of precipitation and humidity, are at the origin of these differences. For instance, the continuous ablation during the year in tropical glaciers, in conjunction with their steep slopes, make them react more rapidly to changes of the local climate than glaciers in mid and high latitudes (IPCC, 2008).

Most of the tropical glaciers of the world are located in the Andean mountains, with 99% =2758 km² of the world's tropical glacier-covered area. The Cordillera Blanca in Peru, covering an area of 527.62km² (Autoridad Nacional del Agua, 2014), is by far the mountainous area with the biggest extension of tropical glaciers and accounts for around 26% of the tropical glacier area of the world (Kaser and Osmaston, 2002). Consequently, the Cordillera Blanca turns out to be an important area to study the tropical glacier retreat. In addition, shrinkage of the glacierized area of the Cordillera Blanca affects distinctly the water supply of the local population which lives mostly in the mountain areas. It also affects agriculture and hydropower generation (Chevallier *et al.*, 2011). Therefore, it is essential to estimate the likely magnitude of the variance of the water resources derived from the tropical glacierized areas and to predict their repercussions on the environment and the population.

The tropical glaciers have been particularly suffering from retreat during the last 40 years, affecting the glacier's capacity to store water and release it. Some reports of tropical glacier's retreat are:

- a) the disappearance of some of the smallest and low-altitude glaciers, such as Chacaltaya in Bolivia which some 10 years ago was still the site of the highest ski lifts in the world (Chevallier *et al.*, 2011),
- b) losses of ice volume of up to 43% for 376 glaciers in the Cordillera Real in Bolivia between 1963 and 2006 (Sorucu *et al.*, 2009),

c) estimations that the Cordillera Blanca glaciers have lost approximately 8% of their surface area between 1948 and 1990 (Kaser *et al.*, 2003). More recent estimations indicate a 27% glacierized area loss between 1960 and 2000 (UGRH, 2010).

d) glacier area shrinkage of 32% between 1962 and 2006 of glaciers in Cordillera Vilcanota in Peru, (Salzmann *et al.*, 2013). Moreover, Tompson *et al.* (2006) studied the Quelccaya ice cap of Cordillera Vilcanota, finding 10 times more area losses between 1991 and 2005 than between 1963 and 1978.

e) decrements of ice area of 26% on Coropuna in the Cordillera Ampato in Perú between 1962 and 2000 (Racoviteanu *et al.*, 2007)

f) losses of 50% of the area covered by Colombian glaciers in the past 50 years (Ceballos *et al.*, 2006). Latest estimations with satellite images in 2016 state that the extent of Colombian glaciers is 36% less than in the mid- 1990s (Rabatel *et al.*, 2017).

g) Cotopaxi's glacier in Ecuador which lost approximately 30% of its surface area between 1976 and 1997 (Jordan *et al.*, 2005). Besides, Caceres (2010) estimates area losses of 57%, 37% and 33% in Chimborazo between 1962 and 1997, and Cotopaxi and Antizana between 1979 and 2007 respectively. Francou *et al.* (2013) report losses of areas of Ecuadorian glaciers of 50% since 1956.

Gaining deeper knowledge of the causes of these glacier retreats is still in process. To understand the relations between climate and tropical glaciers, an adaptation of the methods and models to local conditions and more simulations of the dynamics of the tropical glaciers are required. Besides, the deficiencies of information hinder the possibility to not only to determine the causes of retreat of tropical glaciers, but also to foresee how the responses of tropical glaciers to atypical variations of climate are.

In this context, some authors state the need to deepen certain research lines to which this research seeks to contribute:

For instance, Juen (2006) expresses the need to carry out more studies on the glacier mass balance and the energy budget of the glacier surface to improve the comprehension of the glacier-climate interaction in the tropics.

Braithwaite (2011) proposes to run energy balance models and degree-day models in parallel, in order to understand the possible variations of degree-day factors. These degree-day factors roughly defined as the coefficient of proportionality between surface ablation and temperature above freezing. In addition, Braithwaite (2011) states the need for understanding the roles of sublimation and of the debris cover in the high mountains in the Andes.

Hock (2003) concludes that temperature index models need to be enhanced, in order to bridge the gap between restricted data availability and increased demand for high space-and- time resolution estimates of melt rates.

Studies of the mass balances and energy budgets of tropical glaciers serve as an important key to understand how tropical glaciers behave in response to climate variations. Some studies carried out in the Andean Tropics explain how parameters, such as temperature, precipitation, humidity

and solar radiation, influence the physical dynamics behind mass balance. However, the studies show different results on which of the climatic parameters are the drivers of the energetic balance in tropical glaciers' environments and, therefore, of the changes in mass balances. In addition, gaps in the various hydro-meteorological time series data are a problem which forestalls the application of models that are able to simulate the physical characteristics of energy budgets in tropical glaciers over long periods of time. Incomplete climate records occur often as a consequence of the difficult accessibility of high mountain glaciers, such as those in the Cordillera Blanca.

In this framework, this research aims to make some contributions to the understanding of the dynamics of tropical glaciers in the light of assessing the distributed contribution of energy fluxes to the physical processes leading to ablation and accumulation in the glacier Artesonraju. In addition, and considering the difficulties of obtaining sufficient and accurate data for modelling mass balances, this study also presents the degree-day melt factors that could be applied to modelling mass balance and discharge in this glacier with Temperature Index Models.

1.1 Aim of the Research Project

The aim of this thesis research is to contribute to the understanding of glacier-climate interactions in tropical areas by simulating energy fluxes that act at the glacier surface, leading to ablation- and accumulation processes. Additionally, the study looks for deepening the knowledge of the seasonal behaviour of the glacier. Therefore, and taking into account the limitations of the field data availability, a typical problem of the Andean Mountains, this research explores the possibility to simulate mass balance and discharge with just the use of temperature and precipitation variables as the unique input data.

Specific objectives of the research are:

- Determine and evaluate the characteristic climate, the relation among climatic variables and the historical trends in the climatic variables of the Cordillera Blanca, focusing the analysis to glacierized areas.
- Generate continuous series of data of the climatic variables required to glacier simulation by the use of appropriate statistical models.
- Determine the current state of research related to energy fluxes and degree-day melt factors in tropical glaciers.
- Analyze the dynamics of the climatic variables that influence most the glacial dynamics in tropical glaciers.
- Simulate mass balance and surface runoff of the tropical glacier Artesonraju and the Basin of Artesoncocha with energy balance- and temperature index models.
- Explore degree-day factors in order to obtain sufficiently realistic results that can represent the glacier mass balance with easily obtainable data.

1.2 Structure of the Thesis

The thesis starts with creating a baseline of the climatic conditions that influence the glaciers in the Cordillera Blanca and then presents, specifically, an analysis of measured energy fluxes and current mass balance calculations in the Artesoncocha basin. Later on, the results of two

different glacier simulation models applied in parallel to each season in the Cordillera Blanca, are presented. One chapter is dedicated to energy fluxes in tropical glaciers, in which the first part presents the current state of the investigations on energy budget in the Andean Mountains and the following part the results from the current application of the physically based model, Energy balance Model (EBM). Another chapter discusses various topics related to the Temperature Index Model (TIM), namely, a literature review and results of the application of a temperature index model. A final chapter makes a comparison of the results. In total, the thesis document comprises 9 chapters structured as follows:

Chapter 1 (the present chapter) gives an overview of the thesis, objectives, scope and study area.

Chapter 2 presents the study area and the data used for the current research.

Chapter 3 identifies the climate conditions in the Cordillera Blanca and the current results of mass balance calculations for three glaciers there. The main characteristics, such as seasonality, trend, interannual behaviour and a cross-correlation analysis of the main climate variables, i.e. temperature, precipitation, relative humidity and wind are exposed.

Chapter 4 shows the overview of the topic of mass balances and present the current data related to mass balances in the Artesonraju glacier.

Chapter 5 analyzes the measured energy fluxes data in the Artesonraju glacier, showing their characteristics, seasonality and cross-correlation with other climatic variables.

Chapter 6 presents the statistical method and the results for filling data gaps in the available data. This has the purpose to generate more complete time series which are required in the simulations of the glacier mass balance and discharge.

Chapter 7 composed of two parts is dedicated to the energy fluxes in tropical glaciers. The first part reviews the state of art of the investigations related to energy fluxes in the Andean tropics, identifying the main conclusions and the aspects that should be studied more thoroughly. The second part describes the methodology and the parameterization of the model which is applied in this research. Additionally, it presents the results of the mass balance- and discharge simulations, with a discussion about the distributed energy fluxes and the mass balance in the Artesonraju glacier.

Chapter 8 also composed of two parts is related to temperature index models in the tropical glaciers. The first part reviews the conceptual framework of the temperature index model presenting the state of art in regard to degree-day melt factors in the Andean tropical glaciers. The second part describes the methodology and parameterization of this model and the results of the temperature index models. The latter includes a validation of the degree- day factors for calculating mass balance for the Artesonraju Glacier and the discharge for the Artesoncocha Basin.

Chapter 9 makes a comparison of the results of the simulations of (EBM) and (TIM).

2 Study Area and Data

2.1 Study Area

The glaciated area of La Cordillera Blanca has a surface of 527.62 km² (**Figure 2.1**), and is the mountain chain with the largest extension of glaciers in the tropics. Located between 8° 12' and 10°01' of latitude south in the Department of Ancash of Peru and at longitude 77° 40', this mountain chain comprises 775 glaciers (Autoridad Nacional del Agua, 2014), with more than 200 with peaks over 5000m and 30 more with peaks over 6000 m.a.s.l. (Ames and Francou, 1995). The glaciers of the Cordillera Blanca are an important water reserve and resource for many users downstream.

The waters of the Cordillera Blanca drain through rock slide valleys and some of them are temporarily discharged into lakes before they reach the Rio Santa. These waters from the Cordillera Blanca supply the irrigation system of the extensively cultivated zone called Callejón del Huaylas. Afterwards, parts of the water from the Rio Santa are deviated for hydropower generation in the Cañon del Pato and delivered again to the Rio Santa in their lower part. The Rio Santa flows finally into the Pacific Ocean, where at its mouth supplies much of the water for irrigation (Kaser *et al.*, 2003). This project called Chavimochic is developed for covering the irrigation needs of an area of 144385 ha, in the northern provinces of Viru, Trujillo and Ascope (Chavimochic Project, 2018)

The Cordillera Blanca is very important for the local population and their economic development. Their sloped areas, between 2000 and 4000 m altitude, which have been used for centuries by the Quechua peasants, are irrigated with glacier waters. Additionally, these waters contribute to the feeding of many irrigation projects (e.g. Chavimochic) extending over the coastal region north of the mouth of the Rio Santa, which is used for agriculture production dedicated mainly to exportation and encompasses nowadays a significant proportion of Peru's national income. The Huallanca hydroelectric plant accounts for 5% (270MW) of Peru's electricity and it depends on the generation of water in some glaciers as well. The glaciers are also an important touristic attraction, thus contributing to the local economy of the region (Chevallier *et al.*, 2011). These glaciers make an important contribution to the total annual discharge in the basin of Santa River in Peru. Indeed, Mark and Seltzer (2003) estimate that between 30% and 45% of the discharge in each glacierized catchment in the Cordillera Blanca comes from meltwater. All these glaciers together account for 12% of all annual discharge of the Santa River.

The importance of the tropical glaciers in the region resides not only in the amount of water they provide during the hydrological year, but also in the regulation of this amount of water for each season. This regulation of streamflow especially in the dry season consists in that the ice acts as a buffer of low flows. This characteristic leads to a diminishing of the seasonal variation of discharge in glacierized catchments, a fact which marks a difference with high-latitude glaciers (Mark and Seltzer, 2003). Therefore, the retreat of tropical glaciers documented over the last 40 years could have an enormous impact on the availability of water in the dry season and produce unexpected flooding in the wet season.

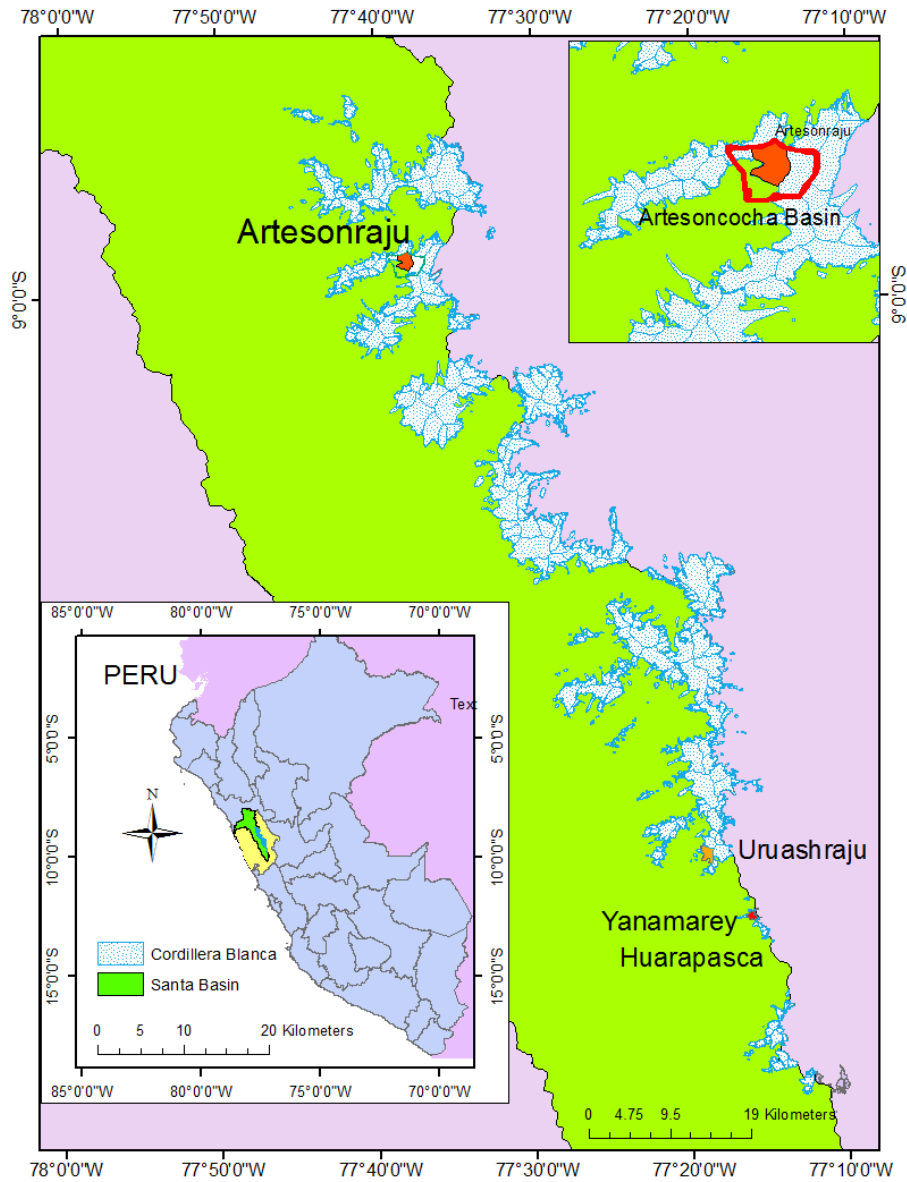


Figure 2.1. Location Cordillera Blanca, Artesonraju glacier and Artesoncocha basin

The glacier studied as part of this thesis research is Artesonraju (see **Figure 2.2**) in the Cordillera Blanca and which is located in the basin of Artesoncocha that is part of the Santa River basin.

In the Artesoncocha basin, there are 3 important peaks, which make up the snow-covered mountains: Artesonraju (north), Parón Grande or Paria (northeast) and Piramide (south) (see **Figure 2.3**). The Artesoncocha lake is a body of water of glacial origin located at the foot of the Artesonraju mountain. This lake is fed by the water of a recently formed small lake, called Laguna Nueva Artesoncocha Alta, (located in the tongue of the Artesonraju glacier) and some of the waters coming from the Caraz- snow covered areas. Artesoncocha lake has an elevation of 4288 m.a.s.l., an area of 6.77 km², stored volume of 637847 m³ and a maximal depth of 17 m. (INAIGEM, 2016).

2. Study Area and Data

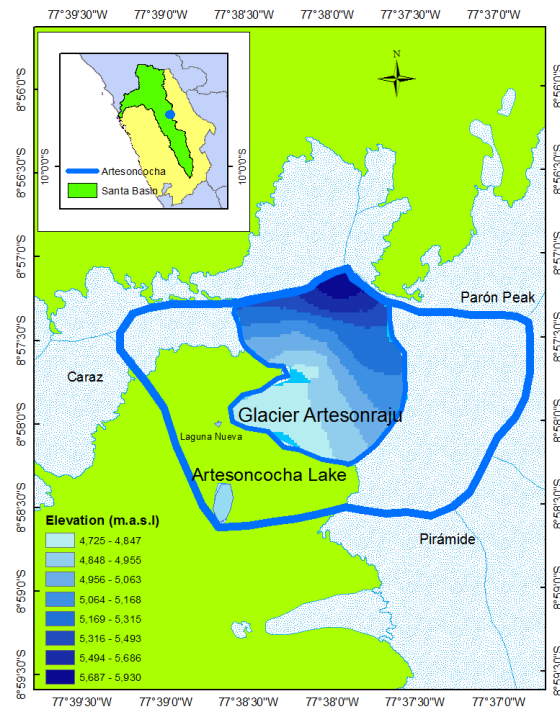


Figure 2.2. Artesoncocha basin, Artesonraju glacier and Artesoncocha lake



Figure 2.3. Satellitel image of the Artesonraju Glacier. Taken from Google Earth 2019

The snout of the Artesonraju glacier is located at 8° 57' 07" S, 77° 37' 56" W (WGS84). This glacier is characterized by having a defined tongue and a longitudinal profile of a waterfall type and has an area of 3.2 km²¹. The glacier's lower altitude varies between 4685² and 4720³ m.a.s.l. the highest is 5979 m.a.s.l. The glacier is predominantly oriented towards southwest and has an average slope of 54% (INAIGEM, 2016).

The Artesonraju glacier shows a retreat of -9.23 m/year between 1970 and 2003 (INAIGEM, 2016), following the increased trend of glacial retreat in the Cordillera Blanca since the end of the 1970s (Rabatel *et al.*, 2013). Consequently, the loss of glacial mass (area and volume) affects the freshwater reserves in the Rio Santa basin, as discussed earlier. Some technical reports of the Artesoncocha basin (INAIGEM, 2016) inform about the recent development of a small lake in the tongue of the Artesonraju glacier, called "The New Artesoncocha Alta " owing to increased ablation over the last 30 years. This small lake drains its water naturally, with an approximate flow of 1.1 m³/s, through an existing fracture to the head of the Artesoncocha lake (INAIGEM, 2016).

2.2 Data

The data used for this research is climate data, with daily records of temperature, precipitation, relative humidity, wind speed and energy fluxes. In addition, mass balance measurements on the glacier and a raster of the digital terrain model are available for this research. The characteristics of this data are described in the following subsections.

2.2.1 Climate data

2.2.1.1 Temperature

The data used from the Cordillera Blanca were taken from 51 gauge stations of daily records from gauge stations from SENAHMI⁴, INRENA⁵, ANA⁶ and DUKE ENERGY⁷ Peru. These data are available between the time period 1970 to 2007. The locations of the temperature stations are presented in **Figure 2.4**. Additionally, two time series with temperature of reanalysis NCEP-NCAR Reanalysis data hereafter called NCEP north and NCEP south (NCEP Reanalysis data provided by the NOAA/OAR/ESRL PSD, Boulder, Colorado, USA, taken from their Website at <https://www.esrl.noaa.gov/psd/>) were used for statistical and trend analyses. The NCEP north is located 224160m E and 9169435 S, 18 UTM, elevation 5500 m.a.s.l.. The NCEP south is located 223509mE and 8892549mS 18 UTM, elevation 5500m.a.s.l.

¹ Average of the annual glacier area, in which, mass balance is calculated by UGRH between the years 2005 and 2008 (WGMS, 2015)

² Lowest glacier elevation reported by INAIGEM (2016) and the WGMS (2015) for the year 2013.

³ Lowest glacier elevation reported by WGMS (2015) for the year 2012.

⁴ Servicio Nacional de Meteorología e Hidrología del Peru. Webpage: www.senamhi.gob.pe.

⁵ Instituto Nacional de Recursos Naturales de Peru. Web page: www.minagri.gob.pe/portal/especial-iv-cenagro/210-especiales/resultados-al-2008/1981-instituto-nacional-de-recursos-naturales-inrena.

⁶ Autoridad Nacional del Agua. Web page: www.ana.gob.pe/

⁷ Duke Energy Peru. Hydroelectric power generation enterprise.

2. Study Area and Data

The temperature time series have many data gaps and most of their records are available only over short periods. Indeed, there are no climate stations without gaps in the data between 1970 and 2007, the available period of records. The most complete records were found for the climate stations Querococha, Recuay, Huamachuco, Santiago de Chuco, Chavin, Anta and Cajabamba. The gaps and the length of the available periods of the largest time series data are detailed in **Table 2.1**.

Table 2.1. Gaps in the temperature series for different climate stations

Station	Start	End	Gaps
Recuay 3394 m.a.s.l.	01.01.1970	31.12.2007	19.4.1970-6.6.1970 6.8.1971-4.12.1972 11.2.1974-31.3.1974 1.6.1974-4.10.1978 18.10.1980-30.11.1980 1.4.1986-30.4.1986 29.6.1987-31.7.1987 1.3.1991-31.3.1991 12.12.1999-19.8.2001 1.10.2002-30.9.2002 10.12.2003-29.12.2003 26.9.2005-10.5.2006 11.7.2006-31.7.2006
Huamachuco 3200 m.a.s.l.	01.01.1970	31.12.2007	7.4.1981-21.8.1981 1.2.1986-1.7.1986 29.1.1991-15.8.1993
Santiago de Chuco 3128 m.a.s.l.	01.01.1970	31.12.1987	20.5.1970-19.10.1970 1.10.1976-12.4.1977 15.7.1982-17.7.1985 31.10.1986-7.12.1986 1.9.1987-23.9.1987
Chavin 3140 m.a.s.l.	9.3.1987	31.12.2007	16.9.1999-1.11.1999 27.9.2000-31.12.2001
Anta 2748 m.a.s.l.	1.1.1973	29.4.1995	9.10.1976-2.12.1976 1.1.1977-31.3.1976 21.1.1988-21.2.1988 1.1.1989-2.2.1989
Cajabamba 2480 m.a.s.l.	1.1.1970	31.12.2007	29.2.1979-31.3.1979 21.2.1980-31.7.1980 1.9.1980-1.10.1984 26.4.1993-6.5.1993
Querococha 4012 m.a.s.l.	1.1.1970	29.12.2007	30.6.1994-30.7.1994 2.7.1996-30.7.1996 2.9.1996-15.9.1996 2.1.2001-30.3.2001 2.5.2001-30.10.2001 2.5.2002-29.4.2005 28.10.2005-3.12.2005 2.3.2007-25.3.2007 29.7.2007-29.9.2007 25.10.2007-29.11.2007

2.2.1.2 Precipitation

Daily precipitation data of 90 stations all over the Santa Basin and surroundings were provided by SENAMHI and INRENA, Peru. These records are available between 1970 and 2007. **Figure 2.5** shows the locations of the precipitation stations. The longest time series exist for the stations Julcan, Milpo2, Chavin, Pira, Querococha, Huacamarcanga, Laguna Huangacocha, Pira, Recuay, Chiquian, Andajes, Malvas, Huamachuco, Mollepata, Oyon, Cotoparaco and Cajamarquilla. The length and the data gaps of these time series are presented in **Table 2.2**

2.2.1.3 Relative Humidity and Wind

Daily records of relative humidity data for the glacier areas of Uruashraju, Yanamarey, Artesonraju and Huarapasca, provided by the INRENA, Peru, are available between 2002 and 2007. In addition, some data are available in Huaraz and Querococha. However, these time series are accessible only for some short periods between 2000 and 2010. The climate stations with daily records of relative humidity are Artesonraju, Parón, Barrick Mine, Querococha and Huaraz (see **Figure 2.5**).

2.2.1.4 Energy Fluxes

Energy fluxes of shortwave- incoming radiation, shortwave-reflected radiation, longwave-radiation incoming from the atmosphere and longwave radiation at the surface, as well as the net radiation, are available every 30 minutes from 2004 to 2008. The data are measured at 4838 m.a.s.l. in the tongue of the Artesonraju glacier. The location of the energy gauge station can be observed in **Figure 2.3**. The data was provided by the ANA, with this data jointly managed by the INRENA and IRD⁸.

2.2.2 Discharge

The discharge data was taken from outlet records of Artesoncocha lake available between 21.06. 1996 and 13.3. 2009. This data was provided by INRENA and is jointly managed by UGRH⁹ and IRD. The gauge of discharge is located at 8° 58' 37" S, 77° 38' 40" W (WGS84), 4254 m.a.s.l. at the outlet of lake Artesoncocha. From instantaneous discharge data (every 30 min), daily averages were calculated as the arithmetic mean of all data during the day.

⁸ Institute de Recherche pour le Développement

⁹ Unidad Glaciológica de Recursos Hídricos. ANA, Peru.

Temperature Stations

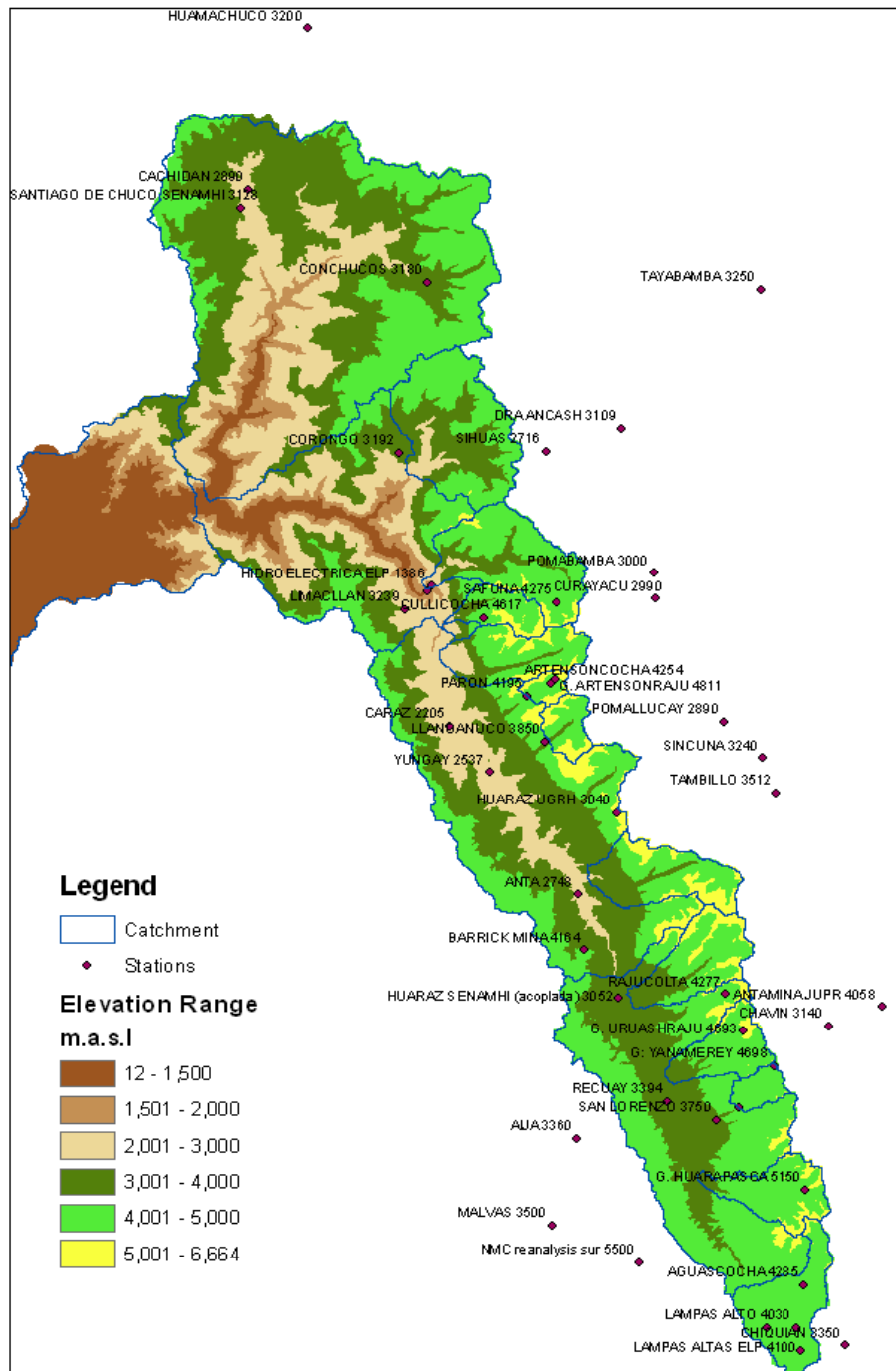


Figure 2.4. Temperature gauge stations in the Cordillera Blanca

2. Study Area and Data

Table 2.2 Length and gaps of the longest daily precipitation time series

Station	Start/Finish	Gaps (more than 3 days)	Station	Start/Finish	Gaps (more than 3 days)
Julcan 3500 m.a.s.l	Start:	21.10.1973-26.10.1973	Chiquian 3350 m.a.s.l	Start:	01.06.1974-10.03.1978
	01.01.1970	01.05.1975-31.05.1975		01.01.1970	09.02.1970-13.02.1970
	Finish:	31.01.1977-31.03.1977		Finish	01.01.1972-14.01.1972
	31.12.2007	01.03.1984-12.31.1984		31.12.2007	01.03.1972-03.12.1972
		10.11.1987-29.11.1987			01.04.1984-30.04.1984
	01.05.1990-31.12.1990		01.02.1985-28.02.1985		
	27.06.1991-30.06.1991		01.11.1985-31.08.1986		
	01.09.1992-01.08.1993		01.09.1987-30.09.1987		
			01.12.1987-12.31.1987		
			01.07.1989-31.07.1982		
			09.05.1995-16.05.1995		
Milpo 2 4400m.a.s.l.	Start:	01.02.1982-30.04.1982	Recuay 3394 m.a.s.l.	Start:	01.04.1986-29.04.1986
	01.07.1980	26.10.1982-30.10.1982		01.01.1970	09.03.1989-13.03.1989
	Finish:	26.10.1982-30.04.1989		Finish:	01.03.1991-30.03.1991
	31.12.2007	16.05.1989-19.05.1989		31.12.2007	01.10.2002-31.10.2002
		25.05.1989-29.05.1989			10.12.2003-30.11.2005
		21.07.1989-05.07.1989			
		19.05.1990-21.05.1990			
		25.06.1990-28.06.1990			
		01.01.1991-14.03.1991			
		01.10.1975-30.11.1975			
Laguna Huangacocha 3920m.a.s.l.	Start:	04.10.2006-07.10.2006	Chavin 3140 m.a.s.l.	Start:	01.01.1986-16.01.1986
	01.07.1971			01.01.1970	01.10.1986-06.03.1987
	Finish:			Finish:	16.03.2005-21.03.2005
31.12.2007		31.12.2007			
Huamachuco 3200 m.a.s.l.	Start:	02.04.1981-20.08.1981	Pira 3570 m.a.s.l.	Start	06.08.1971-08.09.1971
	01.01.1970	18.10.1981-21.10.1981		01.01.1970	27.05.1973-30.05.1973
	Finish:	19.05.1984-22.05.1984		Finish	08.12.1975-10.12.1975
	31.12.2007	31.05.1984-03.06.1984		31.12.2007	11.03.1976-13.03.1976
		01.02.1986-30.06.1986			21.05.1979-04.05.1979
		01.03.1990-05.03.1990			01.07.1971-11.12.1983
		25.03.1990-28.03.1990			17.11.1984-20.11.1984
		29.01.1991-30.04.1992			29.03.1985-31.03.1985
					06.01.1985-31.12.1985
					04.01.1994-29.04.1994
Huacamarcanga 4000m.a.s.l.	Start:	01.02.1985-28.02.1985	Mollepata 3758m.a.s.l	Start:	01.10.1975-31.10.1975
	31.05.1971			01.01.1970	01.04.1988-31.12.1988
	Finish:			Finish	10.01.1999-31.12.1989
31.12.2007		31.12.2007			
Querococha 4050 m.a.s.l.	Start	01.06.1970-06.06.1970	Cotaparaco 3080 m.a.s.l.	Start	01.06.1970-31.12.1970
	01.01.1974	13.07.1994-26.07.1994		01.01.1970	01.12.1983-31.12.1983
	Finish	08.08.1994-15.08.1994		Finish	01.08.1986-31.12.1988
	01.08.2002	25.08.1994-30.08.1994		31.12.2007	01.05.1999-31.05.1999
		01.07.1996-18.07.1996			05.01.2004-31.05.2004
		01.01.2000-31.03.2001			01.10.2006-31.10.2006
	01.05.2001-31.10.2001				
Andaje 3950 m.a.s.l.	Start	04.01.1988-28.02.1989	Oyon 3641 m.a.s.l.	Start	05.01.1982-31.05.1982
	01.01.1970	01.02.2005-10.02.2005		01.01.1970	01.10.1983-30.06.1986
	Finish			Finish	31.08.1994-10.09.1994
01.08.2007		31.12.2007	01.04.2004-30.04.2004		
			01.01.2005-31.01.2005		
			01.04.2006-30.04.2006		
Malvas 3500 m.a.s.l.	Start	01.11.1984-31.12.1984	Cajamarquilla 3028 m.a.s.l	Start	01.03.1982-31.05.1982
	01.08.1981	01.01.1988-29.02.1988		01.01.1970	01.08.1982-31.12.1982
	Finish	01.11.2002-31.01.2003		Finish	01.06.1985-31.07.1985
	31.12.2007	01.05.2005-31.05.2005		31.12.2007	01.03.1986-31.03.1986
			01.02.1990-27.02.1990		
			30.11.2001-06.12.2001		
			01.03.2003-31.03.2003		
			01.01.2005-31.01.2005		

Precipitation Stations

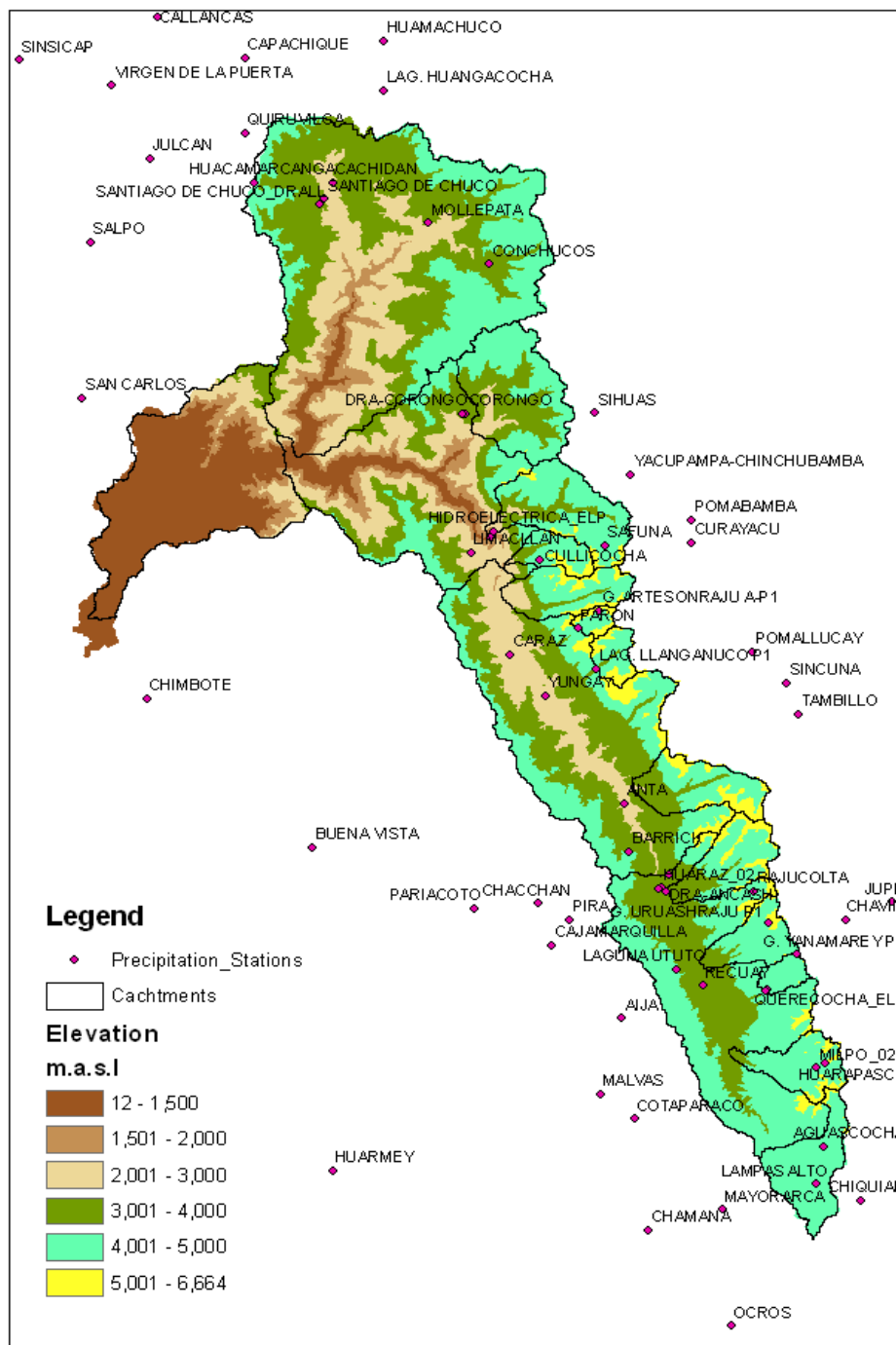


Figure 2.5. Location of precipitation stations in the Santa basin and the Cordillera Blanca

2.2.3 Mass balance measurements

Mass balance measurements between 09.09. 2003 and 18.09. 2008 in each hydrological year that begins in September and finishes in August, were provided by ANA. This data is based on field measurements from the net of stakes and pits operated by IRD and UGRH. The measurements were taken in lapses varying between 20 to 68 days. The net stakes ranges from 29 stakes in 2003 to 34 stakes in 2008 and 2 pits in the accumulation zones, where measurements were made yearly. **Figure 2.6** shows that net of stakes and pits in the glacier Artesonraju. In addition, maps for the glacier variation in the Cordillera Blanca for the years 2000 and 2006 were also provided by the ANA.

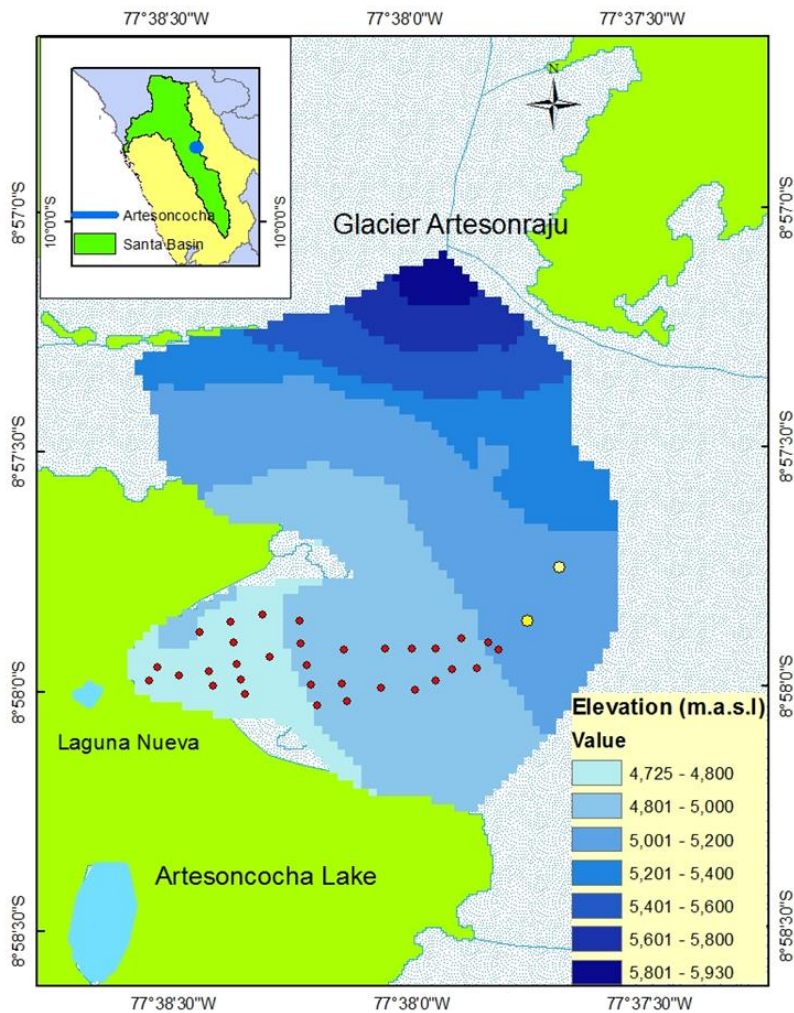


Figure 2.6. Net of stakes (red points) and pits (yellow points) in the Artesonraju Glacier

2.2.4 Grid data

The elevation digital elevation (DEM) model resolution 30x30M provided by the German Earth Observation Center DLR of the SRTM DRL was used. From this DEM, three more rasters required for the EBM model were generated. Slope and aspect rasters were generated by using ArcGIS and Sky view raster by using an specific Sky view factor calculation program from Zakšek, Oštir and Kokalj(2011). The content description of the three mentioned rasters is:

- Slope raster which is the rate of the maximum change in each elevation from each cell in the raster.
- Aspect raster identifies the downslope direction of the maximum rate of change in value from each cell to its neighbors. Aspect can be thought of as the slope direction measured in grades. The values of the output raster will be the compass direction of the aspect.
- Skyview factor defined as the portion of the visible sky limited by relief being 0 when the sky is totally blocked and 1 from unobstructed sky.

3 Analysis of Climate Setting in the Tropical Glaciers of La Cordillera Blanca

This chapter is comprised of two parts. The first part focuses on the climate setting of the glaciers of La Cordillera Blanca. It seeks to analyze the main climatic characteristics of this mountain range, especially, of the glacierized areas. Through the statistical analysis of the main climate variables, their statistical associations, i.e. correlations, their temporal and spatial trends, and the influence of phenomena like el ENSO in the climate setting are found.

3.1 The Climate of the High Mountains in La Cordillera Blanca

3.1.1 General climate characteristics of Andean tropical glaciers

La Cordillera Blanca (CB) is mainly influenced by the easterly winds from the Amazon basin, the westerly winds that comes from the Pacific originated by the Humboldt Current, local orographic effects and the ENSO phenomenon. However, the seasonal influence of the ITCZ is different in CB than in the northern glaciated areas of Colombia and Ecuador. The ITCZ produces not only tropical characteristics, but also certain subtropical climate features in the dry season of the CB, unlike of what is seen in northern glaciers in which tropical conditions prevail during the whole year. Thus, only two yearly seasons, wet and dry, with less humidity and precipitation in the dry season of CB are the main differences, when compared to the climate-typical tropical characteristics of the northern glaciers with the latter having four alternated wet and less continuous precipitation seasons. For this reason, Kaser and Georges (1999) introduced the concept of the “inner and outer tropics” to describe these differences in the climate regimes of the tropical glaciers. Based on this differentiation, the inner tropics are characterized by a regime of permanently humidity, although there are two periods with lower precipitation intensities, whereas, on the contrary, the outer tropics in which CB is located, is characterized by a period of precipitation and a dry period. These concepts will be discussed more extensively in Chapter 7. In the following sub-sections, some characteristics of air temperature, precipitation, relative humidity and wind in the CB are presented.

3.1.2 Air temperature

3.1.2.1 General statistics analysis and mutual station correlations

Despite the lack of data, some patterns can be seen from the available records. The relation of the mean, minimum and maximum temperature with the elevation of the stations located above 3000 m.a.s.l. is displayed in **Figure 3.1**. The overall range is from 10.7°C to 0°C for the lowest (3000 m.a.s.l.) to the highest (5500 m.a.s.l.) station, respectively. The temperature course has an average vertical gradient of -0.65°C/100m, which decreases to -0.62°C/100m for the maximum temperature and to -0.61°C/100m for the minimum temperature. The mean temperature follows approximately a linear trend, especially between 4000 m.a.s.l. and 5000 m.a.s.l.

The station with the longest records of average daily temperature (from 1970 to 2002) is Querococha. This station located at 4012 m.a.s.l. shows a mean temperature of 7.5°C. The highest

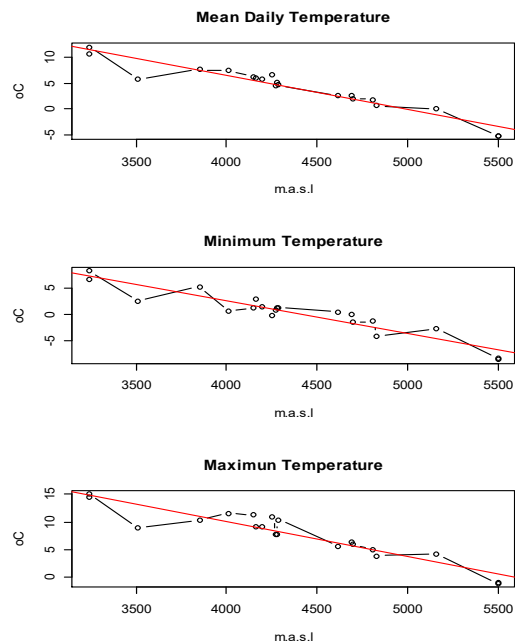


Figure 3.1. Mean, minimum and maximum daily temperature (between 1970 and 2010) as a function of altitude for stations above 3000 m.a.s.l.

station Huarapasca located at 5160 m.a.s.l. has records for only two years. This station shows a mean temperature of 0°C. From the stations located in the glaciers, Yanamarey and Artesonraju have the longest records (from 2001 to 2007). Yanamarey is located at 4698 m.a.s.l. and has a mean temperature of 2.1°C and Artesonraju is located at 4838 m.a.s.l. with a mean temperature of 1.9°C. Further statistics, such as mean, media, minimum and maximum values and lower and upper quartile of the time series of daily temperature, averaged over several years, is presented in **Table 3.1**. Years with more than two consecutive months of gaps were excluded from the analysis. Minor gaps in the time series of the studied years were filled using multilinear regression (Bejranonda, 2015).

Kendall correlation-coefficients of the daily temperature time series for stations over 3000 m.a.s.l. are presented in **Figure 3.2**. The results show especially a high correlation of the stations located over 4.600 m.a.s.l., which are all on glacierized areas. For instance, there is a high correlation for stations Huarapasca, Yanamarey, Artesonraju and Uruashraju. Surprisingly, the station Tambillo exhibits correlation-coefficients, with Huarapasca, Yanamarey, Artesonraju and Uruashraju between (0.46 and 0.61). This station is located at 3512 m.a.s.l. and does not belong to the basin of the Rio Santa. Another important finding is the strong statistical association of time series of temperature between stations located in the same elevation range. Such is the case for Parón, Querococha, Cullicocha and Barrick Mina from one side and Llanganuco and Huaraz from other side. This thermal homogeneity in the Andean glaciers is also mentioned by Pierrehumbert (2005). However, this uniformity in the horizontal elevation band is less at the edge of the tropics according to Kaser and Osmaston (2002). Indeed, some special cases in the CB of unexpected correlations from different elevation ranges are also found in the present analysis. For example, the correlation-coefficient of temperatures between Parón (4195) and Huaraz (3040) is higher (0.55) than that between Parón and Artesoncocha (4254) (0.38). These results indicate that certain local characteristics may influence the temperature gradients.

3. Analysis of Climate Setting in the Tropical Glaciers of La Cordillera Blanca

Table 3.1. Statistics (mean, median, standard deviation (SD), minimum (Min) and maximum (Max), and lower (1stQ) and upper (3rdQ) quartile and variance (VAR)) of daily temperature at stations of CB.

Station	Complete analyzed years	Elevation m.a.s.l	Min	1st Q	Median	Mean	3rd Q	Max	SD	VAR
NCEPnorth	1970-2007	5500	-8.5	-5.8	-5.2	-5.2	-4.6	-1.0	0.9	0.8
NCEPsouth	1970-2007	5500	-8.4	-5.7	-5.1	-5.1	-4.6	-1.1	0.8	0.7
Huarapasca	2006 and 2007	5160	-2.6	-0.7	-0.2	0.0	0.6	4.2	1.0	1.0
Artesonraju	2003-2007	4838	-1.2	1.3	1.8	1.9	2.5	4.9	0.9	0.8
Yanamarey	2003-2007	4698	-1.5	1.4	2.1	2.1	2.7	5.7	1.0	1.0
Uruashraju	2002-2007	4693	0.0	2.1	2.7	2.7	3.3	6.3	0.9	0.8
Cullicocha	2007	4617	0.5	1.9	2.5	2.8	3.0	5.6	0.9	0.7
Aguascocha	2004-2007	4285	1.3	3.9	4.6	4.6	5.4	10.4	1.2	1.5
Rajucolta	2006-2007	4277	1.2	4.6	5.2	5.2	5.8	7.7	0.9	0.8
Artesoncocha	2003-2007	4254	2.9	6.1	6.8	6.9	7.6	10.7	1.1	1.3
Paron	2004-2007	4195	1.5	5.3	5.9	5.9	6.5	9.2	0.9	0.8
BarrickMina	1997-2001, 2005-2007	4164	2.8	5.4	6.1	6.1	6.7	9.1	1.0	0.9
Querococha	1970-2000 and 2006	4012	0.6	6.7	7.5	7.5	8.3	11.5	1.2	1.5
Tambillo	2001-2005	3512	2.6	5.4	5.8	6.0	6.7	8.7	1.0	1.0
Sincuna	2004-2007	3240	8.3	11.5	12.4	12.4	13.2	15.0	1.1	1.1
Recuay	1970-1973,1979-1999and 2002-2007	3394	7.6	11.6	12.6	12.5	13.6	17.4	1.4	1.9
Limacllan	2004-2007	3239	6.7	9.9	10.6	10.6	11.3	14.4	1.1	1.2

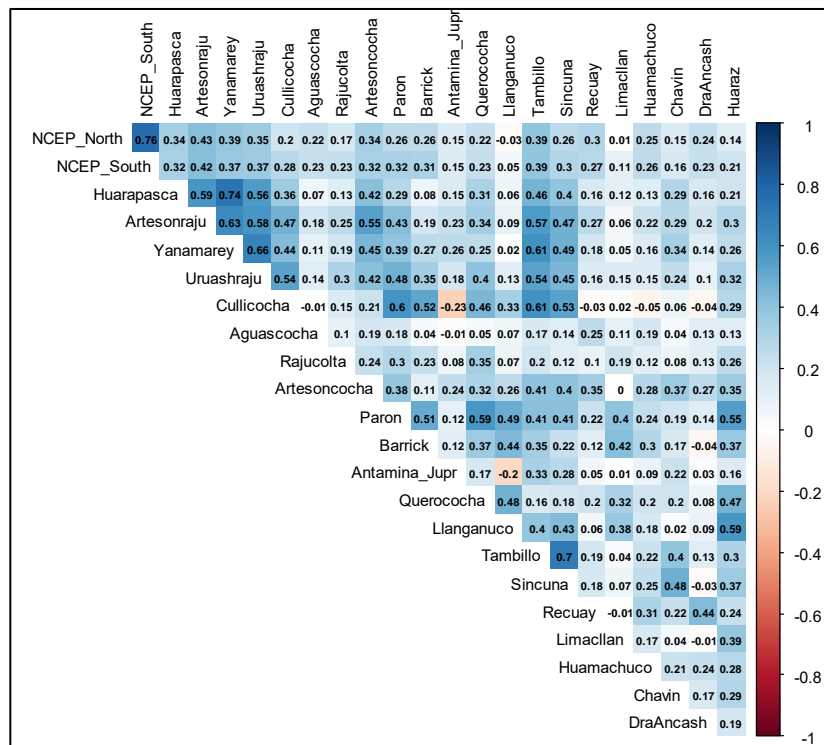


Figure 3.2. Kendall correlation of the temperature of stations above 3000 m.a.s.l.

3.1.2.2 Seasonal patterns of temperature

The Cordillera Blanca has one wet period that starts approximately in September and finishes in April, and a dry period which lasts from May to August. This seasonality manifests itself in slight changes of temperature over the months of the year, as is visualized in **Figure 3.3** which presents box whisker plots of the mean daily temperature in each month of the year of some stations located over 4000 m.a.s.l.

3. Analysis of Climate Setting in the Tropical Glaciers of La Cordillera Blanca

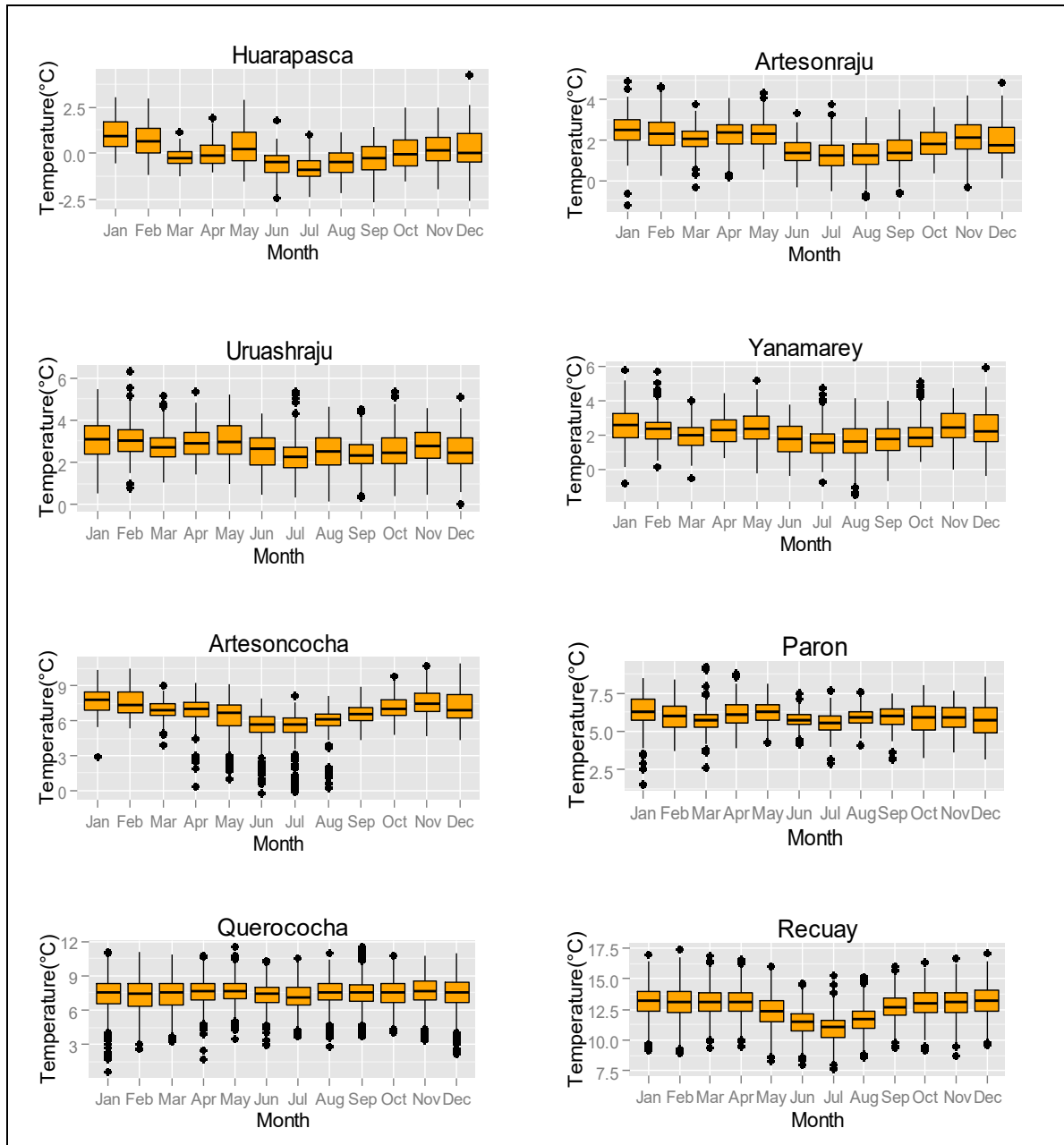


Figure 3.3. Seasonal pattern (box whisker plots) of temperature for each month of a year in the glacier stations and the stations Parón, Querococha and Recuay

In fact, tropical glaciers are known for their low variation of daily temperature in the year, however, minor changes can be noticeable in some of the records of some of the CB glaciers studied here, for instance, Huarapasca, Yanamarey and Artesonraju. In particular, the minimum and maximum monthly mean temperatures of these stations (see **Figure 3.3**) have differences of 1.78°C for Huarapasca (5160 m.a.s.l.), 1.1°C for Artesonraju(4811 m.a.s.l.), 1.28°C for Yanamarey (4698m.a.sl.) and 0.82°C for Uruashraju (4693 ma.s.l.). Non-glaciated stations, like Recuay (3394 m.a.s.l.), Artesoncocha (4811m.a.s.l.) and Querococha (4012 m.a.s.l.) show variations of 2.2°C, 2.5° and 0.5°C, respectively. This shows that differences in seasonal

temperatures are still perceptible, and local conditions may have a certain influence on such variations, as there is not a regular pattern.

The dry period is well marked for most of the stations with their temperatures starting to decline in May and reaching its minimum around June and July. Afterwards the temperatures start to rise again until October. For the wet period two high peaks stand out visibly in most of the cases, wherefore the highest peak is in January, afterwards the temperature decreases between February and March and increases again between April to May. It is also observed that for stations, like Artesonraju, Yanamarey and Uruashraju there is more dispersion of the temperature in the wet season, while the pattern of the dry season are more uniform, however, this feature is inverse in Artesoncocha station which has more data dispersion between April and August.

3.1.2.3 Interannual variability of temperature and correlations with Niño SSTs

The time series of the annual mean temperature (see **Figure 3.4**) shows the minimum and maximum interannual changes relative to the mean annual temperature of each station (hatched line). The red line shows, furthermore, the adjusted linear regression line to the data which provides a first approximation of the temporal trend. A more detailed analysis of the trend will be presented in Section 3.1.1.4. Interannual variability of annual temperature shows a maximum for year 1988 for all, but except for station Santiago de Chuco. For this station and, as well, for the reanalysis data (NCEP south), the highest mean annual temperatures are experienced in year 1997. High peaks of annual temperature are also present in this year for stations Querococha and Cajabamba. The reanalysis data (NCEP north) unveils its peak in 1998. Another peak for the data of NCEP north and south and stations Querococha and Recuay is present in year 1983. There is no data in this year for stations Santiago de Chuco, Chavin and Cajamarca. Furthermore, some smaller peaks are recorded in the NCEP north and south data and of stations Huamachuco, Chavin and Cajamarca for year 2005.

According to the Climate Prediction Center of NOAA, a moderate to strong signal of El Niño SST-anomalies existed in the periods 72/73, 82/83, 86/87/88, 91/92, 94/95, 97/98, 2002/2003, 2004/2005, 2009/2010. In contrast, a strong to moderate signal of La Niña occurred in years 70/71, 73/74, 75/76, 88/89, 95/96, 98/99/2000, 2007/2008 (**Figure 3.5**). The influence of “El Niño” is stronger since the 80s. Thus, both the NCEP data and the times series of stations Querococha and Huamachuco register quite well an increment of the annual temperatures during the years when the El Niño phenomenon occurred, especially, in years 87/88.

Referring back to **Figure 3.4**, the lowest mean annual temperatures are present in year 1999 for stations Querococha and Huamachuco. Both the NCEP data and the records of the Chavin station exhibit a minimum of the mean annual temperature in that year. However, for station Cajabamba the temperature in 1999 is above its long-term average. Similar patterns are noticeable for the various stations in year 2000. Low annual temperatures occurred also in 1971 and between 1973 and 1976, and all stations reported these years as a long cold period. In the years 1984 and 1985, lower than average annual temperatures are found for stations Querococha, Recuay, Huamachuco, Cajabamba, NCEP north and NCEP south; in fact, during these years a weak sign of La Niña is noticeably in **Figure 3.5**. In year 1989, troughs are seen in the temperatures of NCEP

3. Analysis of Climate Setting in the Tropical Glaciers of La Cordillera Blanca

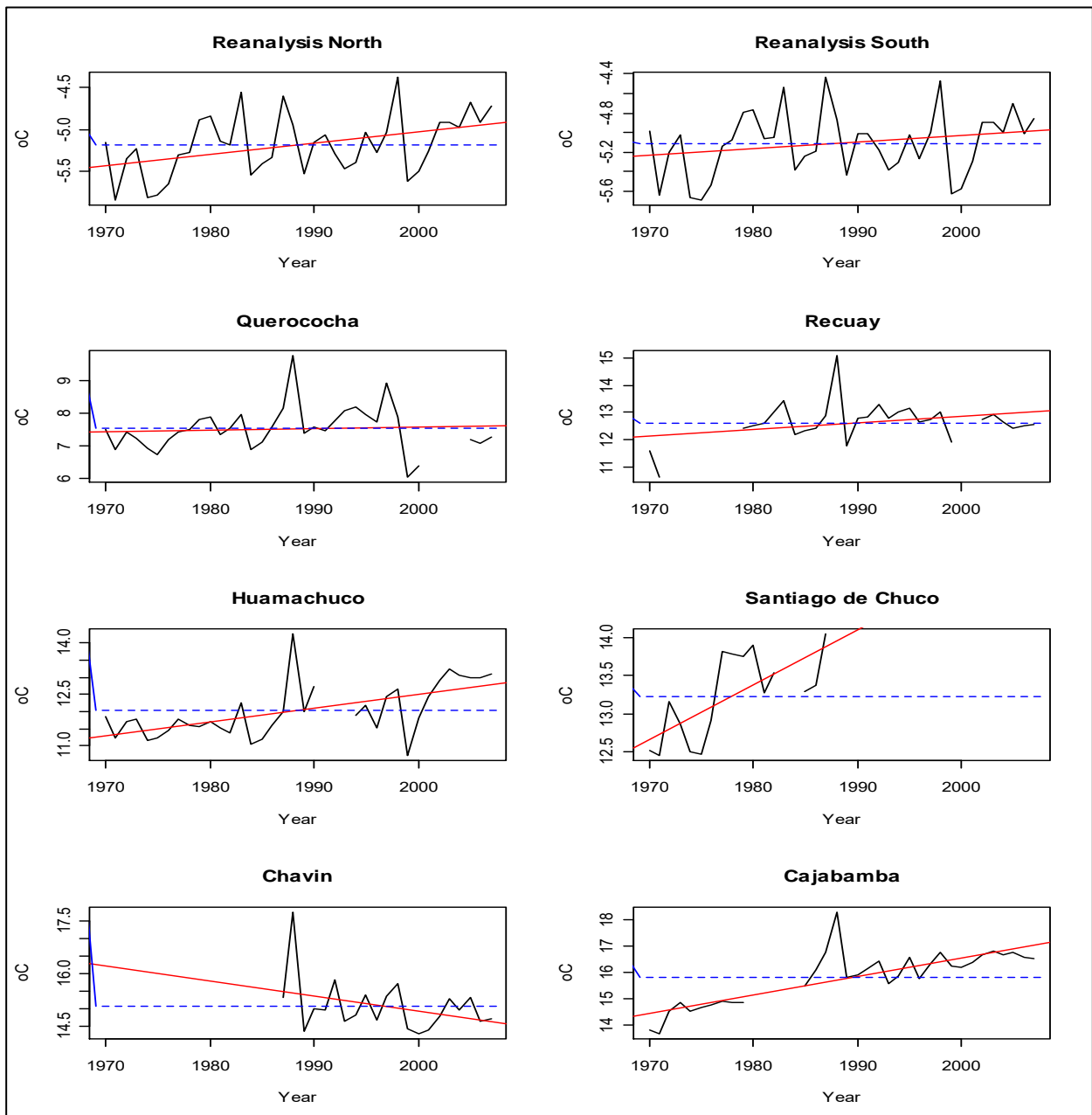


Figure 3.4. Annual mean temperatures of the reanalysis data (NCEP) and of various CB- stations

north, NCEP south, and stations Querococha, Recuay and Chavin. Lows exist also in 1984-1985 for Huamachuco, Querococha and in the NCEP data, and in 1992-1993 for Querococha and Chavin. During the La Niña years, e.g. the periods 1971-1972 and 1973-1976 most of the stations registered minima of the temperature. Other Niña periods seem to have less effect on the climate of the studied area, with barely lower-than-average- or even higher-than-average temperatures, as is the case for the 1995/1996 – and 2007- La Niña (see **Figure 3.4**).

The above results for the stations with the longest temperature records indicate that the El Niño/La Niña phenomenon has an important influence on the temperatures in the Cordillera

3. Analysis of Climate Setting in the Tropical Glaciers of La Cordillera Blanca

Blanca. Hence, the El Niño generates an important increment and La Niña a reduction of the mean annual temperature. This behavior is in agreement with that observed in previous studies made in the Cordillera Blanca (Francou *et al.*, 2004; Vuille, Kaser and Juen, 2008; Maussion *et al.*, 2015). However, it is important to recall that, especially, in the case of La Niña, the reduction of the temperature is not a typical feature of this phase of ENSO, as temperature reductions were not detectable in certain La Niña years, for instance, 1988/ 1989 and 1995/1996.

A correlation of SST temperatures of the regions Niño 1, Niño 3 and Niño 3.4 (with their locations depicted in **Figure 3.6**) with the monthly station temperatures is presented in **Figure 3.7**.

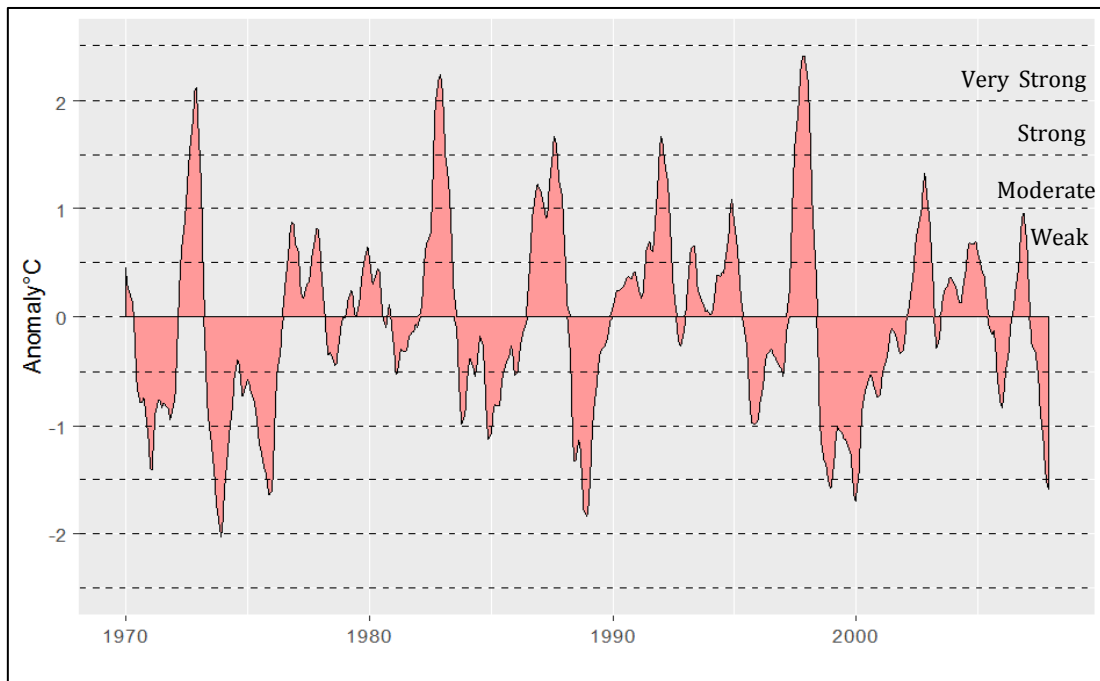


Figure 3.5. Ocean Niño Index (ONI)¹⁰, 3-month running mean SST anomaly

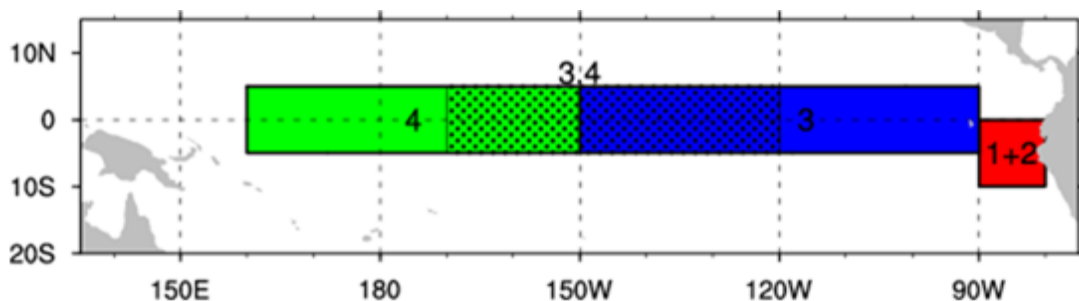


Figure 3.6. Niño SST Regions (SST)

¹⁰ Data provided by the NOAA/ESRL Physical Sciences Division, Boulder Colorado from their Web site at <http://www.esrl.noaa.gov/psd/>.

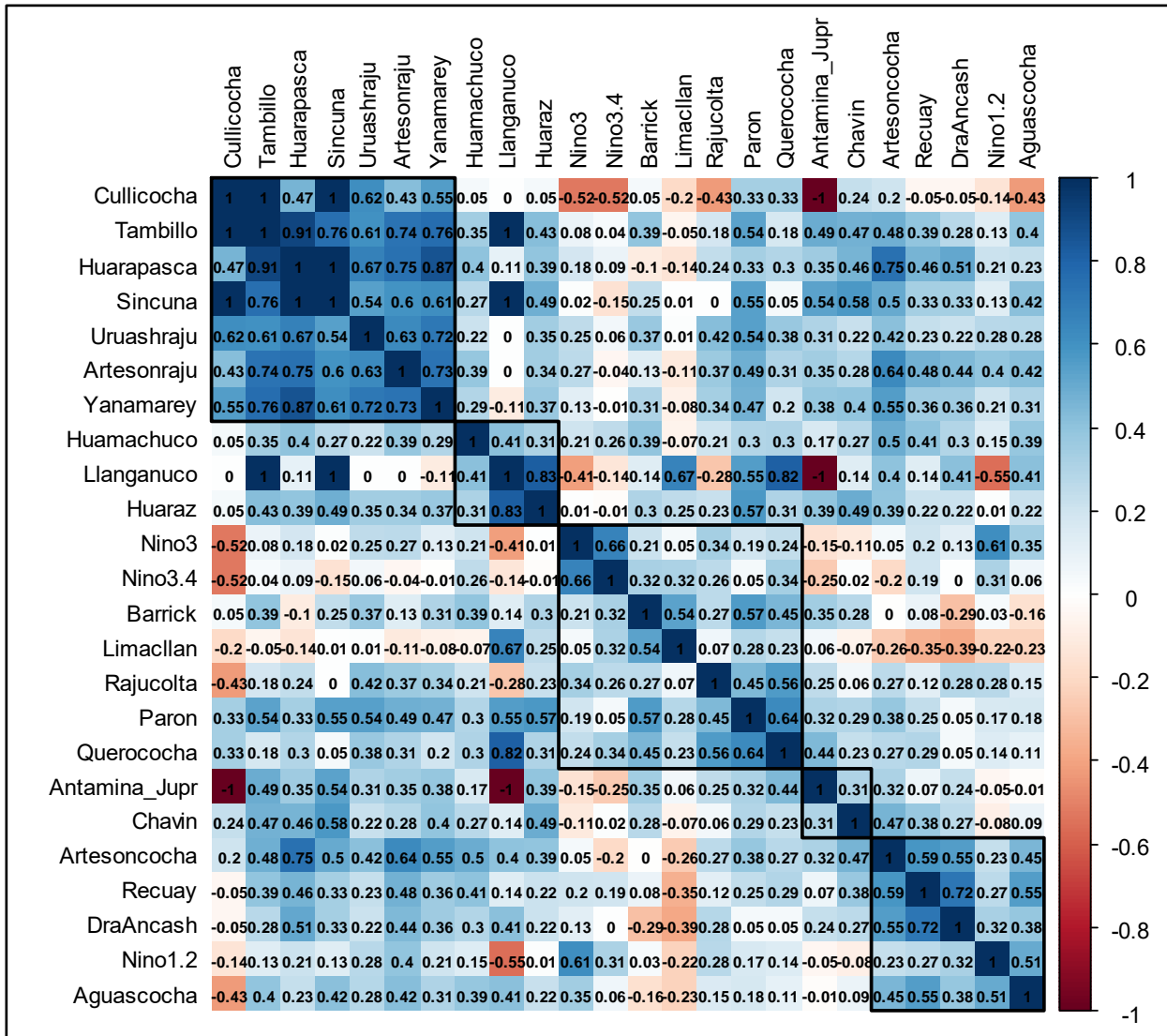


Figure 3.7. Correlations for lag=0 of El Niño 1.2, 3, and 3.4 with time series of daily temperature at stations of the study area

El Niño 1.2 which is the closest Niño region, located in the coastal zone of Peru (0-10S, 90W-80W), shows the highest statistical association, as measured by the correlation coefficient ($r=0.51$) with the daily temperature of Aguascocha. This correlation is followed by the glaciers Artesonraju ($r=0.4$) and Uruashraju ($r=0.28$). A lower statistical association with El Niño 1.2 occurs with Recuay ($r=0.27$), Artesoncocha ($r=0.23$), Yanamarey ($r=0.21$), however, these correlations are not significant. A negative correlation is also found at stations Llanganuco ($r=-0.55$), and lower with Limacllan ($r=-0.22$).

Certain positive statistical association of ENSO with time series of temperature in the glaciers is also found with the SST of the Niño3 region located in (5N-5S, 150W-90W). This is the case for stations Artesonraju and Uruashraju where correlations with SST of Niño3 of $r=0.27$ and $r=0.21$, respectively, are obtained. Daily temperatures at station Huamachuco are also correlated with SST in the Niño 3 region ($r=0.21$), whereas negative correlations occur for stations Cullicocha ($r=-0.55$) and Llanganuco ($r=-0.4$).

In regard with El Niño 3.4 (5N-5S, 170W-120W), which is one of the most used index for defining Niño and Niña events, some correlations are also obtained. For instance, for Querococha, $r=0.34$; Limaclan, $r=0.32$; Barrick Mina, $r=0.32$; and Huamachuco, $r=0.26$. Similar to the Niño3 negative correlation with the daily temperatures at station Cullicocha, a negative association with El Niño 3.4 SST is also found here ($r=-0.52$).

Monthly lagged correlations of El Niño 1.2, 3 and 3.4 SST with the temperatures of the stations located in the glaciers and Artesoncocha basin are also investigated (see **Figure 3.8**). For this purpose the Cross-Correlation Function (CCF) of R° was used. The CCF was applied between the monthly SST temperature data of each Niño region, as a predictor variable, and monthly temperature time series of glaciers Artesonraju, Yanamarey, Huarapasca, Uruashraju and Artesoncocha basin as the response variable.

The CCF between Niño regions and monthly temperature indicates that the temperature response of the stations Artesonraju, Artesoncocha, Yanamarey, and Huarapasca have a stronger positive statistical association with SST of the region Niño 1.2 and a slightly lower one with the SST of Niño 3. The temperature of Uruashraju is the only one that correlates more with the SST of el Niño 3. The mentioned significant positive correlations occur especially between lag 0 up to lag 2 for the southern glaciers Yanamarey, Uruashraju and Huarapasca and between lag 0 up to lag 3 for the northern glaciers Artesoncocha and Artesonraju., indicating that the former group responds slightly faster to increments of the temperature in the Niño regions than the latter.

In contrast, changes in surface temperatures of El Niño 3.4 seem to have no short-term impact on the temperatures of the glaciers in the Cordillera Blanca. Significant, but mostly negative correlation are found for Uruashraju at lags 6-7, Artesonraju at lags 6-10, Yanamarey at lags 8-9 and Artesoncocha at lags 8-10.

Generally, the increments of temperature at the glaciers are more retarded by about one month for region Niño 3 than for region Niño 1.2, owing most likely to the larger distance of the former than of the latter to the CB glaciers. For instance, for the lag-correlation between Artesonraju and Niño 1.2, the maximum, with $r=0.6$, is reached at lag 1, but occurs at lag 2 for the correlation with El Niño 3, though with a somewhat smaller peak, which holds also for all other glaciers mentioned, except for Uruashraju.

The strongest positive correlations of the glacier temperatures with those of the Niño regions are found for Artesonraju/Niño 1.2 ($r=0.6$) at lag 1, Artesoncocha/Niño 1.2 ($r=0.57$) at lag 2 (a slightly difference with lag 1), Yanamarey/Niño 1.2 ($r=0.45$) at lag 1, Uruashraju/El Niño 3 ($r=0.4$) at lag 0 and Huarapasca/El Niño 1.2 ($r=0.55$) at lag 1, i.e. as discussed, mostly for the correlations of the glaciers with the closest Niño region in the eastern Pacific.

3. Analysis of Climate Setting in the Tropical Glaciers of La Cordillera Blanca

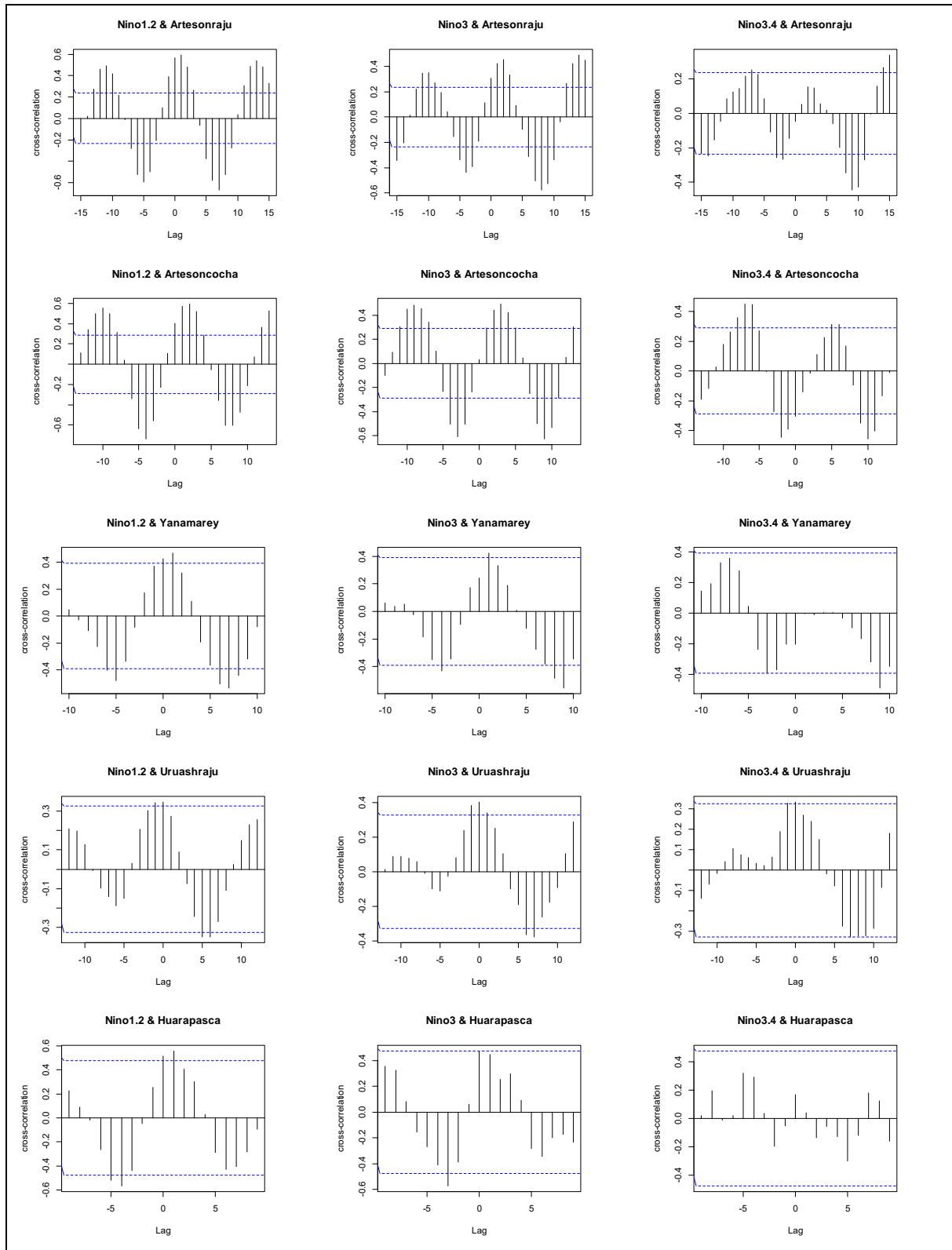


Figure 3.8. Lagged cross correlations of monthly SSTs of Niño 1.2, 3 and 3.4 regions with the monthly temperature in the glacier stations Artesonraju, Yanamarey, Uruashraju and Huarapasca and the Artesoncocha station

The sinusoidal variations of the various CCFs of **Figure 3.8** reflect the seasonal cycles of the glacier temperatures. These cycles show gradual increments of temperature during 6 to 7 months, followed by decrements during 5 to 6 months. They are particularly well established for the CCFs of the temperature of glacier Artesonraju with the various SSTs, but less so for those of Huarapasca, due to the fact that its temperature was only available for a short period of 2 years.

3.1.2.4 Temperature Trends

3.1.2.4.1 Methodology: Mann Kendall test

In order to detect a trend in the time series of annual temperatures, the Mann Kendall test (MK) is used. This test is widely used in trend analyses of climatologic and hydrologic time series (eg (Hirsch, Slack and Smith, 1982; Puertas, Carvajal and Quintero, 2011; Karmeshu, 2015; Khavse *et al.*, 2015). The advantage of this test is that is nonparametric, so that it does not require the data to be normally distributed and, in addition, it has low sensitivity to abrupt breaks in non-homogeneous data, as it the case in the data available in la Cordillera Blanca and the neighboring areas studied here.

The null hypothesis (H_0) in the MK test is that the data has not trend and is randomly ordered, wherefore the alternative hypothesis (H_1) states that the time series has a trend. The MK test compares the relative magnitudes of a sample data rather than the data value themselves. The calculation of the Statistics Mann Kendall (S) of a time series $x_1, x_2, x_3, \dots, x_n$ which represent n data points and x_j represent the data points at time j , then S is represented in Eq. (2.1)

$$S = \sum \sum sign(x_j - x_k), \quad j = 2, 3, \dots, n, \quad k = 1, 2, \dots, j - 1 \quad (2.1)$$

where

$$sign(x_j - x_k) = \begin{cases} 1 & \text{if } x_j - x_k > 0 \\ 0 & \text{if } x_j - x_k = 0 \\ -1 & \text{if } x_j - x_k < 0 \end{cases} \quad (2.2)$$

Positive values of S are an indicator of an increasing trend, and a low negative value indicates a decreasing trend. In order to quantify the significance of the trend, the probability (*p-value*) associated with S and the sample size (n) is computed.

When $n < 10$ the value of $|S|$ is compared directly with the theoretical distribution of S derived by Mann and Kendall. The two tailed test is used. At a certain probability level $(1-\alpha)$, H_0 is rejected in favor of H_1 , if the absolute value of S equals or exceeds a specific value $S_{\alpha/2}$, where $S_{\alpha/2}$ is the smallest S which has the probability less than $\alpha/2$ to appear in case of no trend.

When $n \geq 10$ the normal approximation is used in the Mann Kendal test wherefore the variance (σ_s) of S is obtained as:

$$\sigma_s = \frac{[n(n-1)(2n+5) - \sum tp(tp-1)(2tp+5)]}{18}, \quad p = 1, 2, \dots, q \quad (2.3)$$

where t_p is the number of ties for the p -th value and q is the number of tied values.

The standard test statistic Z_S is then calculated as follows

$$Z_S = \begin{cases} \frac{S-1}{\sigma} \text{ for } S > 0 \\ 0 \text{ for } S = 0 \\ \frac{S+1}{\sigma} \text{ for } S < 0 \end{cases} \quad (2.4)$$

If $|Z_S|$ is greater than $Z_{\alpha/2}$, where α represents the chosen significance level (in this case $\alpha=5\%$ corresponds to a $Z_{0.025}=1.96$), then the null hypothesis H_0 is rejected, since the probability of drawing a sample within that distribution belonging to H_0 (or a more extreme one) is only α , i.e. the alternative hypothesis H_1 of trend is more likely.

A more precise characterization of the test is achieved by means of the *p-value*. Thus, if the *p-value* is less than the significance level $\alpha=0.05$, H_0 is rejected in favor of H_1 , i.e. there is a trend in the time series.

The MK test is applied to annual temperature data, with the results summarized in **Table 3.2**.

For monthly data the Seasonal Mann Kendall (SMK) Test (Hirsch, Slack and Smith, 1982) described in VSP (2018) was applied. This test is used when the trend may or may not be linear but the variable consistently increases (decreases) over time as it can occur with some climatic variables. As same as Mann Kendall test, the H_0 null hypothesis establishes that there is no a trend in the time series, while the alternative hypothesis H_1 states that there is a trend at a significant level.

The notation in SMK test of x_{ij} correspond to the datum obtained for a month i in year j . Thus, the SMK Statistic S_i is calculated as follows:

$$S_i = \sum_{k=1}^{n_i-1} \sum_{j=k+1}^{n_i} \text{sign}(x_{ij} - x_{ik}), \quad (2.5)$$

S_i shows accumulated sign of the differences for the i^{th} month, where the year $j > k$. If S_i is a positive number, observations made in month i in later years tend to be larger than those made in month i in earlier years. If S_i is a negative number, then observations made in month i in later years tend to be smaller than those made in month i in earlier years.

$$\text{sign}(x_{ij} - x_{ik}) = \begin{cases} 1 & \text{if } x_{ij} - x_{ik} > 0 \\ 0 & \text{if } x_{ij} - x_{ik} = 0 \\ -1 & \text{if } x_{ij} - x_{ik} < 0 \end{cases} \quad (2.6)$$

The total of the time series S' is then

$$S' = \sum_{i=1}^m S_i \quad (2.7)$$

The variance σ_{S_i} of each month i^{th} is calculated as follows

$$\sigma_{S_i} = \frac{[n_i(n_i-1)(2n_i+5) - \sum_{p=1}^{g_i} t_{ip}(t_{ip}-1)(2t_{ip}+5)]}{18} \quad (2.8)$$

where g_i is the number of tied groups for the i^{th} month and t_{ip} is the number of data in the p^{th} group for the month i^{th} .

The variance for the whole time series is:

$$\sigma_{S'} = \sum_{i=1}^m \sigma_{S_i} \quad (2.9)$$

The standard test statistic for SMK test, Z_{sk} is then calculated as follows

$$Z_{sk} = \begin{cases} \frac{S'-1}{\sigma} \text{ for } S' > 0 \\ 0 \text{ for } S' = 0 \\ \frac{S'+1}{\sigma} \text{ for } S' < 0 \end{cases} \quad (2.10)$$

If the *p-value* is less than the significance level $\alpha=0.05$, H_0 is rejected in favor of H_1 , i.e. there is a trend in the time series. The sign of S' indicates if the trend is positive or negative.

Practically in many statistical packages, like R[®], Kendall's tau, defined similarly to Eq. 2.10, but using a slightly different expression in Eq. 2.8, is employed as the test statistics and which appears to have some advantages, particularly, for small numbers n of data.

3.1.2.4.2 Discussion and results of temperature trend analysis

Table 3.2 summarizes the results of the application of the SMK test for monthly temperature averages and of the MK test for annual means. The ranking of *p-values* for stations are presented for positive and negative *S-values* separately. The yellow color marks those stations which reject the null hypothesis of no trend H_0 at the 95% level of significance, i.e. the alternative hypothesis H_1 of a trend is accepted. Due to gaps in the data of certain stations, some time series could not be analyzed.

For the annual temperatures 26 out of the 37 stations confirm the null hypothesis of no trend, 10 stations have a positive trend and 1 station has a negative trend. None of the stations located in the glaciers show a significant trend. This is due to the fact that these stations have short time series and, therefore, these results may not be trustworthy. The NCEP north shows a positive trend, while the NCEP south has no trend.

Similar to the trends of the annual temperature averages, the results for the SMK tests for monthly temperature data exhibit also positive trends for most stations. Additionally, positive trends in the monthly data which are not seen in the annual time series appear for stations of NCEP South, Antamina Jupr, Recuay, Aija and Chiquian. That means that they have a monotonic upward trend, at least for one or more seasons (in this case months). Negative trends at the 95% significance level occur at stations Corongo, Hidroeléctrica Duke, Conococha, Limacllan and Lampas Altas.

The locations of the stations with positive trend do not show a particular geographical pattern, as these stations are located in the study area from north to south and cover an elevation range between 2500 and 4000 m.a.s.l.

The SMK test confirms more stations with negative trends in the monthly data (4) against (only 1) for the MK test with annual data. These stations are located across the study area and they have an elevation range between 1450 and 4100 m.a.s.l. These results may be produced by two

3. Analysis of Climate Setting in the Tropical Glaciers of La Cordillera Blanca

Table 3.2. Trends of monthly and annual temperatures using the SMK and MK test, respectively. Stations with significant trends (reject H_0 (no trend) in favor of H_1 (trend)) for both monthly and yearly data are marked in yellow and ones with different results in white

SMK Test				MK Test			
Station	S'	Kendall's Tau	P-value	Station	S	Kendall's Tau	P-value
Positive S^(c)							
Huamachuco	2889	0.408	2.22E-16	Cajabamba	340	0.64	1.50E-07
Cajabamba	3786	0.588	2.22E-16	Huamachuco	273	0.46	1.12E-04
Santiago de Chuco	465	0.410	9.12E-13	Conchucos	24	0.86	4.43E-03
NCEP South	1892	0.225	6.47E-12	NCEP North	215	0.31	7.14E-03
Anta	664	0.239	6.68E-08	Santiago de Chuco	58	0.48	1.03E-02
Antamina Jupr	92	0.575	7.80E-08	Anta	89	0.39	1.31E-02
Recuay	1000	0.197	1.51E-07	Pomallucay	10	1.00	2.75E-02
Conchucos	150	0.444	1.04E-07	Yungay	15	0.71	3.55E-02
Huaraz	477	0.267	1.04E-07	Antamina Yana	15	0.71	3.55E-02
Antamina Yana	112	0.455	6.34E-06	Huaraz	55	0.36	4.08E-02
NCEP North	1044	0.124	1.50E-04	NCEP South	133	0.19	9.70E-02
Aija	106	0.315	1.53E-04	Aija	14	0.50	1.08E-01
Chiquian	114	0.303	1.67E-04	Recuay	73	0.17	1.99E-01
Yungay	72	1.000	1.43E-03	Querecocha	87	0.16	2.02E-01
BarrickMina	61	0.152	5.41E-02	Artesonraju	7	0.47	2.60E-01
Querecocha	6	0.063	7.21E-02	Antamina Jupr	7	0.47	2.60E-01
Hidroeletrica ELP	52	0.125	1.09E-01	Tayabamba	15	0.27	2.76E-01
Pomallucay	20	0.208	1.10E-01	Yanamarey	7	0.33	3.68E-01
Tayabamba	70	0.109	1.10E-01	Antamina Ayash	4	0.40	4.62E-01
Yanamarey	34	0.153	1.14E-01	Huallanca	6	0.21	5.36E-01
Antamina Ayash	21	0.182	1.29E-01	Uruashraju	5	0.24	5.48E-01
Artesonraju	31	0.091	1.48E-01	Hidroeletrica ELP	6	0.17	6.02E-01
Uruashraju	31	0.140	1.48E-01	BarrickMina	6	0.17	6.02E-01
Huallanca	22	0.076	3.85E-01	Chiquian	5	0.11	7.21E-01
Artesoncocha	45	0.040	7.19E-01	Artesoncocha	1	0.07	1.00E+00
Negative S^(c)							
Corongo	-89	-0.614	3.08E-08	Hidroelectrica Duke	-15	-1.000	8.53E-03
Hidroelectrica Duke	-69	-0.462	2.59E-05	Limacllan	-8	-0.800	8.64E-02
Conococha	-66	-0.262	4.22E-03	Corongo	-6	-0.600	2.21E-01
Limacllan	-29	-0.287	2.31E-02	Conococha	-9	-0.429	2.30E-01
Lampas Alta ELP	-79	-0.160	3.06E-02	Chavin	-38	-0.181	2.64E-01
Malvas	-15	-0.022	1.32E-01	Malvas	-4	-0.667	3.08E-01
Chavin	-137	-0.057	2.17E-01	Huaraz UGRH	-4	-0.667	3.08E-01
Paron	-15	-0.143	2.51E-01	Salpo	-3	-0.200	7.07E-01
Pomabamba	-60	-0.069	2.66E-01	Paron	-2	-0.200	8.06E-01
Salpo	-17	-0.103	3.30E-01	Pomabamba	-4	-0.051	8.55E-01
Huaraz UGRH	-9	-0.143	3.40E-01	Lampas alta elp	-3	-0.067	8.58E-01
Cachidan	-6	-0.041	7.11E-01	Cachidan	1	0.067	1.00E+00

factors: 1) the trend in these stations occurs just for certain months or seasons, 2) monthly data present a larger sample size that provides more statistical evidence to detect a trend.

The stations with the lowest p -values, i.e. those with maximal trends not only from the seasonal MK test, but also with the normal annual MK test, are Huamachuco and Cajamarca.

Both the MK and SMK confirm the positive trends established earlier by the linear regression lines depicted by the red lines for stations Huamachuco, Santiago de Chuco, Recuay and Cajabamba in **Figure 3.4**. In contrast, for stations Querococha and Chavin, there is not enough evidence for a trend.

3.1.3 Precipitation

3.1.3.1 General statistical analysis and mutual station correlations

Precipitation is a meteorological variable that determines important characteristics in the study area in which the influence of the ITCZ is very important. In addition, orographic phenomena also have an effect on the intensity and volumes of snow/rain fall at high elevations. A rather low homogeneity in the behavior of the daily precipitation as a function of the elevation range in the Andean Mountains is observed from **Figure 3.9**. This graph shows that there is no clear positive relationship between daily precipitation and elevation range, suggesting that local climate and geographical conditions of each basin alter the precipitation homogeneity in the elevation range. For example, the daily precipitation registered at the Llanganuco station located at 3845 m.a.s.l. exceeds that of station Querococha located at 4050 m.a.s.l. by 1.3 mm. This is more likely due to the proximity of Llanganuco station to the glacierized peak Huaraz (6746 m.a.s.l.) which may lead to additional rain formation from an orographic effect.

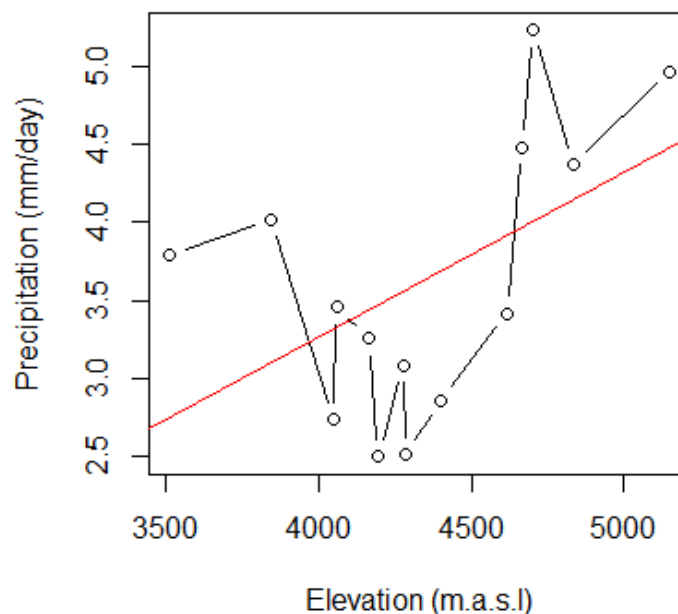


Figure 3.9. Mean daily precipitation in the CB as a function of elevation

3. Analysis of Climate Setting in the Tropical Glaciers of La Cordillera Blanca

The main statistical characteristics of the mean daily precipitation of the stations located above 3500 m.a.s.l. are presented in **Table 3.3**. One may notice that this quantity is higher at the Yanamarey glacier than that at Huarapasca, Artesonraju and Uruashraju glaciers. Amazonian air masses cross the Cordillera Blanca at the lower mountains and condensate afterwards, generating more precipitation (Gallaire *et al.*, 2007), for instance in the influence area of Yanamarey (4.91 mmd^{-1}). The Uruashraju glacier (neighbor of Yanamarey) could also be influenced owing to this effect, because the precipitation here (4.25 mmd^{-1}) is slightly higher than at Artesonraju (3.95 mmd^{-1}), although the former is located 170 m lower than the latter. In spite of the fact that the precipitation does not follow a clear linear relation to elevation, an overall positive trend is observed, though with some minor variability. Indeed, spatial variations of precipitation, in regard to elevations, are very variable in mountain regions (Alpert, 1986; Valéry, Andressian and Perri, 2010; Eackman *et al.*, 2017) and depend on different local factors e.g. wind. For instance, some high peaks of the Cordillera Blanca act as a barrier to the humidity that originates from the Santa River and the Pacific Ocean which may lead to more precipitation in these mountains.

The cross-correlation analysis for the daily precipitation is made with 23 stations. The results are listed in **Figure 3.10**, which indicates that the cross-correlation coefficients for the daily precipitation in the glaciers vary between 0.5 and 0.72, i.e. are rather high. However, two tendencies can be distinguished from this cross-correlation analysis:

Firstly, there is a high correlation of precipitation for some stations located within a similar range of elevation; such is the case for stations Artesonraju and Yanamarey (0.7) and Uruashraju and Yanamarey (0.71); however, as the geographical distance increase between some glaciers, these correlations diminish, as is the case for stations Huarapasca and Artesonraju (0.64).

Secondly, there is a high correlation of precipitation of stations located in the same basin or the neighboring basins, even if they are not in the same elevation range; this is the case for stations Artesonraju and Parón (0.64), Parón and Cullicocha (0.64), Parón and Llanganuco (0.47), Yanamarey and Huarapasca (0.7), and Yanamarey and Uruashraju (0.71).

Table 3.3. Statistics (mean, median, standard deviation (SD), minimum (Min) and maximum (Max), and lower (1stQ) and upper (3rdQ) quartile and variance (VAR)) of the daily precipitation for stations located above 3.500 m.a.s.l.

Station	Complete analyzed years	Elevation	Min	1st Q	Median	Mean	3rd Q	Max	SD	VAR
Huarapasca	2000-2007	5150	0	0.13	1.84	4.59	8.67	50.38	6.25	39.07
Artesonraju	2000-2007	4836	0	0.01	1.43	3.95	6.30	45.40	5.35	28.57
Yanamarey	2003-2007	4701	0	0.00	1.80	4.91	7.60	45.60	6.77	45.78
Uruashraju	2005-2007	4666	0	0.00	1.20	4.25	6.60	47.00	6.10	37.17
Cullicocha	2002-2006	4617	0	0.00	0.30	3.33	5.13	30.30	5.22	27.25
Milpo2	1981, 1983-1988, 1990and 1992-2007	4400	0	0.00	0.15	2.90	4.00	55.60	5.00	56.25
Aguascocha	2004-2007	4285	0	0.00	0.30	2.55	3.30	30.70	4.51	20.35
Rajucolta	2007	4277	0	0.00	1.20	3.18	5.10	24.40	4.34	18.83
Paron	1971,2000-2003 and 2005-2007	4195	0	0.00	0.30	2.36	3.20	28.50	4.00	16.03
Barrick	1997-2007	4164	0	0.00	0.00	3.32	4.50	43.00	5.71	32.65
Querococha	1970-1993, 1995 and 1997-2000	4050	0	0.00	0.10	2.70	3.30	42.90	4.94	24.45
Llanganuco	2005-2007	3845	0	0.00	1.52	3.68	5.80	34.19	5.19	26.98

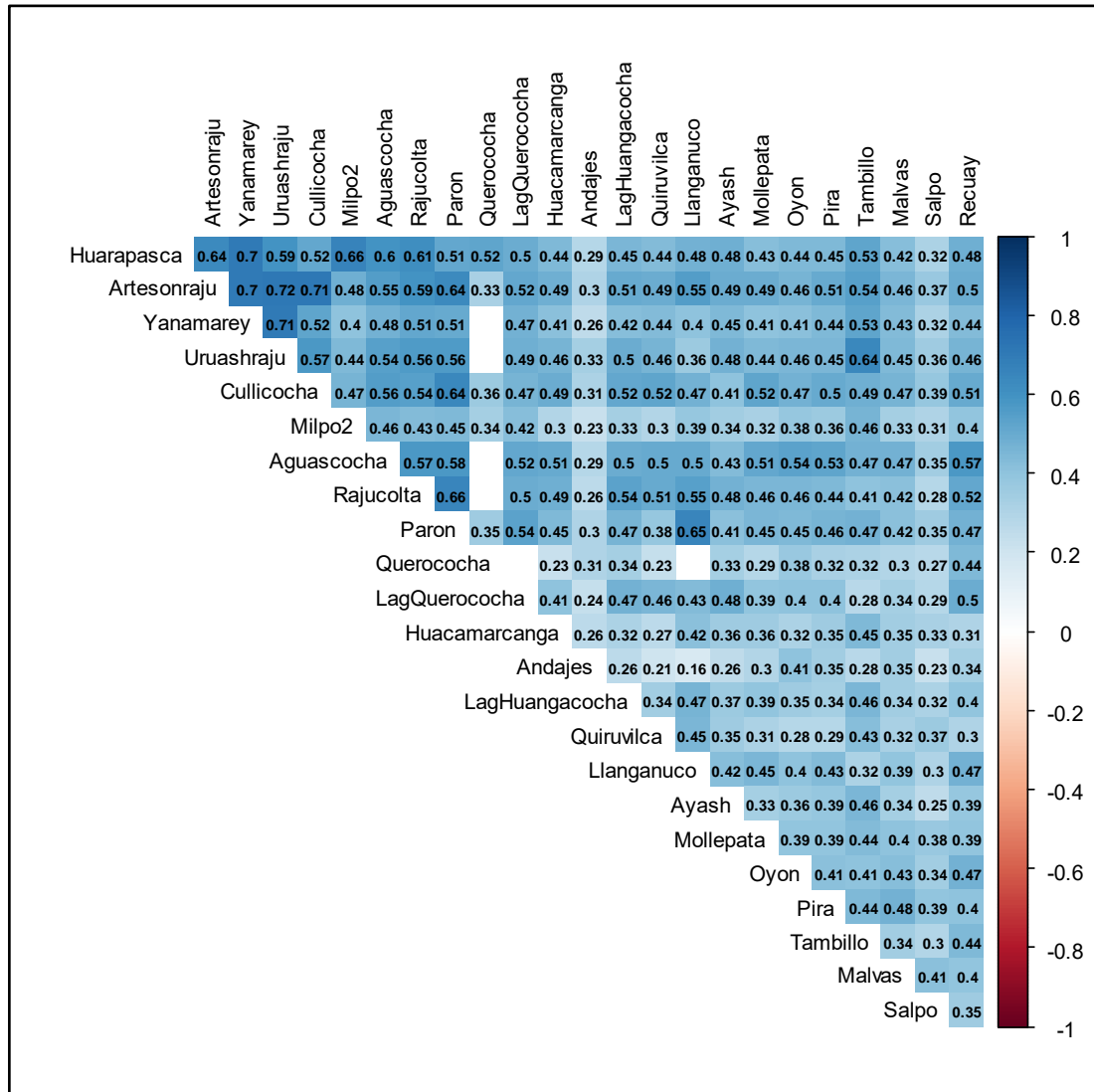


Figure 3.10. Correlation coefficients of daily precipitation data above 3000 m.a.s.l.

3.1.3.2 Seasonal patterns of precipitation

Similarly to the temperature, box whisker plots of the distribution of daily precipitation for each month of the year of the different stations located in the glaciers and those with large records of precipitation are presented in Figure 3.11.

The study area has one wet period lasting from September to April, and one dry period between May to August. For all stations, March is recognized as one of the rainiest months, whereas June and July are the driest months. This seasonal pattern fits quite well that described for the outer tropics, i.e. subtropical influence in the dry season and tropical behaviour in the wet season (Kaser and Georges, 1999).

In a typical manner, the box-whisker plots of the months of the wet season are characterized by more dispersion of precipitation time series data than those of the dry season.

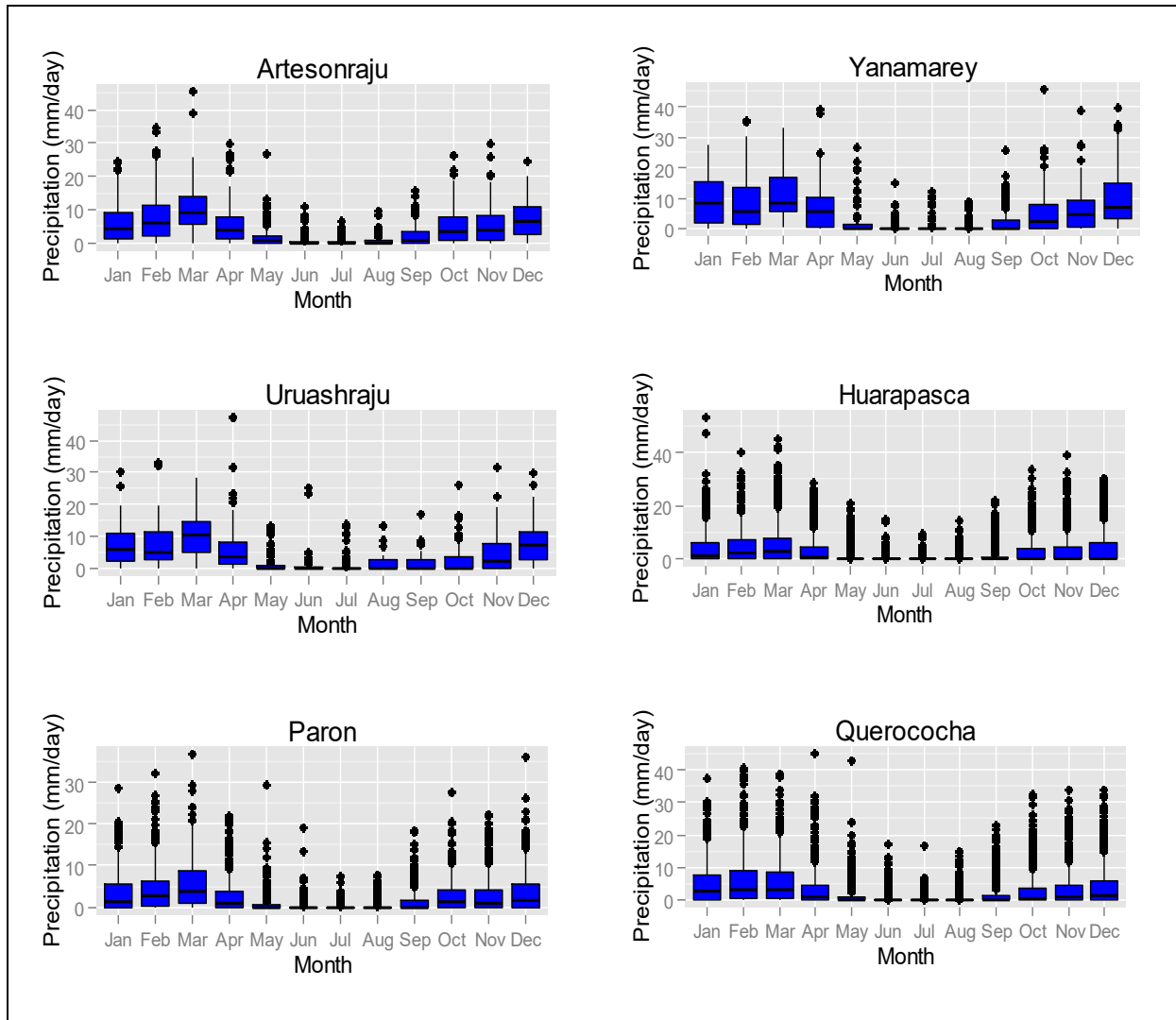


Figure 3.11. Seasonal pattern (box whisker plots) of daily precipitation for each month of the year for stations located in the glaciers, Artesonraju, Yanamarey, Uruashraju, Huarapasca and in their basins, Parón and Querococha

3.1.3.3 Interannual variability of precipitation and correlations with Niño

The assessment will be carried out with regard to two aspects, firstly, looking at the influence ENSO has on the annual precipitation and, secondly, analyzing the trends in the precipitation records. Time series of the annual precipitation for stations with the longest records of data are presented in **Figure 3.12**.

According to the literature, most of the authors coincide that El Niño is characterized by dry conditions, while La Niña by increments of precipitation, for instance, in the Zongo glacier in Bolivia, in Antizana in Ecuador, and in the Cordillera Blanca in Perú (Wagnon *et al.*, 1999; Favier, Wagnon and Ribstein, 2004; Francou *et al.*, 2004; Vuille *et al.*, 2008; Maussion *et al.*, 2015). Thus, it will be interesting to see if there is a similar behavior of precipitation in the Cordillera Blanca in relation to ENSO.

3. Analysis of Climate Setting in the Tropical Glaciers of La Cordillera Blanca

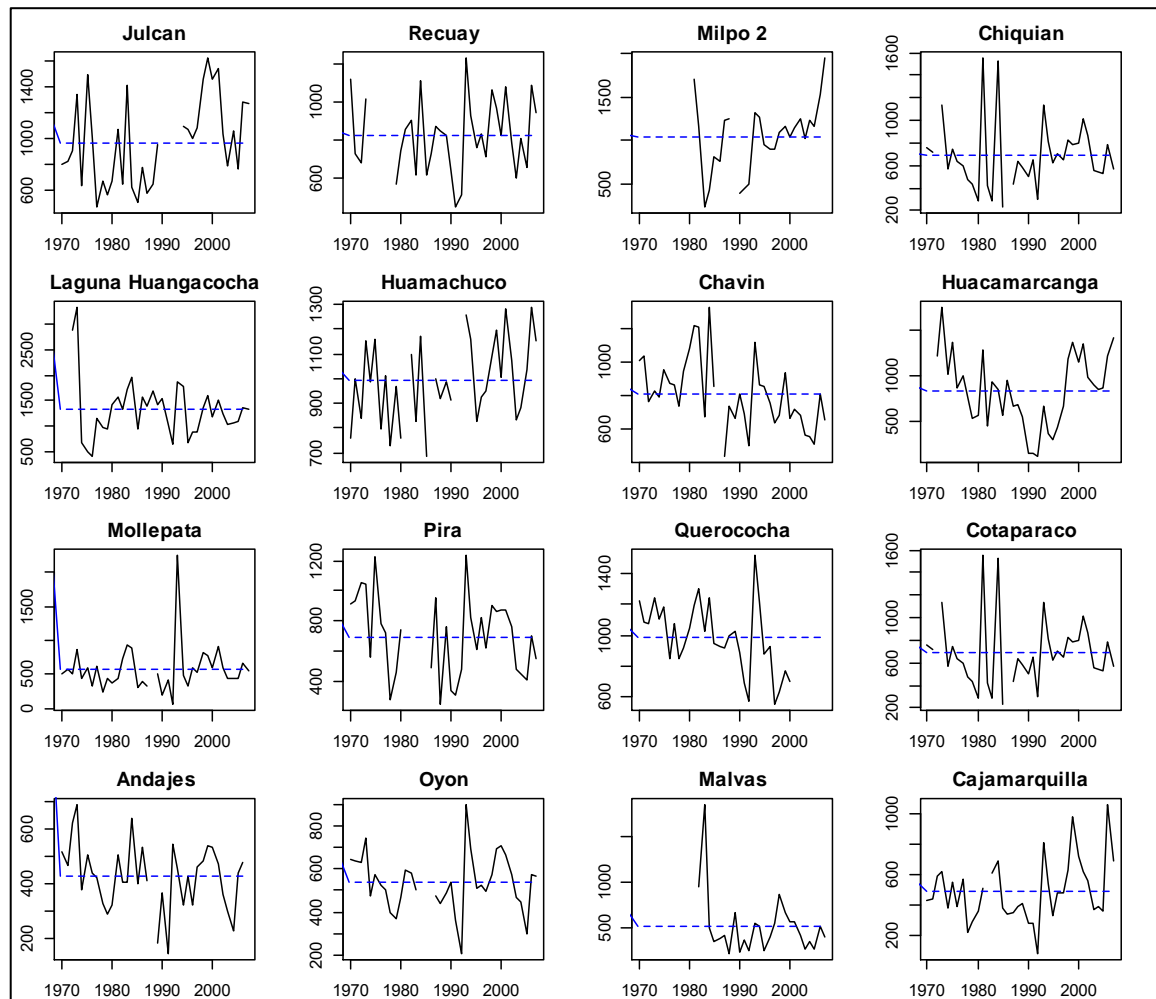


Figure 3.12. Annual precipitation (mm year⁻¹) at stations with largest records of precipitation

The Climate Prediction Center NOAA shows that moderate to strong anomalies of El Niño occurred in the periods 1972/1973, 1982/1983, 1986/1987/1988, 1991/1992, 1994/1995, 1997/1998, 2002/2003, 2004/2005, 2009/2010.

Analyzing the minimum annual precipitations of the graphs (driest conditions), the following aspects can be seen from the various time series plots: In 1972/1973 El Niño years, expected decrements less than the mean annual precipitation are found at stations Julcan and Recuay, however, unusual trends of precipitation increments are also found, for instance, at Pira, Oyon and Andajes for these years.

The year 1979 registered also minimum values of annual precipitation in several station records, like at Julcan, Recuay, Chiquian, Laguna Huangacocha, Huacamarca and Andajes, though neither an El Niño nor a La Niña occurred in that year.

In agreement again with the general correlation trend, in El Niño year 1983, a diminishing of the annual precipitation was registered at most stations, including Julcan, Recuay, Milpo2, Chiquian, Huamachuco, Chavin, Huacamarca, Cotaparaco, Andajes, Malvas, and near average precipitation in Querococha. In contrast, for the El Niño 1986/1987 years there are minimum annual records of precipitation at stations Milpo 2, Recuay, Pira, Malvas and Cajatambo.

Troughs of annual precipitation were registered for the El Niño years 1990 to 1992 for the stations Querococha, Milpo2, Recuay, Huacamarcanga, Mollepata, Pira and Cotaparaco, and only for the years 1991 and 1992 in Laguna Huangacocha, Chavin and Oyon, and 1990 and 1991 in Chiquian. A slightly decreased annual precipitation was observed in years 1994/1995 at Laguna Huangacocha, Huamachuco, Huacamarcanga, Malvas and Cajamarquilla, however, at stations like Recuay, Julcan, Milpo2, Querococha, Cotarapaco and Oyon, the precipitation are close to the mean long-term annual precipitation.

For the El Niño year 1997, a common minimum annual precipitation was measured again for stations, Querococha, Milpo 2 and Recuay. This trough of annual precipitation extends into 1998 for Querococha station.

For the period 2002-2005, many records show minimum values of annual precipitation reflecting dry conditions, such as Julcan, Recuay, Chiquian, Huamachuco, Chavin, Mollepata, Pira, Cotaparaco, Andajes, Oyon, Malvas y Cajamarquilla, however, the effect of this El Niño was less detectable at Milpo2, Laguna Huangacocha, Huacamarcanga.

The above results indicate that, on average, most of the past the Niños are indeed felt in terms of a reduction of precipitation in the Cordillera Blanca. However, some exceptions to this pattern appear also in some records. This could suggest that possible local meteorological variables, for instance, the wind may interfere with the effects of ENSO (Vuille, Kaser and Juen, 2008) or may lead to a lag of these effects in certain areas.

The phenomenon of La Niña occurred in the years 1970/1971, 1973/1974, 1975/1976, 1984/1985, 1988/1989, 1995/1996, 1998-2001, 2007/2008, and some characteristics of those years are:

In the years 1970 and 1973, maxima of annual precipitation are observed for stations Querococha and Recuay, Chiquian, Pira, Oyon and Cajatambo. In these two years both La Niña and El Niño phenomena occurred which explains why the earlier mentioned negative anomaly of El Niño in 1972 was not so strong at certain stations, such as Querococha, for which during that year the annual precipitation was above the mean annual precipitation. On the other hand, in agreement with the earlier mentioned literature, for La Niña years 1975/1976, a maximum of precipitation occurred at stations Julcan, Huamachuco, Huacamarcanga and Pira. However, that La Niña did not increment precipitation as expected at stations like Laguna Huangacocha, Oyon and Cajamarquilla, but shows even decrease of the precipitation at the former station.

In the period 1981 to 1984, high values of annual precipitation were registered at most of the stations, but not in the same way for all these years. For instance, Querococha showed high rates of precipitation, especially, in 1982, 1984 and 1981, but its precipitation was barely above the mean in year 1983. On the other hand, in 1981 all stations had annual precipitations above the mean average, except for station Mollepata. At station Milpo 2 the annual precipitation for year 1981 was very high, and above the mean for year 1982, whereas for years 1983 and 1984 the lowest precipitation values of the entire period were measured. In the year 1993, maximum annual precipitation occurred at stations Querococha, Recuay and Milpo 02. In addition, at stations Mollepata, Pira, Cajamarquilla, Malvas, Cotaparaco and Ocros, which are all located in neighboring basins, the largest amounts of precipitation were recorded in this year.

3. Analysis of Climate Setting in the Tropical Glaciers of La Cordillera Blanca

The above results indicated that in most of the cases, the La Niña's are linked to increments of precipitation; however, it is also observed that the precipitation anomalies do not correspond to the intensities of La Niña's for all cases. According to Vuille, Kaser and Juen (2008) the upper tropospheric flows, in certain areas of the tropics, influence the way the precipitation respond to ENSO. In addition, the correlation of temperature and precipitation in ENSO years, makes that wet summers tend to be cold and dry summers tend to be warm, thereby enhancing precipitation, however, the two variables can neutralize each other, and so generating near average annual conditions for certain years.

The correlation matrix of SST temperatures of the regions Niño 1, Niño 3 and Niño 3.4 with monthly precipitation at the various stations is presented in **Figure 3.13**. The SSTs of El Niño 1.2 region, which is the closest to the coastal zone of Peru(0-10S, 90W-80W), shows moderate positive correlation with most of the analyzed stations, with correlation coefficients that vary between $r=0.32$ to $r=0.44$ for stations Artesonraju, Yanamarey, Uruashraju, Huarapasca, Llanganuco Aguascocha and Cullicocha. A lower statistical association of the SSTs of the El Niño 1.2 regions occurs also with the precipitation at stations Parón ($r=0.25$) and Rajucolta ($r=0.23$). All this agrees with the earlier found fact of different respond of precipitation during La Niña years for which the SSTs at Peruvian coast are the highest per definition of this phenomenon.

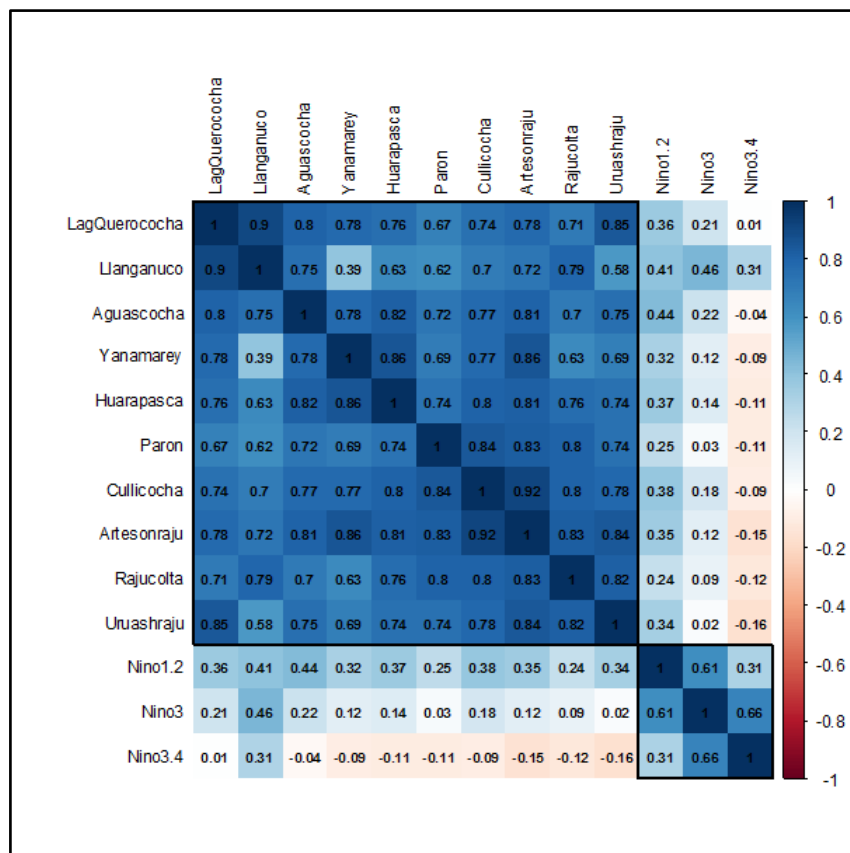


Figure 3.13. Correlation coefficients of Niño 1.2, 3 and 3.4 with daily precipitation in the glaciers stations and Parón, Aguascocha, Llanganuco and Lag. Querococha

Positive statistical correlations of SSTs in the Niño3 region with time series of the monthly precipitation at the analyzed stations also exists. This hold especially for station Llanganuco ($r=0.46$), LagQuerococha ($r=0.21$) and Aguascochas ($r=0.22$), but less so for the three glacier stations, Yanamarey, Artesonraju and Huarapasca with r - values varying between 0.12 and 0.14.

The correlations of the monthly SSTs of the El Niño 3.4 region with the CB- precipitation are overall negative, with r - values ranging between -0.16 and -0.9, except for station Llanganuco, where r is positive ($r=0.31$). This suggest that when the precipitation anomalies are in the view of SSTs of the Niño 3.4 region, the precipitation is observed to decrease. This aspect correspond to the general condition of decresed precipitation to the ocurrence el ENSO phenomenun. But, how this differences in each data series of the ENSO regions occurs?.

Further lagged cross correlation tests for the precipitation in the glacier basins and the SSTs of Niño 1.2, 3, and 3.4 regions reveal possible lags for the effects of ENSO on the increments or reductions of the precipitation in these basins (**Figure 3.14**).

For instance, for glacier stations Artesonraju, Parón and Huarapasca a similar behaviour of the CCF needle plots is observed for all three Niño regions, namely significant positive correlations of the precipitation with the surface temperatures of region ($r > 0.6$)

- Niño 1.2 between lags 0-3, with a peak at lag 1,
- Niño 3 between lags 1-4, with a peak at lag 2,
- Niño 3.4 between lags 2-5, with a peak at lag 3.

In contrast, following the seasonal precipitation cycle negative correlations are significant for stations Artesonraju, Parón and Huarapasca of the precipitation with the surface temperatures of region

- Niño 1.2 between the lags 6-9, with the lower trough at lag 8,
- Niño 3 between the lags 7-10, with lower troughs at lag 8 for Huarapasca and at lag 9 for Artesonraju and Parón,
- El Niño 3.4 between lags 9-11, with minimum peaks at lag 10 for Huarapasca and at lag 11 for Artesonraju and Parón.

The strengths of the lagged correlations of the monthly glacier precipitations with the various SSTs are similar for the combinations of Artesonraju and Huarapasca with regions Niño 1.2 and 3. Exception is the temperatures at station Parón which possesses stronger correlations with the SST of El Niño 1.2 than with Niño 3, let alone with El Niño 3.4 (more distant region). Again, as seen before for the temperature CCFs (see **Figure 3.8**), the precipitation CCF- needle plots exhibit a systematic cyclic pattern with a one-month retarded maximum, the further away is the El Niño region considered (El Niño 1.2 -> Niño 3 -> El Niño 3.4). This seasonality is less clear for stations Yanamarey and Uruashraju, where the displayed lags are less, due to the short evaluation period of only 5 and 3 years, respectively.

3. Analysis of Climate Setting in the Tropical Glaciers of La Cordillera Blanca

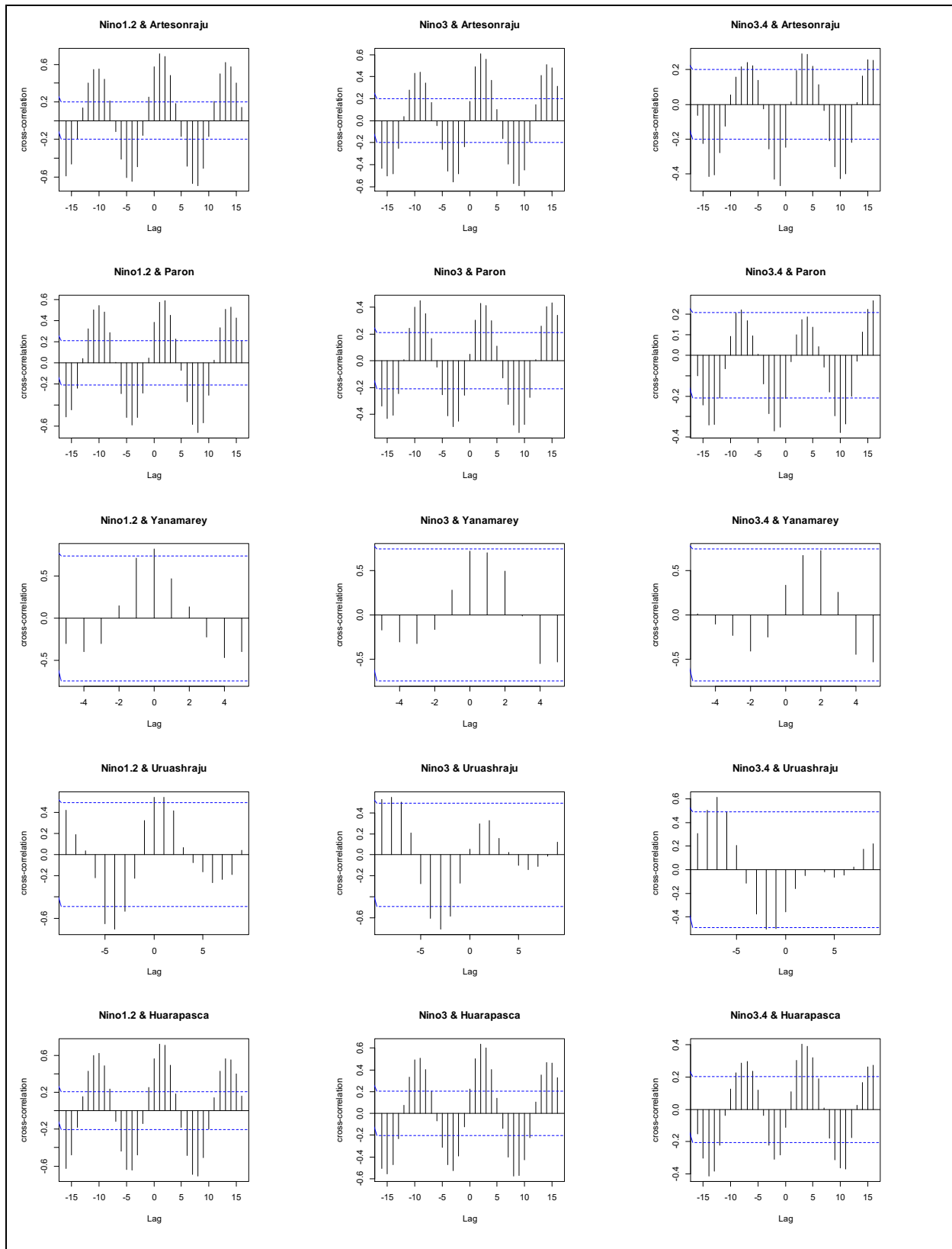


Figure 3.14. Lagged cross correlations of monthly SSTs of Niño 1,2,3 and 3.4 region with monthly precipitation

3.1.3.4 Precipitation Trends

Similar to the temperature series earlier, the Mann-Kendall test is also applied to the annual time series of precipitation, whereas monthly data is tested with the Seasonal Mann Kendall Test. The results are shown in **Table 3.4**. The ranking of the p -values for the different stations is presented separately for positive and negative S -values. The yellow color shows the stations for which the null hypothesis H_0 of no trend at the 95% significance ($p < 0.05$) is rejected in favor of the H_1 alternative hypothesis of trend. Due to gaps in the data of certain stations, some time series could not be analyzed.

For the annual precipitation at 6 out of the 42 stations the alternative hypothesis of trend is confirmed, wherefore 4 stations have a positive trend and 2 stations a negative trend. None of the stations located in the glaciers show a significant trend.

The analysis made with the SKM test for the monthly precipitation increases the number of station with trends to 14. Because of the SKM test is specialized in detect trends in seasonal time series, as is the case the precipitation, more trends are detected for the monthly time series. This may indicate that some trends are found in at least one or more seasons or months. Moreover, the monthly time series with negative trends (9) exceed those with positive trends (5).

These results show that there is not a typical pattern of precipitation trend in the area. However, the time series from stations, such as Querococha and Parón located in the same basins of Yanamarey and Artesonraju, respectively, show a negative trend. Furthermore, contrary to the temperature series, there are regions in the study area that exhibit steady reductions of precipitation rather than increments. Nevertheless, local regional precipitation characteristics may still change in few locations, resulting in upward trends there.

3.1.4 Relative humidity

The Cordillera Blanca's climate is influenced by the humid air that comes from the Amazon basin to the East, the dry air from the West, and by its proximity to the equatorial line. The statistics of the relative humidity data (see **Table 3.5**) shows that its mean at the glacier stations increases slightly from north to south. For instance, the mean relative humidity at the northern station of Artesonraju with 93.8% is lower than that at the southern glacier station, Huarapasca, with 97.92%. In certain cases, and in agreement with the thermodynamic laws of the atmosphere, the relative humidity may decrease with altitude, aspect that is reflected in this case.

The cross correlation coefficients of the relative humidity at the various stations show high correlation among those located above 4500 m.a.sl (see **Figure 3.15**), albeit, this correlation is reduced as the elevation differences increase. An exception to this is the data from station Querococha which shows high correlations with most of the other glacier stations, which is decreased to $r=0.4$ only for station Huarapasca. Indeed Huarapasca is the climate station whose records are the less correlated with those of the other stations.

3. Analysis of Climate Setting in the Tropical Glaciers of La Cordillera Blanca

Table 3.4. Annual mean precipitation trend using the Mann-Kendall test

SMK Test				MK Test			
Station	S	Kendall's Tau	P-value	Station	S	Kendall's Tau	P-value
Positive S⁽⁺⁾							
Cotaparaco	1422	0.271	2.51E-12	Quiruvilca	188	0.356	3.76E-03
Quiruvilca	1781	0.218	3.75E-07	Cotaparaco	159	0.283	1.92E-02
Milpo 2	851	0.211	1.52E-03	Milpo 2	103	0.317	2.46E-02
Cajatambo	584	0.119	1.81E-03	Julcan	151	0.254	3.32E-02
Julcan	687	0.096	5.18E-03	Huamacucho	129	0.230	5.78E-02
L.Ututo	115	0.117	5.31E-02	Huarapasca	14	0.500	1.08E-01
Caja/quilla	417	0.062	7.99E-02	Yanamarey	9	0.600	1.33E-01
Limacllan	17	0.225	1.13E-01	Caja/quilla	90	0.135	2.44E-01
Ocros	363	0.056	1.19E-01	Huaraz ELP	63	0.145	2.69E-01
Pomabamba	123	0.070	1.69E-01	L.Ututo	14	0.212	3.73E-01
Huamacucho	323	0.044	1.97E-01	Limacllan	4	0.400	4.62E-01
Mayorarca	121	0.056	2.45E-01	Mollepata	44	0.066	5.74E-01
Huarapasca	31	0.094	2.62E-01	Cajatambo	30	0.074	5.86E-01
Huaraz ELP	190	0.039	3.11E-01	Recuay	32	0.061	6.31E-01
Recuay	220	0.035	3.21E-01	Ocros	35	0.050	6.69E-01
Cullicocha	12	0.120	3.43E-01	Chiquian	32	0.051	6.73E-01
Mollepata	134	0.018	5.95E-01	HuarazUGRH	2	0.333	7.34E-01
Barrick	18	0.030	6.67E-01	Tambillo	2	0.333	7.34E-01
Chiquian	78	0.011	7.48E-01	Ayash	2	0.200	8.06E-01
Aguascocha	3	0.048	7.50E-01	Barrick	3	0.055	8.76E-01
Malvas	2	0.001	9.89E-01	Salpo	2	0.011	9.74E-01
HuarazUGRH	1627	0.020	4.60E-01				
Negative S⁽⁻⁾							
Andajes	-864	-0.121	4.69E-04	Chavin	-244	-0.366	1.48E-03
Conchucos	-132	-0.212	2.11E-03	QuerecochaELP	-187	-0.402	1.57E-03
Chavin	-807	-0.099	2.78E-03	Santiago	-32	-0.410	5.86E-02
Pira	-675	-0.100	4.35E-03	Conchucos	-21	-0.382	1.19E-01
QuerecochaELP	-1055	-0.182	4.88E-03	Milpo 1	-9	-0.600	1.33E-01
Milpo 1	-54	-0.258	8.26E-03	Yana	-9	-0.600	1.33E-01
Huaraz 02	-72	-0.192	1.73E-02	Artesonraju	-12	-0.429	1.74E-01
Santiago	-144	-0.129	2.59E-02	Pira	-81	-0.144	2.36E-01
Paron	-138	-0.117	3.94E-02	Paron	-21	-0.231	2.74E-01
Oyon	-353	-0.052	1.38E-01	Andajes	-76	-0.121	3.07E-01
Yana	-27	-0.136	1.73E-01	Oyon	-51	-0.086	4.78E-01
Tambillo	-107	-0.150	1.85E-01	Pomabamba	-19	-0.124	4.95E-01
LHuancanocha	-331	-0.043	1.98E-01	Mayorarca	-13	-0.076	6.75E-01
Ant Jupr	-18	-0.100	3.29E-01	Malvas	-19	-0.058	6.92E-01
Huacamarcanga	-253	-0.033	3.30E-01	Huaraz ELP	-3	-0.200	7.07E-01
Ayash	-15	0.108	3.39E-01	Ant Jupr	-3	-0.200	7.07E-01
Artesonraju	-24	-0.071	3.91E-01	Aguascocha	-2	-0.333	7.34E-01
Huallanca	-14	-0.049	5.81E-01	Cullicocha	-2	-0.333	7.34E-01
Salpo	-57	-0.025	5.90E-01	Huacamarcanga	-20	-0.032	7.96E-01
Yanamarey	-44	-0.059	6.00E-01	LagHuancanocha	-16	-0.025	8.38E-01
				Huallanca	-1	-0.048	1.00E+00

3. Analysis of Climate Setting in the Tropical Glaciers of La Cordillera Blanca

Table 3.5. Statistical of mean, median, standard deviation (SD), minimum (Min) and maximum (Max), and lower (1stQ) and upper (3rdQ) quartile and variance (VAR) of daily relative humidity

STATION	Elevation m.a.s.l	Complete analyzed years	Min.	1st Qu.	Median	Mean	3rd Qu.	Max.
Artesonraju	4811	2002-2007	21.2	92.4	100	93.8	100	100
Uruashraju	4693	2003-2007	26.5	95.3	100	94.88	100	100
Yanamarey	4698	2002-2007	38.3	95.3	99.6	95.9	100	100
Huarapasca	5150	2006-2007	40.7	100	100	97.92	100	100
Querocochoa	4012	1970-1998	33.4	84.1	96.9	90.56	100	100

The seasonal relative humidity follows essentially that of the precipitation, i.e. maximum relative humidity in the wet season and reductions in the dry season (see **Figure 3.16**). The most humid month is March and the driest month is July. More variations of daily humidity are found especially in January. However, at the highest weather station (Huarapasca), two minima of humidity are seen, namely, not only July, but also May.

The seasonality of the relative humidity follows more that of the precipitation than that of the temperature, shown earlier. On average, the relative humidity decreases by 25% in the dry months.

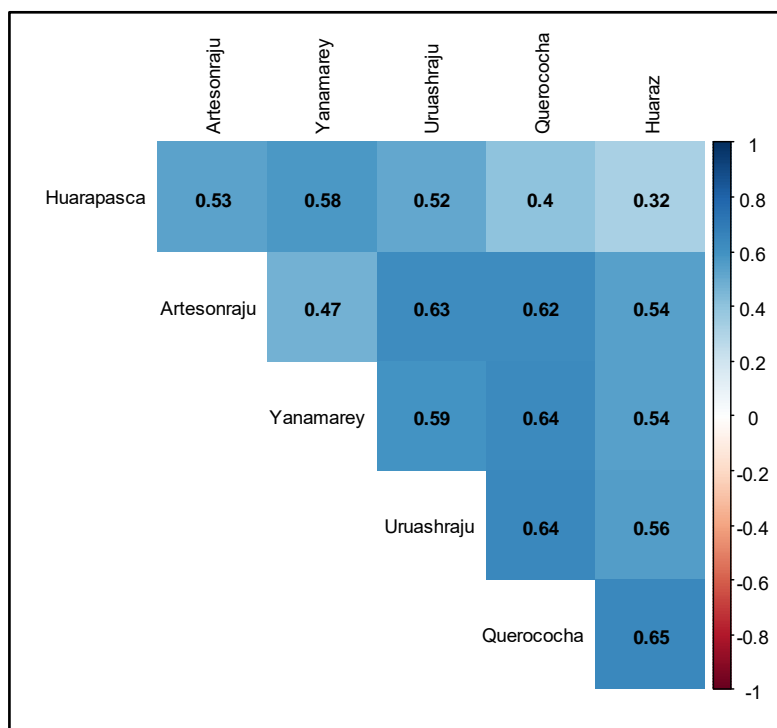


Figure 3.15. Cross-correlations of the time series of relative humidity

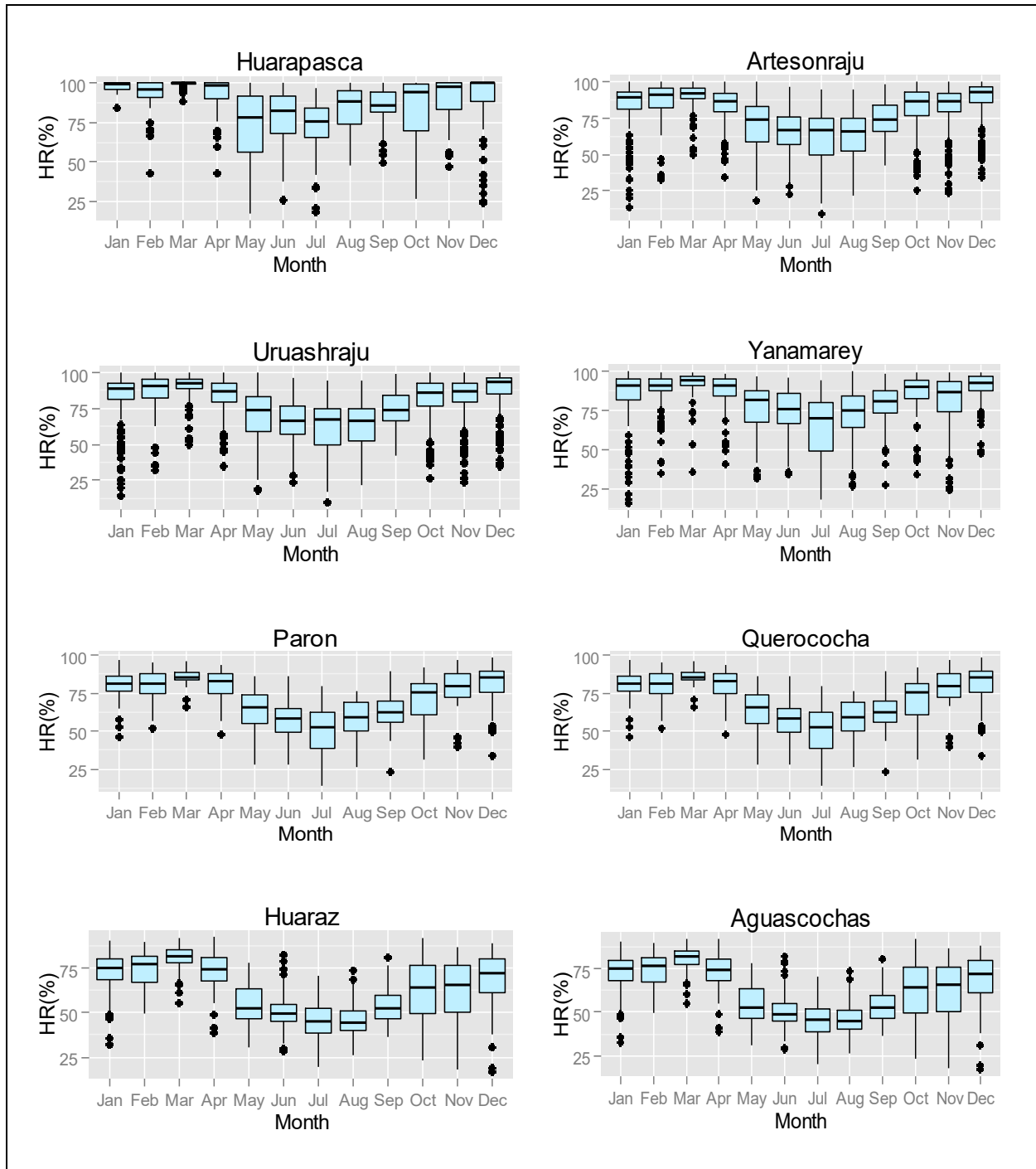


Figure 3.16. Seasonal pattern of relative humidity

3.1.5 Wind

The statistics of the wind data in **Table 3.6** shows that the wind increments with altitude for the climate stations located in the same basin; such is the case for Parón and Artesonraju. However, station Querococha located in another sub-basin exhibits a daily mean wind speed of 4.30 ms^{-1} , whereas station Barrick located at the east side of the Cordillera Blanca has a daily mean of only 2.59 ms^{-1} . This shows that the local geographical pattern have a large influence on the wind. Because the daily wind speeds time series differ in the periods they are available, only few

3. Analysis of Climate Setting in the Tropical Glaciers of La Cordillera Blanca

correlation coefficients could be estimated. These are listed in **Figure 3.17** and show relative low statistical associations among the wind speeds of the analyzed station data, namely, of $r=0.3$ between Artesonraju and Parón and Parón and Barrick.). Lower - but not unexpected - r - values are obtained between station Artesonraju and the others analyzed ones, as there is no clear connection among these stations.

For the other stations, the correlations are even less. Regarding the seasonal variability of the wind speed (see **Figure 3.18**), there are large differences for the stations located in the glacier and those located below 4000 m.a.s.l. Thus, in the glacier, large standard deviations are observed for months June and July. In addition, in August and September, there is an increment of wind speed at the weather stations located in the glaciers. Climate stations, like Aguascocha, Huaraz and Barrick, show clearly less variations of the wind speed. For the climate stations located between 4000 and 4200 m.a.s.l. (Parón and Querococha), variability and seasonality of the wind speed decrease, but are still noticeable.

Table 3.6. Statistics (mean, median, standard deviation (SD), minimum (Min) and maximum (Max), and lower (1stQ) and upper (3rdQ) quartile and variance (VAR)) of daily wind speed

STATION	Complete analyzed years	Elevation m.a.s.l	Min	1st Q.	Median	Mean	3rd Q.	Max.	SD	VAR
Artesonraju	2004-2007	4811	0.00	1.62	2.15	2.44	2.90	10.70	1.38	1.90
Paron	2003-2007	4195	0.08	0.96	1.35	1.62	1.88	10.00	1.09	1.20
Huaraz Electroperu	1983-1994	3200	0.00	0.60	0.80	0.83	1.10	6.80	0.36	0.13
Barrick	1997-2000	4164	0.00	2.09	2.37	2.43	2.76	6.47	0.57	0.33
Querococha	1970-1991	4050	0.00	3.70	4.75	5.25	5.30	7.70	2.31	5.32

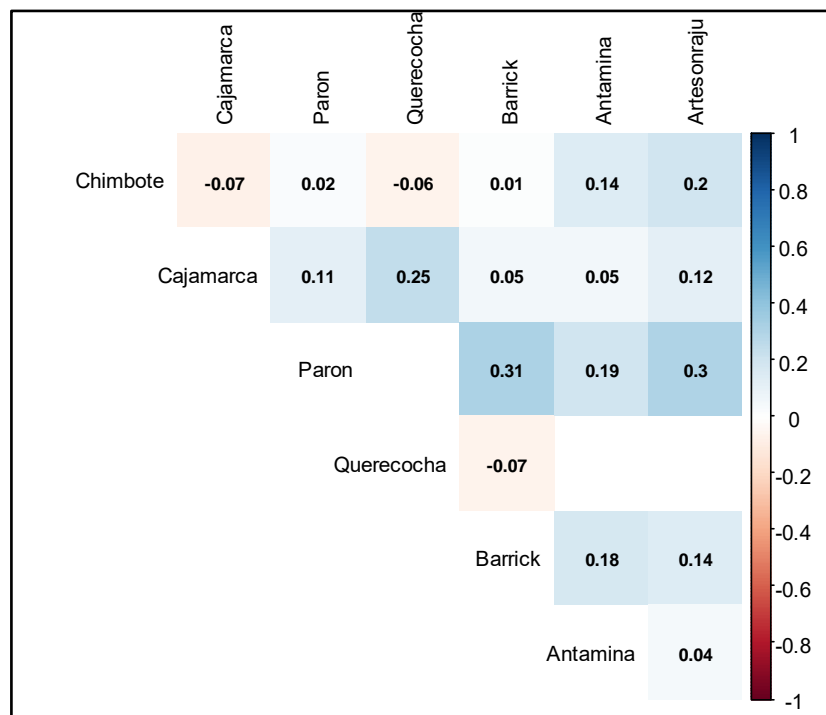


Figure 3.17. Correlation coefficients for daily wind speed

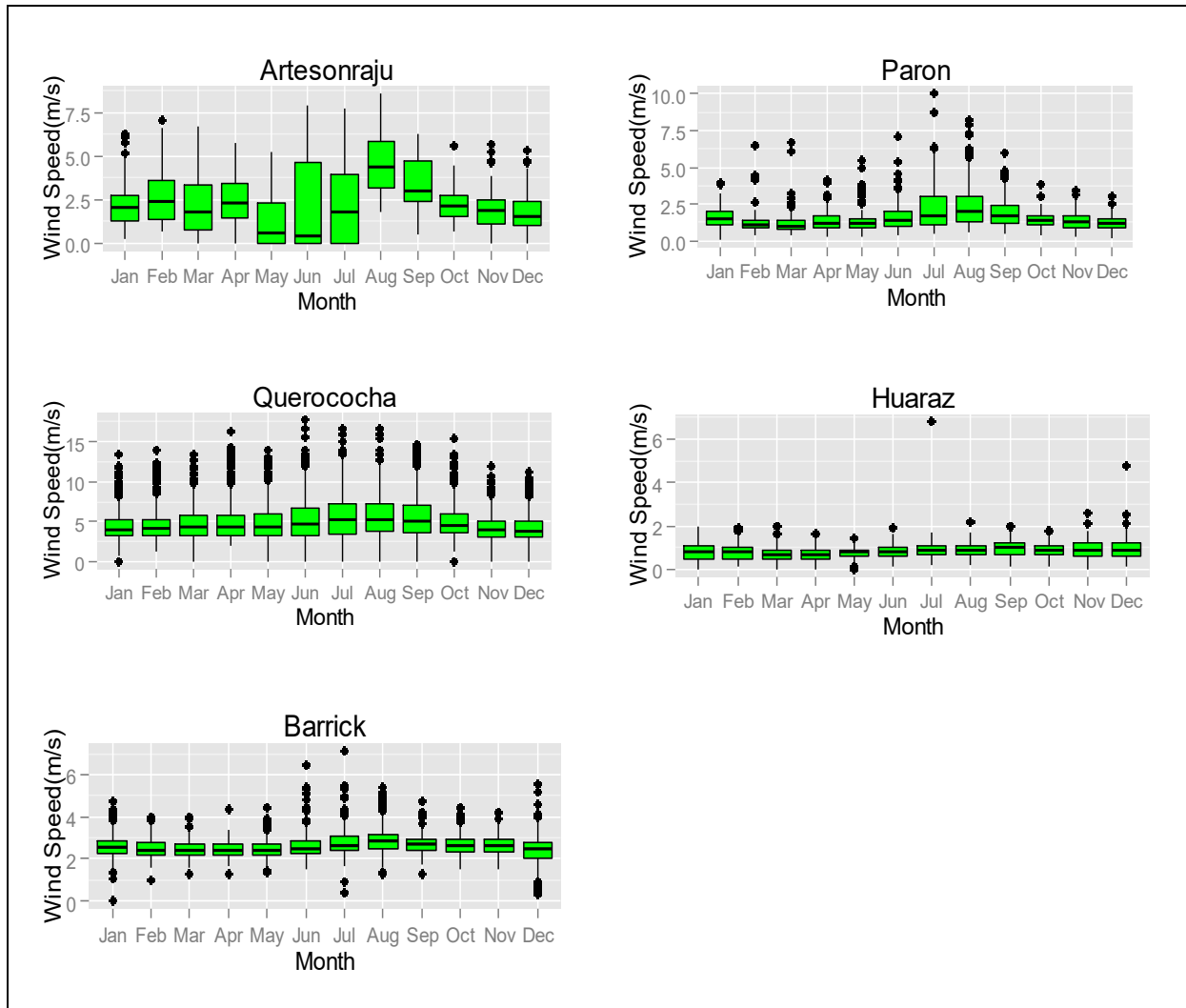


Figure 3.18. Seasonal pattern of daily wind speed

3.2 Concluding Remarks

Although the difficulties to find times series of data with long records and good quality, the present analysis found some relevant information that help to clarify the climate characteristic of La Cordillera Blanca focused in the glacierized areas. Some data gaps and short time series hinder the possibility to deep specifically in the knowledge of the glacierized areas and the correlation and trends of climatic variables.

The climate of cordillera Blanca is characterized by having two different seasons, marked more for seasonal precipitation and humidity. However, low variability in temperature is still detectable.

There is a homogeneous behavior of temperature at the horizontal plane, as it is shown by the high correlation of temperature especially in the high elevations. Precipitation shows different patterns influenced by local geographical characteristics of each catchment, which determine that precipitation becomes a more difficult parameter to predict.

Certain temperature stations with sufficient records show positive trends of temperature in the annual and monthly data. This is the cases of Santiago de Chuco and Huamachuco for annual temperature and Recuay and Querococha for monthly temperature, some minority of stations, however, show negative trends (Limaclan and Hidroeléctrica Duke).

In the case of precipitation, trends are more difficult to find although there are more climate stations, therefore the stations which have trends are relatively less than in the case of temperature. Positive trends appear in most of the cases; however, an important climate station for the glacier areas, like Querococha, shows a negative trend.

The ENSO phenomenon in la Cordillera Blanca has an impact not only in temperature but also in precipitation; however, the answer to the intensity anomalies is not always from the same character. Possible lags of ENSO influence in glaciers and local climate conditions could modify the expected proportional anomalies of temperature and precipitation in ENSO periods.

4 Analysis of Current Data of Mass Balances in the Glaciers in La Cordillera Blanca

This chapter has the purpose to introduce some concepts related to mass balance in glaciers and present the available data related to measurements in three glaciers in the Cordillera Blanca.

4.1 General Concepts and Notations

Mass balance refers to the gains and losses of snow/firn/ ice which determines the size of the glacier. The cumulative difference between accumulation and ablation can be interpreted as a mass budget (**Figure 4.1**). This budget can be estimated in the whole glacier, in particular areas of the glacier or in specific points, the last refers to the specific balance. Thus, specific balance represents a change of mass per unit area, or also is usually presented as a thickness per unit time usually reported as water equivalent rates.

Accumulation and ablation are caused by masses exchanges by processes such as snowfalls, avalanching, melt, sublimation and calving.

4.1.1 Accumulation

The accumulation includes all the processes in which snow and ice are added to the glacier surface, net accumulation is the positive results of the accumulation minus ablation. The inputs to a glacier are:

- Snowfall which is the main input to the tropical glaciers. Snowfall is mainly determined by temperature and the vapor content.

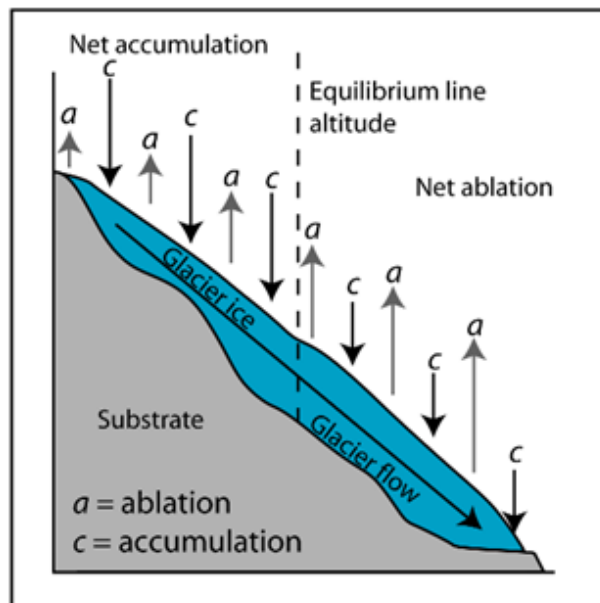


Figure 4.1. Accumulation and ablation scheme

(Figure taken from <http://www.antarcticglaciers.org/glacier-processes/introduction-glacier-mass-balance/>)

- Redistribution by wind, which refers to the snow transported by wind in the glacier surface. Interactions between topography and wind can persist creating induced accumulations by wind scour.
- Avalanching which is a sudden flow of a large mass of snow or ice down the snow sometimes up to the speed of 160 km hour⁻¹. Avalanches occurs more frequent in slopes exceeding 30 degrees (Min Raj Lamsal, 2012)
- Refreezing of melt water, which forms an ice layer in the firm.
- Deposition occurring when a substance goes directly from the gas state to the solid state. Like sublimation, the intermediate liquid phase is skipped over and in contrast to sublimation, the process of deposition or re-sublimation releases energy. It occurs by low temperatures and saturated atmosphere in a process call re-sublimation or deposition. An example of deposition is the formation of frost. In cold temperatures, water vapor undergoes deposition to form a thin layer of solid ice on the surface.

4.1.2 Ablation

The loss of mass in a glacier surface is mostly by melting and sublimation processes:

- Melting is the most important mechanism of mass losses on land-based glaciers. Melt water that re-freezes onto another part of the glacier is not referred to as ablation.
- Sublimation occurs at all temperatures and dominates ablation in very cold environment where the surface temperature does not reach the melting point. Dry air and strong wind increase the sublimation. This state change of water from solid to vapor is important, for instance, at high altitudes in low latitudes (tropical glaciers), in dry climates, and on blue-ice zones in Antarctica. (Hock, 2010a)
- Calving occurs when the glacier nourishes an ice shelf, ice discharge across the grounding line): Calving is iceberg discharge into seas or lakes; important, for example, in Greenland and Antarctica (Hock, 2010a) and in the Andes of the Patagonia (Chevallier, personal communication, October 31th 2019).
- Avalanching can also cause not only accumulation, but also ablation in the same process.

4.1.3 Surface mass balance

Mass balance determines either if a glacier to expand or to recede and how it flows. Changes in thickness and slope cause a glacier to retreat or to advance (Cuffey and Paterson, 2010). For instance, a surplus in mass balance will thicken and steeper the glacier, this act in the gravitational flow while a deficit will cause rapid melting of snow leaving the firm and the ice areas exposed to more radiation as they have less albedo.

The (cumulative) mass balance, b , is the sum of accumulation, c , and ablation, a (the ablation is defined here as negative). The symbol, b (for point balances) and B (for glacier wide balances) has traditionally been used in studies of surface mass balance of valley glaciers (Hock, 2010a). The surface mass balance is denoted by the following equations:

$$b = c + a = \int_{t_1}^t c + a dt \quad (4.1)$$

and

$$B = \int b \, dA \quad (4.2)$$

where

b is the specific mass balance (w.e)

c is the accumulation (w.e)

a is the ablation and (w.e)

B is the mass balance in the whole area (we)

4.1.4 Equilibrium Line Altitude (ELA)

The ELA separates the accumulation zone from the ablation zone. The elevation on the surface of the glacier where the climatic mass balance is zero at a given moment, defines the equilibrium line ELA. It coincides with the snowline only if all mass exchange occurs at the surface of the glacier and there is no superimposed ice.

Mass balance terms are usually stated as mass of snow, ice or firn, converted to water volume and afterwards to water equivalent (w.e.) which allows doing comparisons between different glaciers and different years. Water equivalent represents the volume of water that would be obtained from melting the snow or ice. The value in water equivalent is obtained through dividing the volume by the area, i.e. the mass balance value states how much the glacier has become thicker (accumulation) or thinner (ablation) (in water depth) if the mass addition or loss is distributed over the whole glacier surface (Hock, 2010a). Although accumulation and ablation are usually seasonally varying (see below), so that the mass balance undergoes an annual cycle of growth (positive mass balance) and diminishment (negative mass balance), it is common in glacier studies to compute the mass balance over one year (annual mass balance).

4.2 Seasonal Variations of Mass Balance

In tropical glaciers, there is mainly seasonality in the accumulation, however, ablation occurs during the whole year, as the seasonality of temperature is low. Unlike for mid-latitude glaciers, accumulation and ablation in tropical glaciers occur simultaneously in the rainy season. The annual mass balance b_{ann} can then be described as the sum of the wet season balance (b_{ws}) and the dry season (or season with lower precipitation) balance which number of seasons vary depending on the location within the tropics (b_{ds}).

The mass balance in tropical glaciers depends on two regimes linked to the prevailing climatic characteristics there. Both of them are characterized by the ablation process which lasts the whole year. However, the accumulation period can vary, according to whether the glacier is located in the inner tropics¹¹ or outer tropics¹². The inner tropic area is distinguished for having a permanently humid climate with relatively continuing precipitation throughout the year, though with two periods of intensity increments over a year during which accumulation of the glacier occurs.

¹¹ Northern tropical glaciers located in Colombia, Venezuela and Ecuador.

¹² Southern tropical glaciers located in Perú and Bolivia.

The outer tropics, in contrast, in which the glaciers of the Cordillera Blanca are located, are characterized by just one wet period (around September-March) in which tropical conditions are dominant, and a dry period (around April-August), in which subtropical conditions prevail. The accumulation in these glaciers is produced mainly during the wet period (Kaser and Osmaston, 2002).

4.3 Measurements of Glaciers Mass Balance

There are several techniques of the estimation of mass balance of glaciers which can be categorized either as indirect (estimation or measurements of the various mass exchanges or fluxes to and from the glacier, as in the process or hydrological methods) or direct, as is the widely used glaciological method which consists in the objective measurement of ablation and accumulation on the glacier's surface by a net of stakes and snow pits, respectively (e.g. Cuffey and Paterson, 2010). For a good representation of the glacier's total budget, the measurement net should be sufficiently dense and cover a wide horizontal and vertical range of the glacier's surface.

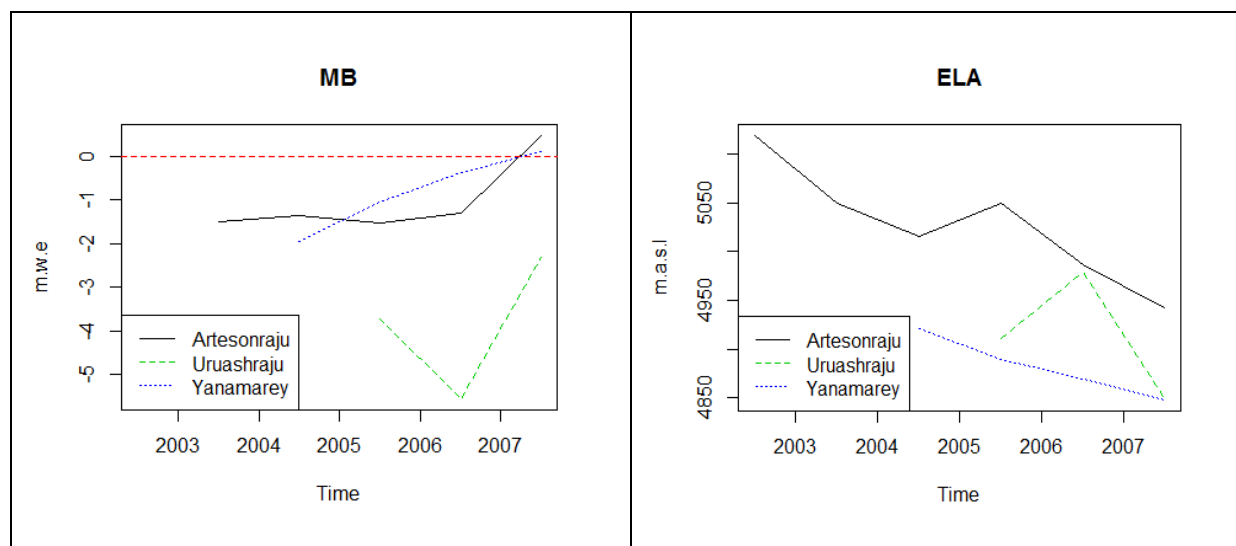
Such a net was installed in the CB glaciers Artesonraju, Yanamarey, Uruashraju and Shallap by the French Institute of Research Development- IRD (Gallaire *et al.*, 2007) and measurements of the ablation- and the accumulation heights were made in the time period 2002-2008. These were converted to m.w.e. (meters of water equivalent) using the density of the snow or ice, according to what was measured. For the case of the Artesonraju glacier it was observed that the stakes cover the total elevation range in the ablation area (see **Figure 2.6**), while the pits were restricted to 5200 m.a.s.l. in the accumulation zone, due to difficulties in finding differences of layers from the previous years.

Measuring the losses and gains of the glacier's mass balance has faced many difficulties in the Cordillera Blanca. Steep slopes, thin glaciers, heavily fissured and fed from steep sides and avalanches make measurements generally difficult and some areas even inaccessible. Also, isothermal conditions in the snow cover and the firn body aggravate the determination of the stratigraphy of the snow package in the accumulation zone (Kaser and Georges, 1999). In addition, the net to measure mass balance is relatively young and data is not public.

With the measurements of m.w.e. in each elevation range, linear regression allows to find the intercept where sum of accumulation and ablation is 0 m.w.e, i.e. the ELA (Equilibrium Line Altitude). This linear regression is used to find the ablation/accumulation in m.w.e in each band. This ablation/accumulation is multiplied for the relative weight of the area of the band and summed over the whole glacier to give the total amount of loss/gain of the glacier area. As mentioned, this procedure of determining the mass balance of a glacier is called the glaciological method. The results of the m.w.e. estimations for each observation period and the ensuing ELAs are presented in **Table 4.1** and **Figure 4.2** for each year of the 2002-2008 observation period.

Table 4.1. 2002-2008 annual mass balances (MB) and ELAs in Artesonraju, Yanamarey and Uruashraju glaciers (data taken by Gallaire *et al.*, 2007 and WGMS, 2015)

Years	Artesonraju		Yanamarey		Uruashraju	
	MB (m.w.e.)	ELA (m.a.s.l.)	MB (m.w.e.)	ELA (m.a.s.l.)	MB (m.w.e.)	ELA (m.a.s.l.)
2002-2003					-5.633	5011.9
2003-2004	-1.48	5048.5			-5.472	4964.8
2004-2005	-1.55	5014.6	-1.96	4921	-5.711	4923.9
2005-2006	-1.67	5049.9	-1.05	4889	-3.728	4911
2006-2007	-1.52	4986.3	-0.38	4870	-5.560	4979
2007-2008	0.47	4943.2	0.09	4848	-2.354	4850

**Figure 4.2.** Annual mass balance profiles MB (left panel) and ELA (right panel) of the glaciers Artesonraju, Uruashraju and Yanamarey from 2003-2007

The short records of the mass balances show mostly negative values for the three glaciers. However, a small recovery of the m.w.e. is observed for Yanamarey and Artesonraju glaciers which reach equilibrium in the hydrological year 2007-2008, a year in which a La Niña phenomenon occurred. However, for the Uruashraju glacier, the specific balance of the mass remains negative for the whole observation period. In addition, a minimum of mass balance is observed in the years 2006-2007 for Artesonraju and Uruashraju, though not for Yanamarey. On the other hand, the ELAs are consistent with what happens with the mass balance, i.e. at higher mass losses the ELAs increase, but decrease when the former are reduced (see **Figure 4.2**).

Although the observation period analyzed above is very short to reliably analyze mass trends in these glaciers, they appear to be consistent with estimates of the retreat of the glaciers' tongues from satellite images, as presented by local authorities (Autoridad Nacional del Agua, 2014). More specifically, comparing the glacier surface recorded in the national inventory of the 1970s with that of 2014, one finds that the Cordillera Blanca has lost approximately 27% (195.75 km²) of its total glacier area over the last 40 years.

4.4 Concluding Remarks

Few are the studies with measurements of mass balance in tropical glaciers of CB, so that much discussion about the physical dynamics of these glaciers in the Andean Mountains is still on the table. Lack of field measurements and, especially, the difficulty of determining the firn layer in the accumulation zone, makes it difficult to understand properly the whole complexity of the physics of the mass balances in the glaciers of the Cordillera Blanca.

Despite the lack of long records of mass balance measurements and estimations in the glaciers of Cordillera Blanca, the limited data indicates a common loss of glacier mass (m.w.e) in consecutive years for three glaciers, wherefore the condition improved somewhat in the La Niña year 2007-2008.

5 Review and Analysis of Measured Energy Fluxes Data in the Artesonraju Glacier

This chapter has the purpose to introduce the topic of energy fluxes of the earth atmosphere system and give an overview and a statistical analysis of the field data of energy fluxes measured at one site of the tongue of the glacier Artesonraju.

5.1 General Concepts and Notations

The cycle of solar energy is one the fundamental in the atmosphere. The energy balance on the earth-sun system is explained by an equilibrated interchange of radiative fluxes that allows maintaining the life in earth. The atmosphere is a key factor to sustain the equilibrium between the incoming solar radiation and the emitted infrared radiation of the earth.

The main source of the earth energy is the solar radiation. The sun has an effective temperature of about 6000K (Cuffey and Paterson, 2010). The solar radiation covers the whole electromagnetic spectrum from gamma waves to the radio waves, however the major radiation is in the ultraviolet visible and infrared, the last three with wavelength of (0.4-0.7 μm). The visible range correspond to 40% of the incoming energy, while 10% correspond to ultraviolet (0.2-0.4 μm) and 50% to the infrared near to (>0.7 μm) (Qiang, 2003).

The Earth which is the other points of the energy system earth atmosphere has an effective temperature slightly less than 300 K. The earth absorbs approximately half of the incoming energy at the top of the atmosphere (radiation at the top atmosphere 340.4 Wm^{-2} , radiation absorbed 163.4) and emits energy in long wave radiation (>3 μm) in the infrared. Most of this energy is absorbed for the water vapor and the carbon dioxide and the ozone in the atmosphere and the rest approximately 10% scape to the space through the atmospheric window in the infrared (8 – 10 μm) called like this for its high transparency of the atmosphere (Oke, 1987) to this range of wavelengths (see **Figure 5.1**).

Figure 5.1 shows the absorptivity of the atmosphere in its constituents gases. A different capacity of the atmosphere to absorb shortwave and long wave radiation is observed. Approximately, 18% of the energy is absorbed for water vapor and ozone. The water vapor absorbs many spectrum bands between 0.9 μm and 2.1 μm while the ozone absorption is concentrated in three spectral bands 0.2 – 0.31 μm , 0.31 – 0.35 μm and 0.45 – 0.85 μm . The radiation of waves less than 0.285 rarely reach the atmosphere under 20 km. Wave lengths between 0.4 and 0.6 μm in the visible spectrum have less absorptivity for the water vapor, the carbon dioxide and the ozone. However, ozone is very good filtering wavelength inferior to 0.3 μm and water vapor at wave lengths between 0.8 and 3 μm . For longwave radiation the absorptivity increased by the three gases water vapor, carbon dioxide and ozone, except for the narrow band between 8 and 10 μm , where the atmosphere becomes more transparent. This gap is called the atmospheric window (Oke, 1987).

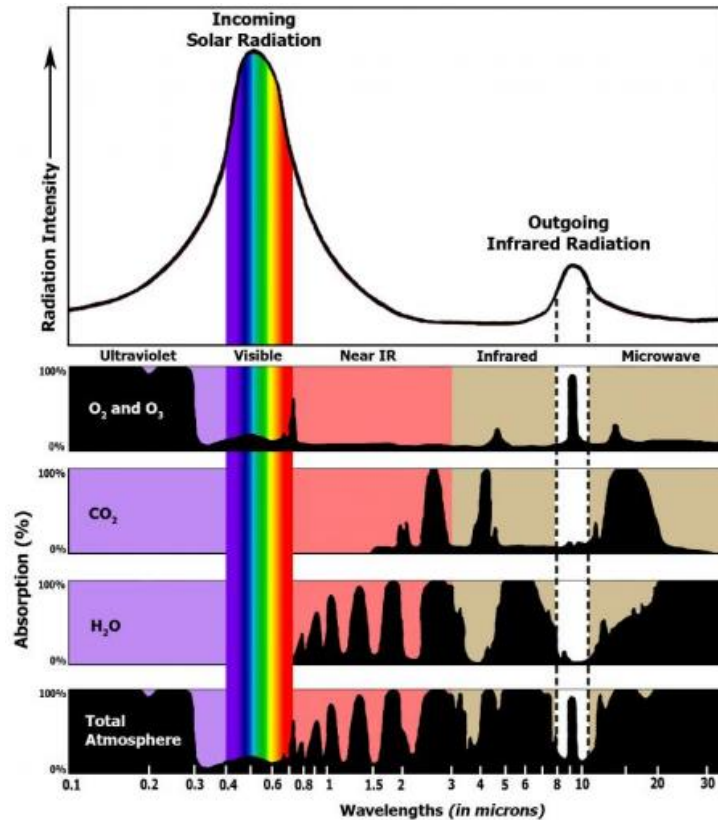


Figure 5.1. Absorption capacity of the gases in the atmosphere for shortwaves and longwaves (taken from <http://www.ces.fau.edu/nasa/module-2/how-greenhouse-effect-works.php>)

The solar energy flux radiation is given by the solar constant 1367 Wm^{-2} (Hartmann, 1994). The solar constant is defined as the sun irradiance outside the atmosphere on a perpendicular surface to the rays for the mean distance between the sun and the earth. However, at the top of the atmosphere mean sun energy flux incident is approximately 340.4 Wm^{-2} .

When this energy enter to the atmosphere certain amount scatters back to space /reflection to the space) (see **Figure 5.2**) and some other is absorbed by clouds, water vapor and particles (atmosphere absorption) and the final one is transmitted to the earth. The shortwave radiation that reaches the surface can be direct and diffuse. As its name indicates the direct radiation is the one that come from the sun without suffering any process of atmospheric dispersion. The diffuse radiation is the energy that has been dispersed in the atmosphere. In clear sky condition the diffuse radiation can reach between 10 to 20% (Hock, 2010b). However, the presence of clouds is a very sensible factor that can increase considerable the proportion of diffuse radiation.

From the incident solar radiation at the top of the atmosphere around 20 % is absorbed by the atmosphere and clouds and contributes to warm the atmosphere. The retrodispersion and reflection outside the space due to clouds conditions accounts for 30%. Therefore around 50% of the solar radiation reaches the earth surface where according to the surface conditions around (8%) of the solar energy is also reflected. From the 50% and average of 30% comes from direct radiation and 20% from diffuse radiation.

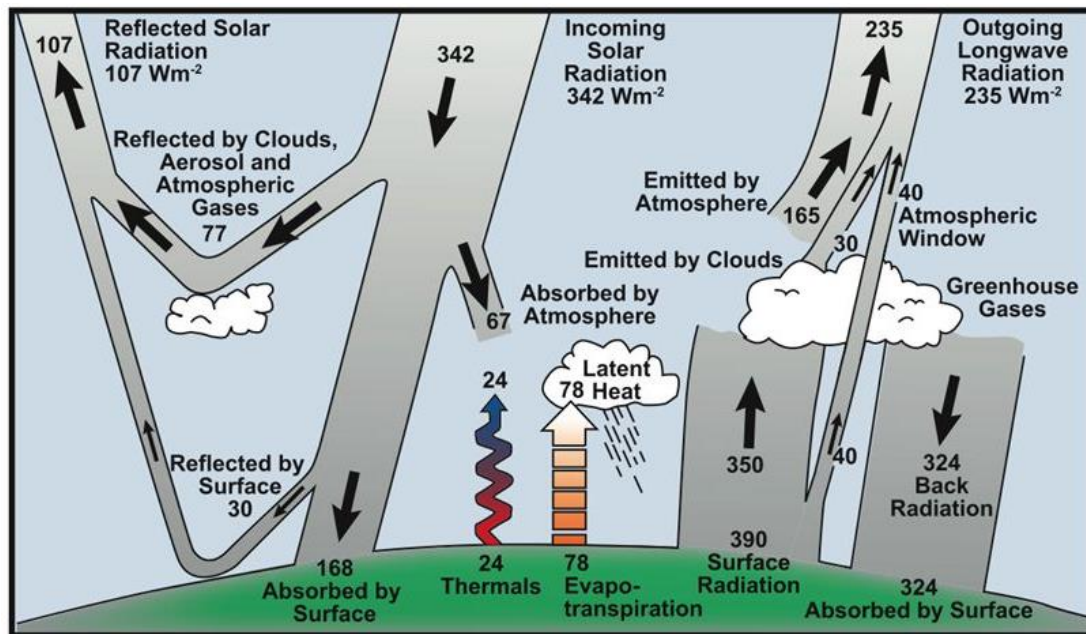


Figure 5.2. Energy budget in the Earth and Atmosphere System, Kiehl and Trenberth (1997)

The emitted radiation of earth of longwave has a yearly mean of 390 Wm^{-2} , around 114% of the solar radiation. The atmosphere blocks partially the loss of the longwave emitted radiation allowing warming the atmosphere, this effect is the so called greenhouse effect. Another important characteristic of this longwave emission is that it is emitted in the entire earth surface although the shortwave radiation is receiving in the sunlit hemisphere (Oke, 1987). On a mean annual basis around 57%¹³ of the longwave radiation emitted by the atmosphere and the clouds leave to the space, and additionally around 12% leaves to the space through the atmospheric window. Exits a net downward emission of longwave radiation by the atmosphere is estimated in 95% and contributes to the warming of the earth surface (see **Figure 5.2**).

The atmosphere absorb longwave radiation according to amount of the gases present in the atmosphere and reemitt longwave radiation according to the temperature and the emissivity. This emitted radiation has not and specific direction it can be downward or upwards. The process of absorption and emission can be more important in the lower layers of the atmosphere where are major concentrations of water vapor and carbon dioxide (Oke, 1987).

Turbulent convection carries some of the heat absorbed by the ground to the atmosphere in this system, closing the energy balance (Fuchs, 2005). Convection transports both sensible and latent heat in the atmosphere on in certain cases from the atmosphere to the surface, this depends on the difference of temperature and humidity between de surface and the lower boundary layer. If the overlayer of the surface is cooler than the surface the sensible heat is release from the surface upon mixing with the air and the water vapor is liberated when the surface is more saturated as the air. However, in certain cases the atmosphere can be warmer as the surface, such as in cases where snow or ice are present. In such cases, the transfers of heat occur from the

¹³ Relative to shortwave incoming radiation at the top of the atmosphere.

atmosphere to the surface. In addition, when the atmosphere is saturated of water vapor and the temperature is low, condensation or deposition on the surface can occur (Cuffey and Paterson, 2010)

From **Figure 5.2** showing the mean values of radiation fluxes on the earth, it can be noticed that the energy balance fluxes act in three separated layers of the atmosphere: its top, the atmosphere itself and the bottom, i.e. the earth's surface. The focus of this research is the balance on the earth surface it means the balance between the energy entering the earth surface and the energy leaving the earth surface. The short wave energy absorbed for the earth (168 Wm^{-2}) plus the back radiation of longwave radiation (324 Wm^{-2}) is balanced by the long wave radiation emitted (390 Wm^{-2}) by the surface plus the sensible (24 Wm^{-2}) heat and the latent heat (78 Wm^{-2}).

The general equation of the energy balance at the earth's surface is:

$$Q_{surf} = Q_N + Q_H + Q_L \quad (5.1)$$

where

$$Q_N = Sw_{inc}^{\downarrow} + Sw_{ref}^{\uparrow} + Lw_{inc}^{\downarrow} + Lw_{sufc}^{\uparrow} \quad (5.2)$$

with

- Q_{surf} energy absorbed by the surface (Wm^{-2})
- Q_N net radiation (Wm^{-2})
- Q_H flux of sensible heat (Wm^{-2})
- Q_L flux of latent heat (Wm^{-2})
- Sw_{inc}^{\downarrow} shortwave incoming radiation (Wm^{-2})
- Sw_{ref}^{\uparrow} shortwave reflected radiation (Wm^{-2})
- Lw_{inc}^{\downarrow} longwave incoming or back radiation (Wm^{-2})
- Lw_{sufc}^{\uparrow} longwave radiation emitted by the earth surface (Wm^{-2})

A brief description of each term of Eq 5.1 and the variables that intervene for calculating each flux needed is presented as follows based in Cuffey and Paterson (2010). However, a more thorough explanation of the parameterization of each flux for the application of the distributed energy balance model, will be presented in subchapter 7.2.2.

Shortwave radiation incoming (Sw_{inc}^{\downarrow}) As it was introduced previously, shortwave radiation incoming is the total solar flux which reaches the ground, also called insolation or global radiation, is constituted by: direct solar beam, the diffuse light due to scattering in the atmosphere and the reflected light from surrounding areas. The term for a horizontal surface is:

$$Sw_{inc}^{\downarrow} = I_o \cos Z \quad (5.3)$$

with

- I_o solar flux at the top of atmosphere, about 1367 Wm^{-2} but zero at night.
- Z zenith angle, the angular distance of the sun below a vertical line.

ψ effective transmissivity expresses how much of the possible total solar radiation strikes surface. The effective transmissivity depends on cloud cover, altitude and haze.

Shortwave radiation reflected: Reflected shortwave radiation can be presented as a fraction of the downward flux which reflected by the surface.

$$SW_{ref}^{\uparrow} = \alpha_s * SW_{inc}^{\downarrow} \quad (5.4)$$

with

SW_{ref}^{\uparrow} reflected shortwave radiation (Wm^{-2})

α_s albedo of the earth surface

Longwave radiation emitted by the surface: Using the law of Stefan-Boltzmann, the emission of longwave radiation from the earth surface will be:

$$LW_{sufc}^{\uparrow} = \epsilon_s \sigma T_s^4 \quad (5.5)$$

with

ϵ_s emissivity of the surface

σ Stefan Boltzmann constant ($5.67 \times 10^{-8} Wm^{-2}K^{-4}$)

T_s surface temperature ($^{\circ}K$)

Longwave radiation incoming or back from the atmosphere: The longwave radiation incoming is constituted by the emissions from clouds, atmospheric water vapor, carbon dioxide, ozone, methane and in general from greenhouse gases. The flux depends on the amount and temperature of these constituents at different heights

The emission are represented as well for the Stefan Boltzmann emission law for grey bodies, thus for the case of downward longwave radiation, the emissivity of the atmosphere differs from one, because the greenhouse gases absorb and emit less energy than a black body, and only for certain wavelengths bands.

$$LW_{inc}^{\downarrow} = \epsilon_a \sigma T_a^4 \quad (5.6)$$

with

ϵ_a emissivity of atmosphere

T_a air temperature ($^{\circ}K$)

The emissivity can vary from 0.95 with completely cloudy skies (Konzelmann *et al.*, 1994), for clear skies with dry air values can be less than 0.5. A rough estimation of the determining factors of the atmosphere that influence in the downward longwave flux is described by Cuffey and

Paterson (2010): warm, humid conditions increase, heating the surface in periods of low cloud cover. Cold and dry conditions reduce and allow the surface to cool.

Turbulent fluxes of sensible heat and latent heat: The sensible heat transfer between the atmosphere and the glacier surface can be described by the Bulk Aerodynamic approach as:

$$Q_H = \rho_a c_a C_H u [T_a - T_s] \quad (5.7)$$

with

Q_H sensible heat flux (Wm^{-2})

ρ_a density of air (Kgm^{-3})

c_a specific heat capacity of air at constant pressure ($Jkg^{-1}K^{-1}$)

C_H bulk exchange parameter for heat

u wind speed a few meters above the surface (ms^{-1})

T_a temperature of the lower boundary layer ($^{\circ}K$)

T_s surface temperature ($^{\circ}K$)

$$Q_L = \rho_a L_{V/S} C_E u [q_a - q_s] \quad (5.8)$$

with

Q_L latent heat flux (Wm^{-2})

ρ_a density of air (Kgm^{-3})

$L_{V/S}$ latent heat of sublimation or evaporation (Jkg^{-1})

C_E bulk exchange parameter for moisture

u wind speed a few meters above the surface (ms^{-1})

q_a absolute humidity boundary layer ($kg m^{-3}$)

q_s absolute humidity of the surface ($kg m^{-3}$)

5.2 Field Data of Energy Fluxes at the Artesonraju Glacier

The data of energy fluxes was provided by the UGRH to the University of Kassel. The climate station is jointly managed by the UGRH and the IRD. The climate station is located in the $8^{\circ} 58' 77'' S$, $77^{\circ} 38' 67'' W$ (WGS84), in the altitude of 4838 m.a.s.l. The resolution of the data is available every 30 min. The data was first reviewed and arranged in daily records, as the precipitation, wind and humidity were available at this temporal resolution.

Some of the first corrections made to the data concerned the physical characteristics of each flux and the range of radiation fluxes. These ranges are listed in the manual of the EBM (Hock and Tijm-Reijmer, 2012). The corrections made are as follows:

- Negative values of shortwave radiation, during the night period, were replaced by 0.
- Exclusion of inconsistent values of shortwave reflected.

- Values of shortwave incoming and reflected radiation superior to 1500 Wm^{-2} were disregarded.
- Values of longwave incoming radiation superior to 900 Wm^{-2} and inferior to 50 Wm^{-2} were disregarded.
- Values of longwave emitted at the atmosphere superior to 320 Wm^{-2} and inferior to 50 Wm^{-2} were disregarded.
- Values of net radiation superior to 1000 Wm^{-2} and inferior to 400 Wm^{-2} were disregarded.

5.3 Daily Measured Energy Fluxes

The statistics of daily energy fluxes are presented in **Table 5.1**; in addition, a normality test was applied to the measured variables, with the results of this test shown in **Table 5.2**

The statistic of daily radiation fluxes are quite consistent with the behaviour of energy balance of the earth atmosphere systems described in the subchapter 5.1. The incoming shortwave radiation with a mean of 234 Wm^{-2} is slightly superior as the mean shortwave radiation of the earth. This can be consistent considering that the location of the glacier is in the tropics. The mean reflected shortwave radiation of 95.64 Wm^{-2} is inferior to shortwave incoming radiation and shows a mean reflection of 60%, this is relatively high in relation to the mean earth reflection, however, it is important to consider that the surface of the glacier is composed of ice, firn and snow, materials which has a relative high albedo between 0.4 and 0.9.

Table 5.1. Statistical of mean, median, standard deviation (SD), minimum (Min) and maximum (Max), and lower (1stQ) and upper (3rdQ) quartile and variance (VAR) of daily energy fluxes at Artesonraju glacier between 2004-2007

Radiative Fluxes (Wm^{-2})	Min	1st Q	Median	Mean	3rd Q	Max	SD	VAR
Sw_{inc}	110	182.40	227.50	234.60	282.60	408.80	65.76	4325
Sw_{ref}	6.97	60.56	91.01	95.64	126.50	248.14	48.23	2327
Lw_{inc}	194.3	254.20	290.70	280.60	311.10	369.40	36.36	1322
Lw_{surf}	287.7	303.90	309.70	308.50	313.50	320.00	6.80	46.3
Q_N	-38.8	44.26	80.68	87.87	123.02	266.38	56.51	3193

Table 5.2. Results of normality tests on time series of daily energy fluxes

Radiative Fluxes	SHAPIRO TEST (Shapiro and Wilk, 1965)		KOLMOGOROV TEST (Wayne, 1990)	
	W	p -value	D	p -value
Sw_{inc}	0.98	1.88E-09	0.05	5.40E-08
Sw_{ref}	0.98	2.77E-12	0.05	1.23E-07
Lw_{inc}	0.69	2.2E-16	0.22	2.2E-16
Lw_{surf}	0.97	2.76E-14	0.07	1.82E-15
Q_N	0.97	3.37E-13	0.06	4.20E-11

The mean of longwave incoming radiation is under the longwave emitted by the surface, as it observed in the energy balance of earth-atmosphere. The net radiation has positive mean of 87.87 Wm^{-2} , however, the existence of negative values of net radiation are also observed. The latter suggest for certain cases, either increments in the outgoing radiation, through high values of albedo and/or very low surface temperatures, or the increments in the incoming radiation. Considering that the analysis is made in snow or ice surface areas the first situation is more likely.

The normality tests applied to the data, Shapiro (Shapiro and Wilk, 1965) and Kolmogorov (Wayne, 1990) indicate through p -values ≤ 0.05 , that none of the time series follow a normal distribution (hypothesis H_0 is rejected, as the probability that data oblige H_0 is only p , i.e. very low), therefore, the data are considered non-parametric for further analysis.

5.3.1 Shortwave incoming radiation

The daily mean shortwave incoming radiation varies between 110 Wm^{-2} and 408 Wm^{-2} . The mean of the daily shortwave incoming flux is 234.6 Wm^{-2} . The descriptive statistical parameters of this variable are presented in **Table 5.1**. From this statistical description, it is observed that the shortwave radiation incoming present higher standard deviation (65.76 Wm^{-2}) as the longwave radiation emitted by the surface (6.8 Wm^{-2}) and emitted by the atmosphere (36.36 Wm^{-2}).

The daily means of the shortwave fluxes measured at the glacier are presented in **Figure 5.3**. It can be seen from the figure that there is a slight seasonality, with increased shortwave incoming radiation in the middle of each year, especially, for years 2004 and 2006, unfortunately, there are long gaps in the middle of the year 2007 and 2008. Shortwave incoming radiation does not follow a normal distribution.

5.3.2 Shortwave reflected radiation

The mean daily shortwave reflected flux is 94.64 Wm^{-2} , the minimum value is 6.97 Wm^{-2} and the maximum value is 248.14 Wm^{-2} . The seasonality of the shortwave reflected radiation is more marked as the shortwave incoming radiation. In most of the cases, less variability of shortwave reflected radiation is presented in the cold and dry season and more variability in the wet season. Maximum values occur just after precipitation events and minimums or low peaks occur not only in the dry season but also in the wet season. The shortwave reflected data does not follow a normal distribution, as it was revealed by the normality tests which results are shown in **Table 5.2**. The patterns of the time series of the shortwave reflected have a slight change from 2006, especially in the first semester; this corresponds to the higher annual precipitation (1453mm) of this year, among the evaluated years.

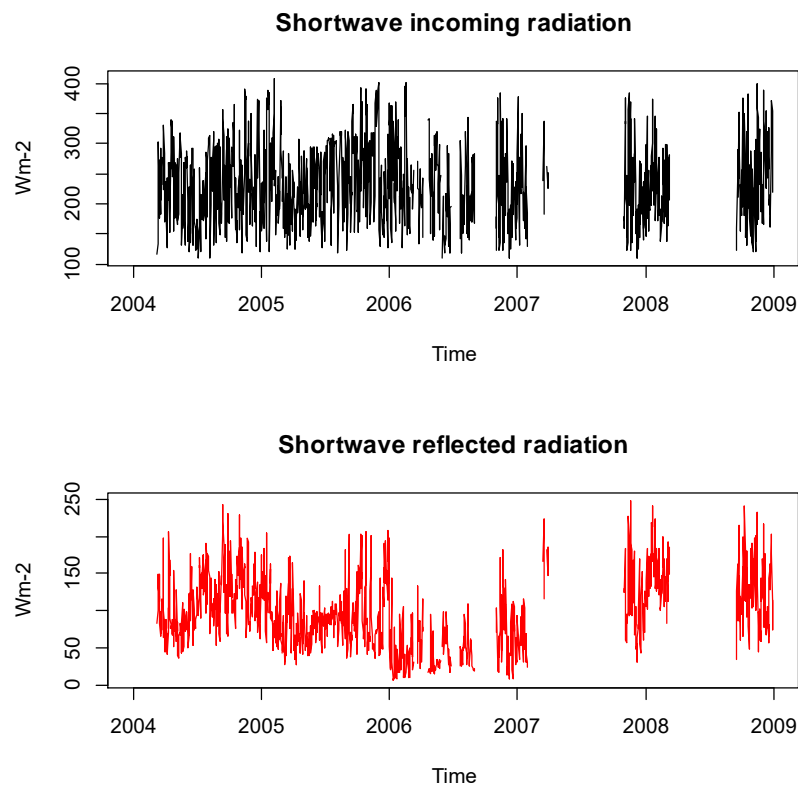


Figure 5.3. Daily shortwave incoming and reflected radiation at glacier Artesonraju

5.3.3 Longwave incoming radiation (from the atmosphere)

The daily means of longwave incoming from the atmosphere are presented in **Figure 5.4**. Longwave radiation incoming shows very elevated values for some days of the years 2007 and 2008. These values break the behavior of this variable which, until 2005, had a mean of only 276.2 Wm^{-2} . A comparison of the longwave incoming radiation with the temperature was made (not presented) and showed that the outliers of the longwave radiation at the atmosphere did not correspond to increments of the temperature. Therefore, these extreme values were taken out. The longwave incoming radiation series varies between 194.3 Wm^{-2} and 369.4 Wm^{-2} with a mean of 280.6 Wm^{-2} . The extreme values correspond to the dates 22.03.2006 and 12.07.2005, respectively.

5.3.4 Longwave emitted radiation (longwave radiation by the surface)

The daily longwave emitted radiation has a mean value of 308.5 Wm^{-2} , with the flux ranging between 287.7 Wm^{-2} and 320 Wm^{-2} . These values occurred on 07.29.2004 and 4.2.2006 respectively. The longwave emitted by the surface presents a more marked seasonality.

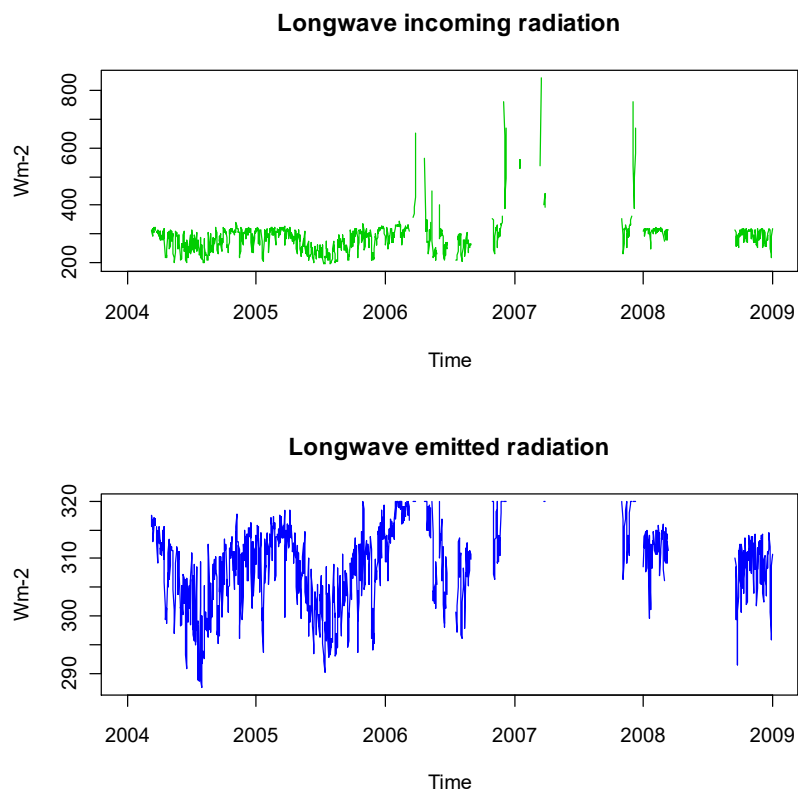


Figure 5.4. Daily longwave incoming radiation and longwave emitted radiation at glacier Artesonraju

5.4 Analysis of Seasonality and Trends of the Energy Fluxes

Establishing categorical conclusions of the variables and their patterns through time is not the purpose of this analysis, as the available data of energy fluxes are rather short-timed. Nonetheless, some aspects that characterize the seasonality of the time series of the data at one gauge station – originally taken at a resolution of 30 min and then averaged for each day for the 5 years 2004-2008 - can be seen from the whisker plots for each month in **Figure 5.5**.

The daily averages of the shortwave incoming radiation do not vary much through the year, which means that there is not a well-defined seasonality in this variable. However, it is observed that some monthly averages tend to fall, as it is the case for months of June and December. On the contrary, August, September and November have the highest average radiation. In general, there is a high dispersion of the daily radiation in all months, though the former decreases in March and April.

Regarding the shortwave reflected radiation, the monthly averages show a lot of variation between the months of January and March, and greater data dispersion as well. The lowest daily

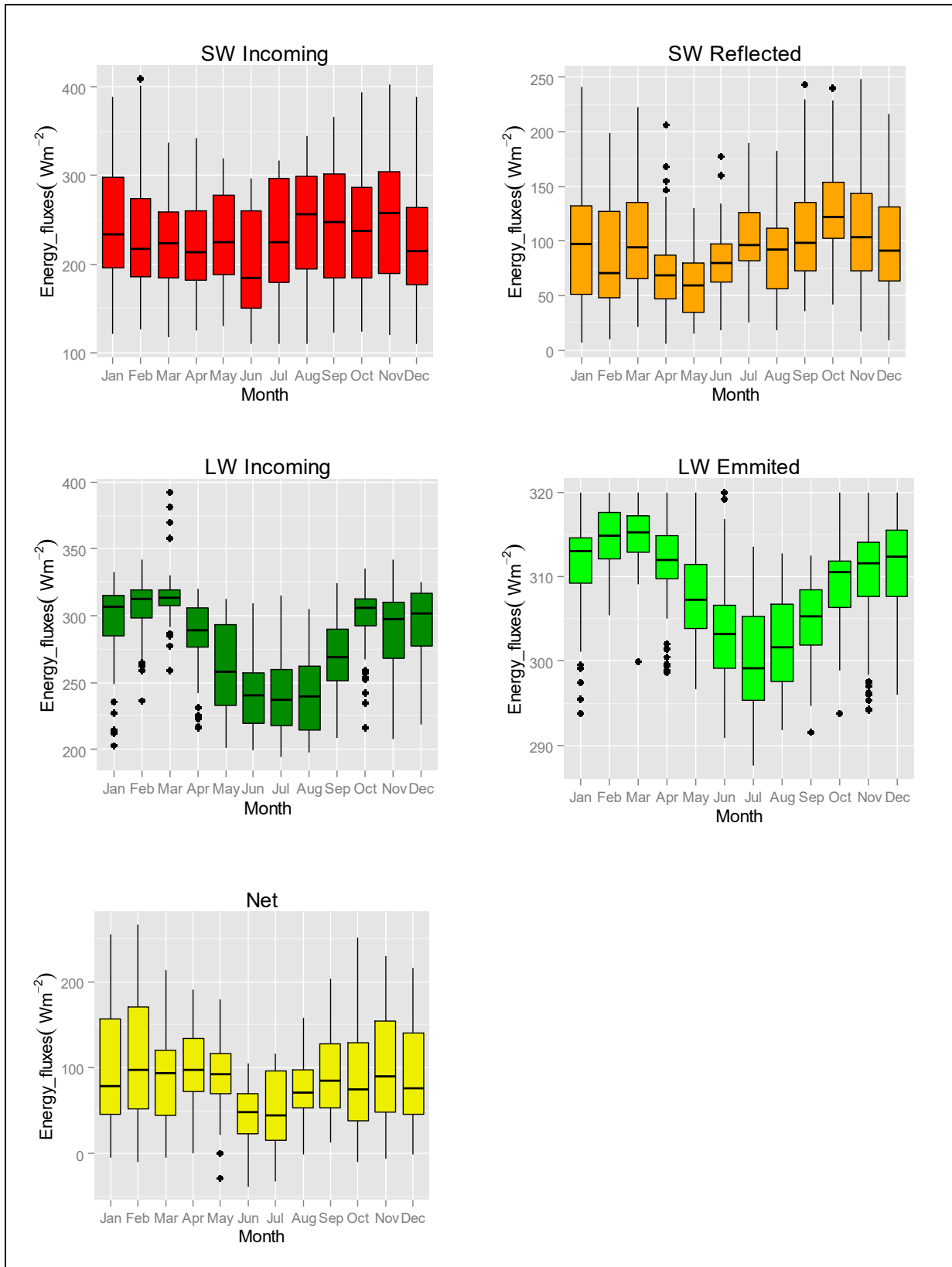


Figure 5.5. Artesonraju daily averages (2004-2008) of various energy fluxes for different months of a year

averages are presented in February, April and May. Lower data dispersion of daily data is presented in April, May, June, July, than the rest of the months of the year. October is the month with the highest average reflected radiation of the year; this average tends to decrease gradually and slightly until December. Comparing the seasonality of shortwave reflected radiation (see **Figure 5.5**) with precipitation of Artesonraju in Chapter 4 (see **Figure 3.11**), it is observed that this two variables do not totally correspond to each other in the seasonality, for example, the highest precipitation characteristic of March did not generate an immediate increase of shortwave reflected radiation as expected, and the low precipitations of June and July did not decrease as expected the shortwave radiation, this was observed also by Juen (2006) who explain this phenomenon. In the wet season, some months like in February are expected to have precipitation that falls as rain and thus albedo decrease while for July for instance, whatever snowfall can keep the albedo high.

Certainly, both longwave radiations have marked seasonality. However, longwave incoming radiation from the atmosphere, present the greatest seasonal differences (up to 175 W m^{-2}) between the dry and the wet season. The highest averages are located in the wet season. Months of transition from the maximum to the minimum averages are observed, these transition months are April, May and September. The minimum averages of longwave incoming radiation are presented in May and August and the maximum average in March and October. It is observed that most of the outliers of longwave incoming radiation are presented in March. The longwave radiation emitted by the surface, has seasonality with fewer differences between the maximum and minimum average, but likewise, as longwave incoming, higher values are observed in the wet season and lower values in the dry season.

There is certain seasonality in the net radiation daily averages; however, this seasonality is determined mainly by minimum averages in the months of June and July. For the rest of the year, it is presented daily averages that have slight variations and that alternate between August and May.

Taking into account the above, it can be partially determined that longwave radiation has the most marked seasonality in energy fluxes. This seasonality influences the net radiation to a greater extent in the dry season while shortwave radiation influences net radiation in the wet season. However, it is necessary to precise that these are data from a specific site in the tongue of the glacier and that these characteristics can change according to other factors. Such factors are for instance: a) the reflections caused by the different surfaces that compose the glacier or b) the shade in some sectors of the glacier at certain times that may influence the amount of shortwave radiation received or emitted. Therefore, distributed energy studies are required in order to study how these energetic fluxes may be affected in the different areas of the glacier.

5.5 Correlations of Energy Fluxes, Temperature and Precipitation

Cross-correlations of the energy fluxes, precipitation in Artesonraju, discharge in Artesoncocha, and the daily temperature in each glacier and the NCEP data are computed, with the results shown in the cross-correlation matrix of **Figure 5.6**.

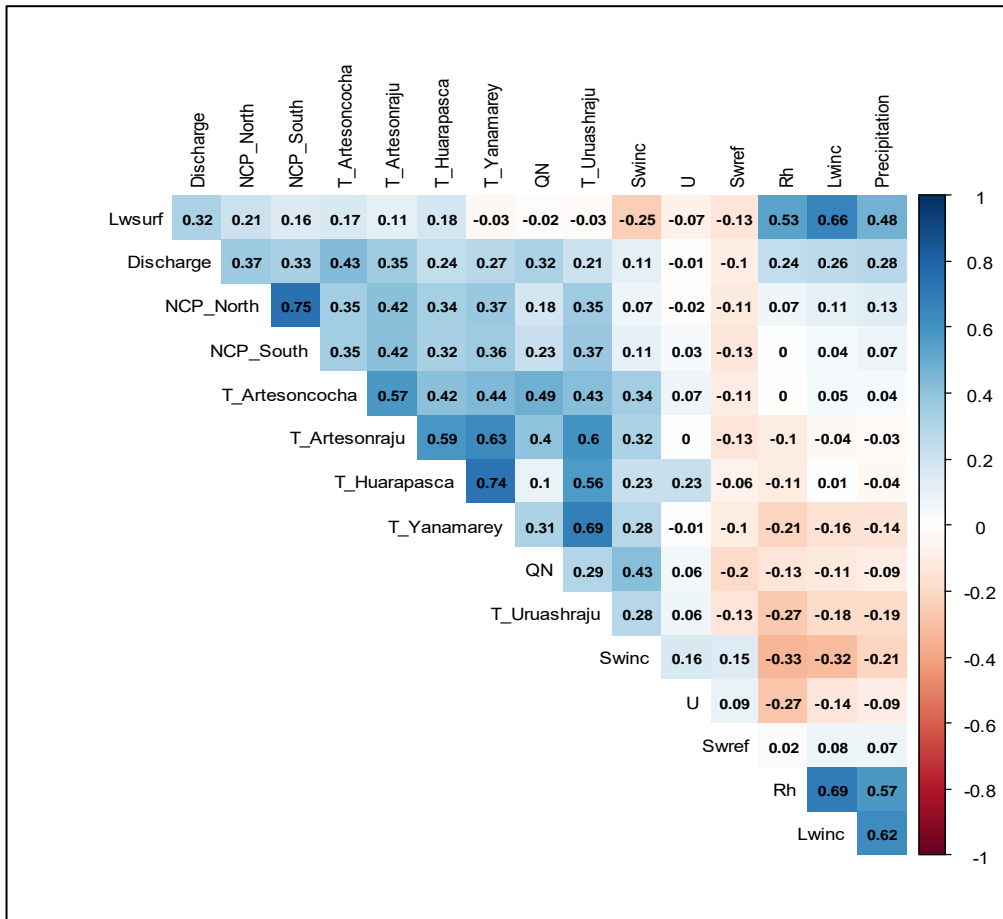


Figure 5.6. Correlation coefficients among the energy fluxes variables, Shortwave radiation Incoming (SW_{inc}), Shortwave radiation reflected (SW_{ref}), Longwave radiation incoming (LW_{inc}), Longwave radiation emitted by the surface (LW_{surf}), Net Radiation (Q_N), Temperature ($T_{glacier}$'s name), Precipitation, Relative Humidity (R_h), Wind Speed (U) and discharge in Artesoncocha and the closest reanalysis data NCEP in the north and in the south.

Figure 5.6 indicates that there is a high correlation between relative humidity and longwave incoming radiation ($r=0.69$), and longwave emitted by the surface ($r=0.53$). In addition, longwave incoming and longwave emitted have also a high statistical correlation with precipitation, (0.62) and (0.48) respectively. The temperature daily times series at the glacier of Artesonraju shows a correlation of ($r=0.4$) with net radiation, but does not show a high correlation with any shortwave radiation and long wave radiation as it would be expected. There is also a high correlation between longwave radiation incoming and emitted ($r=0.66$).

This high correlation between longwave incoming and emitted radiation with humidity and precipitation is not surprising, as atmospheric radiation is affected by cloudiness which, in turn, is related with the water vapor content in the air. This means that the tropical characteristics of the wet season in the outer tropics and the atmospheric characterization of the subtropical dry season help to understand the seasonal behavior of the longwave radiation.

Another significant correlation is obtained between the temperature of Artesoncocha and the net radiation, ($r=0.49$), with the latter also correlated well with the temperature of Artesonraju ($r=0.4$), Yanamarey ($r=0.31$) and Uruashraju ($r=0.29$). For the southern glacier, Huarapasca, this

correlation is reduced. This good correlation of temperature with net radiation can hint of the possibility to extrapolate energy flux data to other glaciers. Net radiation has a good correlation with shortwave incoming as well ($r=0.43$), this reflects the not-well defined seasonality in both variables, although in net radiation there are two months when marked decreased radiation occurs, this is not the case for the rest of the months, and this low seasonality for most of the time is also characteristic of shortwave incoming and the temperature. The discharge in Artesoncocha also exhibits some correlation with the temperatures in all glaciers.

Although some authors state that the temperature is not the most important climate parameter driving seasonality in the outer tropical glaciers (Kaser and Georges, 1997), as it has not a marked seasonality as precipitation or humidity, the results of the correlation analysis show certain sign of interaction between the temperature and the net radiation which in turn suggests a relevant role driving the energetic balance in the tropical glaciers, although the low annual variation of the daily means of temperature. Therefore, more investigations with regard to the mechanism that uses temperature to drive the physical dynamics and the seasonal patterns of the tropical glaciers are required.

5.6 Concluding Remarks

The analysis made in the present chapter considerer the measured data of energy fluxes in the climate station of Artesonraju. Therefore, it should be seen as the conditions presented in just one site on the glacier which may not be representative of all the physical processes that occurs in the whole glacierized basin. However, these results can be a preliminary outline of the understanding of energy fluxes on tropical glacier environments. Besides, it can be used as comparative element of site analysis in regard to the whole context of the glacier.

Some of the most important aspects related to the site analysis of measured energy fluxes average to daily means are the following:

The statistical correlation of the different energy fluxes suggest that the observed seasonality of the net radiation may be more influenced by the reflected shortwave radiation in the wet season and by the clear seasonality of longwave radiation in the dry season.

The correlation of the net radiation with temperature can be explained by the similar seasonal patterns of these two variables in most of the months. Therefore, further investigations should establish how temperature interferes in maintaining the snowpack in the glacier and thus regulating the amount of energy available for melting. Furthermore, this correlation of two variables, more than with, for example, precipitation, opens the way to investigate if empirical models like the temperature index model could be applied in tropical glaciers, despite the low seasonality of temperature.

A reasonable correlation of precipitation, humidity, and in less extend to temperature, with the longwave radiation was also observed. In fact, the latter seems to be an important variable for determining the seasonality of energy fluxes in outer tropical glaciers, as also stated by Sicart *et al.* (2011).

6 Filling of Data Gaps in the Climate Data Series

6.1 Rational and Overview

The models of the energy balance and the temperature index, in the subsequent chapters can only be used with complete time series of the data. Therefore, the data gaps in the energy fluxes as well as other climate variables require the use of statistical methods in order to fill in the former in a reasonable manner.

This chapter presents the methodologies, the validation and the results of the application of various statistical models used for filling gaps in order to obtain complete time series of the climate data. The latter is used afterwards as input for the physical and empirical models for calculations of mass balance and glacier discharge modelling.

The objective of this chapter is then to partially reconstruct some missing periods in the time series in a period from 2000 to 2007. The selected period is relatively short, because of the scarce availability of important data necessary for the validation of the main models used in this research.

For the filling of the data gaps, two different methods are used. The first method is multiple linear regression which offers the possibility to use the data from neighboring stations, taking advantage of possible correlations among their data, to rebuilt gaps or extrapolate the time series. This approach works particularly well for temperature data, because of its high thermal homogeneity for stations in a similar elevation range. However, for the times series of energy fluxes this method turns out to have no good results, due to the low correlation of these parameters and that they have gaps in the same time lapses.

The second method used is optimal interpolation based on seasonal trends and autoregression properties of the time series. This method uses basically the memory of the time series, in order to fill the data gaps and turns out to be useful for the time series which do not have a high correlation among each other, which is the case for the majority of energy fluxes. This data goes back to 2004 and covers a maximum period of 4 years, i.e. until 2008, therefore, the idea is to make interpolations to find the missing data in order to apply the energy balance model at least for 4 years. Considering the good records of energy fluxes for the years 2004 and 2005, the autoregressive memory of these data can help to find a regression model that allows filling of the missing data of 2006 and 2007.

6.2 Gap Filling by Multiple Linear Regression

6.2.1 Theoretical basis of multilinear regression

The multiple linear regression model seeks to explain the change in the response variable y by the change ($\beta_i, i=1, \dots, p$) of some predictor variables (x_1, \dots, x_n). The linear function form is:

$$y_i = \beta_0 + \beta_1 x_{i1} + \beta_2 x_{i2} + \dots + \beta_p x_{ip} + \varepsilon_i \text{ for } i = 1, 2, \dots, n. \quad (6.1)$$

Eq. 6.1 indicates that

- each predictor variable in the function is multiplied by an unknown regression coefficient or parameter,
- there is at most one unknown parameter with no corresponding explanatory variable,
- all of the individual terms are summed to produce the final function value,
- the regression coefficients represent the linear dependency between multiple variables and they are related to multiple correlations.

The data reconstruction of a time series uses then the multiple linear regression model above with available predictors among the neighborhood data sets. The program of multiple linear regression (Bejranonda, 2015) formulates all the regression equations with possible combinations of 2 to 5 available predictors which are then solved by the classical least squares method. Afterwards, the goodness of the fit of the predictor model to the observed data is evaluated by means of the Nash Sutcliffe Efficiency Coefficient (E).

6.2.2 Results

The application of the multilinear regression program of Bejranonda (2015) for the different time series with gaps generate the results discussed in the subsequent sub-sections.

6.2.2.1 Temperature data

The reconstruction and the filling of data gaps of the temperature time series of Artesonraju weather station were made for years 2000 to 2007. The selected period is that when the precipitation and discharge are also available for modelling the temperature index model. The regression model selected three main predictors for filling the data gap. These are the daily temperatures at stations Cullicocha, Uruashraju and Yanamarey.

Figure 6.1 shows the results of the application of the multiple linear regression model to this data. Obviously, the method is able to make a reconstruction of the time series between 2000 and 2002 and some data additional gaps are filled between 2002 and 2007. The validation of the simulated model, i.e. its capability to rebuild and fill data gaps, results in goodness of fit parameter E between 0.42 and 0.85 and with values of 0.75-0.85 for the time period 01.01.2000-24.04.2002. For the filling of data gaps between 08.04.2002 and 31.12.2007 quite satisfactory E between 0.75 and 0.85 are obtained. These good results of the multiple linear regression model for reconstructing certain periods and filling in data gaps in the temperature can be explained by the high correlation of temperature at station Artesonraju with that of neighboring stations in a similar elevation range.

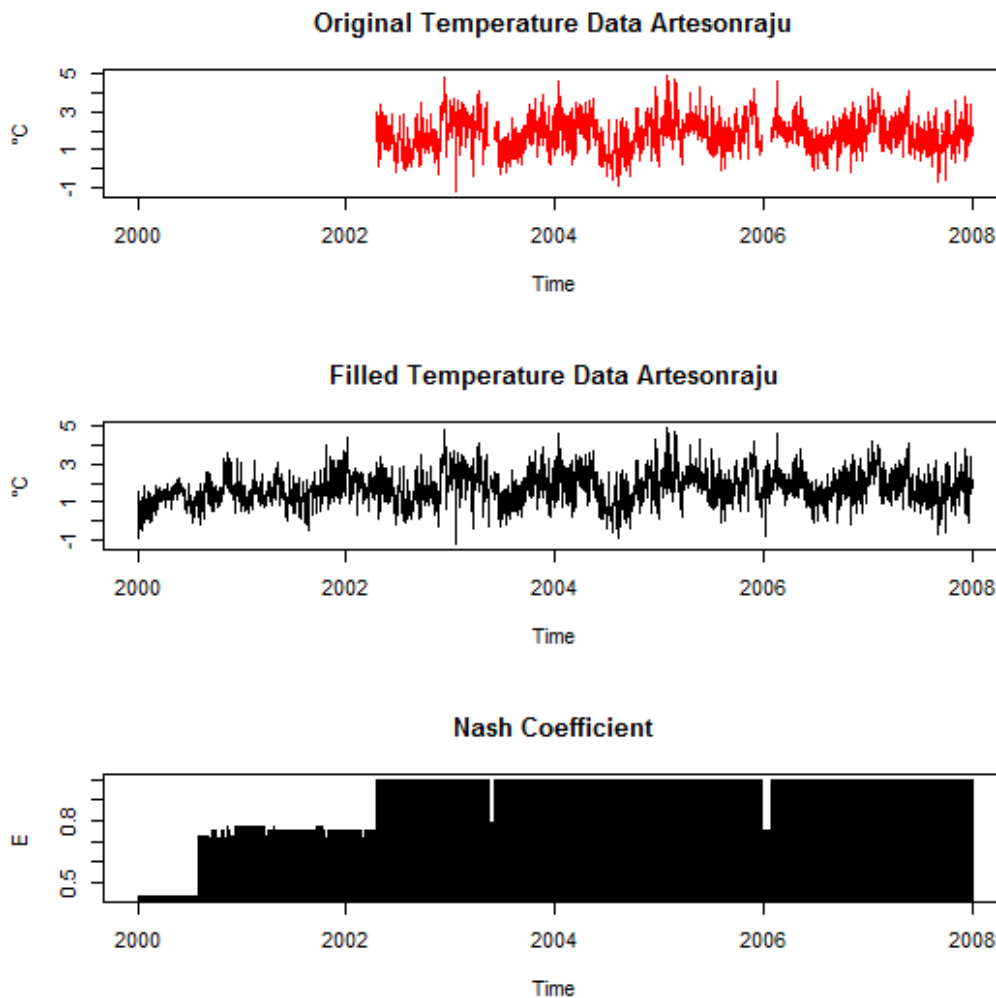


Figure 6.1. Results of application of the multiple linear regression model for filling in and extrapolating daily temperature at Artesonraju station

6.2.2.2 Energy Fluxes

Multiple linear regression was also applied to fill in missing data in the energy fluxes. The predictors used for the modelling are the same energy fluxes and additional climatic variables, such as the temperatures of the NCEP- reanalysis, measured temperatures at Artesonraju, Artesoncocha and Parón stations, as well as precipitation and relative humidity in the basin.

6.2.2.2.1 Shortwave incoming radiation

The regression model for the shortwave incoming data results in E ranging between 0.26 and 0.35 for filled data gaps between years 2008 and 2009. The period between 03.11.2008 and 09.19.2008 could not be rebuilt, owing to a lack of data for the other variables. The filled data between 2007 and 2008 presents less dispersion than the original data (see **Figure 6.2**).

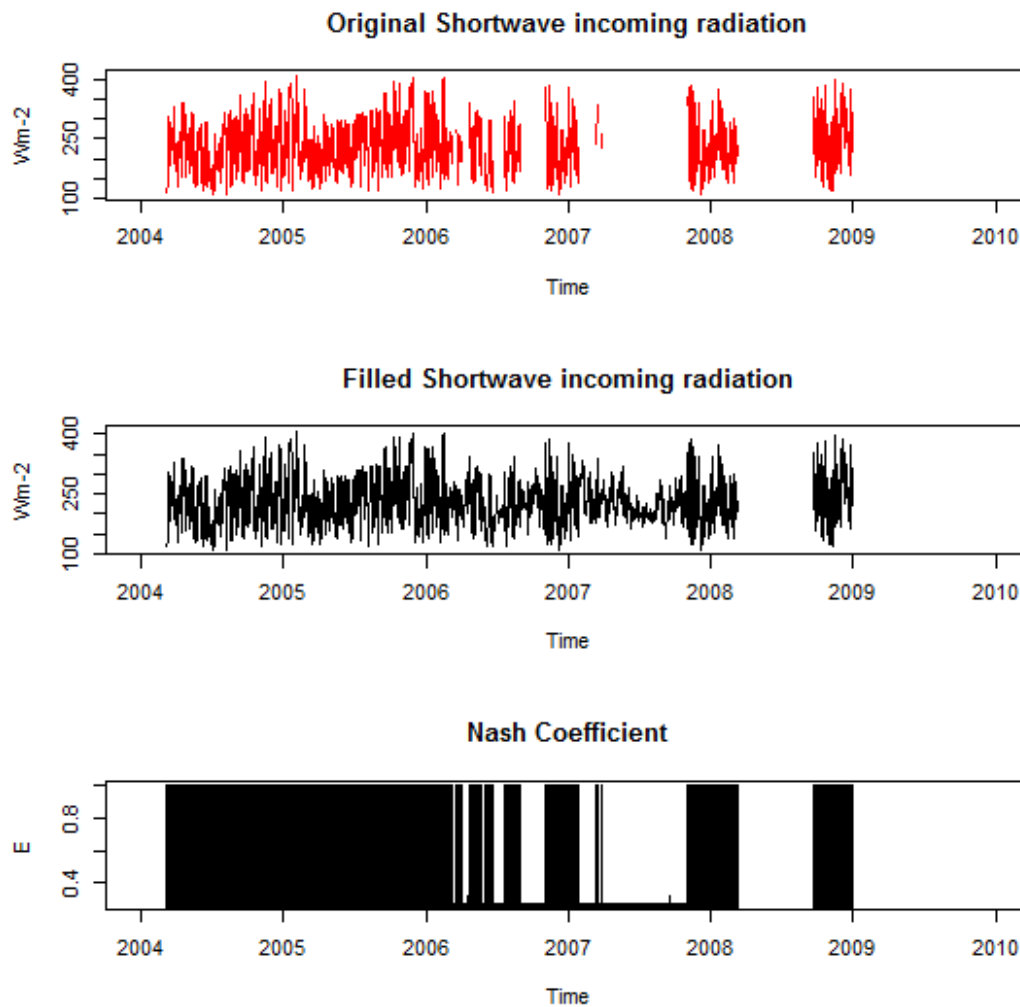


Figure 6.2. Results of application of the multiple linear regression model for filling in and extrapolating daily shortwave incoming radiation at Artesonraju station

6.2.2.2.2 Shortwave reflected radiation

The shortwave reflected radiation measured and filled data at Artesonraju is presented in **Figure 6.3**. The Nash coefficients values (E) of the model which simulates the data are -0.27, showing that the modelled data will not represent adequately the real pattern of these time series. The model can follow mean values but the results don't follow either the typical dispersion data of the shortwave incoming radiation nor the seasonal data pattern. The period between, 11.03.2008 and 19.09.2008 could not be rebuilt to the lack of data of the other variables.

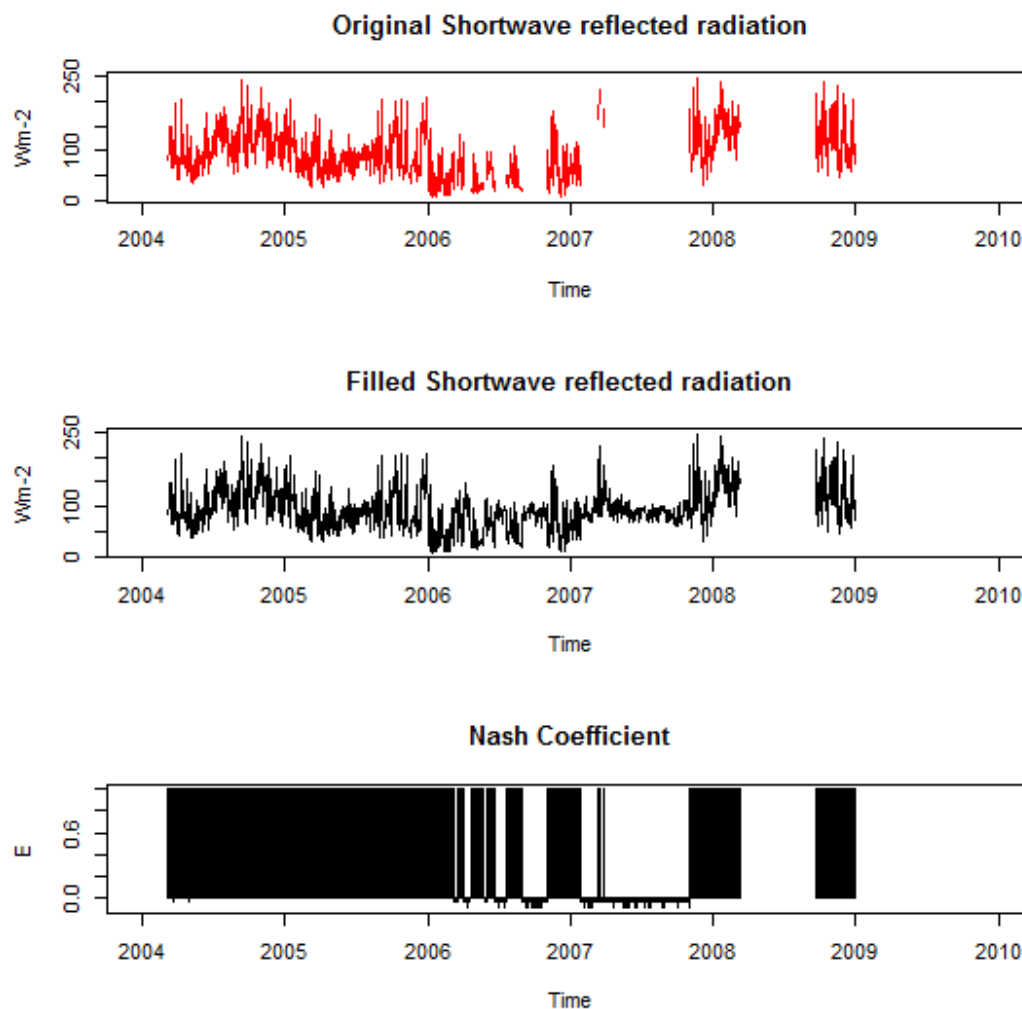


Figure 6.3. Results of application of the multiple linear regression model for filling in and extrapolating daily shortwave reflected at Artesonraju station

6.2.2.2.3 Longwave incoming radiation

The multiple linear regression model for the longwave incoming radiation shows Nash-Sutcliffe coefficients E between -3.53 and 0.8. The majority of filled data show E with negative values, which, are not satisfactory enough to validate the model. The filled data also differs considerably from the patterns of the original series, (see **Figure 6.4**, in black) and the data dispersion of the majority of the filled data has untypical upper and lower outliers. The Nash-Sutcliffe coefficients confirm the non-adequacy of the multiple linear regression model for filling gaps in the time series of longwave incoming radiation.

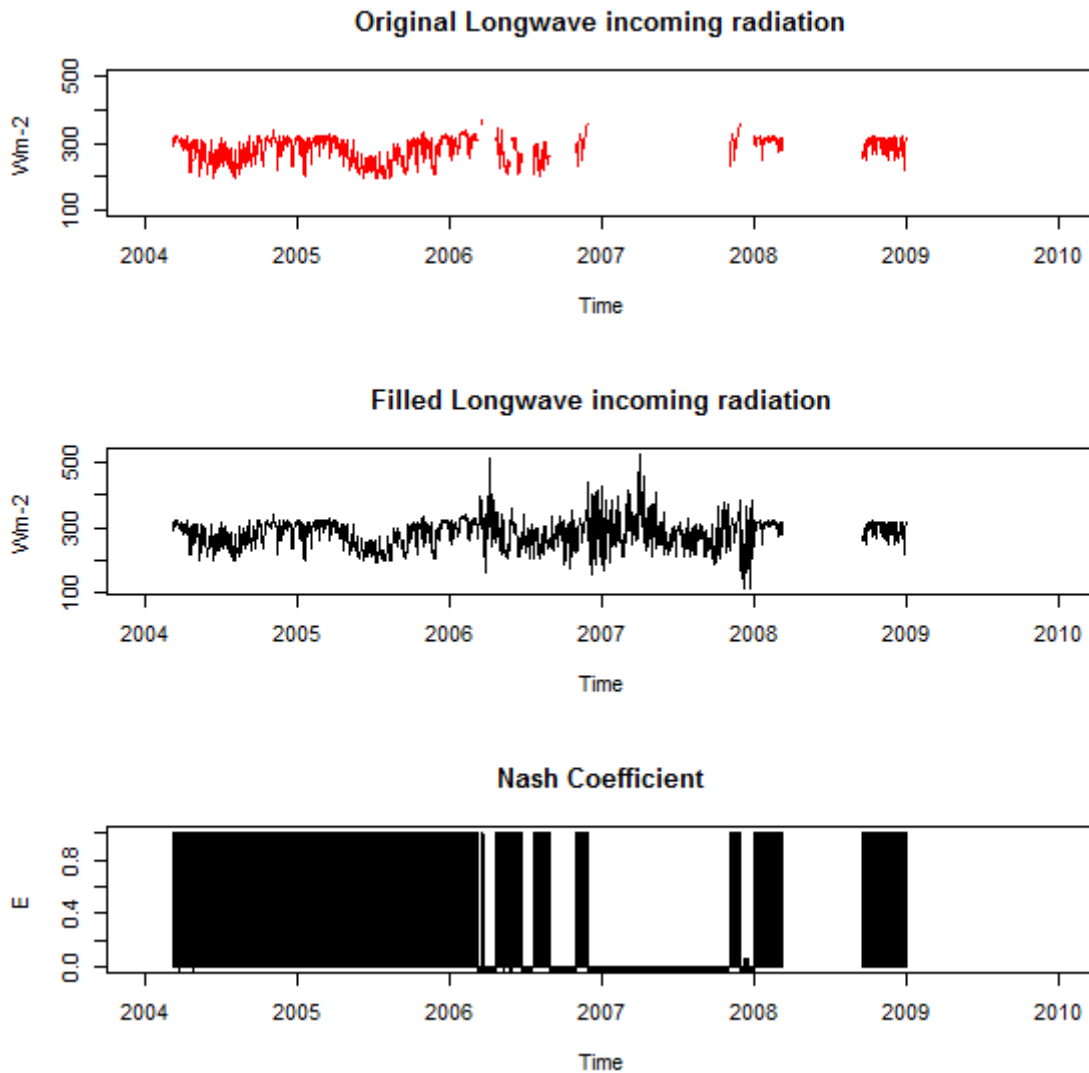


Figure 6.4. Results of application of the multiple linear regression model for filling in and extrapolating daily longwave incoming radiation at Artesonraju station

6.2.2.2.4 Longwave emitted by the surface

The Nash-Sutcliffe coefficient E for the fill-in of the longwave emitted radiation by the surface is between -0.07 and -0.08, i.e. not very satisfactory. Indeed, the filled data shows a much different pattern of dispersion from that of the original data (see **Figure 6.5**). Thus the multiple linear regression model does not work well for the fill-in of the longwave emitted radiation by the surface neither.

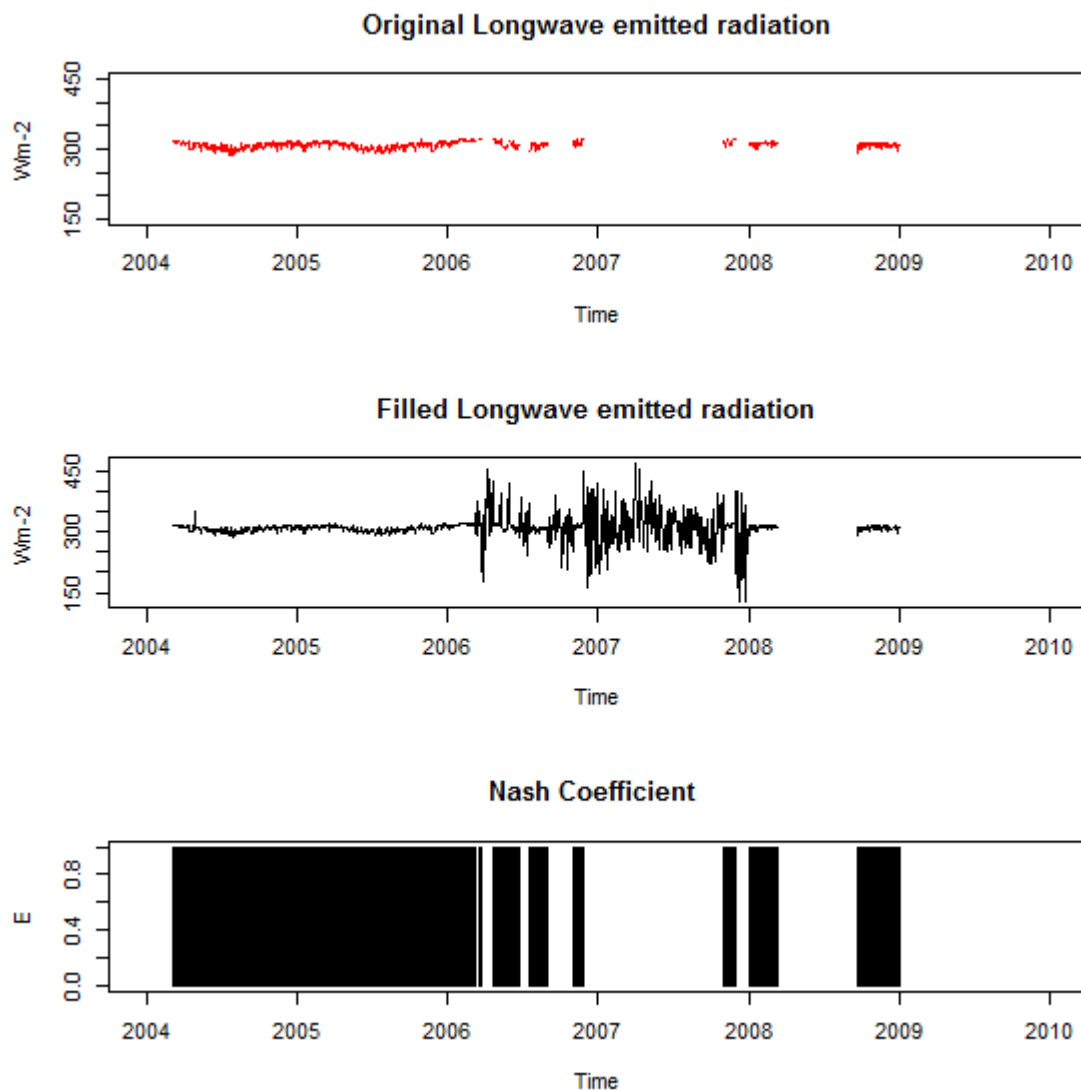


Figure 6.5. Results of application of the multiple linear regression model for filling in and extrapolating daily longwave emitted radiation by the surface at Artesonraju station

6.3 Interpolation of Energy Fluxes by Seasonal Decomposition of Time Series by Loess (STL), Harmonic Analysis and Fitted Optimal Autoregression (AR) Models

Due to difficulties of reconstructing the energy fluxes with the multiple linear regression model, an alternative methodology consisting in a combination of (1) Seasonal decomposition of time series by lowess/loess (STL) (Cleveland *et al.*, 1990), (2) Harmonic analysis, and (3) Fitted optimal autoregression (AR) models, programmed in the R[®]-environment (Koch, 2014), developed internally at Kassel University and used by courtesy of M. Koch, is applied to interpolate missing data in the energy fluxes. The details of the methodology are outlined in the following sub-section.

6.3.1 Basis of STL, harmonic analysis and AR

As mentioned above, the new gap filling methodology developed here (e.g. Koch, 2014), internal report consists essentially of three consecutive steps of time series analysis, i.e.

(1) STL seasonal decomposition by lowess/loess

The first step in the interpolation of missing data is made by through a seasonal decomposition of the time series of interest based on lowess/loess (STL). STL is a filtering procedure for decomposing a seasonal time series into three components, the trend, the seasonal cycle and the noisy remainder, i.e. the part which cannot be explained and so constitutes random errors (Cleveland *et al.*, 1990):

$$Y_t = T_t + S_t + R_t \quad (6.2)$$

where

the trend T_t shows the low-frequency variation of the data together with non-stationary long-term changes,

the seasonal component S_t shows the variation of the data at or near the seasonal period, which for most hydro-climate time series is one cycle per year.

the remainder R_t denotes the random error not explicable by the previous two terms.

STL consists of a sequence of smoothing operations each of which, with one exception, employs the same smoother: LOWESS and its most recent version used in the R[®]-packaged, called LOESS

Lowess fits simple models to a localized subset of the data to build up a function that describes the deterministic part of the variation of the data point by point. It means that there is not specified a global function to fit a model to the data, instead there some low degree polynomial functions that fit a segment of the data. These low degree polynomial functions have predictor variables near the point whose response is being estimated. The polynomials are fit using weighted least squares, giving more weight to the points, near the point whose response is being estimated and less to points further away.

The seasonal component is found by lowess smoothing of the seasonal local sub-series. The seasonal values are removed from the series and the remainder smoothed to find the trend. The overall level is removed from the seasonal component and added to the trend component. This process is iterated a few times. The remainder component is the residuals from the seasonal plus trend fit.

As lowess requires full data series, initial data gaps in the time series are firstly filled in by substituting there the statistical mean of the available data series as the most simple gap estimator. These mean values are then replaced by statistically more representative values - by abiding by the seasonality of the data - in the subsequent steps of the total gap filling procedure, as outlined below.

The automatic extraction of the seasonal, i.e. the annual cycle, in the measured energy flux series by lowess, turned out to be often difficult, if not impossible, most likely due large noise in the original data (see figures in the subsequent results section). For that reason, and due to the fact that an inherent annual cycle must be present in the climate data, an explicit harmonic analysis of the mean-interpolated data series is carried out as step 2:

(2) Harmonic analysis:

Harmonic (Fourier) analysis permits a complex time series curve to be expressed as the sum of a series of cosine waves (terms) and an additive term (Rayner, 1971; Davis, 1986). Each wave is defined by a unique amplitude and a phase angle, where the amplitude value is half the height of a wave, and the phase angle (or simply, phase) defines the offset between the origin and the peak of the wave over the range $0-2\pi$. Each term designates the number of complete cycles completed by a wave over the defined interval. Successive harmonic terms are added to produce a complex curve, and each component curve, or term, accounts for a percentage of the total variance in the original time-series dataset (Jakubauskas, Legates and Kastens, 2002). This harmonic analysis looks for the signals as the superposition of waves of sin or cosine functions of the original data.

As in the present application the annual cycle is of only interest, the data series is fitted by using only one cos/sin - harmonic with that period.

(3) Fitting of optimal autocorrelation (AR) model

The analysis of autocorrelation (AR) of a time series is a mathematical tool for finding repeating patterns, such as the presence of a periodic signal obscured by noise, or identifying the missing fundamental frequency in a signal implied by its harmonic frequencies. It is often used in signal processing for analyzing functions or series of values, such as time domain signals. The autocorrelation, defined by the autocorrelation coefficients r_i at different lags i allows, in particular, to find the amount of randomness, or its opposite, the persistence or memory in a seemingly chaotic time series.

Once the statistically significant discrete autocorrelation coefficients r_i ($i=1,\dots,p$), with p the maximum of significant lags has been determined, the data series can be fitted by a so-called AR- model:

$$X_t = \sum_{i=1}^p \varphi_i X_{t-i} + \varepsilon_t \quad (6.3)$$

which indicates that each value X_t in the (mean-corrected) time series at time t is a linear combination of up to $t-i$ ($i=1,\dots,p$) previous values, with coefficients φ_i , that are determined in the least-squares fitting process (=minimizing the error terms ε_t in Eq. (6.3)), by solving the so-called Yule-Walker equations (e.g Brockwell and Davis, 1991).

In the present application of gap-filling, the residuals between the observed data-values and the previously harmonic fitted data values are used in the determination of the optimal AR-model in Eq. (6.3). This is done internally in the corresponding R[®] - program by increasing p and finding

the $\max p$ giving the best fit of the model to the data based on the AIC, which in turn penalizes the use of higher p , i.e. the procedure attempts to find low p - structured models.

Once the optimal AR-model (Eq. 6.3) is found, the latter is used to generate new, random time series data, which abides by the original autoregressive structure of the model. This data is added – after inflation of the variance to reflect the variance of the original data – to the previously harmonic fitted data in the locations of the data gaps.

In conclusion of this tree-step gap-filling procedure, programmed in the R[®] -environment, missing data in the time series are replaced with fitted values of the harmonic analysis and added random numbers taken from the fitted optimal autoregression (AR) model of the observations.

6.3.2 Results

6.3.2.1 Shortwave incoming radiation

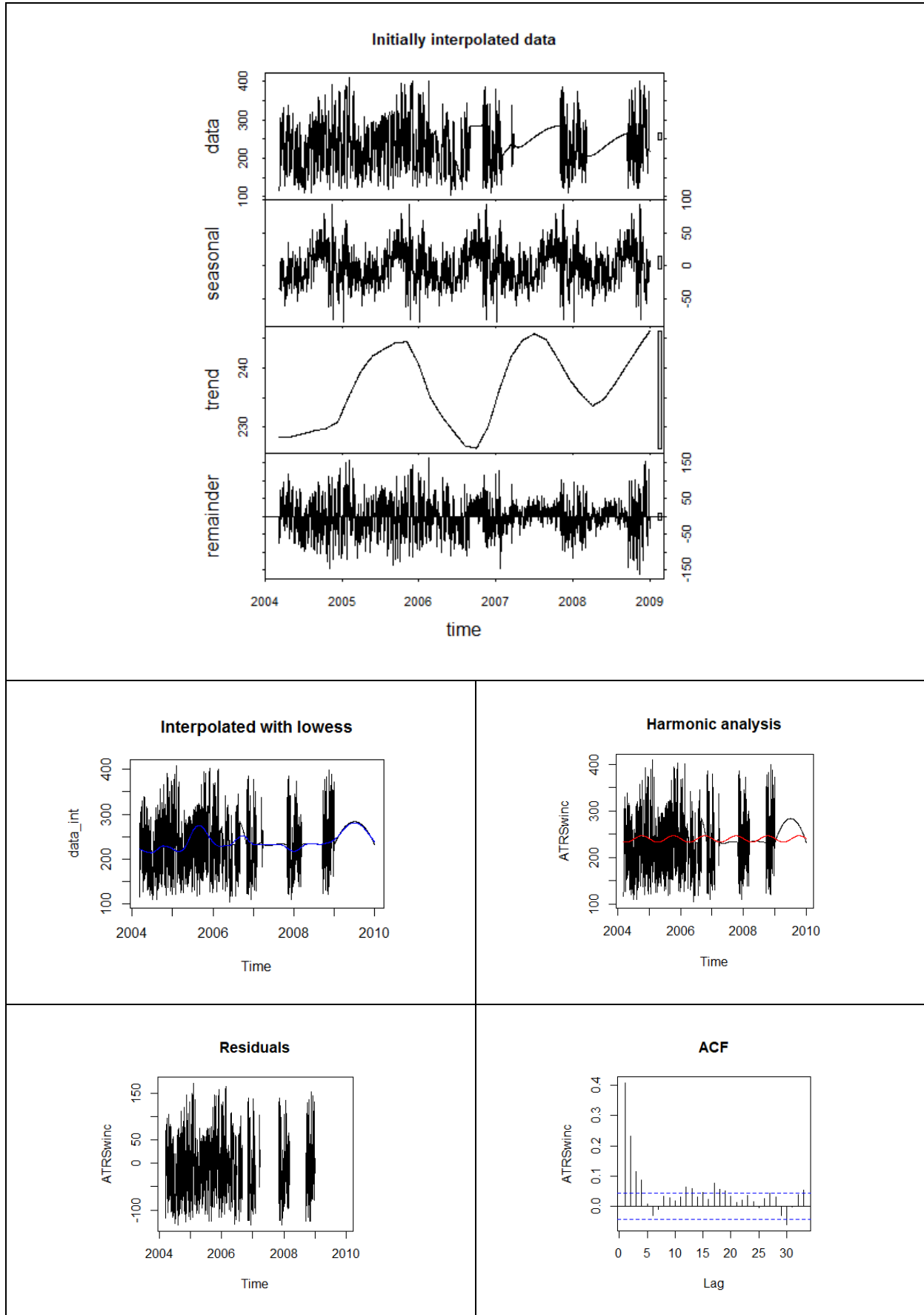
Figure 6.6 shows the various plots related to the gap-filling procedures discussed for the shortwave incoming radiation.

The STL- seasonal decomposition of the data (2nd upper panel from above) shows a certain seasonality sign with a period of one year, though superposed with random fluctuations, as presented in the lowest values around the middle of the time period analyzed. However the trend has also some periodicity of about 2 years, with fluctuations that change from positive until 2006, afterwards become negative towards the middle of the year of 2007 and again positive until the half year of 2008, and start to be negative again in the first trimester of 2008 and end positive. However, as the variation of the trend is only between 230 and 245 Wm⁻², and much smaller than the seasonal amplitude changes, it may not be of the relevance. In fact, visually, the raw data (upper panel) does not appear to have much of a trend.

The fitted lowess regression shows some similar dynamics, but does not follow the annual cycle as stringent and as it should be as the fitted harmonic function with the annual period enforced (second row of **Figure 6.6**). Thus, the harmonic fitting methodology appears to be superior than the lowess regression model for this rather noisy radiation data and so the former is used in the subsequent steps of the gap-filling procedure.

The autocorrelation function shows significant correlations up to lags of about 4 months (i.e. correlation-coefficients outside the confidential interval of 95%). It means that there is a some auto-correlation between the residuals, which moreover follow a normal distribution. Using this information, and as discussed in the previous section, the optimal AR model is build and used to generate missing data in the gaps.

The filled-in data is presented in red in the last panel of **Figure 6.6**. From this time series, it is observed that the generated data has some large negative outliers, which is most likely a consequence of some random numbers drawn from the tails of the normal distribution. Other realizations would result in slightly different pattern. In spite of these caveats, the performance of this stochastic gap-filling model appears to be better than the multiple linear regression of the last section.



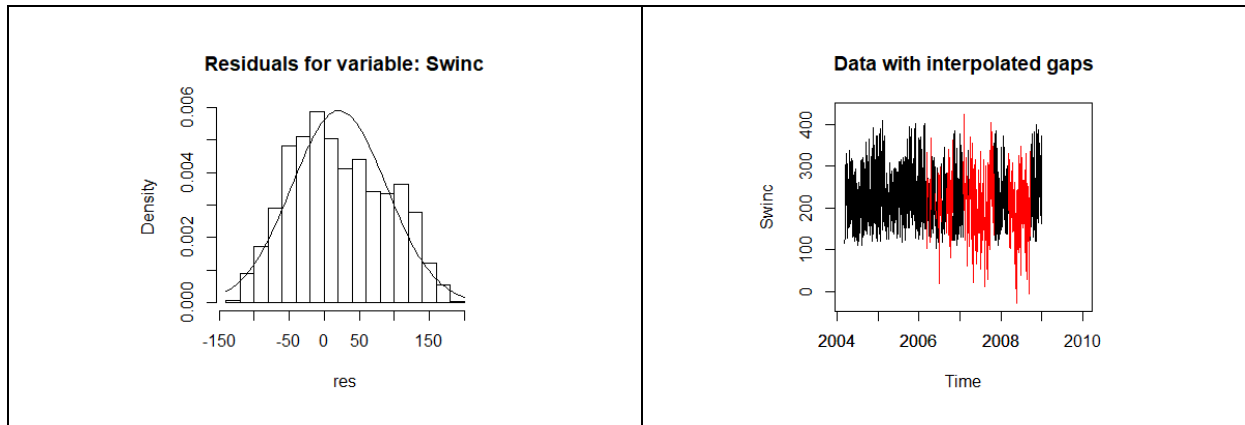


Figure 6.6. Plots showing various results of the different steps of the gap-filling procedure of Koch (2014) for the shortwave incoming radiation

6.3.2.2 Reflected shortwave radiation

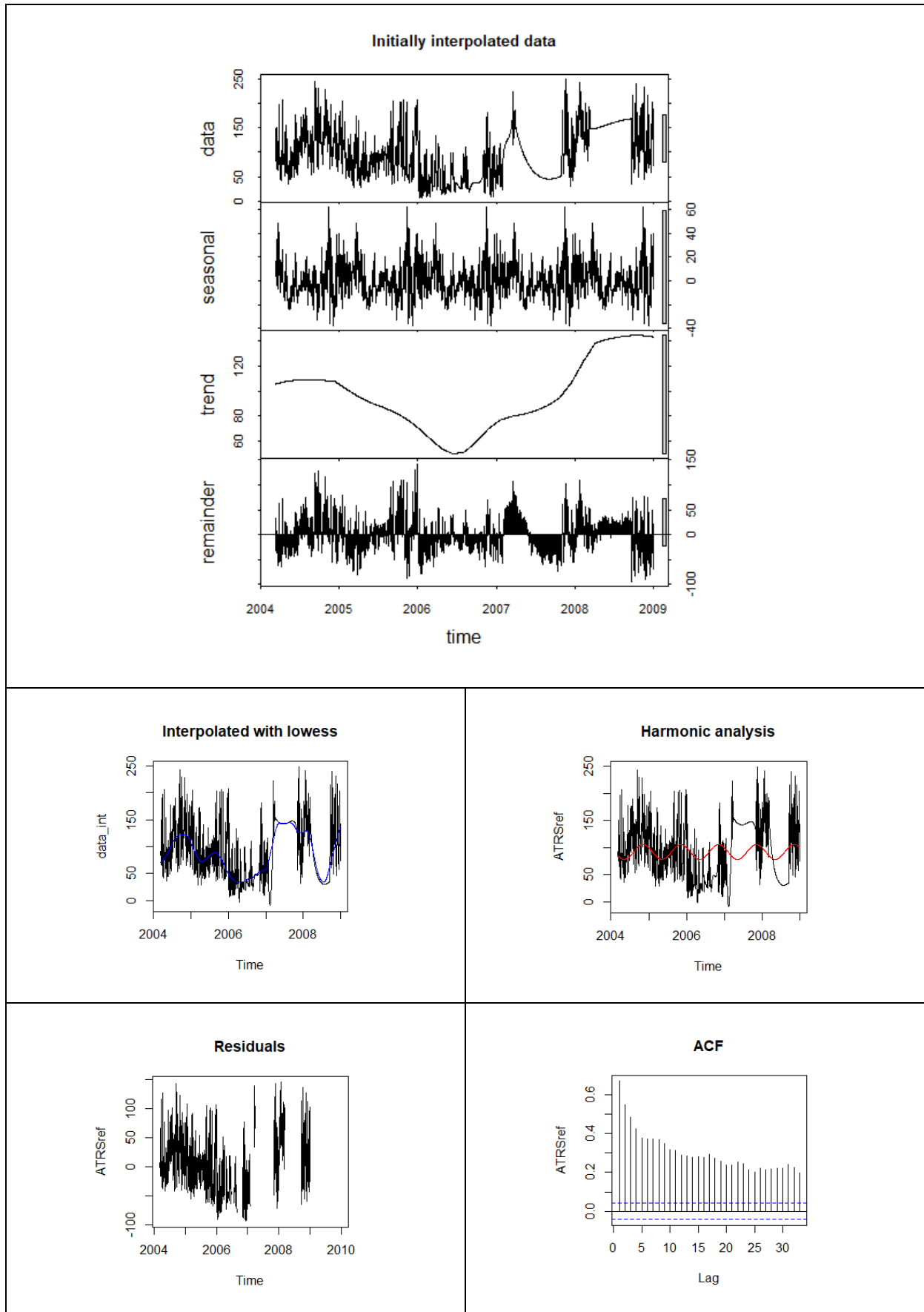
Figure 6.7 shows the various plots related to the gap-filling procedures discussed for the shortwave reflected radiation.

The STL- seasonal decomposition of the data (second upper panel from above) shows a certain seasonality sign with a period of one year, though superposed with random fluctuations, as presented in the lowest values around the middle of each year and the highest peaks at the of the time period analyzed. However, the trend has not a clear periodicity. The trend has fluctuations that change from negative until middle of 2006, afterwards become positive towards the end of the year of 2009. Certainly, the trend shown in the STL does not allow concluding that the trend has a defined pattern.

The fitted lowess regression shows some similar dynamics, but does not follow the annual cycle as stringent and as it should be as the fitted harmonic function with the annual period enforced (second row of **Figure 6.7**). Thus, the harmonic fitting methodology appears to be superior than the lowess regression model for this rather noisy radiation data and so the former is used in the subsequent steps of the gap-filling procedure.

The autocorrelation function shows significant correlations which decrease every lag, however the correlation-coefficients fall for all the lags outside the confidential interval of 95%. It means that there is certain auto-correlation between the residuals, which in most of the residuals follow a normal distribution. Using this information, and as discussed in the previous section, the optimal AR model is build and used to generate missing data in the gaps.

The filled-in data is presented in red in the last panel of **Figure 6.7**. From this time series, it is observed that the generated data has some negative outliers for the years 2007 and 2008, which is most likely a consequence of the negative tails of the normal distribution. Other realizations would result in slightly different pattern. In spite of these caveats, the performance of this stochastic gap-filling model appears to be better than the multiple linear regression of the last section.



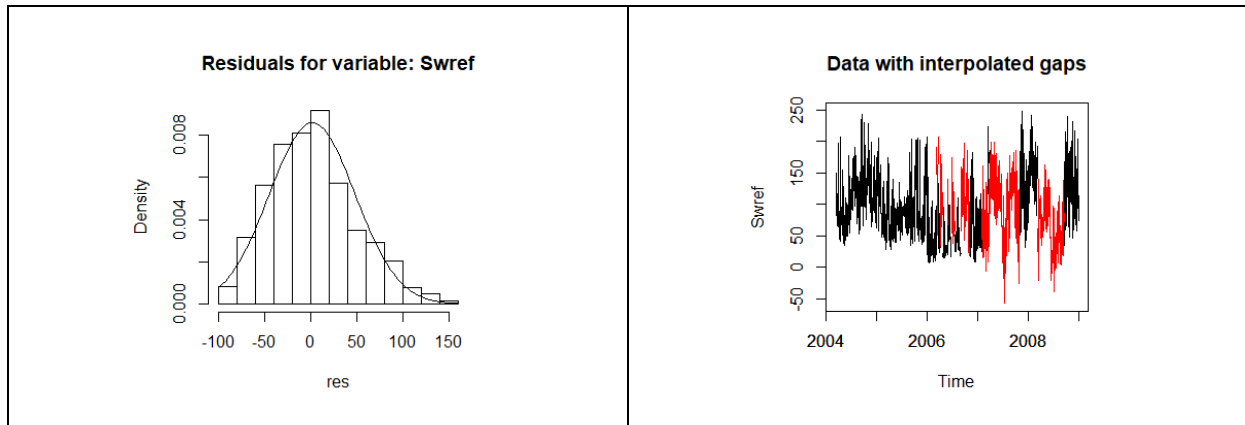


Figure 6.7. Plots showing various results of the different steps of the gap-filling procedure of Koch (2014) for the shortwave reflected radiation

6.3.2.3 Longwave incoming radiation

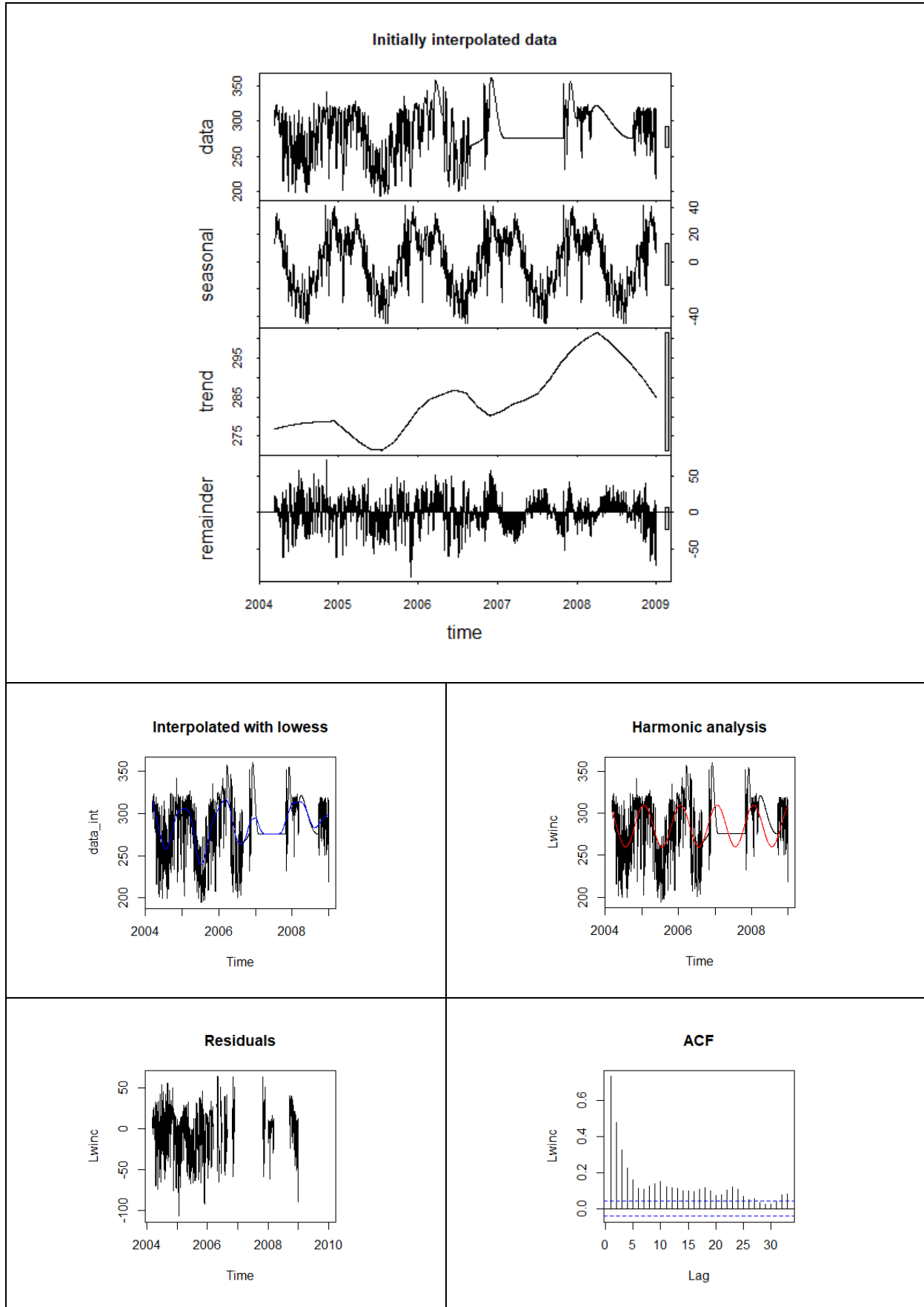
Figure 6.8 shows the various plots related to the gap-filling procedures discussed for the longwave incoming radiation.

The STL- seasonal decomposition of the data (second upper panel from above) shows a clear seasonality sign with a period of one year, though superposed with random fluctuations. Troughs occur around the middle of each year and the highest peaks at the end of each year and beginning of the following year. These troughs correspond to the lower cloudy conditions that characterize the dry season between May and August and the peaks to increments of clouds in the rainy period that begins usually in September and increase between December and March. The trend has fluctuations that change from slightly positive until the end of 2004, afterwards become negative middle of 2005 and again positive until the middle of 2009 with a small trough in between and the end of 2007. Despite these alternate fluctuations, the trend has not a clear periodicity. In addition, the STL-trend does not allow discerning a pattern.

The fitted lowess regression shows some similar dynamics, but does not follow the annual cycle as stringent and as it should be as the fitted harmonic function with the annual period enforced (second row of **Figure 6.8**). Thus, the harmonic fitting methodology appears to be superior to the lowess regression model for this rather noisy radiation data and so the former is used in the subsequent steps of the gap-filling procedure.

The autocorrelation function shows significant correlations which decrease every lag, however the correlation-coefficients fall for all the lags outside the confidential interval of 95%. It means that there is certain auto-correlation between the residuals, which does not seem to follow a normal distribution. Using this information, and as discussed in the previous section, the optimal AR model is build and used to generate missing data in the gaps.

The filled-in data is presented in red in the last panel of **Figure 6.8**. From this time series, it is observed that the generated data has some minor positive outliers for the end of the year 2006 and beginning of 2007, which is most likely a consequence of some random numbers drawn from the positive tails of the residual distribution. Other realizations would result in slightly different pattern. In spite of these caveats, the performance of this stochastic gap-filling model appears to be better than the multiple linear regression of the last section.



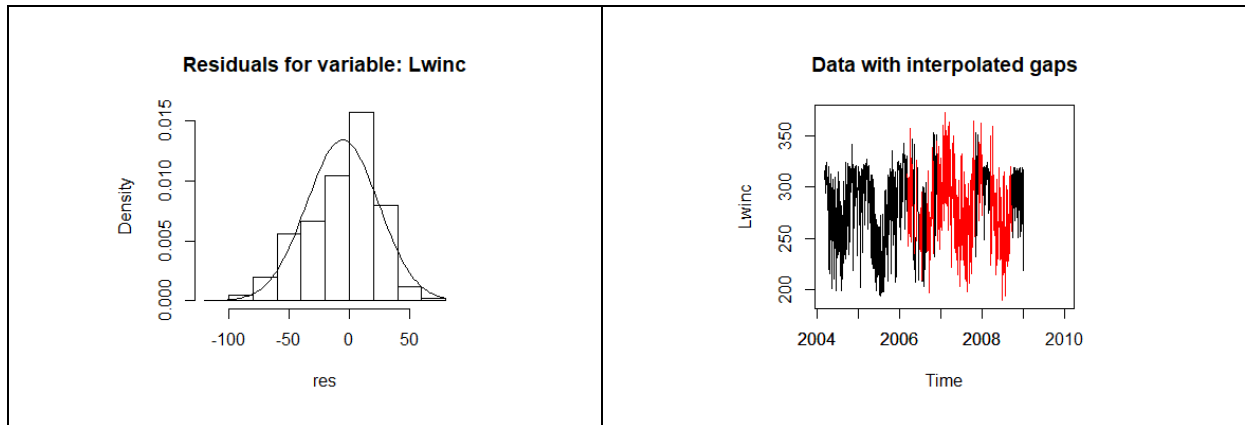


Figure 6.8. Plots showing various results of the different steps of the gap-filling procedure of Koch (2014) for the longwave incoming radiation

6.3.2.4 Longwave emitted by the surface

Figure 6.9 shows the various plots related to the gap-filling procedures discussed for the longwave emitted radiation.

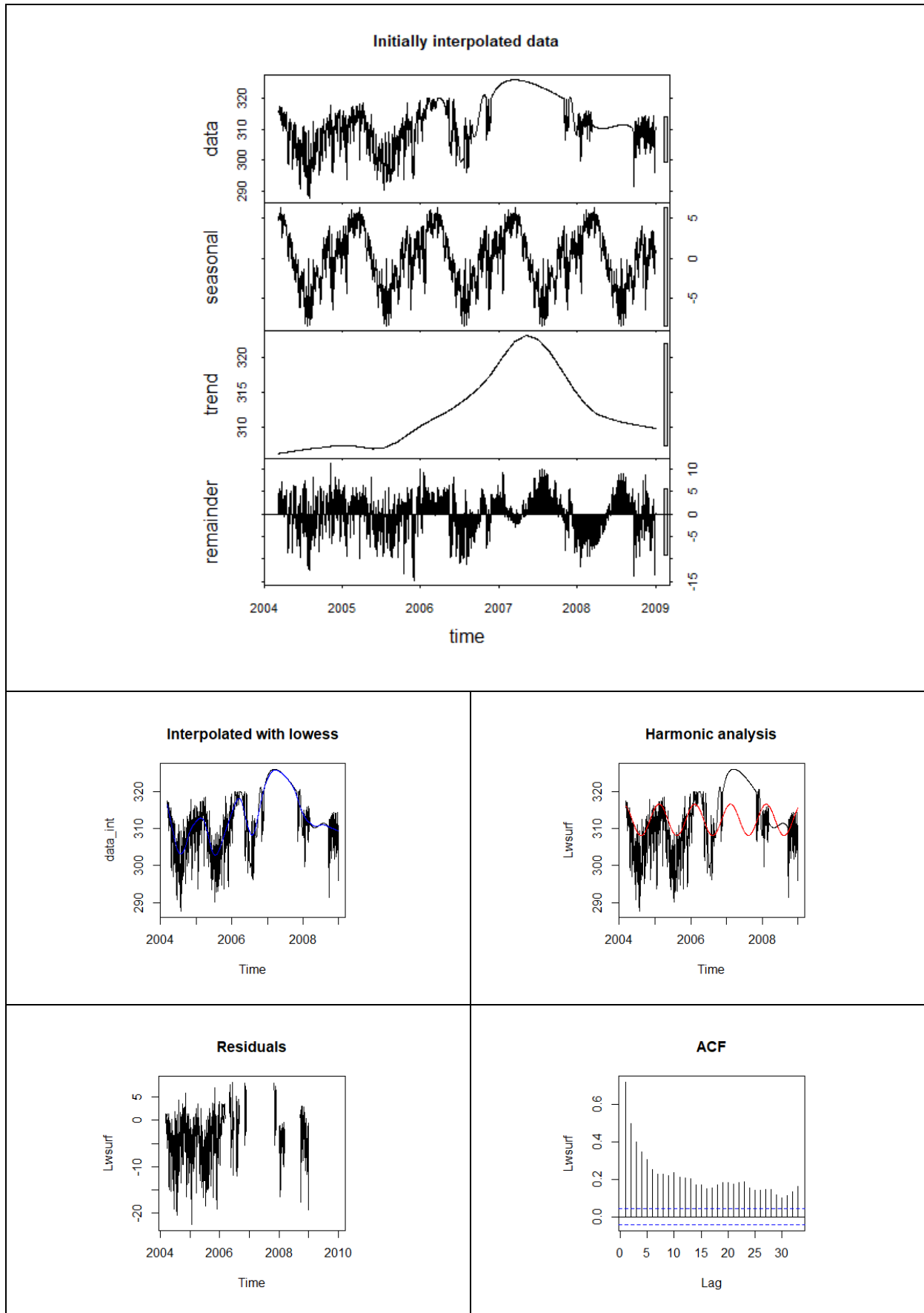
The STL- seasonal decomposition of the data (2nd upper panel from above) shows a clear seasonality sign with a period of one year, though superposed with random fluctuations. Troughs occur around the middle of each year and the highest peaks at the end of each year and beginning of the following year. This seasonality corresponds to the slight temperature variations of the year. Surprisingly, not only the seasonality but also the trend is pretty similar to the longwave incoming radiation. The trend has fluctuations that change from slightly positive until the end of 2004, afterwards become negative middle of 2005 and again steadily positive until the middle of 2007 and finalize being negative until the end of 2008. Nonetheless, the trend has neither a clear periodicity nor a clear pattern.

The fitted lowess regression shows some similar dynamics, but does not follow the annual cycle as stringent and as it should be as the fitted harmonic function with the annual period enforced (second row of **Figure 6.9**). Thus, the harmonic fitting methodology appears to be superior to the lowess regression model for this rather noisy radiation data and so the former is used in the subsequent steps of the gap-filling procedure.

The autocorrelation function shows significant correlations which decrease every lag, however the correlation-coefficients fall for all the lags outside the confidential interval of 95%. It means that there is certain auto-correlation between the residuals, which does not seem to follow a normal distribution. Using this information, and as discussed in the previous section, the optimal AR model is build and used to generate missing data in the gaps.

The filled-in data is presented in red in the last panel of **Figure 6.9**. From this time series, it is observed that the generated data has some positive outliers for the beginning of 2007 and the troughs are also conservative overestimated in the middle of the same year, which is most likely a consequence of some random numbers drawn from the positive tails of the residual distribution. Other realizations would result in slightly different pattern. In spite of these caveats, the performance of this stochastic gap-filling model appears to be better than the multiple linear regression of the last section.

6. Filling of Data Gaps in the Climate Data Series



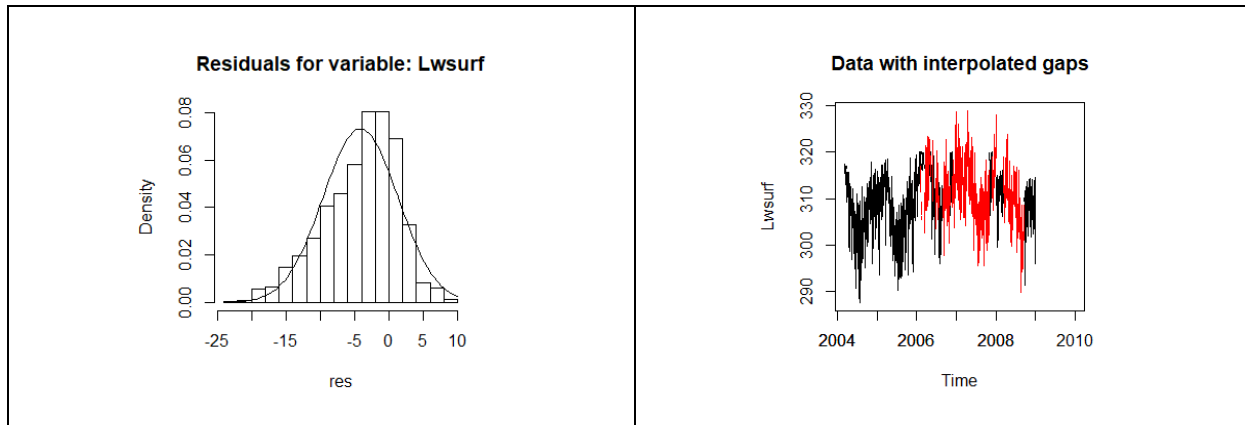


Figure 6.9. Plots showing various results of the different steps of the gap-filling procedure of Koch (2014) for the longwave emitted radiation by the surface

6.4 Concluding Remarks

Results should be considered, however, in light of the difficulty to rebuild large periods on a series. Therefore, although the gap-filled in data may not represent the true data values (which are not known), they reflect the general statistical properties of the time series analyzed. Consequently, they are sufficient to obtain a continuous series in order to apply the energy balance model for the case of energy fluxes and the temperature of the case of temperature index.

For fulfilling the time series of temperature, the multiple linear regression methods shows to be appropriate due to the high correlation of temperature with the different records especially with temperature data from stations located in the similar altitude.

For the case of filling up time series of energy fluxes, the results of the multiple regression method applied to the data are not realistic. Mean values are properly generated; however, typical variations of the data series are not presented especially for the longwave incoming and longwave emitted radiation. This can be explained due to many data gaps are simultaneous in many other variables, and the predictors are not enough to generate the new data.

The autoregression model using STL by Lowess, harmonic analysis and AR models are more suitable for filling gaps of the energy fluxes time series. However, the residuals generated by the AR selected function for the stochastic part of series tend to generate a bias, explained by some random numbers drawn from the tails of the normal distribution. By this method in all the cases the seasonal characteristics of the time series are better represented by the harmonic function than the lowess function, therefore this first one were for all the cases taken for the gap filling procedure.

7 Energy Balance in Tropical Glaciers

7.1 Review on Climactic Factors Influencing Mass Balance Changes in Andean Tropical Glaciers (Energy Fluxes Current Results)

The mass balance changes of tropical glaciers have produced a retreat of masses in the last 40 years (Ames and Francou, 1995; Autoridad Nacional del Agua, 2014). This glacier retreat is the result of an unusual warming trend (Pierrehumbert, 2005), owing to the fact that all physical processes and interchange fluxes between the atmosphere and the glaciers are strongly affected by changes in the various climatic factors. Alterations of glaciers' dynamics generate synergic impacts on the water system not only on the global but also on the local scale. The case of the Cordillera Blanca is crucial at the local level, as this mountain range makes an important contribution to the total annual discharge in the basin of Santa River in Peru. In fact, some of the estimations of the contribution of discharge indicate that between 16- 20% (Schaner *et al.*, 2012) or 30-45% (Mark and Seltzer, 2003) of the discharge in each glaciated catchment in the Cordillera Blanca comes from meltwater.

Furthermore, the importance of the Andean tropical glaciers resides not only in the amount of water they provide during the hydrological year, but also in the regulation of the water discharge in each season. Thus, the tropical glaciers act as water storage systems that supply water during the whole year. This storage is important, especially in the dry season, when precipitation reduces drastically. Therefore, changes in its seasonal behavior can have impacts on the availability of water, especially, in the dry season, and also on the occurrence of flooding in the rainy season (Villacís *et al.*, 2010; Schoolmeester *et al.*, 2018).

Consequently, the accelerated loss of mass of tropical glaciers has created a need to determine the climatic variables which drive these (negative) changes. Some studies carried out on the Andean Tropics explain to what extent, variables such as temperature, precipitation, humidity and solar radiation influence the physical dynamics behind mass balance (Kaser and Georges, 1997; Favier, Wagnon and Ribstein, 2004; Francou *et al.*, 2004; Juen, 2006; Wagnon *et al.*, 2009; Sicart *et al.*, 2011; Gurgiser *et al.*, 2013). Similar studies focused on determining the effects of climate phenomena, like ENSO, on tropical glaciers (Francou *et al.*, 2004; Vuille *et al.*, 2008; Maussion *et al.*, 2015) or the effect of climate change on mountain hydrology (Vergara *et al.*, 2011).

The generalized retreat of glaciers across the Andean suggests the existence of a common pattern of causality (Pierrehumbert, 2005). However, the studies lead to different conclusion as to which climatic variables are the driving factors of the energetic fluxes in tropical glaciers. For the studied cases, the different influencing factors which explain the response of glaciers to climate variations, seem to depend on specific location within the tropics (Favier *et al.*, 2004b), and/or range of elevation (Rabatel *et al.*, 2013). In addition, differences in the driving factors of the energy balance, specifically, of the ablation and the accumulation zones, were found (Gurgiser *et al.*, 2013).

First of all, this chapter will analyze the results of such studies and will focus on the different perspectives trying to clarify the current state of investigations. Furthermore, it will review the

main conclusions related to climatic drivers of the mass balance and proglacial runoff of tropical glaciers and their seasonal variations. Lastly, it will examine the investigations of the influence of ENSO in the studied glacier cases.

7.1.1 Approaching energy balance studies on Andean tropical glaciers

Research on energy balance fluxes on tropical glaciers is relatively recent. The most studied glaciers in regard to their energy dynamics are Antizana in Ecuador (Wagnon *et al.*, 1999; Favier *et al.*, 2004), Zongo (Wagnon *et al.*, 1999; Vuille *et al.*, 2008; Sicart *et al.*, 2011), Charquini (Lejeune *et al.*, 2007), and Chacaltaya (Francou, 2003) in Bolivia, Shallap (Gurgiser *et al.*, 2013; Maussion *et al.*, 2015) and Artesonraju in Peru (Juen, 2006; Winkler *et al.*, 2009).

As can be seen in **Table 7.1**, which presents a summary of the most important characteristics of these studies, the studied periods comprise just short periods, with a maximum of seven years, except for the downscaling of energy fluxes made by Maussion *et al.* (2015). In fact, one limitation of studying energy balance on tropical glaciers in the Andean mountains is the scarce data. Thus, the longest records of measured energetic fluxes extend over 10 years, but, in most cases, the available records last only 1 to 4 years.

The studies aiming to determine the main factors that lead to the melting of the tropical glaciers, have different approaches and so it is of no surprise that some of their results are also different. The main focus and the different outcomes obtained in each research will be presented and discussed in this chapter.

Some studies (see **Table 7.1**) carried out an evaluation of energy fluxes measured at the site gauge, whereas others use distributed models for extrapolating the fluxes in the complex topography. In the first set of case studies, the assessment of site measurements could lead to a rough understanding of the behavior of the balance equation describing the energy fluxes. However, these assessments have the disadvantage of disregarding the spatial changes of fluxes in distinct areas of the glacier, as the climate station records of energy fluxes reflect only the situation at a specific area in the glacier. Moreover, in some cases, such areas can be affected by temporary changes in snow coverage, so that the gauge information gained cannot be representative of the whole glacier dynamics. Such a point scale analysis disregards the fact that topographic complexity may affect some components of the energy balance equation (Rabatel *et al.*, 2013). In complex topography, the main variability on energy fluxes are expected for albedo and the diffuse component of shortwave and longwave incoming radiation (Hock and Holmgren, 2005).

All studies listed in **Table 7.1** warn about the pattern of the retreat of the tropical glaciers which incur clearly a generalized loss of mass. However, the causes of this common problem seem to be different. For instance, (Favier *et al.*, 2004b) suggest that there are different climatic factors which drive the melting and ablation processes depending on whether the glaciers are located either in the inner or in the outer tropics. In addition, it is important to consider that the current study results show that the mass balance is influenced by different climatic factors in each season (Juen, 2006; Winkler *et al.*, 2009; Sicart *et al.*, 2011; Gurgiser *et al.*, 2013). Fact is that the meltwater reductions in tropical glaciers are more pronounced in the dry season and can lead to

Table 7.1. Energy balance studies made in the tropical Andean glaciers

Glacier Name	Analyzed period	Author	Location	Type of data/model	Maximal elevation and glacier area
Zongo	29.03.1996 to 01.10.1997	(Wagnon <i>et al.</i> , 1999)	Bolivia Cordillera Real	Analysis of direct measurements	Elevation max: 6000 m.a.s.l. Area: 2.4 km ²
Zongo	1997 /1998	(Wagnon <i>et al.</i> , 2001)	Bolivia Cordillera Real	Analysis of direct measurements	Elevation max: 6000m.a.s.l. Area: 2.4 km ²
Zongo	1999/2000	(Sicart, 2001)	Bolivia Cordillera real	Analysis of direct measurements	Elevation max: 6000 m.a.s.l. Area: 2.4 km ²
Zongo	1999/2000	(Sicart <i>et al.</i> , 2011)	Bolivia Cordillera real	A distributed model of energy balance	Elevation max: 6000 m.a.s.l. Area: 2.4 km ²
Zongo	11-30.05.2006 and 18.11 to 7.12.2006	(Vuille <i>et al.</i> , 2008)	Bolivia Cordillera real	Analysis of direct measurements	Elevation max: 6000 m.a.s.l. Area: 2.4 km ²
Charquini	14.05.2002-15.07.2003	(Lejeune <i>et al.</i> , 2007)	Bolivia Cordillera Real	Coupled ISBA/CROCUS Model	Elevation max: 5392 m.a.s.l. Area: 5 km ²
Antizana 15	06.95 to 12.2002	(Francou, 2003)	Ecuador	Analysis of direct measurements	Elevation max: 5760 m.a.s.l. Area: 0.71 km ²
Antizana		(Favier <i>et al.</i> , 2004)	Ecuador	Analysis of direct measurements	Elevation max: 5760 m.a.s.l. Area: 0.71 km ²
Artesonraju	08.2004	(Winkler <i>et al.</i> , 2009)	Peru Cordillera Blanca	Measured sublimation	Elevation max: 5800 m.a.s.l. Area: 5.7 km ²
	04.12.2005	(Winkler <i>et al.</i> , 2009)		Sublimation Model ITGG	Elevation max: 5800 m.a.s.l. Area: 5.7 km ²
Artesonraju	04.2004-03.2005	(Juen, 2006)	Peru Cordillera Blanca	Measured data	Elevation max: 5760 m.a.s.l. Area:5.7 km ²
Shallap	08.2006-08.2008	(Gurgiser <i>et al.</i> , 2005)	Peru Cordillera Blanca	A distributed model of energy balance	Elevation max: 5800 m.a.s.l. Area: 7km ²
Shallap	09.2006-08.2008	(Gurgiser <i>et al.</i> , 2013)	Peru Cordillera Blanca	A distributed model of energy balance	Elevation max: 5800 m.a.s.l. Area: 7km ²
Shallap	1980-2013	(Maussion <i>et al.</i> , 2015)	Peru Cordillera Blanca	Reanalysis data DownGlacier Model	Elevation max: 5800 m.a.s.l. Area: 7km ²

a decrease of the average discharge of up to 30% for the glaciers in la Cordillera Blanca (Baraer *et al.*, 2012).

The seasonality of the climate of the inner and outer tropics (see upper and middle panel of **Figure 7.1**) is described by Kaser and Osmaston (2002). As already pointed out in a previous section, within the tropics, the annual variation of temperature is very small, however, this variation increases slightly in the south towards the Tropic of Capricorn. Nevertheless, the changes of temperature over the whole year are not enough to make a distinction of a proper summer and winter, as is the case in the mid-latitudes (lower panel, **Figure 7.1**). The moisture has a bigger and more differentiated variation which marks the named two zones within the tropics.

7. Energy Balance in Tropical Glaciers

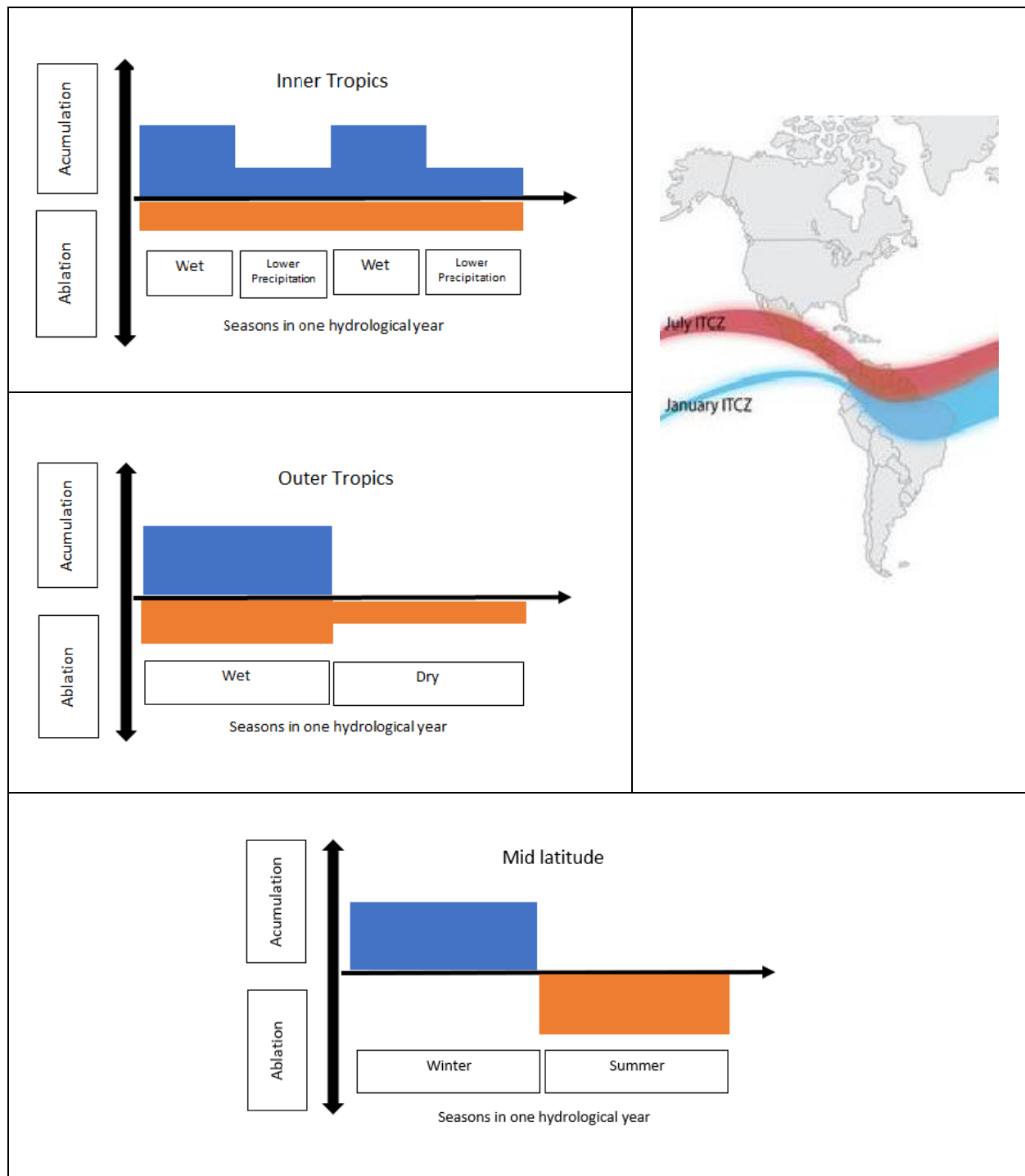


Figure 7.1. Inner (upper panel) and outer (middle panel) tropics glaciers-regime, mid latitude glacier-regime (lower panel) and the seasonal differences of the location of the ITCZ (right panel). Figure based on (Kaser and Osmaston, 2002)

The regime in the inner tropics: in these zones, precipitation occurs during the whole year, but with a decreased intensity twice a year, which corresponds to the two movements of the Intertropical Convergence Zone (ITCZ). The glacier regime is influenced by tropical conditions during the whole year. The small variation of temperature leads to constant ablation during the hydrological year. Although accumulation is presented during the entire year, the amount of

7. Energy Balance in Tropical Glaciers

accumulation is reduced in two periods according to the annual cycle of the ITCZ. To this regime belongs the glacier Antizana glacier in Ecuador. In the outer tropics: in this zone, there is a dry and a humid period, wherefore the humid period corresponds to the occurrence of the ITCZ. The regime is partially influenced by tropical conditions, but subtropical climate can also characterize the dry season. In the outer tropics, the ablation is presented during the whole year due to low variation of the annual temperature; however, lower net radiation may reduce ablation rate in the dry period. The outer tropics are considered as a transition between the tropics and the mid-latitudes. To this regime belong the glaciers Zongo, Chacaltaya in Bolivia, and Shallap and Artesonraju in the CB Peru.

The generalized retreat, not only in the inner, but also in the outer tropic, could indicate that a particular climatic variable, which is common for all the glaciers there, is responsible for the accelerated mass losses. Pierrehumbert (2005) suggests that it is not illogical to think that temperature could be this variable, due to its high correlation in the horizontal plane. In fact, in Subchapter 3.1.2, correlations of daily temperatures in similar elevation bands above 4500 m.a.s.l., with coefficients ranging between 0.56 and 0.76, were found in some glaciers of la Cordillera Blanca (see **Figure 3.2**). Indeed, the homogeneous gradient of temperature in the high mountains is not comparable to any other climatic variable, like precipitation (see **Figure 3.10**), humidity (see **Figure 3.15**) or wind (see **Figure 3.17**). However, studies made in different locations (see **Table 7.2**) within the tropics reveal that the climatic factors which drive the annual mass balance on those glaciers are different in each location. Therefore, in order to address the same patterns and differences found in such studies in regards to the driving climatic factor controlling seasonality of tropical glaciers, a brief description of the main characteristics of each component of the energy fluxes stated by the previous authors will be shown.

Table 7.2. Some reported energy fluxes in the Andean tropical glaciers

	Antizana	Artesonraju	Shallap		Zongo				Shallap				Zongo					
	Annual figures								Seasonal and monthly figures									
Periodo	3/2002-3/2003	04/2004-03/2005	1980-2013	2006/2008 Site A	2006/2008 Site B	1996/1997	1997/1998	1999/2000	1996-1997	10/2006-04/2007	05/2007-09/2007	10/2007-04/2008	05/2008-08/2008	12/1999	01/2000	07/2000	11/1996-02/1997	05-08/1997
	(Favier <i>et al.</i> , 2004)	(Juen, 2006)	(Mausson <i>et al.</i> , 2015)	(Gurgiser <i>et al.</i> , 2005)		(Wagnon <i>et al.</i> , 1999)	(Sicart <i>et al.</i> , 2002)	(Wagnon <i>et al.</i> , 1999)		(Gurgiser <i>et al.</i> , 2013)				(Sicart <i>et al.</i> , 2011)		(Wagnon <i>et al.</i> , 1999)		
	(W/m ²)								(W/m ²)									
<i>Sinc</i>	239	231	208	211	211		209	211.3		198	215	201	207				196	220
<i>Sref</i>	-116	-110	-112	-86	-116		-137			-122	-90	-142	-106					
<i>Sbal</i>	123	121	96	125	95		72			76	125	59	101	52	26	31		
<i>Linc</i>	272	281	310	274	273		258											
<i>Lsurf</i>	-311	-310	-277	-311	-310		-303											
<i>Lbal</i>	-39	-28	33	-37	-37		-45	-55.5		-25	-53	-29	-49	-32	-6	-82		
<i>QNet</i>	84	92	129	88	58	15.8	48.7	27	16.5	51	72	30	52	19	19	-51	12.7	10.5
<i>QH</i>	21	9	14	13	13	6.1	9.8	21	6	10	21	10	20	2	-2	5	4.4	9.1
<i>QL</i>	-27	-13	-11	-13	-13	-18.1	-11.6	-31	-17.7	-4	-28	-5	-25	-11	-5	-25	-7.3	-30.9
<i>Tf</i>	-6	-4	3	0	0			-10	-11.7	6	-7	5	-5	-9	-7	-21		
<i>QGround</i>			9					2.8		-10	-14	-6	-10				0.8	4.1

Red numbers indicate difference estimations in the energy balance (own calculations) from the original results see (Eqs.5.1 and 5.2), negative values means upward fluxes from the surface.

7.1.1.1 Radiative fluxes

7.1.1.1.1 Shortwave radiation

The annual averages of shortwave incoming radiation (link panel in the **Table 7.2**) vary between 208 Wm⁻² in Shallap Glacier (1980/2013) and 239 Wm⁻² in Antizana (2002/2003). There is a slight decreasing difference between the northern glaciers, for instance Antizana and the southern glacier Zongo. Some main characteristics of the shortwave incoming in the Cordillera Blanca specifically in Artesonraju, are shown by Juen (2006). Her studies indicate that the hourly shortwave incoming has a high variability in a day, however, the daily average of shortwave incoming during the year are relatively constant.

The seasonal figures show slightly lower values for the wet season than for the dry seasons for Shallap and Zongo glacier. The possible trivial seasonal variation of the shortwave incoming is an effect of the cloudy conditions (Sicart *et al.*, 2011). Although the extraterrestrial solar radiation is higher in the wet season, cloudy conditions reduce the possible differences between wet and dry season (Gurgiser *et al.*, 2013).

The annual average of reflected shortwave radiation varies between 86 and 137 Wm⁻², which correspond to Shallap (1999/2000) and Zongo (2006/2008 Site A) respectively. The albedo for Artesonraju glacier is constant in July, but it is variable in March. The variability of albedo in March is explained by the high precipitation of this month. After some days of snowfall, the albedo is reduced and the melting process is enhanced. In this way, the same ablation and accumulation is maintained in this period (Juen, 2006). Seasonal values of shortwave reflected in the Shallap glacier shows more reflection for the wet than for the dry seasons. The albedo plays the main role in controlling melting in the wet season of the inner and outer tropics (Francou *et al.*, 2013).

Table 7.2 shows that shortwave radiation balance is the main source of energy, while the longwave represent and energy sink and turbulent fluxes are very low or null. The annual averages of the shortwave radiation vary, depending on the author and the year, between 72 Wm⁻² (outer tropical glacier Zongo (1999/2000)) and 125 Wm⁻² (outer tropical glacier Shallap (2006/2008 Site A)).

The shortwave radiation budget is the driving factor of melting in the ablation zone of Antizana, Shallap and Artesonraju. However, the seasonal variations of melting seem to be more influenced by shortwave radiation reflected than by shortwave radiation incoming, as the latter is characterized by a very low seasonality. Ablation depends mainly on surface albedo and snow cover which, in turn, depend on the amount of solid and liquid precipitation (Favier *et al.*, 2004; Juen, 2006; Gurgiser *et al.*, 2013). So, the area covered by snow is, therefore, decisive for controlling the melt. This area is determined by the temperature at which precipitation falls as rain or snow. The temperature that divides rain/snow has, therefore, an important effect on the mass balance of the inner tropical glaciers and the Shallap Glacier in the outer tropics (Favier *et al.*, 2004; Gurgiser *et al.*, 2013). Increments of the temperature are expected to raise the E.L.A, even for conditions when increased precipitation occurs (Pierrehumbert, 2005).

The fact that the temperature controls the rain/snow partition, may be an indirect effect of the energy budget, as temperature is the result of a thermal equilibrium on the surface. In addition, humidity and the atmospheric pressure influence the temperature threshold (Jennings *et al.*, 2018), thus these variables may have an effect on the rain/snow phase limit as well.

7.1.1.1.2 Longwave radiation

The annual average of longwave incoming radiation varies between 258 Wm^{-2} and 310 Wm^{-2} which corresponds to the Zongo (1999/2000) and Shallap glacier (1998/2013) respectively. The annual average of longwave emitted radiation varies between 277 and 311 Wm^{-2} .

The longwave radiation balance is in all the cases a sink of energy that varies between -28 to -54 Wm^{-2} (see **Table 7.2**). This energy sinks is major in the Zongo Glacier in the dry season. For the Zongo and Shallap Glacier this major sink in the dry season remains between -49 and -82 Wm^{-2} while in the wet season the longwave radiation balance is reduced and show values between -32 and -6 Wm^{-2} . The longwave radiation balance is determined mostly by the longwave emitted by clouds. A reduced cloudy condition in the dry season and slightly reduced temperatures at the surface generate bigger negative values of longwave balance. However, this effect is more marked in the Zongo Glacier. For Sicart *et al.* (2011), the longwave radiation has a clear seasonality, thus, it can have an effect on the amount of melting. The author states that the reduction of melting during the dry season is caused mainly by the reduction of longwave emission.

Gurgiser *et al.* (2013) and Juen (2006) showed as well the seasonality of the net longwave radiation. Additionally, Gurgiser shows also that the net longwave radiation varies little in regard to the altitude. However, for this author, melting is most restrained by diminished net shortwave radiation than by longwave emission or sublimation. The longwave radiation in the case of the Shallap Glacier only offsets a third and a half part of the energy gain by net shortwave radiation (Gurgiser *et al.*, 2013).

7.1.1.1.3 Net radiation

The annual net radiation prevails over the turbulent fluxes in the tropical glaciers in most of the cases being positive between 15.8 and 92 Wm^{-2} . This net radiation is larger in the Antizana, Shallap and Artesonraju glacier and diminishes for the southern Zongo Glacier (see **Table 7.2**). It has low seasonality, as it is shown in the wet period of the Shallap Glacier (Gurgiser *et al.*, 2013), in which net radiation is less in the wet season than in the dry period, this is caused by more shortwave reflected in the wet season. Contrary, the net radiation can even be negative in the dry season of the Zongo Glacier. In the dry season, there is a diminishing in reflection, however, a reduction of emitted radiation by clouds is more marked in June to August in the Zongo Glacier (Sicart *et al.*, 2011), which facilitates that net radiation can reach negative figures for the same period.

7.1.1.2 Turbulent fluxes of heat:

The turbulent fluxes are a small source of energy or loss in the energy balance during the year. The annual averages of turbulent fluxes fluctuate between -11.7 and 3 Wm^{-2} . The results of the

modelling on the Shallap Glacier and in the Artesonraju showed that they have seasonality. These losses are more significant in the dry season (Sicart *et al.*, 2011; Gurgiser *et al.*, 2013) and it can even be an energy source in the wet season (see **Table 7.2**). For Zongo glacier, in all the cases the turbulent fluxes corresponded to energy sinks.

The Turbulent fluxes exchanges (loses) are mostly larger in the dry season mainly because the gradients of humidity and temperature between the atmosphere and the glacier surface are higher in the dry season. In addition, the wind speed increases in this season favoring this exchanges (Juen, 2006).

7.1.1.2.1 Sensible heat flux

The sensible heat flux in most of the reported studies is a source of energy which annual averages varies between 6 and 21 Wm^{-2} , only in July of 2000, a negative sensible heat flux was reported in the Zongo Glacier (see **Table 7.2**). In the different studies, it can be analyzed that sensible heat flux in the tropical glaciers does not have an appreciable role in the energy balance for melting, as it has in mid-latitude glaciers. For the case of tropical glaciers, it has the effect of offsetting the latent heat flux, and therefore diminishing the sublimation. However, unexpected increments of temperature due to Phenomena such as ENSO, could have a repercussion on the gradients of temperature in the boundary layer and thus in the sensible heat (Wagnon *et al.*, 1999).

The sensible heat is low in the wet season and increases in the dry season. For instance, in the case of Shallap Glacier, this is due to larger vertical gradients of temperature and enhanced wind speeds. But this flux is not relevant for melting process because it occurs when there is a high albedo due to a snow layer covering the surface (Gurgiser *et al.*, 2013)

It was found that the sensible heat is predominantly positive in the energy budget. For instance, in the Zongo and Artesonraju Glaciers, suggesting that the surface boundary layer is almost always in a stable condition (Wagnon *et al.*, 1999). In Artesonraju, negative sensible flux occurs 5% of the hourly measurements when the surface temperature is higher than air temperature Juen (2006).

7.1.1.2.2 Latent heat flux

The annual averages of latent heat flux vary between -11 and -31 Wm^{-2} . These values are presented in Shallap (1980/2013) and Zongo (1999/2000) respectively (see **Table 7.2**). In all the cases, latent flux is a sink of energy. This sink is larger in the dry season as it observed in the reported data from Shallap and Zongo.

The role of sublimation in tropical glaciers should not be underestimated at all. Due to the consumption of energy that sublimation takes, the melting process is restrained when sublimation occurs. As climate change can cause important changes in humidity, it is by these changes in humidity that the glaciers in the outer tropics can be very sensitive to climate change. An increment in atmospheric humidity can considerably reduce the sublimation and, and above freezing, increase melting (Francou *et al.*, 2005).

In addition, it was found that in the tropical glaciers of the Andeans, the negative latent heat flux is presented through the whole year causing sublimation. Positive latent fluxes only occur in 12% of the hours mainly between October to February in Artesonraju (Juen, 2006).

On the other side, one of the differences between inner tropical glaciers and outer tropical glaciers is that in the latter one the role of sublimation could be more important. This is because of the dry air conditions that prevail in the dry season (Kaser and Georges, 1999), which is due to their subtropical influence. Indeed, the authors coincide that the loss of energy caused by latent flux is stronger in the dry season (Kaser and Georges, 1999; Wagnon *et al.*, 1999, 2009; Juen, 2006; Winkler *et al.*, 2009). Wagnon *et al.* (1999) state that the humidity has a very important role in the seasonality of discharge through influencing latent heat flux. The sublimation reduces melting as it was observed in the dry season of the Zongo Glacier. This means that the possible surplus of energy on the surface, with less humidity in the atmosphere than at surface and the surface temperature of 0°C or below, favors sublimation instead of melting. These are typical conditions in the dry season of Zongo. Favier, Wagnon and Ribstein (2004) also consider that the sublimation plays a role in the inner tropics decelerating melting but in contrast to Zongo, the humidity in the Antizana Glacier does not have seasonality and is, therefore, the increments in wind speed the cause of larger exchanges of latent flux in the dry season.

Winkler *et al.* (2009) made a study of sublimation in Artesonraju. This author quantified that sublimation consumed 10 -15% of the energy available for ablation during the wet season and 60-90% during the dry season. Low humidity and high surface roughness favor the transition from ice to vapor.

However, it seems that the importance of the sublimation is minor in the Shallap than in the Zongo Glacier. Although, the Shallap Glacier is also located in the outer tropics, the turbulent fluxes partially compensate each other in the ablation area, and therefore this fluxes did not significantly alter the radiation fluxes (Gurgiser, *et al.*, 2013; Maussion *et al.*, 2015).

7.1.1.3 Conductive heat flux from/into the ground and rain fluxes

According to Wagnon *et al.* (1999), in the Zongo Glacier, the conductive heat flux in the snow/ice was unimportant in the wet season. The results of the energy balances in Shallap Glacier revealed that the mean ground heat flux was always negative and with a small magnitude. However, the maximal magnitudes of the ground heat flux were close to those of the turbulent fluxes in the lower parts of the glacier. The downscaling made by Maussion *et al.* (2015) indicated that conductive flux was positive in the same glacier.

Reports and discussions about the effects of rain fluxes are scarce. Juen (2006), for instance, neglected precipitation as a source of energy since, notwithstanding that it can fall as rain in the lower sections of the tongue of Artesonraju, its intensities are weak and the rain temperatures are close to 0 °C.

7.1.2 The drivers of melting processes on tropical glaciers

The studies on tropical glaciers focus on finding physical explanations of the seasonal and interannual variability of their mass balances. Most studies hint of a trend of a common pattern of dynamics leading to glaciers' retreat and these are related to whether glaciers are located in

the inner or outer tropics. However, the results of these studies indicate that this pattern is not clear enough to establish categorically which are the major climatic factors and physical processes that lead to the variability of glacier ablation for each case.

What are the main climatic parameters which control the mass balance and its seasonality in the tropical glaciers?

For most studies there is the common conclusion that the net radiation, namely, its contribution from net shortwave radiation, is the main source of energy for melting in the ablation zone, with the albedo as the major influencing parameter. There are differences though with regard to which parameters affect the albedo. In the case of most northern glaciers, the so-called inner tropic glaciers, the temperature plays a stronger role in the glacier dynamics, as it regulates the liquid and solid phase of precipitation and, consequently, the area where snow fall, which reduces the rate of melting. However these statements are true only white glaciers, while debris covered glaciers show different energy fluxes dynamics (Francou *et al.*, 2013)

This influence is not explicit in the outer tropic glacier with a more subtropical climate, such as the Zongo glacier. There, indeed, the solid precipitation extends over the whole glacier which so retains melting in the dry season, producing a reduction of melting and discharge. However, it cannot completely ruled out neither that the temperature is not a determining variable in outer tropics glaciers, as it appears to be the case for the Shallap glacier, where it was shown that the temperature can also have an important influence on albedo by controlling the solid-liquid phase of precipitation (Gurgiser *et al.*, 2013).

In Zongo glacier, the effects of temperature are felt through the humidity. The latter is an important climatic factor which controls and enhances the sublimation (Kaser and Georges, 1999; Wagnon *et al.*, 1999), which so constitutes a more important physical process in this subtropical environment. This also occurs in the tropical glacier of Kilimanjaro where sublimation dominates ablation (Mölg *et al.*, 2008). However, some studies contradict previous conclusion and state that the role of sublimation is not as important as that of the longwave fluxes (Sicart, 2011), because the latent flux and sensible heat offset each other (Favier *et al.*, 2004; Gurgiser *et al.*, 2013; Maussion *et al.*, 2015). The marked seasonality of longwave radiation fluxes and the critical reduction of the sky emission in the dry season is for (Sicart *et al.*, 2011) the cause of the extreme abatement of melting in the dry season of the Zongo glacier. This research reports also that 60% of the radiation-fluxes exchange in the dry season is due to longwave radiation losses.

For Zongo glacier, where liquid precipitation almost never occurs, it is the amount of snowfall and not the temperature which determines the snowline (Favier *et al.*, 2004b). This is also supported by Francou (2003) who attribute seasonal variations of the latter in the Chacaltaya Glacier in Bolivia to changes of precipitation and humidity. Although this author found a correlation between reanalyzed temperatures on interannual timescales with the mass balance of Chacaltaya, he explains this with the interrelation of temperature with other climatic variables, such as humidity.

Despite of the different results from previous studies regarding the seasonal climate drivers, especially in the glaciers of the outer tropics, the retreat and mass loss is a common problem

affecting all tropical glaciers. Increments of annual temperature along the Andes show a direct negative correlation with mass balances (Francou *et al.*, 2013). However, because of the different results from the aforementioned studies, one must put forward the idea that increments on temperature may have different mechanisms which can act directly or indirectly with local climatic factors that, in turn, influence mass balances. For instance, the strong sensitivity of glaciers to minimal changes of temperature gradients determines the phase of precipitation and, thus, albedo, while the temperature influences also the humidity and, therefore, has an indirect influence on threshold temperatures (Jennings *et al.*, 2018) and sublimation (Francou *et al.*, 2005) and so, eventually, on glacier mass loss.

The statements above indicate that more studies are required to investigate the spatial and temporal dynamics of energy fluxes and the role of other climatic variables in tropical glaciers. Thus, this theme constitutes an ample study field, as the state of research shows that many aspects are not still clear, for instance, the outlined differentiated glacier pattern of seasonal climate drivers in the glaciers located in inner and outer tropics (Favier *et al.*, 2004b). The physics of tropical glaciers requires a better understanding and more case studies should be carried out for building a detailed baseline of the dynamics of these ecosystems affected by global climate change.

7.1.3 The effect of ENSO on tropical glaciers

There is now sufficient evidence that the climate variability in the central Andes and specifically that in the glacier is associated with the El Niño Southern Oscillation (ENSO). Therefore, the study of the climatic factors and physical processes involved in the mass balance of the tropics cannot disregard the influence that the ENSO phenomenon has on them. The relation of this phenomenon with the variability of the mass balance in tropical glaciers has been studied by (Ribstein *et al.*, 1995; Arnaud *et al.*, 2001; Wagnon *et al.*, 2001; Francou *et al.*, 2000, 2004, 2005; Vuille *et al.*, 2008; Vuille *et al.*, 2008b; Veettil *et al.*, 2014; Maussion *et al.*, 2015). The different observations on the glaciers of Los Andes Cordillera indicate a high correlation of ENSO with the mass balances.

On the one hand, El Niño in the Andean high mountains is usually related to temperature increments and precipitation deficits. This leads to predominantly negative mass balances anomalies. On the other hand, la Niña which is characterized by increments on precipitation leads to slightly positive or neutral mass balances anomalies. It was found a negative correlation of the mass balance of the Antizana, Shallap, Chacaltaya glaciers with tropical SSTA of El Niño 4 Chacaltaya Glacier (Francou, 2003) found that the best predictor for mass balance was the SSTA in El Niño1+2 region during the spring and early summer with a lag of two months.

But the general relation pattern of ENSO with mass balance is not totally uniform in the tropical zone, especially since 1980 (Vuille *et al.*, 2008b). Some break-down periods which do not follow negative/positive mass balance with El Niño/La Niña are presented in **Table 7.3**.

The years in the **Table 7.3** differ from the typical pattern of mass balance expected by the occurrence of the El Niño phenomenon. Some explanations to this behaviour are the major influence of anomaly precipitation from this phenomenon. The possible changes produced by the ENSO in the upper tropospheric zone determine the amount of snowfall during the wet season,

Table 7.3. Reported ENSOs and mass balance signals in the Andean glaciers

Location	Year	SST signal	Mass balance signal	Author
Central Andes	1972/1973	El Niño (wet)	Not reported. But amount and sign of Altiplano rainfall anomalies are highly dependent on location of zonal winds.	(Garreaud and Aceituno, 2001)
Cordillera Blanca	1979/1980	El Niño (weak)	Most negative mass balance	(Vuille <i>et al.</i> , 2008)
	1982/1983	El Niño second largest	Mass balance near average	(Vuille <i>et al.</i> , 2008)
	1993/1994	Neutral conditions	Strongest positive mass balance	(Vuille <i>et al.</i> , 2008)

but this effect is especially unstable and oscillates latitudinal along the subtropics producing breakdowns in the typical response to ENSO (Vuille *et al.*, 2008). ENSO is different in terms of the spatial pattern of SST anomalies in the Pacific, determining the upper-level wind anomalies

thereby shifting precipitation anomalies away from their typical location (Garreaud and Aceituno, 2001). However, “these breakdown periods” 1983 and 1994 were not found by Maussion *et al.* (2015) in the studies made on the Shallap Glacier. Other studies found that the periods with less systemic respond to ENSO were between 1992-1995 and 2001-2005 (Rabatel *et al.*, 2013; Maussion *et al.*, 2015). While the temperature anomalies seem to be the same along the Andes, the anomalies in the precipitation seem to have more variability. This is shown in some studies in which El Niño presented wet conditions. For instance, Salzmann *et al.* (2013) and Perry *et al.* (2014) found a Niño/wet signal in the Cordillera Vilcanota south of the Cordillera Blanca. Ronchail and Gallaire (2006) reported opposite ENSO effects within short distances with a Niña/dry signal in the Zongo valley lowlands and a Niña/wet signal on the higher Altiplano (Maussion *et al.*, 2015). The signals of ENSO are stronger in low altitudes although in high altitudes remains detectable.

Another important aspect found was that the ENSO effect has a lag of three months (Francou *et al.*, 2004) to four months (Rabatel *et al.*, 2013) in the case of Antizana. This lag explains the occurrence of the largest differences in mass balances between two phases of ENSO from February to May. The temperature anomalies are a very important mechanism by which mass balances are affected in the inner tropics (Francou *et al.*, 2004). Lags of two months on the effect of ENSO on temperature on glaciers of the CB were also found in the present in section 3.1.1.3. Lags of increments of precipitation between 2 to 4 months and decrements between 6 to 10 months are shown in section 3.1.2.3.

All these findings point out that the specific causality of ENSO on the climatic factors that governs mass balance is not systematic in the inner and outer tropics. For instance, in the Antizana Glacier, the cause of the negative mass balances during the El Niño period is the increment of temperature and less precipitation (Francou *et al.*, 2004). The increment of temperature favors rain over snowfall and thus, a reduction of the accumulation and less albedo. In addition, there is a reduction of the amount of precipitation enhancing the effect of maintaining low albedo (Favier *et al.*, 2004; Francou *et al.*, 2004; Rabatel *et al.*, 2013). Less cloudy conditions represent an increment of solar radiation. In addition, a reduction of the normal winds in El Niño favors melting over sublimation. All these conditions lead the energy balance to increase the melting process. In la Niña, opposite conditions prevail such as reduction of temperature and increments in the amount of precipitation which lead to an increase of albedo, and an increase of the effect of wind which favors sublimation and thus retaining melting. In addition, cloudy conditions reduce

the shortwave incoming radiation. Therefore, the mass balances in the La Niña period are mostly positive to neutral. In the case of the Cordillera Blanca and the glacier in Bolivia, it was stated that the climatic factors linking to ENSO are anomalous tropospheric flow from westerly (El Niño) and easterly (La Niña), produced by changes in the temperature gradient between the tropics and mid-latitudes. These changes affect the moisture influx and generate dry /wet conditions in El Niño/La Niña. It is also known that these changes are stronger in the southern tropical glaciers, such as Zongo or Chacaltaya (Vuille *et al.*, 2008). Furthermore, it was found that ENSO influences sensible heat flux to a certain extent (Vuille *et al.*, 2000; Lozano and Koch, 2014; Maussion *et al.*, 2015). However, it is not clear regarding longwave radiation or sublimation (Maussion *et al.*, 2015), notwithstanding that it should be expected that changes in atmospheric temperature have an effect on longwave incoming radiation.

7.2 Modelling Mass Balances and Discharge with Energy Balance Fluxes in the Artesonraju glacier and the Basin of Artesoncocha

7.2.1 General overview and approach

This sub-chapter presents the methodology and the results of modelling the mass balance of the glacier Artesonraju, and the ensuing discharge of the glaciated basin of Artesoncocha. For this purpose, the energy balance model of Hock (1998) is used. It is a distributed model, applied, in this case, on a daily time scale to the time period between 24.08.2004 and 31.12.2007, as some variables were available only on this scale and time period. In the first part, the methodology and parameterization applied to the model is presented, whereas in the second part the results of the simulations for each hydrological year are shown.

The energy model allows calculating the specific mass balance and discharge by estimating firstly the amount of melting derived from the interaction of the energy fluxes at the glacier's surface. The energy gained is used for fusion of the ice or the snow to water when the surface temperature is 0°C or above. Another considered state of water change by the model is sublimation. Sublimation is estimated always when there is a loss of latent heat from the surface. In the case of gains of latent heat at the glacier's surface, condensation and refreezing /deposition are obtained.

The calculation of the mass balance of the glacier considers the accumulation, deposition, fusion, sublimation and condensation in each grid, in other words, the specific feeding and loss of the Artesonraju glacier (3.2 km²) that belongs to the Artesoncocha basin (7 km²). The calculation of the discharge takes into account not only the Artesonraju glacier area, but also the melting of snow zones from other nearby snowcapped mountains as well as runoff of some areas devoid of snow that contribute to inflow to the Artesoncocha Lake (see **Figure 2.2**).

7.2.2 Methodology and parameterization

First of all, the focus will be on the computation of each component of the energy balance equation, how each flux is calculated and which parameters are considered. Afterwards, it will be explained how this energy is related to melting and how it is converted in water equivalent for the reckoning of discharge and the specific mass in the glacier.

The energy balance model (EBM) which will be described as follows was developed by Hock (1998) is based on the energy balance equation 5.1 and stated again here in modified form:

$$Q_M = Q_N + Q_{HS} + Q_{HL} + Q_P + Q_G \quad (7.1)$$

where:

Q_M is the energy flux available for melting in Wm^{-2}

Q_N is the net radiation in Wm^{-2}

Q_{HS} is the flux of sensible heat in Wm^{-2}

Q_{HL} is the flux of latent heat in Wm^{-2}

Q_P is the heat flux from precipitation in Wm^{-2}

Q_G is the subsurface energy flux in Wm^{-2} .

These flux-variables will be discussed in detail in the following sub-sections. As notation, the downward fluxes towards the surface are considered positive (input gain) and those upward from the surface negative (loss).

7.2.2.1 Net radiation

The net radiation (Q_N) is the sum of net shortwave radiation and net longwave radiation fluxes

$$Q_N = (Sw_{inc}^{\downarrow} + Sw_{ref}^{\uparrow}) + (Lw_{inc}^{\downarrow} + Lw_{sufc}^{\uparrow}) \quad (7.2)$$

where

Sw_{inc} is the incoming shortwave radiation from the atmosphere (Wm^{-2})

Sw_{ref} is the shortwave radiation reflected by the surface (Wm^{-2})

Lw_{inc} is the longwave radiation incoming from the atmosphere (Wm^{-2})

Lw_{suf} is the longwave radiation emitted by the surface (Wm^{-2})

7.2.2.1.1 Shortwave radiation

The incoming shortwave radiation Sw_{inc}^{\downarrow} , also called global radiation G , is the sum of the direct radiation I and the diffuse radiation D .

The reflected shortwave radiation Sw_{ref} is due to the albedo of the surface. Thus, the net shortwave radiation is calculated as:

$$Sw_N = (1 - \alpha) Sw_{inc}^{\downarrow} = (1 - \alpha) (I + D) \quad (7.3)$$

where

I is the direct radiation

$D = D_s + D_t$ is the diffuse radiation, as the sum of the portions that come from the sky (D_s) and from the adjacent terrain (D_t).

Direct radiation I:

The calculation of the potential radiation for clear sky conditions (I), Eq. 7.4, takes into account the following aspects:

- scattering, reflection and absorption of the solar beam by the atmosphere's transmissivity,
- inverse relation between solar radiation and atmospheric pressure,
- variation of the path length with the sun's altitude by means of local zenith angle.

$$I = I_0 * \left(\frac{r_m}{r}\right)^2 * \Psi \left(\frac{p}{P_0 / \cos Z}\right) * \cos Z \quad (7.4)$$

where

I_0 is the solar constant (=1368 Wm⁻²)

r is the distance between the earth and the sun (m refers to the mean)

Ψ is the transmissivity

p is the atmospheric pressure which depends on elevation h through the barometric formula

p_0 is the standard atmospheric pressure and

Z is the zenith angle

The transmissivities Ψ used in the current simulations are taken from the study of Baigorria *et al.* (2004) on seasonal transmissivities in Peru, and vary between 0.5 in the warm/rainy season and 0.6 in the cold/dry season.

The zenith angles Z are calculated according to (Oke, 1987) cited by Hock (2013) as:

$$\cos Z = \sin \Phi \sin \delta + \cos \Phi \cos \delta \cos h \quad (7.5)$$

$$\delta = -23.4 \cos [360^\circ (t_j + 10) / 365] \quad (7.6)$$

$$h = 15(12 - t) \quad (7.7)$$

where

Φ is the latitude

δ is the solar declination

h is the hour angle

t_j is the Julian date

t is the local apparent solar time

In addition, topographic conditions for the calculation of the direct radiation I are taken into account by the model by incorporating the slope and the exposition of the plane in each grid. Thus, the radiation on the slope of a plane is calculated as:

$$I_{slope} = I * \cos \theta / \cos Z \quad (7.8)$$

where

θ is the angle of incidence between the normal to the slope and the solar beam

$$\cos \theta = \cos \beta \cos Z + \sin \beta \sin Z \cos(\Omega - \Omega_{slope}) \quad (7.9)$$

where

β is the slope angle

Ω is the solar azimuth angle

Ω_{slope} is the slope azimuth angle

Diffuse radiation:

For estimation of the diffuse component of shortwave incoming radiation, two methods are used:

The first one is a procedure which determines the portion of the direct radiation from the measured global radiation at a climate station. In this way the portion of the diffuse radiation is easily deducted. The direct portion is invariant in the whole area at an estimate time, contrary the diffuse has certain variability. Therefore, the diffuse component is extrapolated to other parts of the glacier. This extrapolation takes into account sunny and shadow conditions by using the ratio of measured global radiation and calculated clear sky solar radiation at the climate station.

With the use of the global radiation measured at the climate station and the radiation calculated for conditions without any cloud cover (potential clear sky radiation, I), it is possible to estimate, in a specific moment, how much diffuse radiation exists. The ratio between global radiation G and direct radiation I allows to determine for example, whether diffuse radiation from the sky D_s and the surrounding terrain D_t are incrementing the potential solar radiation or if, on the contrary, shade (also from clouds or terrain) diminish the amount of radiation.

Consequently, four circumstances are presented in order to estimate global radiation for the distributed grids (Hock and Tijn-Reijmer, 2012). These are:

- 1) when the location of both climate station and grid which is going to be extrapolated, is under the sunlight,
- 2) when both are shaded,
- 3) when the location of the climate station is under the sun while the extrapolated grid is in the shade or
- 4) when the climate station is in the shade and the grid is under the sun

A more detailed description of the calculations is presented in **Table 7.4**.

The second method for estimating diffuse radiation uses a calculation of radiation from sky and from adjacent terrain.

The total diffusive radiation D is

$$D = D_s + D_t \quad (7.10)$$

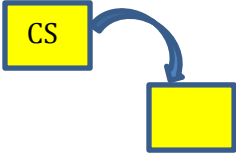
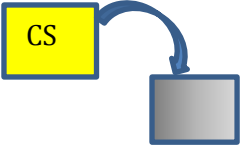
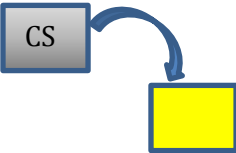
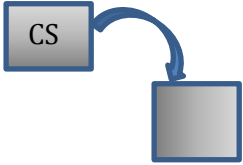
and is the sum of the diffusive radiation D_s that comes from the sky and of D_t that comes from the terrain. D_s is computed as:

$$D_s = D_0 S_f \quad (7.11)$$

where

D_0 is the diffuse radiation from an unobstructed sky (Wm^{-2}) and S_f , is the sky view factor indicating the portion of the visible sky of an element. This was calculated for each grid, with the program of Zakšek, Oštir and Kokalj (2011).

Table 7.4. Conditions for calculating diffuse radiation in the Energy Balance Model (Hock and Tijm-Reijmer, 2012)

Sunny and shade conditions	Characteristics	Calculation
<p>Both, climate station and grid are under the sun</p> 	<p>The location under the sun of both grids: In this case, the portion of diffuse radiation at the climate station and the extrapolated grid is similar. Thus, the ratio of global radiation and potential clear sky radiation at the climate station will probably be the same as the one in the extrapolated grid. As the direct radiation in the grid can be calculated, this is affected in the same way as the climate station.</p>	$G_{grid} = I_{grid} \left(\frac{G_{cs}}{I_{cs}} \right)$ <p style="text-align: right;">(7.12)</p>
<p>Grid to be calculated is in the shade</p> 	<p>There is only diffuse radiation at the grid. Then, global radiation is estimated as a fixed percentage of the clear sky radiation. This percentage was assumed to be 10% according to an empirical equation of diffuse radiation by Hock (1998).</p>	$G_{grid} = I_{grid} (\%10)$ <p style="text-align: right;">(7.13)</p>
<p>Climate station is in the shade and the grid is under the sun</p> 	<p>Global radiation measured at the climate station is only diffuse radiation. The clear sky radiation calculated at the grid is affected by the last ratio of global radiation and clear sky radiation at the climate station just before this came to shade.</p>	$G_{grid} = I_{grid} \left(\frac{G_{cs0}}{I_{cs0}} \right)$ <p style="text-align: right;">(7.14)</p>
<p>Both, climate station and grid are in the shade</p> 	<p>When both grids are in the shade, the global radiation measured at the climate station is diffuse and is taken invariant for the extrapolated grids.</p>	$G_{cs} = G_{grid}$ <p style="text-align: right;">(7.15)</p>

The diffusive radiation from the surrounding terrain D_t is computed as

$$D_t = \alpha_m G (1 - S_f) \tag{7.16}$$

where α_m is the mean albedo of the surrounding terrain and the other variables are as defined. Since D_t depends on the local sky view factor of a slope element, it is variable across the grid.

There has been much research and debate how to estimate or to compute D and/or D_o (e.g. Hock, 1998). When measurements of the global radiation G at a climate station are available, Hock (1998) proposed an empirically corroborated relation of the diffuse radiation D to the global radiation G or (SW_{inc}):

$$\frac{D}{G} = \begin{cases} 0.15 & : \frac{G}{I_{ToA}} \geq 0.8 \\ 0.929 + 1.134 \frac{G}{I_{ToA}} + 5.111 \left(\frac{G}{I_{ToA}}\right)^2 + 3.106 \left(\frac{G}{I_{ToA}}\right)^3 & : 0.15 < \frac{G}{I_{ToA}} < 0.8 \\ 1 & : \frac{G}{I_{ToA}} \leq 0.15 \end{cases} \quad (7.17)$$

where I_{ToA} is the radiation at the top of the atmosphere (which is equal to the solar constant affected by the instantaneous and the mean solar earth distance and the cosine of the zenith).

Eq. (7.17) shows clearly how the ratio D/G increases with the decrease of G due to cloud cover and vice versa. Using Eq. (7.17), the total D for a measured G can be computed and, employing $D=D_s + D_t$, with D_t known by Eq. (7.16), $D_s=D-D_t$, i.e. $D_o=D_s/S_f$. With this computed D_o at the climate station (which it is invariant for the whole area), D for an arbitrary grid element is estimated by the sum of Eqs. (7.11) and (7.10) and using the appropriate sky view factor S_f in these equations.

Albedo:

For the current simulations, corresponding albedos are allocated for each surface type. The considered surface types are areas covered with snow, ice, firn, and rock (no values in table) for which the corresponding albedo ranges are listed in **Table 7.5** (Cuffey and Paterson, 2010)

Table 7.5. Typical albedo ranges for glacier surfaces.

Surface Type	Recommended	Minimum	Maximum
Fresh dry snow	0.85	0.75	0.98
Old clean dry snow	0.80	0.70	0.85
Old clean wet snow	0.60	0.46	0.70
Old debris-rich dry snow	0.50	0.30	0.60
Old debris-rich wet snow	0.40	0.30	0.50
Clean firn	0.55	0.50	0.65
Debris-rich firn	0.30	0.15	0.40
Clean ice	0.35	0.30	0.46
Debris rich ice	0.20	0.06	0.30

The changes of the surface type of the grids around the ELA are very important as they define how the glacier behaves. These changes are calculated from the initial surface maps at the beginning of the hydrological year and the initial conditions of the gains and losses of the surface at the start day of the simulation period. The snow area is determined by the solid precipitation according to threshold temperature rain/snow precipitation. The ice area, located below the

ELA, is the area with bare ice after the snow cover has melted away, and the firn area, above the ELA, is that area which is free of snow.

The meter water equivalent map defining the initial conditions at the start day of the simulation are taken from field data of the mass balance (up to the start day) and interpolated to the whole basin with ordinary kriging.

7.2.2.1.2 Longwave net radiation

The net longwave radiation (LW_N) is calculated as

$$LW_N = LW_{linc}^{\downarrow} + LW_{surf}^{\uparrow} \quad (7.18)$$

with

Longwave incoming radiation LW_{linc}^{\downarrow}

$$LW_{linc}^{\downarrow} = LW_{lincs} + LW_{linct} \quad (7.19)$$

describing the sum of the longwave radiation that comes from the sky, LW_{lincs} , and from the adjacent terrain, LW_{linct} .

LW_{lincs} from the sky (Wm^{-2}) is estimated by:

$$LW_{lincs} = L_0 S_f \quad (7.20)$$

where L_0 is the sky irradiance from an unobstructed sky (Wm^{-2}) and S_f is the sky view factor. L_0 is calculated at the climate station, as follows: $LW_{lincs} = LW_{linc}(measured) - LW_{linct}$ and $L_0 = LW_{linc}/S_f$. L_0 is then used invariant for the whole grids. S_f which is different in each grid, shows the portion of the visible sky and is calculated with the program of Zakšek, Oštir and Kokalj (2011).

The longwave radiation that comes from the terrain, LW_{linct} , is based on a parameterization Plüss and Ohmura (1997), and discussed further by Hock (1998), which considers the part of the sky which is obstructed, the air temperature, and the temperature from the emitting surface. More specifically, LW_{linct} (Wm^{-2}) is computed as:

$$LW_{linct} = (1 - S_f) \pi s r (L_b + a T_a + b T_s) \quad (7.21)$$

where:

L_b is the emitted radiance of a black body at $0^\circ C$ ($=100.2 Wm^{-2}sr^{-1}$),
 a, b are constants ($a= 0.77 Wm^{-2}sr^{-1}C^{-1}$ and $b=0.54 Wm^{-2}sr^{-1}C^{-1}$)
 T_a and T_s are the temperatures of the atmosphere and surface respectively.

Longwave outgoing radiation emitted by the surface LW_{surf}^{\uparrow}

from the surface calculated for each grid which is computed as :

$$LW_{surf}^{\uparrow} = \varepsilon \sigma T_s^4 \quad (7.22)$$

where:

ε emissivity of the surface

σ Stefan Boltzmann constant ($5.67 \times 10^{-8} \text{ Wm}^{-2}\text{K}^{-4}$)

T_s surface temperature ($^{\circ}\text{K}$)

At infrared wavelengths snow and ice act as near perfect radiator, with typical emissivity's ε between 0.94 and 0.99 and most of the cases is taken approximately to 1.

The parameterization of the surface temperature T_s is made through the following options:

- Melting conditions are assumed to be at a temperature of 0°C .
- When the energy balance results in a negative value, the surface temperature is lowered, until the energy balance reaches the balance.
- From measurements of longwave outgoing radiation which, are available for the case of the Artesonraju glacier.

7.2.2.2 Turbulent Fluxes of Latent and Sensible Heat

Turbulent fluxes are calculated with two different methods, allowing comparing their results. These two methods are the following:

First method: The sensible heat flux is calculated by means of temperature T and wind speed u as (Escher-Vetter, 1980; Hock and Tijm-Reijmer, 2012):

$$Q_{HS} = 5.7\sqrt{u} * T \quad (7.23)$$

The latent heat flux Q_{HL} is calculated by means of humidity (saturation deficit) and wind speed.

$$Q_{HL} = 5.7\sqrt{u} * 0.623 * \frac{L_v}{p * c_p(e - e_0)} \quad (7.24)$$

where:

L_v is the latent heat of evaporation ($=2.514 \times 10^6 \text{ J kg}^{-1}$) or sublimation ($=2.849 \times 10^6 \text{ J kg}^{-1}$)

c_p is the specific heat of air at constant pressure ($=1005 \text{ J kg}^{-1}\text{K}^{-1}$)

e_0 is the saturation vapor pressure of melting ice ($=611 \text{ Pa}$)

e is the vapour pressure at 2m, i.e. $e_0 - e$ is the saturation deficit

Second method: This method is called the bulk aerodynamic method. It takes into account the differences of temperature, wind speed and vapor pressure between the surface and a certain height in the atmosphere.

The sensible heat flux Q_{HS} is calculated as follows:

$$Q_{HS} = c_p k^2 \frac{\rho_0}{P_0} P * \frac{u_2(T_2)}{\ln(z/z_{ow}) * \ln(z/z_{oT})} \quad (7.25)$$

where

k is the Karman constant (=0.41)

P is the atmospheric pressure (Pa)

ρ_o is the air density at P_o (=1.29 kgm⁻³)

z_{ow} and z_{oT} are the roughness lengths for the logarithmic profiles of wind and temperature and z the instrument height above the surface (2m).

Winkler *et al.* (2009) report some values of roughness lengths of temperature and water vapor between 1 to 10 mm for the Artesonraju glacier.

The latent heat flux Q_{HL} is calculated as

$$Q_{HL} = 0.623 * L_{v/s} k^2 \frac{\rho_o}{P_o} * \frac{u_2(e_2 - e_o)}{\ln(z/z_{ow}) * \ln(z/z_{oe})} \quad (7.26)$$

where

$L_{v/s}$ is the latent heat of evaporation or sublimation depending on which phenomenon is occurring. With a negative latent heat flux, sublimation will, whereas with a positive flux, condensation will occur for positive surface temperatures and deposition for negative ones

e is the vapour pressure

z_{oe} is the roughness length for a logarithmic profile of water vapour.

7.2.2.3 Ground heat flux and rain energy

Subsurface conductive heat transfer is minor if the temperature of the ice or snow is at its melting point (Cuffey and Paterson, 2010). For temperate glaciers (such as Artesonraju), which are characterized by their temperature at or near its pressure-melting point throughout the ice mass (IACS, 2011), the energy ground flux is usually neglected .

The rain energy is calculated as:

$$Q_R = \rho_w c_w R (T_r - T_s) \quad (7.27)$$

where

ρ_w is the density of water (kgm⁻³)

c_w is the specific heat of water (=4179.6 J kg⁻¹K⁻¹)

R is the rainfall rate (msec⁻¹)

T_r is the temperature of rain assumed to be equal to air temperature (°K)

T_s is the surface temperature (°K)

7.2.2.4 Accumulation

The glacier accumulation is calculated from the snowfall. The state of precipitation is calculated using the threshold temperature snow/rain T_0 . Between the temperature interval of $T_0 - 1^\circ\text{K}$ and $T_0 + 1^\circ\text{K}$, the percentage of snow or rain is linearly interpolated.

7.2.2.5 Ablation

The ablation is due to melting and sublimation.

The melting M (units) is calculated as:

$$M = \frac{Q_M}{\rho L_f} \quad (7.28)$$

where

Q_M is the energy flux available for melting in Wm^{-2}

ρ is the water density

L_f latent heat of fusion ($=334000 \text{ Jkg}^{-1}$)

If the latent heat flux is negative, no matter what the surface temperature is, sublimation S is assumed and computed as:

$$S = \frac{Q_L^\uparrow}{\rho L_s} \quad (7.29)$$

where

L_s is the latent heat of sublimation ($=2.849 * 10^6 \text{ J kg}^{-1}$), if the latent heat flux is positive and the surface temperature is $0 / < 0$, condensation /deposition is expected. Deposition is present when the surface temperature is < 0 .

7.2.2.6 Discharge

The glacier model uses the discharge model of Baker *et al.* (1982), which is based on the idea that different surfaces release water at a rate proportional to the storage amount.

The sum of melt and rainfall is converted into discharge using a linear reservoir approach, which is based on the non-stationary water budget equation:

$$dS/dt = R(t) - Q(t) \quad (7.30)$$

where

t is time;

S is storage, expressed as $S = k*Q$ (linear reservoir, with k , the storage coefficient), and R and Q are inflow and outflow into an area, respectively.

A separate linear reservoir model is set up for snow, ice and firn areas, specified by different storage coefficients k .

The computational, integrated version of Eq. (7.31) (Hock, 1998), is then:

$$Q(t_2) = \sum_{i=1}^3 Q_i(t_1) * e^{\frac{-\Delta t}{ki}} + R(t_2) - R_i(t_2) * e^{\frac{-\Delta t}{ki}} \quad (7.31)$$

According to Cuffey and Paterson, (2010), the cyclic input of melting and precipitation generates a cyclic variation of runoff with peak values delayed relative to the time of maximum input. After the input has finished, the runoff declines exponentially with time.

There is some discussion on the choice of the appropriate k -values for the three glacier area types, i.e. snow, ice and firn (e.g. Hock, 1998; Cuffey and Paterson, 2010). In the present

application, the k -values found in the temperature index model for the Artesonraju glacier were tested and applied in the energy balance model.

7.2.3 Model application and evaluation

7.2.3.1 Overview of modelling approach

The period of simulation covers three hydrological years, 2004-2005, 2005-2006 and 2006-2007 and the beginning of the hydrological years 2007-2008. The model is spatially distributed on a grid of 30*30 m and run temporarily on a daily resolution. The day of the beginning of each hydrological year depends on the first day of the mass balance measurements. In order to take into account as much as possible the variability of some parameters for the different seasons, every hydrological year is evaluated in three seasonal periods (see **Table 7.7**). Thus, parameter such as albedos and storage constants discharges were tested for each period in the hydrological year and trends of those parameters for the same periods were analyzed.

The total modelling area consists of two parts (**Figure 2.2**). The first one is the Artesoncocha basin for which the discharge data at the outlet lake is available. In this area, not only the melting of the glacier Artesonraju contributes to the discharge, but also some snow-covered areas of the Piramide, Paron and Caraz peaks and the free ice/snow covered areas. The total outflow of the Artesoncocha basin is considered for the evaluation of the modeled discharge. The second area is specifically the Artesonraju glacier area proper as the main contributor of discharge in that basin, albeit where only calculation of mass balance is considered. Both areas are delimited using the DTM30- model with the help of the SWAT- basin- delimiting submodule (Arnold *et al.*, 2005).

7.2.3.2 Input data

The input required for the Energy Balance Model is listed in **Table 7.6**

7.2.3.3 Main calibration parameters

7.2.3.3.1 Albedo

Initial model simulation trials showed that a particular albedo value could mimic observations well for one period, but not for the others. Therefore, the model was calibrated using seasonal albedos for the three periods discussed (see **Table 7.6**). Albedos were tested according to the characteristics of the different surfaces for each season (see **Table 7.5**).

7.2.3.3.2 Threshold temperature rain/snow (TO)

This parameter is used to determine the solid and liquid precipitation. In the range of one degree below and above the TO, the precipitation is assumed to be a combination of snow and rain, with the percentage of each phase obtained from linear interpolation (Hock and Tijm-Reijmer, 2012).

Table 7.6. Input data for energy balance fluxes model

Data Type	Data	Observations
Climate Data	Temperature	Daily resolution; climate station at 4811 m.a.s.l.; gradient of Temperature 0.65°C/100m
	Precipitation	Daily resolution; climate station at 4836 m.a.s.l.
	Relative humidity	Daily resolution; climate station at 4838 m.a.s.l.
	Wind	Daily resolution; climate station at 4838 m.a.s.l.
	Shortwave radiation	incoming Daily resolution; climate station at 4838 m.a.s.l.
	Shortwave radiation	reflected Daily resolution; climate station at 4838 m.a.s.l.
	Longwave radiation	incoming Daily resolution; climate station at 4838 m.a.s.l.
	Longwave radiation	outgoing Daily resolution; climate station at 4838 m.a.s.l.
	Discharge	Artesoncocha lake outlet, used for calibration/validation
Grid Data	Elevation	DTM30 m
	Glacier and basin area	From DTM calculations using SWAT
	Slope	From DTM calculated using ArcGIS
	Exposition	From DTM calculated using ArcGIS
	Sky view factor	From DTM calculated using SVF program
	Water equivalent	From measurements, interpolated using kriging , using ArcGIS
	Firn and ice area	Delimited at the beginning of the simulation of hydrological year, for calibration and validation period

Table 7.7. Studied simulation periods

Period		Characteristics
2004-2005	(SO) 24 August-03 November	Transition period, beginning of the rainy season.
	(NDJFM) 04 November-07 April	Core of the rainy season and warmest period
	(AMJJA) 08 April-25-August	Dry season, with slight reduction of temperature
2005-2006	(SO) 26 August-30 October	Transition period, beginning of the rainy season.
	(NDJFM) 31 October-07 April	Core of the rainy season and warmest period
	(AMJJA) 08 April-23 August	Dry season, with light reduction of temperature
2006-2007	(SO) 24 August-30 October	Transition period, beginning of the rainy season.
	(NDJFM) 31 October-07 April	Core of the rainy season and warmest period
	(AMJJA) 08 April-27 August	Dry season, with slight reduction of temperature
2007-2008	(SO) 28 August-30 October	Transition period, beginning of the rainy season.
	(AMJJA)31October-31 December	Dry season, with light reduction of temperature.

7.2.3.3.3 Storage constants

A wide range of discharge constants k (Eq. 7.31) were tested, ranging between 20-510 for snow, 50-2500 for firn, and 0-300 for ice. The first exploratory calibration exercises showed optimal results with various values within a large storage range constants even outside the ranges presented in the literature (Lliboutry, 1971). Therefore, the storage constants were tested simultaneously not only for the present simulation with the Energy Balance Model (EBM), but also for the later Temperature Index Model (TIM), to obtain trend values similar for both models.

7.2.4 Results and discussion

The calibration accuracy of the model is measured with the Nash Sutcliffe coefficient (E) and the RMSE of the simulated versus observed discharge. In addition, a comparative analysis of the mass balance with the results provided by the ANA-UGRH has been carried out. Besides, annual

mass balances and the positions of the ELA are also compared to local estimations included in WGMS (2015). All these comparisons with the mentioned data were considered for the calibration of the model and the selection of the most appropriate parameters which will be described in the section 7.2.4.4.

7.2.4.1 Simulated Discharge

Although the discharge is the final outcome of the whole chain of model driving parameters (energy, meteorology, hydrology), it will be discussed first, as it is the ultimate measured parameter on which all other parameters of the model are calibrated.

Table 7.8 shows the performance of the calibrated model for the four hydrological years in terms of the Nash Sutcliffe Coefficient (E) and the RMSE for the fitted discharge. Based on these values, the adjustment goodness is classified in the last column of the table. The lowest E and maximum RMSE are obtained in the year 2005-2006, but the adjustment quality is still considered as good.

The observed and simulated discharge hydrographs for the various years are illustrated in **Figure 7.2**. One may note from the various panels that the model cannot represent well the biggest discharge peaks; especially, in month December 2005-2006 and to a lesser extent, some peaks of October and April of 2004-2005 and 2006-2007. For the hydrological years 2004-2005, 2006-2007 and the months of ASOND of year 2007 the major discrepancy occurs in October. Important bias in the estimation of some minima occurs mainly in the months of January and February 2005-2006, 2006-2007 and 2004-2005. This differences may be a consequence of the disregard of the rapid fluctuations of albedo that could be produced by quick changes in precipitation (Hock, 2010b). However, the characteristic trends of the season are captured by the seasonal albedos, i.e. despite that seasonal albedos are used in the simulation, the performance of the model to simulate the discharge appears to be good enough. In fact, albedo simulations of the present model EBM (Hock and Tijm-Reijmer, 2012) require hourly resolution of the input data, but not all the climate variables are available at hourly resolution in CB, therefore daily albedo could not be simulated. Albedo simulations may be particularly important in the rainy season when the reflection of shortwave radiation varies more strongly over the days. Nonetheless, the use of seasonal albedos to represent the surface characteristics of each station appears to be warranted for calculating the typical average discharge in an acceptable way and, consequently, the amount of water produced by the glacier.

Table 7.8. Statistical measures of the simulated discharge

Year	E	$RMSE(m^3s^{-1})$	Adjustment quality (Cabrera, 2011)
2004-2005	0.86	0.12	Very Good
2005-2006	0.56	0.23	Good
2006-2007	0.60	0.16	Good
2007-2008	0.77	0.13	Very Good

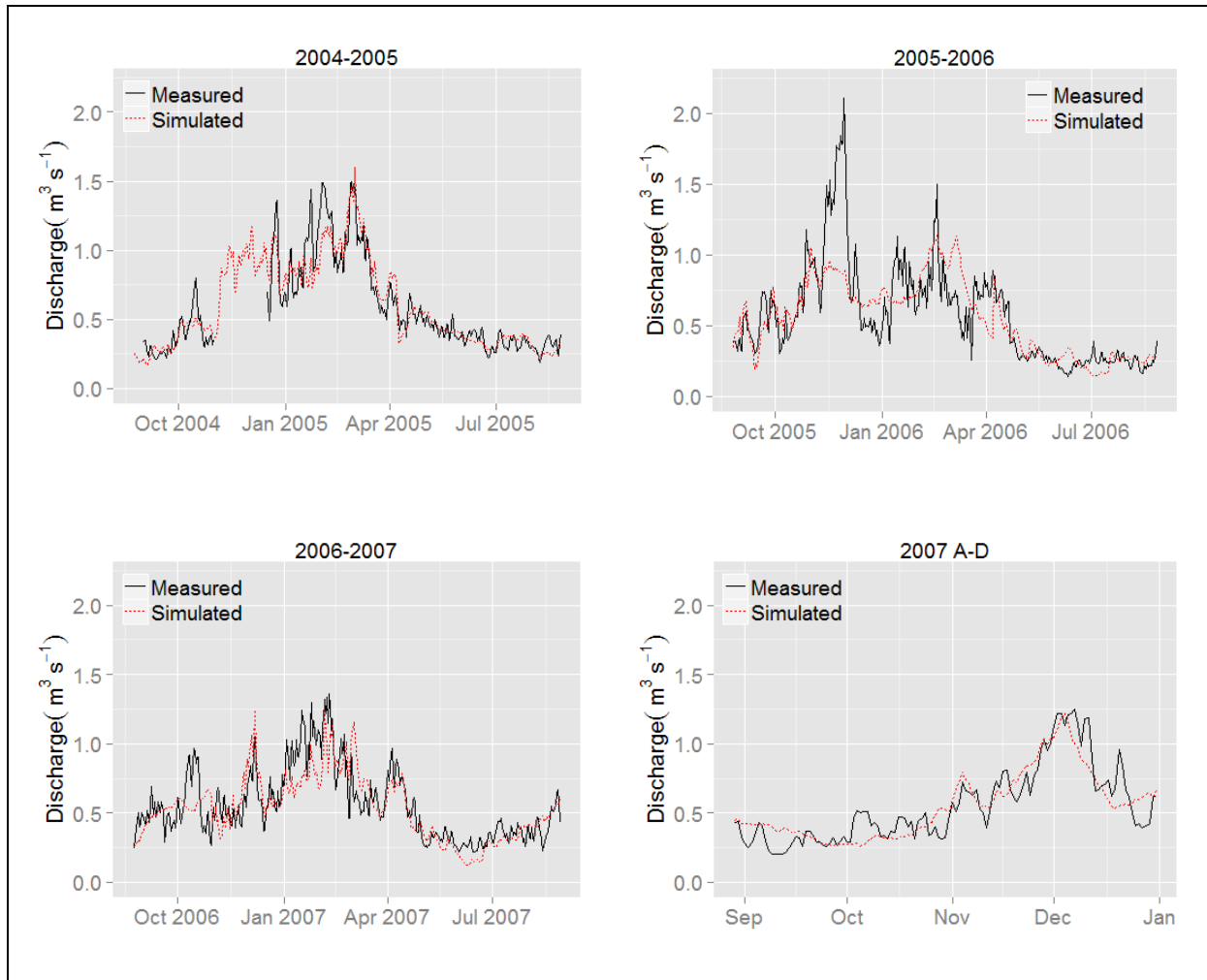


Figure 7.2. Simulated and measured discharge at the outlet of Artesoncocha lake

Furthermore, the best results of E , as listed in **Table 7.8**, were obtained by calculating diffuse and direct radiation separately which correspond to the second method described in the Methodology Section 7.2.2.1. The first method described in that section in **Table 7.4** resulted in values for E of 0.09 for year 2004-2005, 0.27 for 2005-2006, 0.34 for 2006-2007 and 0.44 for year 2007 A-D, i.e. are much lower than those obtained with the second method. Therefore, the latter will not be discussed further in the following sub-sections.

7.2.4.2 Mass balance, mass balance profiles and ELAs

The mass balance is calculated only for the Artesonraju glacier, excluding some snow-covered areas of the Piramide, Paron, and Caraz peaks that also contribute to the discharge, but which do not feed specifically the Artesonraju glacier. The calculation area for the specific mass balance is 3 km², delimited by SWAT with a DTM of 30 m resolution. This area corresponds to the size of the area of mass balance calculation made by the UGRH (WGMS, 2015). The simulated mass balances are compared with the ones measured UGRH, and reported to the WGMS (2015).

Figure 7.3 shows the annual balance profiles for each of the four hydrological years, estimated from the UGRH measurements as well as the ones retrieved from the current simulation results. One may notice from the different panels that for the years 2004-2005 the energy balance model estimates greater amounts of mass loss in the area of ablation over the whole altitude range of the ablation area. This occurs also in the years 2006-2007 and A-D 2007 but to a lesser extent of mass loss overestimations. In years 2005-2006, overestimations of mass loss only occur in the range between 4750 and 4900 m.a.s.l.

In the accumulation area, greater amount of mass gains occurs in the glacier for the years 2004-2005, 2005-2006 and 2006-2007. These alternated under- and overestimations of mass in the ablation and accumulation area result in a compensation of the total calculated annual mass balance in relation to the UGRH estimates, as detailed in **Table 7.9** in which also the measured and simulated ELAs are listed. Differences in the measured and simulated mass balances are progressively reduced and are very low in the vicinity of the ELA, an aspect that is very important, because the ELA separates the surfaces with different albedos, such as snow which prevails in the accumulation zone and ice which prevails in the ablation zone. The ELA- numbers listed in **Table 7.9** indicate a good agreement between the UGRH- reported and the simulated ones.

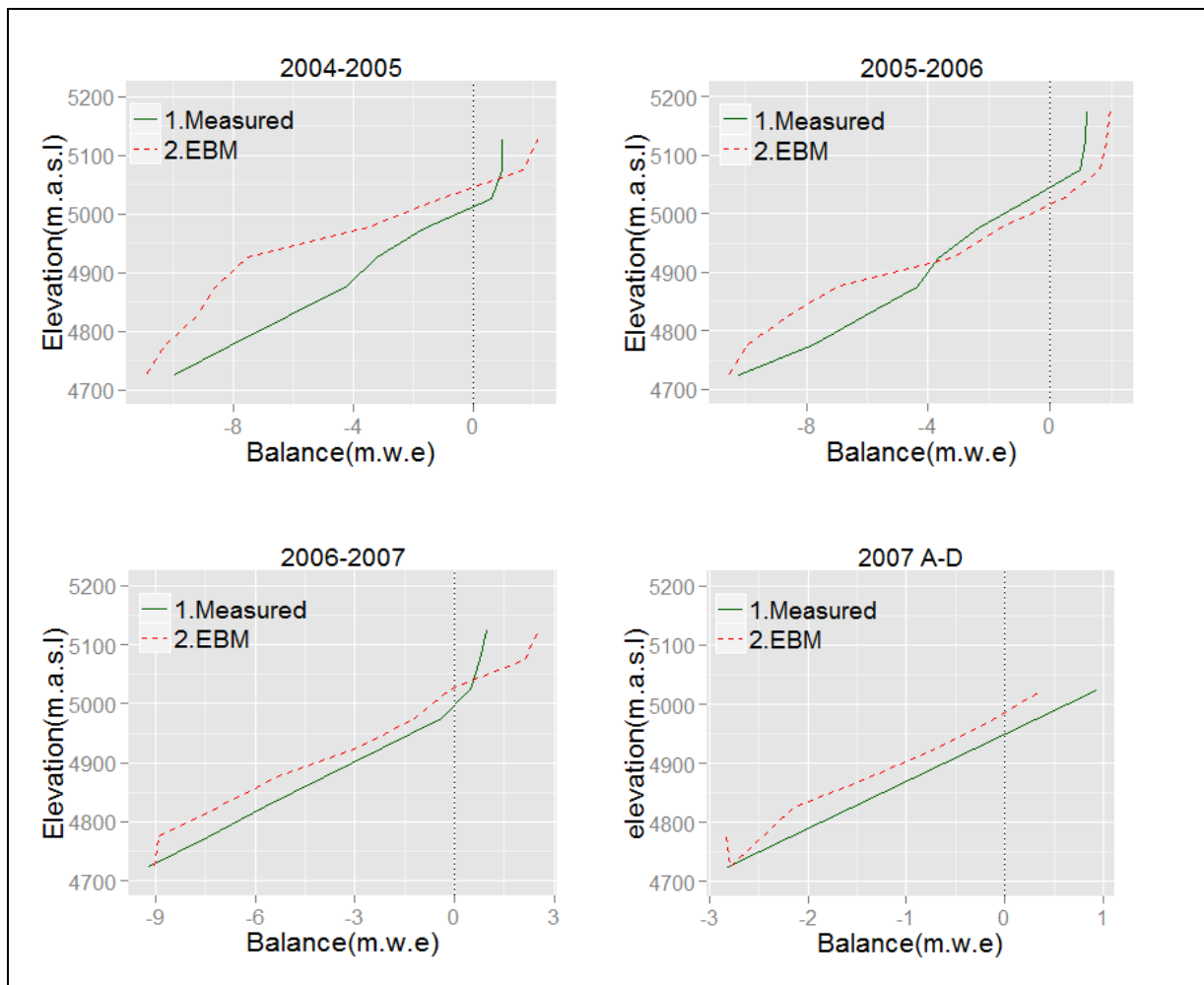


Figure 7.3. Measured and simulated mass balance profiles for the Artesonraju glacier area

Table 7.9. Annual simulated and measured mass balances and ELAs and calculated accumulation-area ratio from simulated data

PERIOD	Mass simulated (m.w.e)	Mass measured ¹ (m.w.e)	ELA simulated (m.a.s.l.)	ELA measured ² (m.a.s.l.)	AAR (%)
2004-2005	-1.91	-1.55	5046	5015	50.9
2005-2006	-1.57	-1.67	5018	5050	55.7
2006-2007	-0.64	-1.52	5025	4986	54.4
2007(A-D)	-0.25	0.47		4943	

¹WGMS (2015); ²Gallaire *et al.* (2007).

Figure 7.4 shows the spatial variation of the simulated mass balance of the Artesonraju glacier, within in the same basin for each of the three years investigated. The red points present the stake measurement of each year. The dark-green stripe is the area close to the elevation line altitude (ELA). Major differences between measures and simulated mass balances occur towards the end of the glacier tongue, but these differences decrease towards the positions of the ELA band.

In the accumulation zone differences between the measured and simulated specific mass balances are also obtained. For example, the simulation shows larger gains (more than 4m.w.e) above 5625m.a.s.l. and 5725 m.a.s.l. in hydrological years 2004-2005 and 2006-2007, respectively. For the years 2005-2006, the accumulation varies between 0.6 and 2.6 m.w.e. whereas the UGRH- estimates hint of a constant accumulation of 0.94 m.w.e, 1.19 m.w.e and 0.97m.w.e in years 2004-2005, 2005-2006, and 2006-2007, respectively. However, the glacier areas with discrepancies above 4 m.w.e., correspond to 6.14%, 0% and 2.64% of the whole glacier's areas, for each of the three hydrological years investigated, respectively.

The differences in the ablation zone, of the simulated mass balance profile with the UGRH- one are bigger between 4800 and 4950 m.a.s.l. for 2004-2005 and between 4800 and 4900 m.a.s.l. for 2005-2006, wherefore the divergence is maximum with 4 m in year 2004-2005 which is not optimal and, so, contributes to the total differences of the annual balances **Table 7.9**. However, it is important to note that 57% of the glacier area has a difference <3 m.w.e in that year and 42% < 2 m.w.e. For year 2005-2006, 81.46% of the area show a divergence <2 m.w.e and 54.26% <1 m.w.e, whereas for years 2007 and 2008 79% is <2 m.w.e and 50 % < 1 m.w.e.

The estimations of the Accumulation Area Ratio (AAR), defining the ratio of the area of the accumulation zone to the area of the glacier, are also presented in **Table 7.9**. The accumulation area varies between 50.9% and 55.7% of the total glacier area. Higher slopes reduce the impact of yearly changes of ELAs on AAR, in these cases AAR changes by up to 4% of the area within a variation of 28 m in the ELA.

The simulated, mostly negative annual balances, agree rather well with the loss trends measured by UGRH and reported by WGMS (2015) (see **Figures 7.4** and **7.5**). Some minor differences are present in years 2004-2005, when the simulated losses are higher than the measured ones. However, these higher losses during these years are congruent to findings in the Zongo glacier where the second largest specific mass balances losses (after 1998-1997) were also measured in year 2004-2005 (-1.69 m.w.e.) by means of the glaciological method (Soruco *et al.*, 2014).

7. Energy Balance in Tropical Glaciers

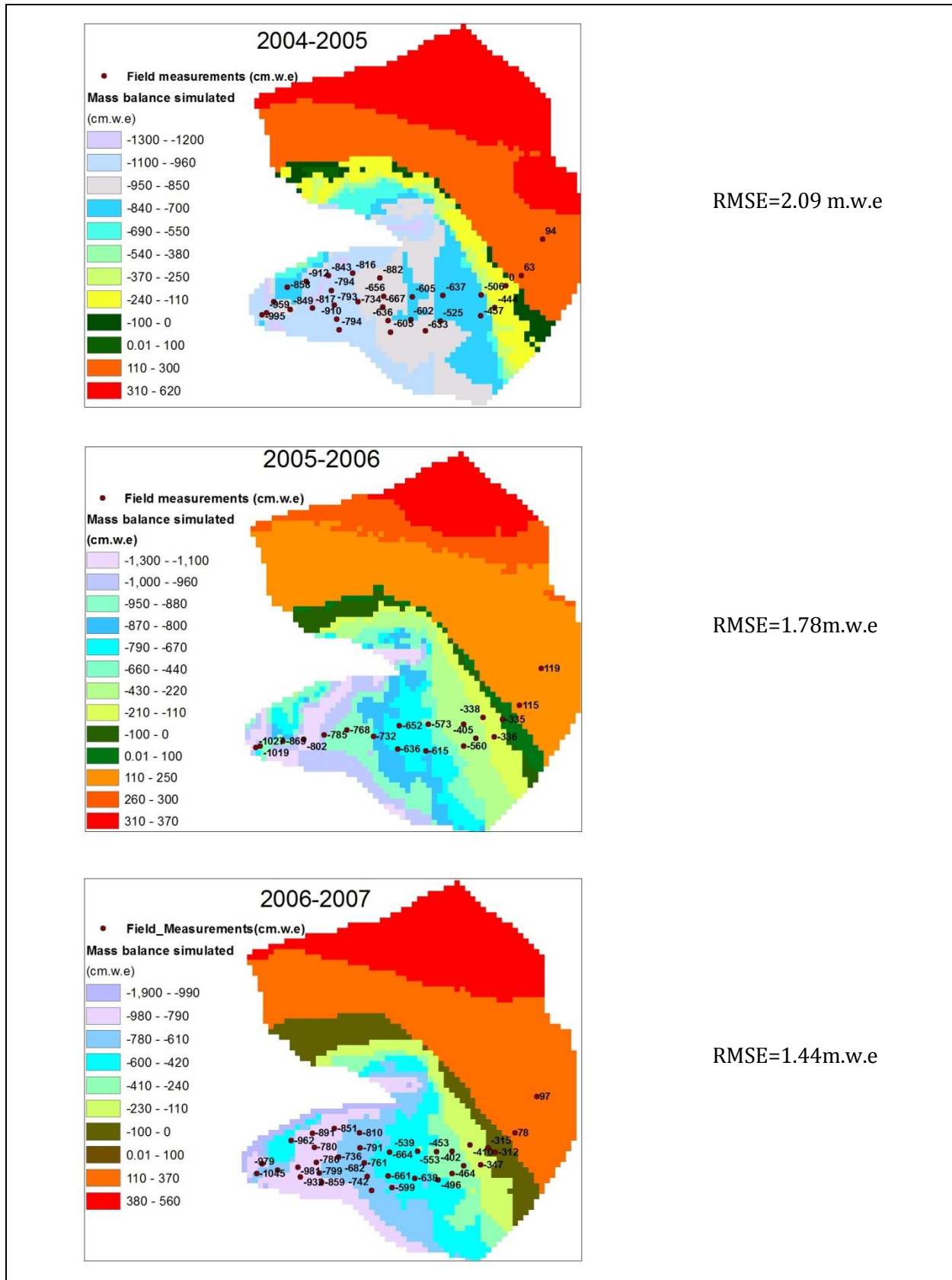


Figure 7.4. Spatial variations of annual measured and simulated (EBM) mass balances in the Artesonraju basin for three hydrological years, with RMSE of each simulation year as indicated.

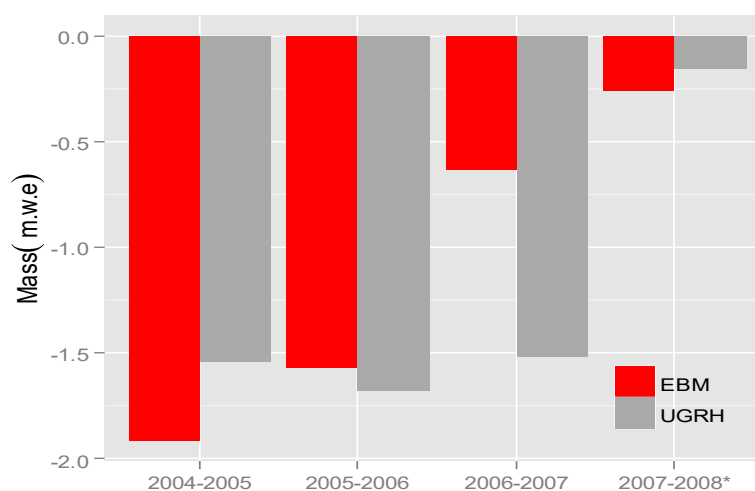


Figure 7.5 Measured and simulated annual mass balance

Higher differences of the annual mass balances simulated versus estimated by local authorities (UGRH) show up in year 2006-2007. The simulation underestimates annual mass balance losses. This is due to the bias generated in SO (2006-2007) by the filled radiation data (section 6.3.2, **Figure 6.6**), especially from underestimations of shortwave incoming radiation.

The RMSE of the simulations at the measurement locations are 2.09 m.w.e for 2004-2005, 1.78 m.w.e for 2005-2006 and 1.44 m.w.e for 2006-2007 (see **Figure 7.4**). The major disagreements between measured and simulated data arise towards the edge of the tongue of the glacier. In the accumulation area, unfortunately, only two measurement gages are present. These errors may be produced by bias in the extrapolation of the initial conditions (see input data map **Table 7.7**) of the water equivalent of the accumulation and ablation. The map of the initial condition of the water equivalent is elaborated with the accumulated measured mass balance up to at the start day of the simulation. However, the extrapolation of the field measurement with Kriging in ARCGIS generates errors (different error for the distributed surface) that increase with increasing distance of the extrapolated grid points from the sample point. This generates a certain uncertainty, especially in the accumulation region where fewer measurements are available which can project into the estimated ablation as well, as the ultimate purpose for calibration is to reach accordance of simulated and measured discharge and water volume data.

Figure 7.6 provides a more detailed picture of the seasonal variations of the glacier's mass balance, together with the seasonal temperatures and precipitation. As mentioned in a previous chapter, these two climate variables and, in turn, the mass balance in the CB glaciers are much affected by El Niño/La Niña events, so that that the observed and simulated seasonal mass balance of Artesonraju may be explained in part by intermittent occurrences of such events. Thus, the months July-March of year 2004-2005 were affected by an El Niño which, although it was weak, because of its long duration, may have affected negatively the glacier's mass balance.

A lapse with Niño occurred also from months August to February, 2006-2007 (GGWS, 2019), when important reductions in precipitation in months September-October (SO) were found. Simultaneously, increments of the shortwave incoming radiation (due to bias in the filled data gaps section 6.3.2). This combination of factors produced the highest daily loss mass during

7. Energy Balance in Tropical Glaciers

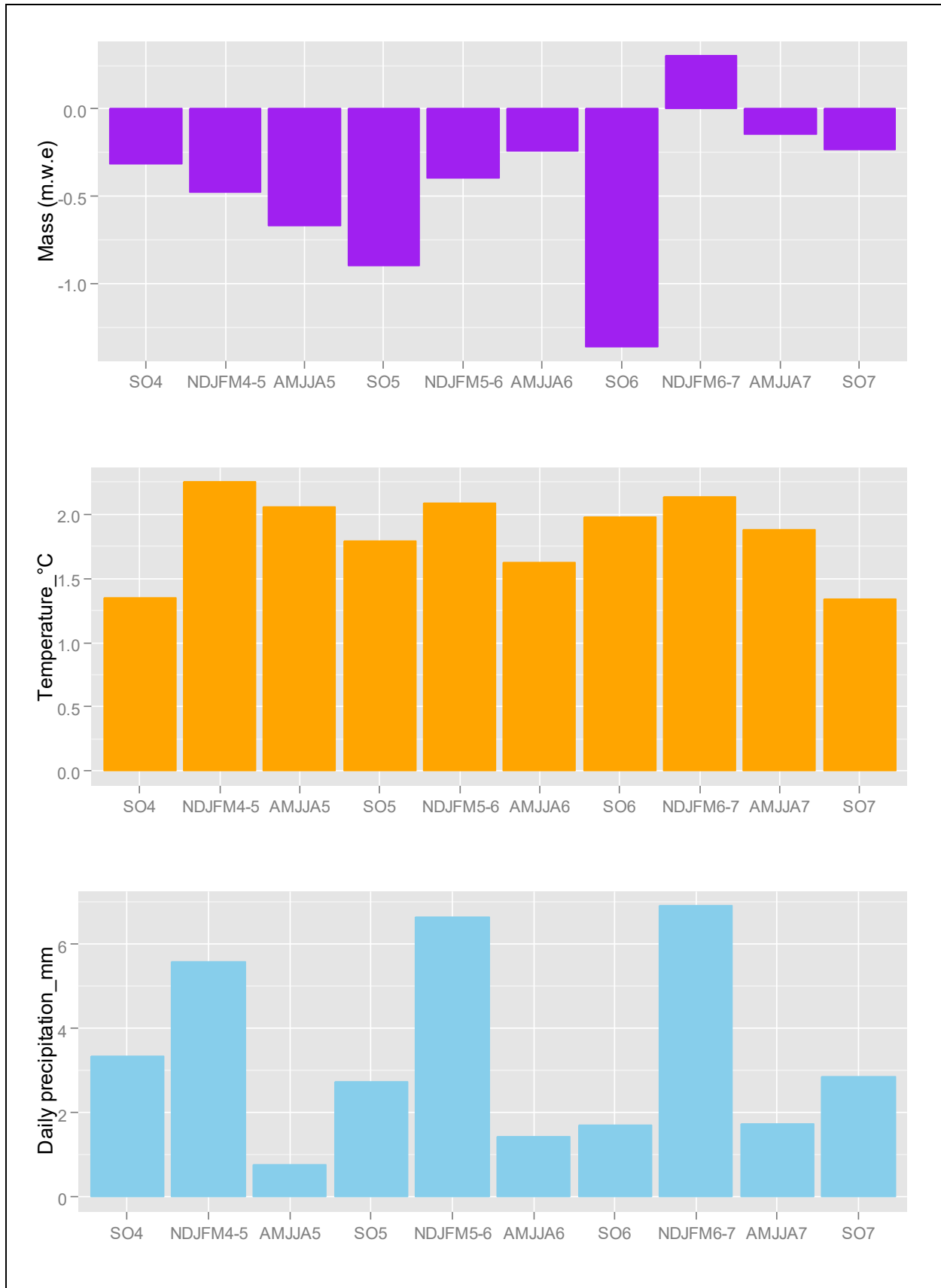


Figure 7.6. Mean daily of the season of simulated mass balances (upper panel), temperature (middle panel) and precipitation (lower panel) for each season of the years studied

these two months; however, this did not have an effect on the total mass balance, because the glacier recovered mass in the following months NDJFMA, when increased precipitation compared with the same period of other years happened. Opposite, La Niña's phenomena occurred in years 2005-2006 and 2007-2008, and had a positive effect on the daily mean specific mass balances in months NDJFM of 2006-2007, and less mass reductions from April 2007 (see **Figure 7.6**), due to increased precipitation during the middle of the wet season.

The above results indicated that in the simulated periods of years 2004-2008 the glacier is far away from reaching equilibrium, as most of the annual periods have losses of mass, with alternating negative and positive trends, marked by ENSO phenomena.

The earlier discussed **Table 7.9** indicates further that the UGHR- measured- and simulated ELA of the Artesonraju glacier range between 4950-5050 m.a.s.l. and 5000-5050 m.a.s.l., respectively. Since this ELA difference does not exceed 50 m, one may deduce that the delimitation of the firn and ice areas is pretty similar in both cases, so that the error is low. However, the trend of the simulated ELA is not clear, while the UGRH- measured ELA decreases for the 2004-2005 year. However, it should be noted that year 2007-2008 is not simulated completely. In this year, a larger mass gain is expected owing to a La Niña. Some slight differences of the snowline movement are shown at the inter-annual scale. For instance, between years 2004-2005 and 2005-2006, the UGHR- reported ELA moves upward from 5015 to 5050 m.a.s.l., whereas the simulated one decreases from 5046 to 5018. This snowline movement differences occurs due to the initial conditions of simulation, which means that the location of ELAs and different surfaces for beginning of each year were taken from the reported ELAs and not from previous simulations.

7.2.4.3 Evaluation of energy fluxes

As discussed earlier in the theory section, the net radiation is one of the components in the total energy flux balance equation (7.1) driving melting in a glacier. Further parameters in this equation are the terms sensible heat Q_{HS} and latent heat Q_{HL} , which are computed using the equations of turbulent fluxes (Eqs. 7.25 and 7.26, respectively). All of which will be discussed in the following paragraphs.

7.2.4.3.1 Shortwave- and longwave radiation balances (comparison between simulation results and measurements)

The measured and simulated net (incoming Sw_{inc} - reflected Sw_{ref}) shortwave- and net (incoming LW_{inc} - emitted LW_{surf}) longwave radiation at the Artesonraju station are compared in **Figure 7.7** and **Figure 7.8**, respectively. It is observed from these figures that there is more disagreement between simulated and measured shortwave- than for longwave radiation. These deviations are possibly due to daily fluctuations of the albedo which, as mentioned, are not taken into account in the model which only uses standard seasonal values. The major discrepancies occur in the

months from November to December when the fluctuations of precipitations are also bigger (not shown).

The measured data of shortwave radiation, longwave radiation and the total net radiation (Q_N) have some gaps¹⁴, mainly in years 2006 and 2007 that were filled using the Autoregressive model, as detailed in Chapter 6. Thus, it is of no surprise that the main deviations of the simulated total of 2006-2007 of shortwave and net radiation, (the latest shown in **Figure 7.9**), occur also during these gap-filled periods. Apart from these lapses, the net radiation exhibits a similar behavior as the measured one, except for the period of October to November of year 2004-2005, when the simulation yields more net radiation, whose effects could be seen in the larger modelled losses of mass and increased discharge, presented earlier in **Figure 7.2** and **Figure 7.3**

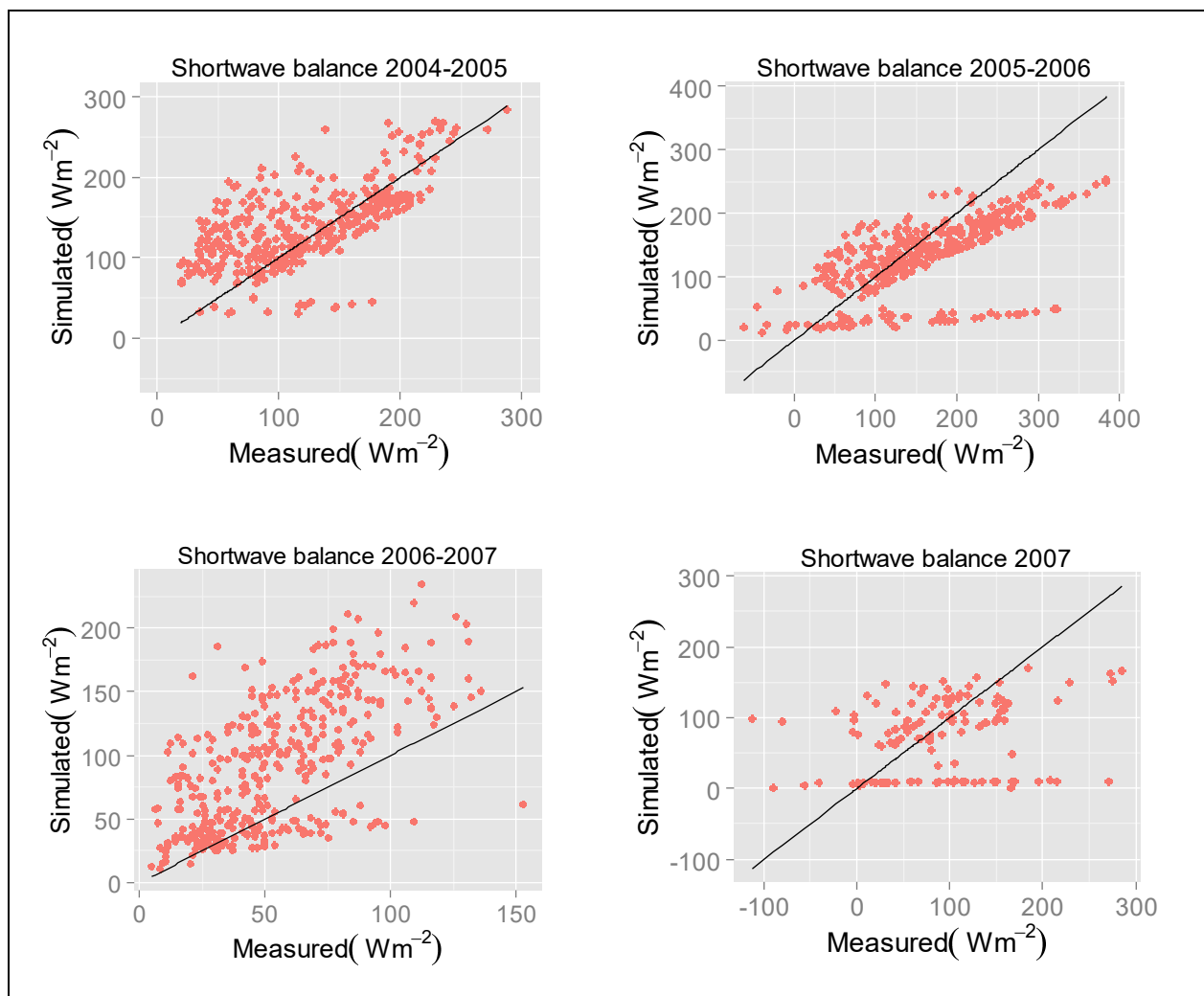


Figure 7.7. Measured and simulated net shortwave radiation at Artesonraju glacier station

¹⁴ Gaps in year 2006: March 9-19, April 4-19, May 25- 31, June 24 to July 19, August 30 to November 1: Gaps in year 2007: January 28 to March 13, March 16-24 and March 29 to November 1.

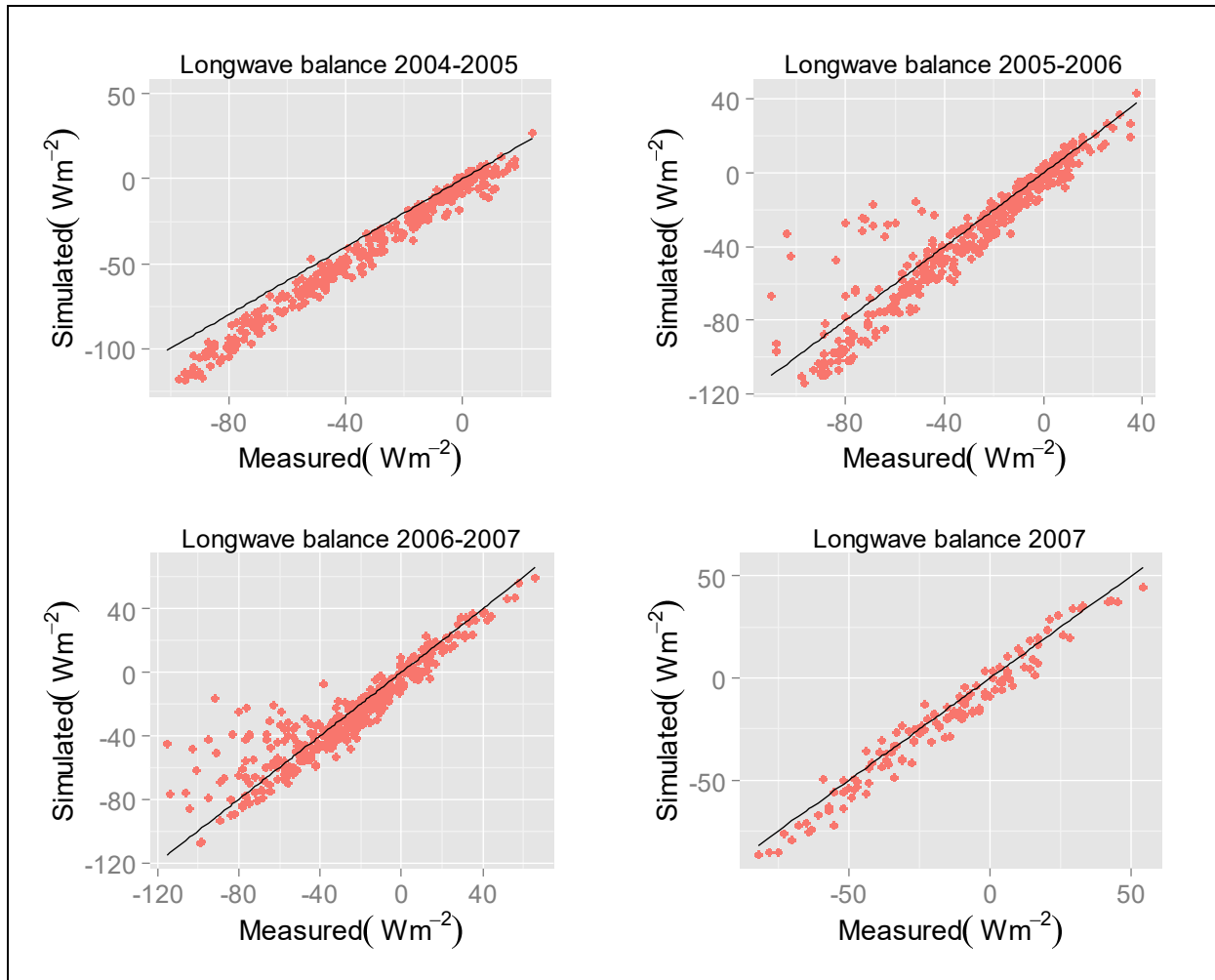


Figure 7.8. Measured and simulated net longwave radiation at Artesonraju glacier station

7.2.4.3.2 Simulated turbulent fluxes (comparison of sensible and latent heat with net radiation)

Figure 7.10 shows the mean simulated time series of sensible and latent heat (daily means) for the time period investigated in the whole area of the glacier, together with that of the net radiation, for comparison. It is observed that for the Artesonraju glacier, the net radiation is really predominant over the two turbulent fluxes and this holds for all times of the study period. This result is not completely new since studies of other glaciers, such as the Antizana in Ecuador (Favier *et al.*, 2004), the Shallap in the Cordillera Blanca Peru (Gurgiser, *et al.*, 2013) and the Zongo in Bolivia (Sicart *et al.*, 2011) obtained a similar behavior.

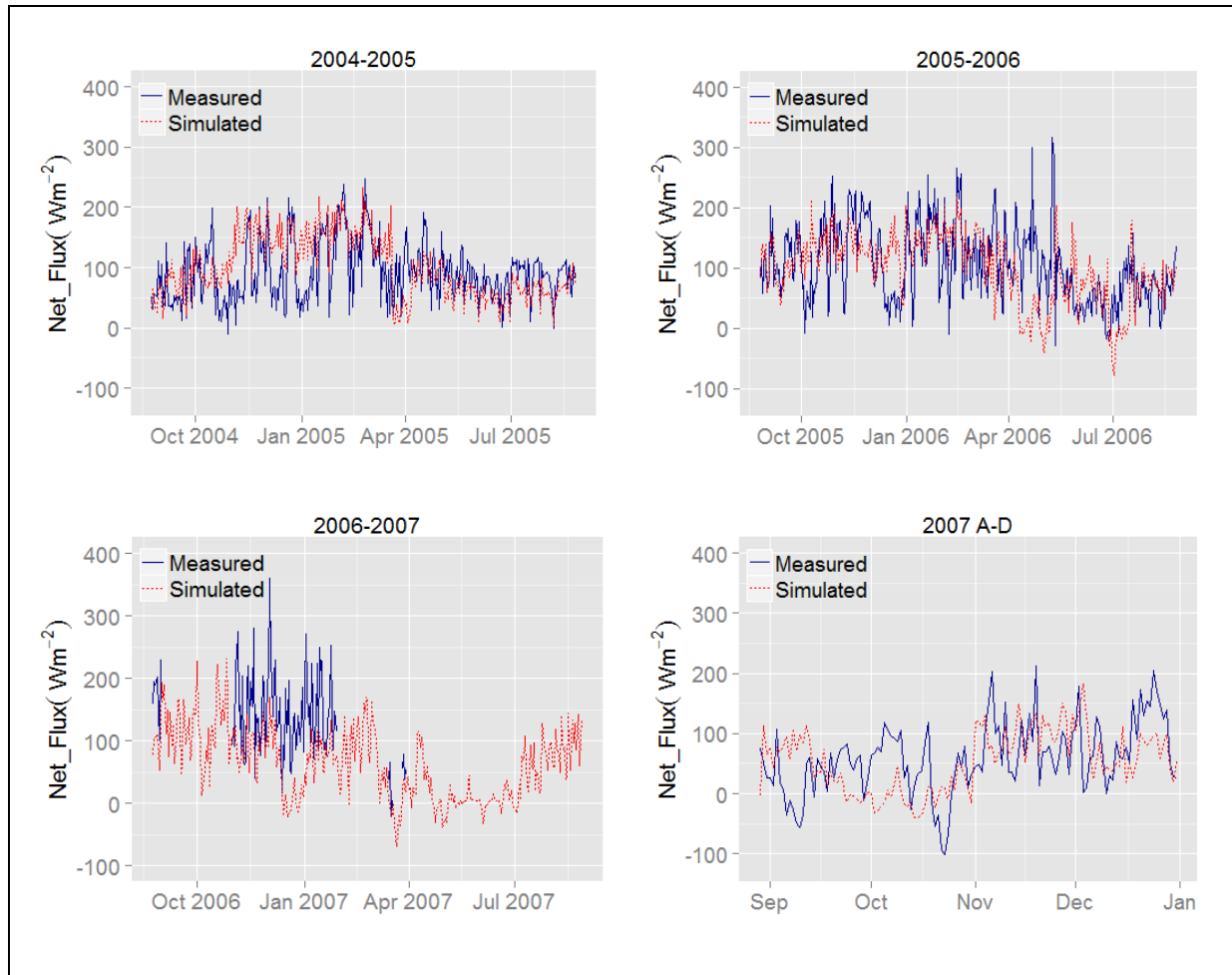


Figure 7.9. Measured and simulated net radiation at the Artesonraju glacier gauge station

However, as can be seen from the four panels of **Figure 7.10** over the course of the study period, sporadic episodes in which the daily net radiation is less than the turbulent fluxes and even negative, are found. These episodes are particularly frequent in the dry season (AMJJA), of the year 2004-2005, coinciding with the occurrence of a strong El Niño phenomenon, which lasted for eight months and showed maximal SST-anomalies of up to $0.7\text{ }^{\circ}\text{C}$ in those years. For two days at the end of July of 2005, the mean net radiation reached -25 Wm^{-2} whereas the mean sensible heat attained 70 Wm^{-2} . This unusual behavior was generated by the combination of increased temperature (above 3°) and higher wind speeds (above 4 m/s). Notwithstanding that a strong El Niño with SST anomalies of up to $0.9\text{ }^{\circ}\text{C}$ also occurred in 2006-2007, the turbulent fluxes did not exceed net radiation in that year as this El Niño although had less duration.

A more detailed analysis of the separate components of the energy balance equation showed that the negative net radiation in the named dry seasons could be associated with lower values of longwave incoming radiation as well as higher reflected short-wave radiation. This often happened after a sporadic snowfall event followed by dry days.

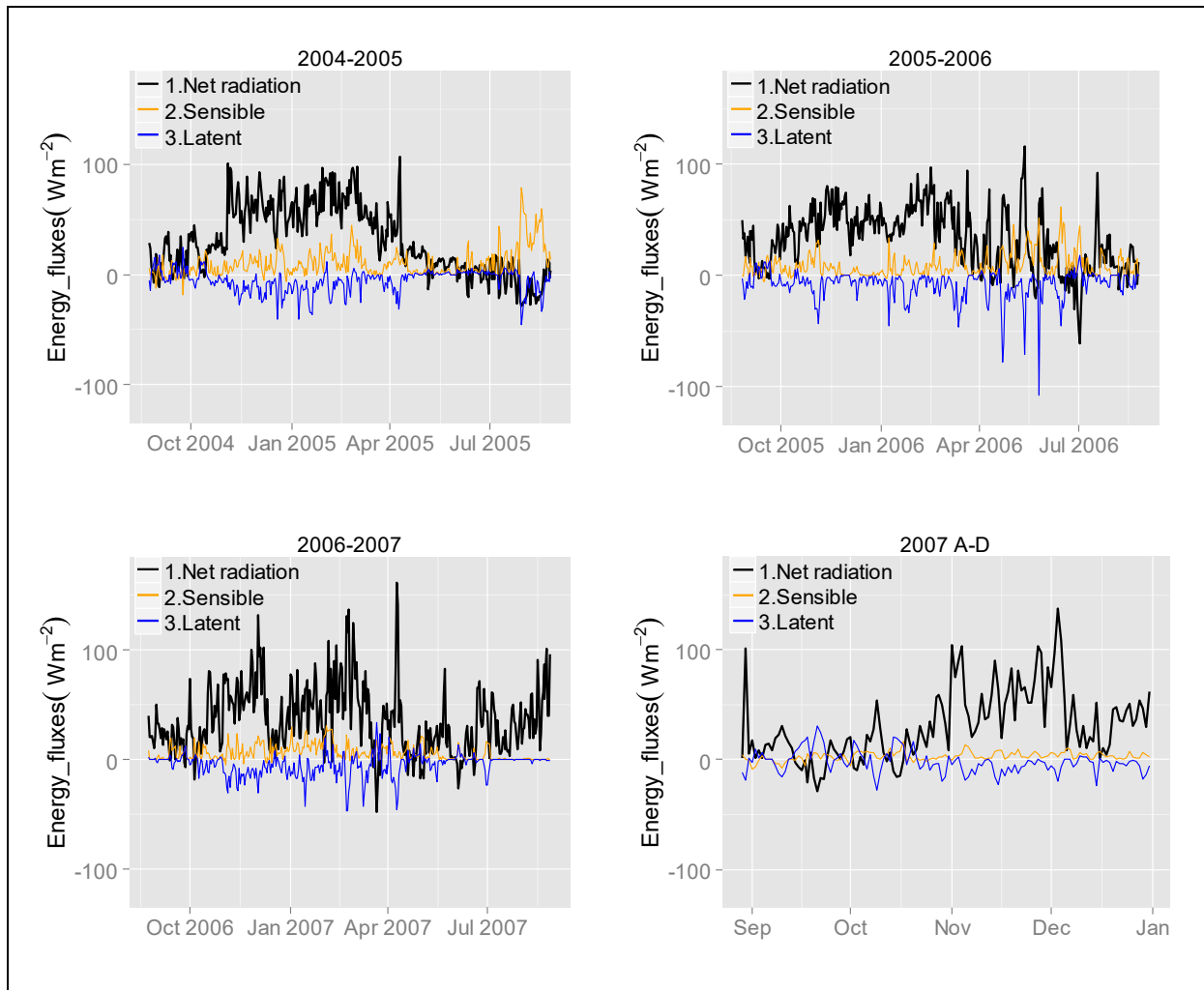


Figure 7.10. Simulated daily net radiation and turbulent fluxes

7.2.4.3.3 Seasonal contribution of energy fluxes in energy balance for melting

The mean seasonal contributions of the different radiation energy fluxes terms are presented in **Figure 7.11** and **Figure 7.12**

The shortwave radiation balance has the greatest weight within the net radiation term. This shows the preponderant role of albedo in guiding the seasonal dynamics of the glacier, as the shortwave incoming present a lower seasonality. This has been concluded in the studies of the tropical glaciers of the Andes (Favier *et al.*, 2004; Gurgiser *et al.*, 2013). Shortwave radiation is higher in the rainy season, when mean seasonal values range from 63 to 73 Wm^{-2} . Although the mean seasonal values of SW_{bal} of the dry season are slightly reduced after the rainy seasons in 2004-2007, this reduction is less in year 2006-2007, in which more precipitation occurred. It was also found that the role of longwave radiation in the seasonality is stronger than that of any other flux. The greater energy sink is longwave radiation (LW_{bal}). This is greater in the dry and cold seasons (see **Figure 7.12**). From means of energy fluxes in each season, (LW_{bal}) represented an offset of 63%, 69% and 68% of the energy obtained by (SW_{bal}) in the dry season, for the years 2004-2005, 2005-2006 and 2006-2007, respectively.

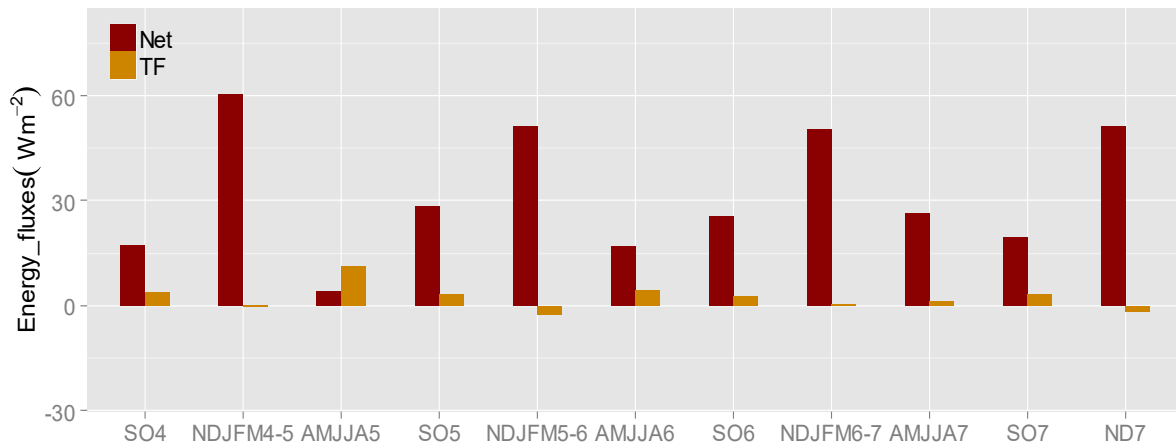


Figure 7.11. Mean seasonal net radiation and turbulent fluxes at the Artesonraju glacier

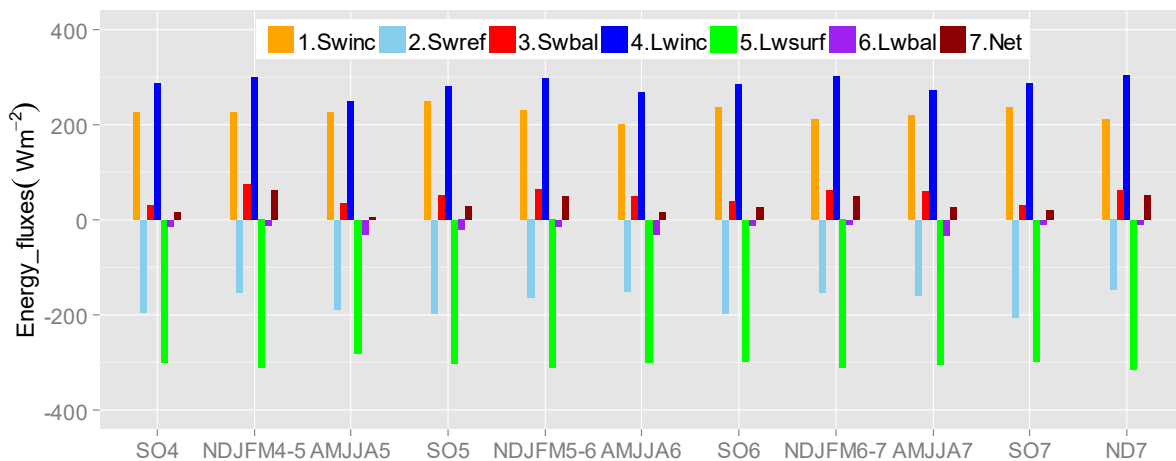


Figure 7.12. Mean seasonal contribution of radiative fluxes terms

The net energy is reduced in the dry season due to a reduction also of shortwave balance (for years 2005-2007). The important sink of energy in the dry and cold period by means of net longwave radiation reduces glacial melting, which under other conditions would be higher. The reductions of incident longwave radiation of the atmosphere primordially are the cause of increased sinking of longwave energy in the dry season **Figure 7.12**.

The mean annual reflected shortwave radiation (148-170 Wm⁻²) (see **Table 7.10**) tends to be a little over the averages of the values reported (see **Table 7.2**), between 90 and 142 Wm⁻², in other studies of tropical glaciers (Wagnon *et al.*, 1999; Favier *et al.*, 2004; Juen, 2006; Sicart *et al.*, 2011; Gurgiser *et al.*, 2013). Four aspects should be considered regarding this result: a) The figures presented here are the mean daily shortwave reflected in the whole area, considering that the AAR is between 51 to 55% the albedo in the accumulation area which is predominantly high, raise the average, instead most of the previous studies presented site values. b) Different local climatic conditions, especially of the influence of charged air masses that arise from the Amazon and that could influence the Artesonraju Glacier. In addition, low precipitation correlation was observed within the tropics. c) The use of seasonal albedos may have an influence on the reflected short-wave results since daily fluctuations are not captured. d) This

study used precipitation gradients for each month calculated from the data of Parón, and Artesoncocha gauges. Former studies with distributed energy fluxes in tropical glaciers assumed precipitation constant (Sicart *et al.*, 2011; Gurgiser, *et al.*, 2013). However, the values of reflected radiation at the altitude of the climate station are similar to those presented at the altitude of the climate station and those presented by Juen (2006)

The annually averaged daily turbulence fluxes are comparatively less than the net radiation (see **Table 7.10**). Over the whole year (but not for separate seasons) the mean daily sensible (Q_{HS}) and latent heat (Q_{HL}) fluxes counterbalance themselves pretty much, with their sum (Turbulent Fluxes, T_f) hovering between +1 and -2 Wm^{-2} . However, increments of sensible heat and latent heat occur in El Niño years (2004-2005).

The data of previous studies for long and shortwave radiation in glaciers shown in **Table 7.2** and the present results are quite similar, with annual averages between (250 and 301 Wm^{-2}) for longwave incoming (LW_{inc}) and between (294 and 312 Wm^{-2}) for longwave emitted (LW_{surf}). The turbulent flows found here are also within the average ranges found for tropical glaciers, with the sensitive heat (Q_{HS}) ranging between -2 and 21 Wm^{-2} and the latent heat (Q_{HL}) between -27 and -4 Wm^{-2} .

Table 7.10. Simulated annually averaged daily energy flux terms in the Artesonraju glacier

Year	Energy flux components (Wm^{-2})									
	SW_{inc}	SW_{ref}	SW_{bal}	LW_{inc}	LW_{surf}	LW_{bal}	Q_{Net}	Q_{HS}	Q_{HL}	T_f
2004-2005	224	-143	76	277	-303	-26	51	9	-6	0
2005-2006	221	-151	69	283	-306	-24	46	8	-9	0
2006-2007	213	-155	58	286	-306	-21	38	5	-5	1
2007AD	225	-170	55	294	-307	-13	42	3	-5	-2

7.2.4.3.4 Seasonally averaged depth variations of energy fluxes

In the present sub-section simulated vertical variations (profiles) of seasonally averaged energy fluxes are presented in the elevation range of the glacier for the three seasons of a year, i.e. the beginning of the rainy season, the core rainy season and the dry season. The maps of the mean seasonal distributed energy fluxes with a horizontal resolution of 30m*30m were divided in 16 horizontal bands, each 50-60 m high, so that the whole glacier area is covered. From the grids of these subareas or bands, statistical calculations of the mean, and the minimum and maximum values of each flux were performed. With these definitions, each profile or ribbon in the following graphs shows the range between the minimum and maximum value of each band, with the mean of the balance of the fluxes represented by the points.

- **Net radiation, turbulent fluxes and melting energy profiles**

The profiles of net radiation, turbulent fluxes and the ultimate energy remaining for melting are illustrated in **Figure 7.13**. The three panels of the figures indicate that the net radiation is much larger in magnitude and more variable and in the lower lying ablation zone (ranging between -7 and 183 Wm^{-2}) than in the higher lying accumulation zone (ranging between -10 and 41 Wm^{-2}). This situation is the reason for the minimization of mass losses in the accumulation zone.

7. Energy Balance in Tropical Glaciers

decreases, as the net radiation is reduced due to the lower emission of atmospheric radiation (longwave incoming radiation).

The panels of **Figure 7.13** demonstrate that the ablation- and accumulation areas have different behaviors. The available energy for changes of the mass state depends to a large extent on the shortwave radiation that is reflected by the different surfaces; with ice prevailing in the ablation- and snow in the accumulation zone. These surfaces influence the vertical gradients of temperature as well and, thus, the vapour pressure differences between the surface and the atmosphere. In this way, turbulent fluxes have a different behavior for the two glacier zones.

- *Sensible/ latent heat and turbulent fluxes profiles*

Profiles of sensible, latent heat and the total turbulent flux are presented for each of the three seasons named in the three panels of **Figure 7.14**. Sensible heat varies between 4 and 23 Wm^{-2} in the ablation zone, and between -37 and 11 Wm^{-2} in the accumulation zone. In the accumulation zone sensitive heats are mainly negative during the wet season. Besides, latent heat is positive in (SO) resulting in energy used for deposition processes and negative in (NDJFM) generating sublimation which require 8 times more energy than melting. The latter prevents melting in the accumulation zone although more net energy is available in the wet periods.

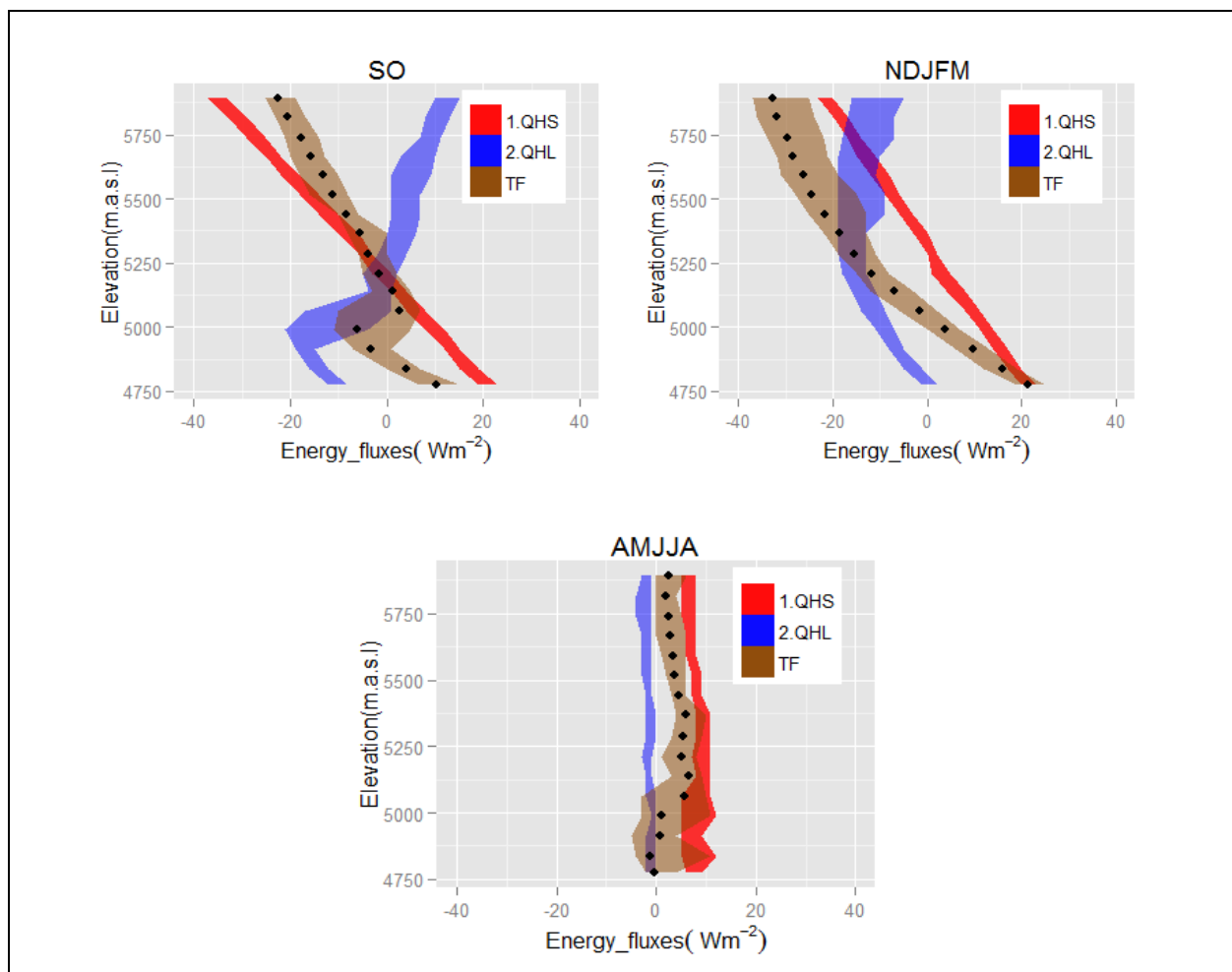


Figure 7.14. Turbulent fluxes profiles for months September–October (SO), November –March (NDJFM) and April–August (AMJJA)

7. Energy Balance in Tropical Glaciers

7.2.4.4 Sensitivity analysis of calibration parameters

The calibration of the model was made by tuning pairs of the different parameters. In the case of albedos, the variation of the parameters was made with a physical basis (see **Table 7.5**). That means between the possible ranges of the albedos for each surface. For each set of albedo combinations, another parameter was tested, the threshold temperature rain/snow T_o . This parameter was set also to the physical limits between 0-5°C. Ultimately, discharge constants were considered. For all the possible combinations of albedo pairs with threshold temperatures, the ranges of 400-1000hour K_{firm} , 100 to 550 hour K_{snow} and 0-300 hour for K_{ice} , E of discharge were calculated. These ranges of the storage constants were selected from the values found for the same parameters in accordance also with the Temperature Index Model that will be explained in 8.2.3.3. The major Nash Coefficients obtained by the best combinations of parameters were evaluated in terms of correspondence with the total mass balance.

7.2.4.4.1 Albedo

One of the most important calibration parameter in the glacier energy balance model turns out to be the albedo. Different combinations of albedos for each of the glacial surfaces were tested, however, by respecting the range of their physical values for the typical glacier surfaces (see **Table 7.5**). The seasonal albedo selection was made by observing their effects on the model outcome, i.e. the model sensitivity under different threshold temperature conditions. Thus, all the possibilities were investigated and, finally, the albedo parameters with a) the best adjustment of the discharge and the best fit of the total water volume and b) those that presented similar trends for the same season of all modelled years were taken in the final simulations.

Figure 7.16 shows the results of the model adjustments in terms of the Nash-Sutcliffe parameter E of discharge for different combinations of snow and ice albedos for each of the modelled periods. It is observed that the albedos are different for each of the three periods in the year, but that they exhibit similar tendencies for the same period in each of the modelled years.

For the SO seasonal period, a high value trend of the snow albedo is observed, varying from 0.87-0.95, whereas the albedo of ice ranges between 0.35-0.48. The high albedo of this period can be explained by the beginning of the wet season in which fresh snow is typical and clean ice prevails in the ablation zone.

For the subsequent wet season period NDJFM, the snow albedo decreases to a range of 0.8 - 0.85. The same holds for the ice albedo which is reduced to a range of 0.25-0.3 for year 2004- 2006 but which increases to a range of 0.45-0.5 for year 2006-2007. In this wet season period larger fluctuations of precipitation and a slightly higher temperature occur normally, so that the glacier melting is higher. The ensuing melt water reduces the snow albedo directly and increases indirectly the grain size of the ice/snow surface which, in turn, reduces albedo (Hock, 2005), explaining the diminished albedo found above. The albedo is expected to fluctuate between those values from fresh snow and old wet snow (see **Table 7.5**).

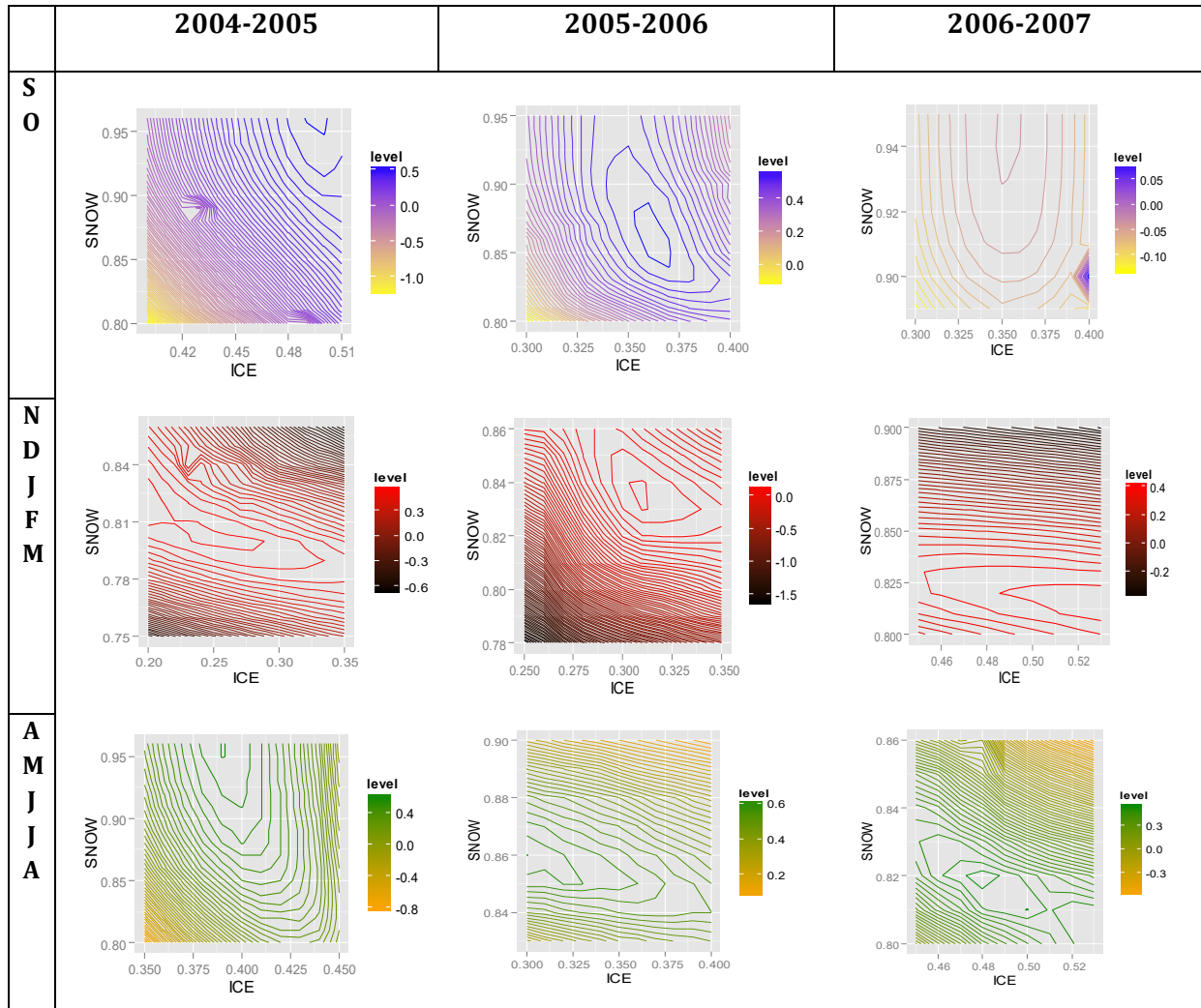


Figure 7.16. Snow and ice albedo sensitivity in terms of the Nash-Sutcliffe parameter E

For the AMJJA dry season period, the snow albedo ranges between 0.82-0.95. The water content during that time of low precipitation is reduced which helps to maintain the snow accumulated in the previous season. Therefore the snow albedo tends to slightly increase compared with the previous season, which is also concordant to what was observed by Juen (2006). In this case, two of the simulated periods between 2005 and 2007 are characterized by albedos of old dry snow. The dry period of 2004-2005, shows a very high albedo 0.95, that may be too high.

7.2.4.4.2 Threshold temperature Rain/ Snow T_0 :

The threshold temperature rain/ snow, T_0 is very important for determining surface conditions in the model, because each surface (snow, ice, firn and debris) owns different physical features influencing the energy budget. It has been found in the literature (see below) that this threshold temperature is variable and depends on geographical and seasonal atmospheric conditions. The latter influences the state of precipitation through different mechanisms. The thickness of the air layer that falling water droplets (leading to precipitation) must go through, the soil heat, the cooling influencing on humidity, and the salt content of the particles affecting freezing point, are some factors that influence the type of precipitation reaching eventually the soil (Dai, 2008; Ye,

Cohen and Rawlins, 2013; Feiccabrino *et al.*, 2015). Some studies present the temperature threshold range in different locations. For instance, August and Auer (2010) found in a study of over 1000 station in the United States that rain never occurred beneath a temperature of 0.8 °C and that snow was never observed when the temperature exceeded 6.18 °C. Another study, specifically in the Cordillera Blanca of interest here, estimated a snow/rain threshold temperature range of 1.1-2.5 °C in the Shallap glacier (Gurgiser, *et al.*, 2013).

Based on these studies, it is of no surprise that the threshold temperature rain/snow T_0 turned out to be a very sensitive parameter in the present model simulations as well. This is demonstrated by **Figure 7.17** which shows the effects of varying T_0 on E for different seasons. The figure indicates that a larger sensitivity of the threshold temperature rain/snow T_0 occurs in the second wet period NDJFM, as small changes in T_0 have a large effect on the Nash-Sutcliffe parameter E . However, for year 2007-2008 the sensitivity of T_0 decreases which may be due to the occurrence of a La Niña at that time. The less sensitive months are SO, but contrary to what has been just said, the T_0 -sensitivity of this period increases for year 2007-2008. 2004-2005, the T_0 of the dry period AMJJA exhibit a high sensitivity as well.

The best threshold temperature range rain/snow lies between 2.8°C and 4°C. The seasonal T_0 differences may depend on certain local atmospheric conditions related, especially, to relative humidity, vapor pressure and wind speed. Also, anomalies generated by ENSO can produce changes in the threshold temperatures, as El Niño can lead to unusual dryness, as it has been the case, for instance, for the one occurring during AMJJA 2005. According to Jennings *et al.* (2018) snowfall events at low relative humidities are more likely to fall as snow at higher T_0 . Indeed, from observational data, the warmest threshold temperatures were shown in mountain regions above 4000 m.a.s.l., in the north hemisphere, e.g., Rocky Mountain 3.8°C and Tibetan Plateau 4.5°C.

In regard to the glacier Artesonraju, the seasonality of the relative humidity shows reductions, especially in the dry season in which higher values of threshold temperature arise. Besides, the relative humidity turns out to be slightly lower here than in the southern glaciers of the Cordillera Blanca (see Section 3.1.3), so that higher threshold temperatures than the 2.5°C found in the southern glacier Shallap by Gurgiser *et al.* (2013) can occur.

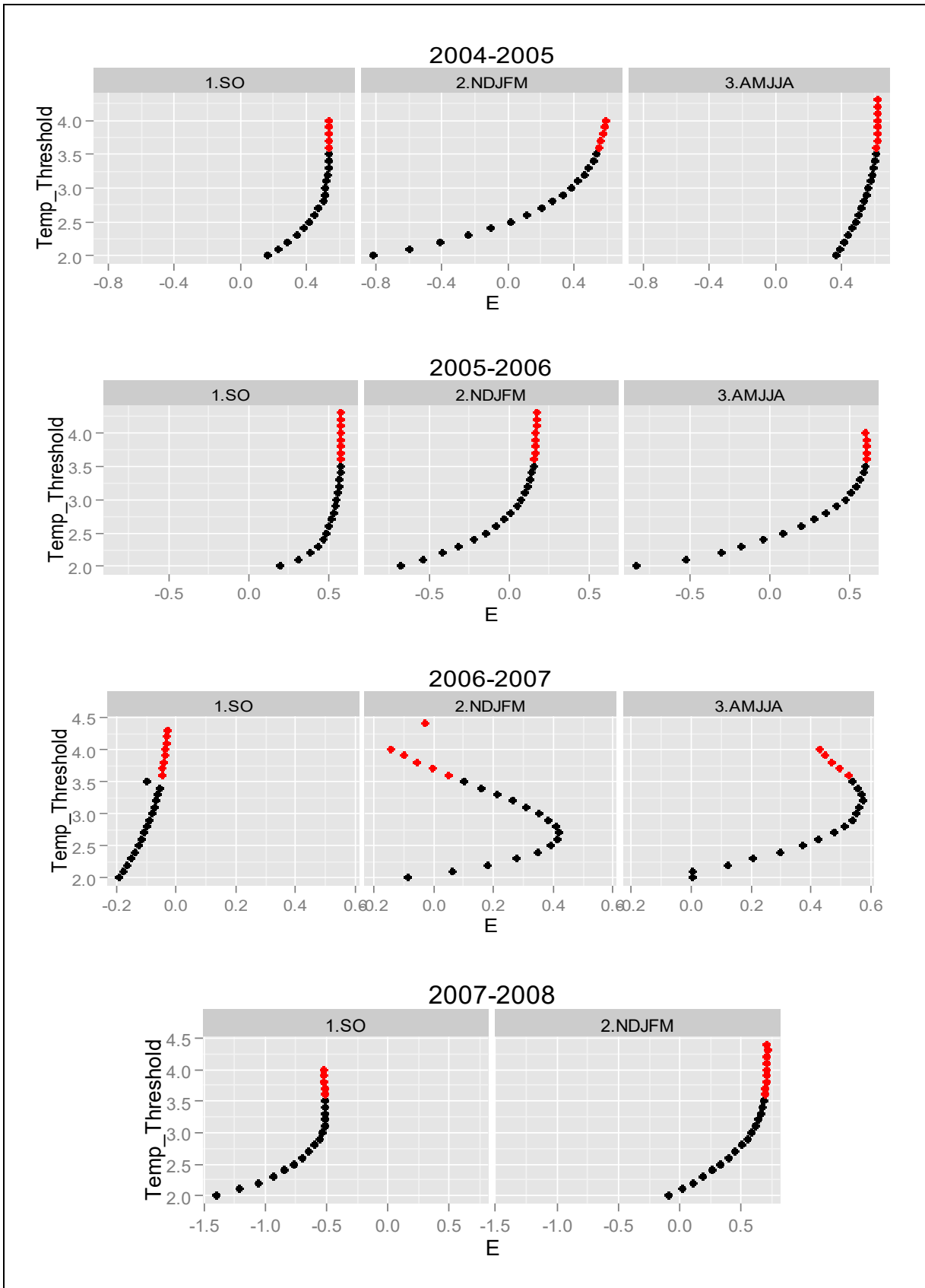


Figure 7.17. Threshold temperature rain/snow T_0 sensitivity in terms of E . Red point shows the points located above 3.5°C

7.2.4.4.3 Storage constants

The storage constants used in the cascade sub-model for routing the discharge within the energy balance simulations were taken from a simultaneous simulation of the same glacier with the temperature index model. The results obtained with this alternative will be presented in Chapter 8. These storage constants also showed satisfactory results with the energy balance model. However, to explore the sensitivity of the model to these storage constants, more simulations were done with varying values depending on the season considered. The optimal constants finally obtained for the three glacier surfaces and the different seasons are listed in **Table 7.11**.

According to **Table 7.11**, for the same season the spread of the storage constants across the four years simulated is rather small. However, differences arise for the individual seasons. Thus, for the first season, SO, values of k_{firm} of 700-800 hour, for the second (rainy) period, NDJFM, of 480-800 hour, and for the third (dry) season, AMJJA, of 1100 hour are observed. The low k_{firm} - values obtained for season NDJFM can be explained by the fact that larger amounts of melting penetrate into the firn interstices. In the SO period the melting is smaller, so that k_{firm} is still larger as a results too of its recent formation from previous period.

For k_{snow} , the corresponding seasonal ranges are 390-400 hour, 390-450 hour and 150-200 hour, respectively, i.e. the k_{snow} - values for the two rainy periods SO and NDJFM are much larger than that of the dry season AMJJA. This is due to the fact, that during the two rainy seasons a greater amount of snow exists which is maintained for a longer time. Indeed, the total accumulation of a year occurs in these seasons, for tropical glaciers.

For k_{ice} , values ranging between 30-120 hour for NDJFM and of 250-300 hours for AMJJA are encountered. However, for season SO of year 2006-2007, an extreme value of 500 hour is found which may not be realistic and is most likely due to gaps in the input data during that time period which made modelling difficult. The table shows further that the highest storage constants are obtained in the dry period, especially, for firn and ice surfaces. This is logical as during that period the glacier, because obtains less energy input, and thus less melting, generates its lowest discharge, leading to a longer storage time of ice. As the solid precipitation is also reduced in the dry period, the smaller amount of snow can melt faster which, consequently, leads to a smaller storage time of the snow. In the case of firn, the dry period is the time when the accumulated

Table 7.11. Optimal seasonal storage constants for the three kinds of glacier surfaces

Year	Period	k_{firm} (hr.)	k_{snow} (hr.)	k_{ice} (hr.)
2004-2005	SO	700	390	150
	NDJFM	500	390	35
	AMJJA	1100	150	250
2005-2006	SO	700	390	50
	NDJFM	480	400	120
	AMJJA	1100	150	300
2006-2007	SO	800	390	500
	NDJFM	800	450	30
	AMJJA	1100	200	250
2007S-D	SO	750	400	250
	ND	400	390	100

snow from previous seasons is becoming firn and therefore more storage times are expected, as it is the case. The storage constants found in this research represent quite well the seasonality of accumulation and ablation of snow ice and firn typical of the outer tropical glaciers.

7.2.4.5 Uncertainties in the simulation

The current EBM simulations, in conjunction with the limited quality of the data are, naturally, fraught with some uncertainty and/or errors. One source of the latter may be due to the few measurements existing in the accumulation zone of the glacier. Normally, these zones are abrupt and dangerous in the high mountain of the Cordillera Blanca, making access for measurements difficult (Kaser and Georges, 1999). The net and the instrumentation of the measurements are also costly and cover generally just some parts of the glaciers (Francou *et al.*, 2013). Therefore, the initial conditions, especially for the accumulations, are still difficult to estimate over the whole area. The estimations of initial surface conditions in the current EBM simulations were made in ArcGIS with geospatial interpolation based on Kriging analysis which introduces additional errors in the estimations of the initial accumulated mass, propagating through the model simulations.

Another source of uncertainty is the variation of the wind on the glacier surface. Wind speed in the EBM is assumed as constant across the whole glacier area. Therefore, the estimation of the turbulent fluxes which depend on wind speed can be fraught with certain inaccuracies. The results of the current simulations suggest that wind represents the most important climatic driver of latent and sensible fluxes. Thus, exploring different parameterizations to account for the wind variability may be an important task for better understanding the role of sublimation, condensation, deposition and other variables all of which depend on wind speed, like relative humidity. Besides, the direct interference of the wind leads to a reduction in the net accumulation at high altitudes, but may produce accumulation of snow in topographic depressions (so-called snowdrift) (Francou *et al.*, 2013), both of which are out of the scope of the present model simulations.

Gaps in the measured energy fluxes that were filled with various statistical methods (see **Chapter 6**) are also a source of uncertainty. Predicting long periods of data gaps, as the one in 2006 (see **Figures 5.3** and **5.4**), was a difficult task. The error generated by interpolation with these models, could affect the performance of the model, as is reflected by the Nash-Sutcliffe coefficients of the present simulations in the corresponding season of SO of years 2006-2007.

Unknown daily variations of albedo are another source of uncertainty. Large variations of albedo are expected in the wet season. The main cause of these variations is attributed to alternate amounts of precipitation and the moisture content that affect the permanence of the snow on the surface. Indeed, snow albedo falls exponentially after a few days of snowfall (Hock, 2005; Sugatan *et al.*, 2014), however, this physical process is not considered in the current simulations.

Finally, rock avalanches that produce important changes of debris mass in the high mountains are another uncertainty. This aspect is very important, as such mass movements could be exacerbated by climate change. Fischer *et al.* (2013) state rapid topographic changes and increased erosion rates caused by massive slope failures (favored by rising temperatures) in glaciated affected high mountains in the alpine areas.

7.2.5 Concluding remarks

The present glacier modelling sought to deepen the understanding of the physical processes and the leading parameters that govern the mass balance in tropical glaciers. Thus, the results of the present simulations contribute to the many studies in this field, in which some results related to the various parameters that drive the seasonal dynamics of tropical glaciers differ in some cases.

Based on the available empirical input data, a period of three years and four months was modelled. Good to satisfactory results, with Nash-Sutcliffe coefficient E between 0.57-0.85 in discharge were obtained. Besides, annual mass balances estimations were compared with previous official calculations by UGRH, reported in the WGMS (2015). Simulated annual mass balances show mass losses between -1.9 and -0.64 m.w.e, show to be concordant to the official estimations. The annual and seasonal balances strongly depend on climatic variation associated with El Niño and La Niña phenomena.

A more detailed analysis of the various components of the energy balance equations indicated that the net radiation governs the energy balance and the melting processes, confirming results of some current studies (Favier *et al.*, 2004; Juen, 2006; Sicart *et al.*, 2011; Gurgiser *et al.*, 2013; Maussion *et al.*, 2015). More specifically, it is the reflected shortwave radiation which is the dominant component here, which in turn is governed by the albedo of the typical different surfaces. Although the daily short-term variations of albedo could not be simulated, the use of seasonal albedos for three different seasons (less rainy, rainy, dry) and from three surfaces (snow, firn, ice) allowed to carry out the modelling satisfactorily. Thus, seasonal albedos appear to reasonably account for the temporary characteristics of the surface conditions over the season under question. On the other hand, longwave radiation plays mainly a role in the dry season by reducing the net radiation then, confirming statements of Sicart *et al.* (2011).

The temporal analysis of the turbulent fluxes shows that their lowest values in the energy balance occur predominantly in the dry season. However, the turbulent fluxes are not mainly responsible for the glacial processes in the ablation zone, as they often counteract themselves. Besides, turbulent fluxes are comparatively lower to net radiation. Only in sporadic days, the turbulent fluxes exceeded the net radiation. Especially, the sensible heat showed a peculiar increase during the long 2004-2005 El Niño period, owing to a sustained rise in temperature which eventually led to increased glacier melting in that period.

In the wet season(s), in particular, the vertical profiles of the energy fluxes across the glacier zone indicate that the turbulent fluxes can overcompensate the net radiation in the accumulation zone, thus the former being an energy sink which helps to maintain the glacier's accumulation, despite an increase of net radiation of this period. Increments/decrements in wind speed in the wet season/dry season are the most important cause of major/minor transfers of turbulent fluxes. Net radiation is more predominant in the glacier's ablation zone, exceeding the turbulent fluxes here to a large extent. These interesting findings should be clarified further by more detailed mass measurements in the glacier.

The role of the snow/rain threshold temperature T_0 turns out to be decisive in the glacial modelling as well, corroborating findings of Favier *et al.* (2004) and Gurgiser *et al.* (2013). A high sensitivity of T_0 is observed, especially, in the rainy season, although it appears to be affected by

La Niña- and El Niño phenomena, such that T_0 is decreased during episodes of the former. In any case, changes in the elevation at which T_0 occurs determine the snow area coverage, i.e. determine its albedo and, eventually, the amount of reflected radiation. Thus, the threshold temperature maintains a balance of the portion of accumulation and ablations areas. This is very important, because the physical surface characteristics control, in turn, the response to certain radiation fluxes, such as shortwave radiation reflected, longwave radiation emitted and turbulent fluxes. Other investigations of threshold temperature in mountain areas show that this variable depends on other meteorological variables, like humidity, pressure, and wind (Jennings *et al.*, 2018). Therefore, the threshold temperature is an important parameter which may show certain variability that depends on geographical conditions or climate events like those produced by ENSO. More investigations to that regard are suggested to better determine the physical behavior of threshold temperature in tropical glaciers.

The optimal discharge storage constants found in parallel simulations with the temperature index were used here and analyzed. These storage constants exhibit a seasonal behavior as well, and represent quite well the characteristic of the typical seasonal ablation and accumulation of snow, ice and firn, of glacier located in the outer tropics.

8 Temperature Index Modelling in Tropical Glaciers

8.1 Review on Empirical Temperature Index Models for Modelling Mass Balance and Discharge in Glaciers

The degree-day models, also called temperature index models, are based on an empirical relation between temperature and melting (Braithwaite and Olesen, 1989; Hock, 2003). This simple relation was proofed to deliver good performance to simulate ablation on many glaciers around the world. Although degree-days models leave out the role of many physical processes behind the ablation, they represent an important tool for cases where data is not available. In addition, they can be used to predict how changes in temperature affect the future of glaciers.

8.1.1 Basis of the temperature index model

The temperature index model considers basically two important terms. One is the so-called **positive degree-day (PDD)**, which is the total sum of daily average temperatures above 0°C in a given time period. The other one is the **degree-day factor (DDF)** which is a factor of proportionality, relating the rate of melting to the mean temperature or the positive degree-day. Basically, the degree-day factor indicates the decrease of the water content caused by one degree above freezing over one day.

The *Positive Degree-Day (PPD)* (°C*day or °K*day) is defined, for a time period Δt (days), as:

$$PDD(\Delta t) = \int_{\Delta t} T_c H(T_c) dt, \quad \text{with } H(T_c) = \begin{cases} 1 & \text{if } T_c > 0 \\ 0 & \text{if } T_c < 0 \end{cases} \quad (8.1)$$

where T_c is the air temperature (°C or °K).

When using daily mean temperatures, $\overline{T_{c_j}}$, Eq. 8.1 is replaced by its discrete counterpart:

$$PDD = \sum_j \overline{T_{c_j}} H_j \quad (8.2)$$

where the sum extends over all days j in the time interval of interest (with zero contributions when $T_c < 0$. Positive degree-day sums can also be accumulated over intervals such as an hour or a month. The latter has also been referred to as the positive degree month sums. Thus *PDD* can lead to a confusion, but positive degree “days” refers just to the name of the unit in which it is measured (IACS, 2011):

The *Degree-Day Factor (DDF)* (mm.w.e. °C⁻¹ d⁻¹) is the coefficient of proportionality between surface ablation m_s (mm.w.e d⁻¹) and *PDD*, i.e. the former is calculated as

$$m_s = DDF * PDD \quad (8.3)$$

The daily melt on an iced or snowed surface is then computed as:

$$m_s = DDF * \overline{T} \quad (8.4)$$

8.1.2 Advantages and disadvantages of temperature index models

Although temperature index models simplify a complex physical process, they are very valuable, as they require only simple input variables, while still performing well in estimating the melting at the scale of a basin (Martinec, 1960; Braithwaite and Olesen, 1989; Braithwaite, 1995; Singh *et al.*, 2000; Hock, 2003; He *et al.*, 2014). As such, they have also been used to study climatic sensitivity, since climate scenarios are usually given in terms of air temperature and precipitation changes (Hock 1998).

According to Hock (2003) and Ohmura (2001) the advantages of temperature index models are:

- Require only air temperature data which are widely available or can be easily extrapolated
- Easy interpolation and forecasting of air temperature
- Good model performance despite their simplicity
- Computational simplicity.

Although the temperature index models work well over long time periods, their accuracy decreases with increasing time resolution. Moreover, they are not good for discharge or flood forecasting, because they cannot capture quick-changing peak discharges, as the degree-day factors are not able to represent the large variability of diurnal cycles (Hock, 1998).

8.1.3 Spatial and temporal differences of the degree-day factors

Results of different studies show a large temporal and spatial variability of the degree-day factors (*DDFs*). These variations occur, because *DDF* accounts basically for all terms in the general melt balance energy equation (7.1) and, as discussed there, these terms vary from site to site and season to season. Lang and Braun (1990) state that, as long as the heat balance conditions do not change, *DDF* can be an index representing the energy for melt for the corresponding time period, but, as changes in climatic conditions over different seasons cause necessarily changes in *DDF*, its applicability for calculating melt over a longer time period has to be put into question.

The *DDF(s)* behaves in response to some other physical variables at the glacier site. For instance, Ambach (1988) concludes in his studies in Greenland ice sheets that low degree-day factors are generally associated with high shares of sensible heat flux there. Degree-day factors are expected to increase with elevation as well, owing to increasing direct solar radiation input, and they increase also with decreased albedo and the portion of sensible flux (Hock, 2003). Therefore, lower degree-day factors should be found for snow (high albedo) than for ice. In addition, some experimental studies report more rapid ablation from ice than from snow (Cuffey and Paterson, 2010). In agreement with the general trends above, *DDFs* ranging between 22 to 5 mm.w.e. °C⁻¹ d⁻¹ for ice and between 11.6 to 2.5 mm.w.e. °C⁻¹ d⁻¹ for snow have been reported (Braithwaite, 1995; Hock, 2003).

According to the reported *DDFs* in different locations, no regional pattern can be discerned, due to the complexity of the melting processes (Hock, 2003). However, maritime locations with higher wind speeds and higher humidity appear to have higher *DDFs*, owing to higher latent heat

of condensation and higher sensible heat transfer. In dry-, high-radiation-, continental regions, where ablation occurs mainly through sublimation, low *DDFs* are found, as sublimation consumes high amounts of energy, i.e. less energy is available for melting (Davies, 2015).

8.1.4 Physical fundamentals of temperature index models

There are not many investigations related to the understanding of the physical bases of the temperature index model (*TIM*), although the latter has been widely used for its good capacity of simulating melt. To that regard, Ohmura (2001) made interesting contributions to the physical bases of this method. His work suggests that *TIM* has been underestimated, despite the fact that it has shown sufficient precision for basin ablation estimations. Among the many aspects presented in the work of Ohmura (2001), the most important ones are:

The surface temperature plays an important role in melting and regulating the equilibrium in the energy equation. The longwave emitted radiation is determined by the other components in the energy balance equation (this aspect is different for other terms of the equation which indeed depend on external factors, not depending on the equation itself). Considering that the glacier surface has a poor thermal conductivity when melting occurs, this means that when the surface temperature reaches 0°C, the majority of the energy sources are funneled to melting. In this way, longwave emitted radiation by surface maintains itself as constant and melt turns into a process with a passive role. For Ohmura (2001), these characteristics of the energy budget and melt make melting easier to predict with the atmospheric data.

Longwave radiation, which is a very important term in the energy budget, is greatly influenced by temperature. This is because an important portion of incoming longwave radiation comes from the atmospheric layer close to the ground (around 67% from the first 100m and 89% for the first 1km). In the first layer, up to 100 m altitude, the presence of water vapor and the effect of longwave radiation are more characteristic, while greenhouse processes occur above 3km height. In this thin layer of the atmosphere, which is very important for high altitudes, the temperature and the vapor concentration have more influence on longwave incoming radiation than other variables. Some authors state that longwave radiation at the atmosphere can be modelled by temperature measured at the screen level¹⁵ (Swinbank, 1963; Saunders and Bailey, 1997; Ohmura, 2001). This is because the temperature measured at this level is representative of the first 100m at the atmosphere.

The high correspondence of temperature and melting can be explained by the correlation of temperature with some of the terms of the balance equation, such as longwave incoming radiation and turbulent fluxes. It has been estimated that longwave incoming radiation, together with sensible heat flux, provide around $\frac{3}{4}$ of the entire energy source used for melting in mid-latitude glaciers (Ohmura, 2001). However, the importance of longwave radiation in the tropical context is not enough discussed. A recent study (Gurgiser *et al.*, 2013) found that yearly average of net longwave radiation offsets between a third and a half of the energy gained via net shortwave radiation in Shallap glacier, whereas Sicart *et al.* (2011) showed that longwave

¹⁵ The thermometer is exposed in a Stevenson screen, at a height of 1.25 m above the ground and aspirated only by natural ventilation through the side louvers.

<https://www.metoffice.gov.uk/weather/guides/observations/how-we-measure-temperature>

radiation contributes with 57% of the whole energy sums in the dry season. For the present findings, the longwave radiation generates and offset of energy of 63 to 69% in the dry seasons (see **Chapter 7**).

It is also important to consider that the temperature itself is affected by global radiation. Certain correlations among these variables have been found by Ohmura (2001), as well in the present study case of Artesonraju in Section 5.5 .

Indeed, thermal conditions of air masses are generated by various components, such as advection, convection, mixing, radiative processes, turnover of latent heat in melting, condensation and evaporation. However, the contribution of each component to air temperature is difficult to elaborate. As long as the contribution of each of these variables change, for instance, due to seasonality, geographical location or weather types, the *DDFs* required for using the temperature index model also change (Lang and Braun, 1990).

8.1.5 Temperature index model in tropical glaciers

In tropical glaciers, the use of temperature index models is not so widespread, due to the low seasonal sign of daily temperature and the low correlation of daily temperature with net radiation (Sicart *et al.*, 2008). Indeed, these authors estimate that the application of temperature indices is more plausible at year-resolution, given the fact that the annual ablation is more correlated with inter-annual temperature variations. Nevertheless, a few studies have shown the possibility to use TIM and obtain satisfactory results in modelling mass balance in tropical glaciers at different resolutions. These studies include:

The glaciated basin of Parón Lake in the Cordillera Blanca, Peru: Application of TIM for simulating discharge between 2000 and 2005 (Suarez *et al.*, 2008). This study applied monthly degree melt factor for ice, using values that varied between 285 to 330 mm.w.e °C⁻¹ month⁻¹ for the Parón Catchment. In addition, a discharge constant for ice (Kice) ranging between 250- 500 (hour) was found.

Santa River Basin in Cordillera Blanca, Peru: Simulation of discharge of that river and glacier areas of this basin between 1979 and 1999 (Condom *et al.*, 2012). The monthly degree factor found for the Santa basin was 380 mm °C⁻¹ month⁻¹ for snow and 600 mm °C⁻¹ month⁻¹ for ice.

Zongo Glacier in Bolivia: Five modified models of temperature index, were applied there between 1997 and 2006 for modelling annual mass balance with a monthly resolution (Blard *et al.*, 2011). The outcomes show degree-day factors or melt factors of snow and ice ranging between 8.7±0.6 mm.w.e °C⁻¹ d⁻¹ and 12.7±1.4 mm.w.e °C⁻¹ d⁻¹, respectively, using different melt factors for snow and ice. However, the study did not find significant improvements in the simulation results when incorporating additional input data into the TIM, such as, for instance, a parameterization which uses the shortwave radiation for factor calculation.

Another application of a (enhanced) temperature index model to the Zongo glacier was carried out for years 2005 and 2006 by Fuchs *et al.* (2013). Their simulations included the use of net global radiation (global radiation minus albedo) to attain seasonal changes and by doing so the authors found optimal Temperature Factors of 0.20 mm d⁻¹ °C⁻¹ for the dry season and of 1.19 mm d⁻¹ °C⁻¹ for the wet season.

8.2 Use of Seasonal Degree Factors for Modelling Discharge and Mass Balance of the Artesoncocha Basin

8.2.1 General remarks on the applicability of *DDFs* in La Cordillera Blanca

The application of degree-day melt factors (*DDFs*) in the TIM – method for modelling discharge and mass balance in the glacier of La Cordillera Blanca has not been greatly explored at daily resolution. The main cause for this deficiency is the little variability of daily temperature in the year whereas the seasonality is more marked by the precipitation (dry and humid). However, some aspects should be considered before disregarding the applicability of the TIM method. Firstly, the daily temperature is not totally constant and some small sign of variability can be found in the data between the seasons. Secondly, although there is not a big variability over the year, the temperature is a parameter that shows a clear trend at the inter-annual scale as an indicator for climate warming. Thirdly, even these small changes of temperature could influence the altitude at which the temperature threshold (T_0) for snow/rain occurs. As it was shown in the energy balance simulations in the previous chapter, the threshold temperature T_0 is one of the sensitive factors which determine the behavior of the glacier's mass balance.

Another point to consider is that the so-called degree-day factors *DDFs* represent indirectly climate conditions of the energy balance equation. Since there are marked seasons and different behaviors of each energy flux for each season, establishing appropriate *DDFs* could open the possibility to use this kind of tool for modelling. Seasonal *DDFs* represent more properly the dynamics of the tropical glaciers, in spite of their rather low temperature seasonality.

However, the lack of complete data sets in the Andean mountains hinders the possibility to use physical based models for predicting the fate of the glaciers in that region of the world for long periods of time. Thus, there is a need to find tools to that avail, using minimal data; in this case, temperature and precipitation. In such a case, temperature index models (TIM) can contribute significantly to the current investigations about the effects of climate change on glacier dynamics. Therefore, this section aims to explore the possibility to use this kind of tool for the tropical glaciers in the Andean Mountains.

8.2.2 Methodology

8.2.2.1 Parameterization

The temperature index model used was is that (Hock, 1998), i.e. the melting is calculated according to Eq. 8.4. The model uses the same discharge routing model of Baker *et al.* (1982) and applied by Hock (1998), as described in Section 7.2.2.6 of the energy balance model.

8.2.2.2 Simulation period and input data

The period of simulation is the hydrological years 2004-2007, since it is the period with the most complete climate data set. The validation period is from 2001 to 2004. The simulation is short because of the lack of data, namely, for discharge at the Artesoncocha Lake outlet which is available only in some periods between 1996 and 2001 and, to a greater extent, between 2002 and 2007. Mass balance measurements of the validation period are not available and the precipitation data was provided just up to 2007.

The input required for modelling with the temperature index model is shown in **Table 8.1**

Table 8.1. Input data for the temperature index model (TMI)

Data Type	Data	Observations
Climate Data	Temperature	Daily resolution, climate station at 4811 m.a.s.l., gradient of temperature -0.65°C/100m
	Precipitation	Daily resolution, climate station at 4836 m.a.s.l.
	Discharge	At the outlet of Artesoncocha lake, used for model calibration and validation.
Grid Data	Elevation	DTM30 m
	Water equivalent at the started day	For calibration period, taken from measurements of mass balance and interpolated using kriging with ArcGIS. For validation period, from results of the last simulated season.
	Firn and ice area	Delimitation of surface areas at beginning of hydrological year, for both calibration and validation period.

8.2.2.3 Main calibration parameters

8.2.2.3.1 Degree-day factors:

Some initial simulations showed that certain *DDFs* could simulate the observations better for certain periods and others for the rest. Therefore, the simulations used seasonal degree factors for three periods according to their seasonal characteristics. The first one, marking the beginning of the rainy season or transition period, lasting from months September to October (SO), the second one, the core of the rainy season, from November to March (NDJFM), and the third one, the dry period, from April to August (AMJJA). A wide range of *DDFs* were explored for each of these three periods. The ranges of *DDFs* tested were between 4-26 mm.w.e °C⁻¹ d⁻¹ for ice and 0.5-20 mm.w.e °C⁻¹ d⁻¹ for snow, ranges that are much in agreement with those found by Singh *et al.* (2000) and Hock (2003) in other glaciers areas around the world, namely, ranges of *DDFs* between 5-20 mm.w.e °C⁻¹ d⁻¹ for ice and between 2.5-11.6 mm.w.e °C⁻¹ d⁻¹ for snow. Combinations of *DDF(s)* of snow exceeding those of ice were excluded in the simulations, because it is generally agreed upon that *DDF(s)* of ice are greater than those of snow (Braithwaite, 1995; Hock, 1998; 2003). This occurs due to the characteristics of the materials. For instance the snow mainly located in the accumulation area, absorbs less energy than ice, indeed net radiation reduces considerably in this portion of the glacier. The ice is a material that characterizes de ablation area. Ice absorbs more energy and therefore more discharge is generated by ice melting than snow.

8.2.2.3.2 Storage Constants

A wide range of discharge constants in the discharge routing equations (see Section 7.2.2.6) were also tested: for snow, values between 20-510 hours, for firn, values between 50-2500 hours and for ice between 1-300 hours. The first exploratory exercises showed good results with larger storage constants as those presented in the literature (Liboutry, 1971). Therefore, their range was expanded and the best storage constant combinations were selected analyzing common

seasonal trends retrieved not only from the temperature index simulations, but also from the energy balance simulations of the previous chapter.

8.2.2.3.3 Threshold Temperature rain/snow (T_0):

This parameter is used to determine the amount of the solid and liquid precipitation. One degree below and above the T_0 , the precipitation is assumed as a combination of snow and rain, with the percentage of each one obtained from linear interpolation (Hock, 1999).

8.2.3 Results and discussion

8.2.3.1 Simulated discharge

The criteria used to evaluate the model performance are again the Nash Sutcliffe Coefficient (E) and the RMSE. These two parameters are presented for each hydrological year in **Table 8.2**. Based on the values of E , the adjustment quality has been evaluated. The table shows that the model results are quite good in simulating the discharge in the calibration period with annual E 's ranging between 0.75 and 0.89 and the best result obtained for years 2004-2005.

However, as can be seen from the simulated and measured hydrographs at the outlet of Artesoncocha lake in **Figure 8.1**, the model is not able to simulate certain peaks of the rainy season. In addition, some deviations, underestimations and overestimations of the observed discharge occur in the dry season of years 2005-2006 and 2006-2007. Nevertheless, the model is able to represent in a satisfactory manner the observed discharge.

Table 8.2. TMI- obtained Nash Sutcliffe Coefficients for discharge in the calibration period.

Year	E	$RMSE$ m^3s^{-1}	Adjustment quality (Cabrera, 2011)
2004-2005	0.89	0.1092	Excellent
2005-2006	0.78	0.1659	Very Good
2006-2007	0.76	0.1264	Very Good
2007-2008	0.75	0.1371	Very Good

8.2.3.1 Mass Balance and ELAs for the calibration period

The mass balance profiles computed by the current TMI- model and those measured by UGRH (reported by WGMS, 2015) are analyzed for each hydrological year. Not included are months of SOND of 2007, because the UGRH-calculation is normally for the whole year. The comparison of the simulated and measured mass balance profiles (see **Figure 8.2** and **8.3**) leads to the following comments:

For the year 2004-2005, in the lower-lying ablation area, the simulated mass balance estimate more losses than measured data, especially between 4700 and 4900 m.a.s.l. These differences are of up to 2.8 m.w.e between the UGRH- measured and simulated. The total area with differences larger than 2m.w.e is 29% of the total glacier's area. The simulated mass gains in the accumulation zone exceed the UGRH- estimated ones by up to 2.5 m.w.e. However, the areas in

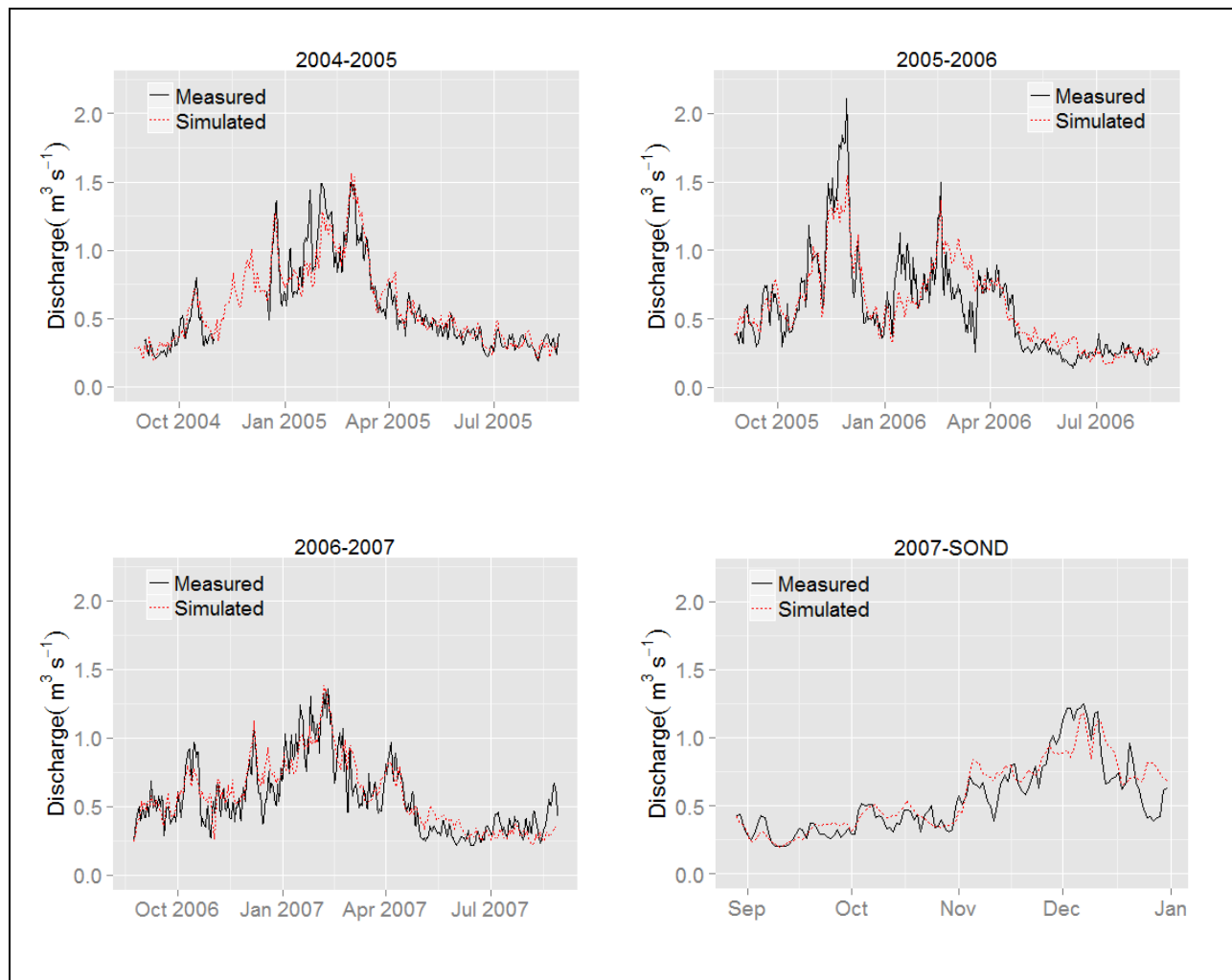


Figure 8.1. TMI-simulated (calibrated) and measured discharge at Artesoncocha lake outlet

which differences above 2 m.w.e. occur correspond to 12% of the total glacier's area. It is important to clarify that above 5075m elevation, the estimation of the UGRH indicates a constant accumulation of 0.94m.w.e, an aspect that should be subjected to more investigations. The RMSE of the simulations in regard to measured data is of 2.21 m.w.e.

For the year 2005-2006, in the ablation zone, there are again positive differences of up to 2.4 m.w.e., with those exceeding 2 m.w.e representing 18% of the total glacier's area. The corresponding panel of **Figure 8.3** shows that there are no differences in the simulated and measured profiles in the accumulation zone exceeding 2 m.w.e., wherefore the UGRH measured a constant accumulation of 1.2 m.w.e. above 5175 m.a.s.l. In general, for this year, the measured and simulated profiles are more congruent, especially, in the upper and lower areas of the glacier, where differences are more pronounced in the previous year. The RMSE of the simulated against the measured data is 1.92 m.w.e.

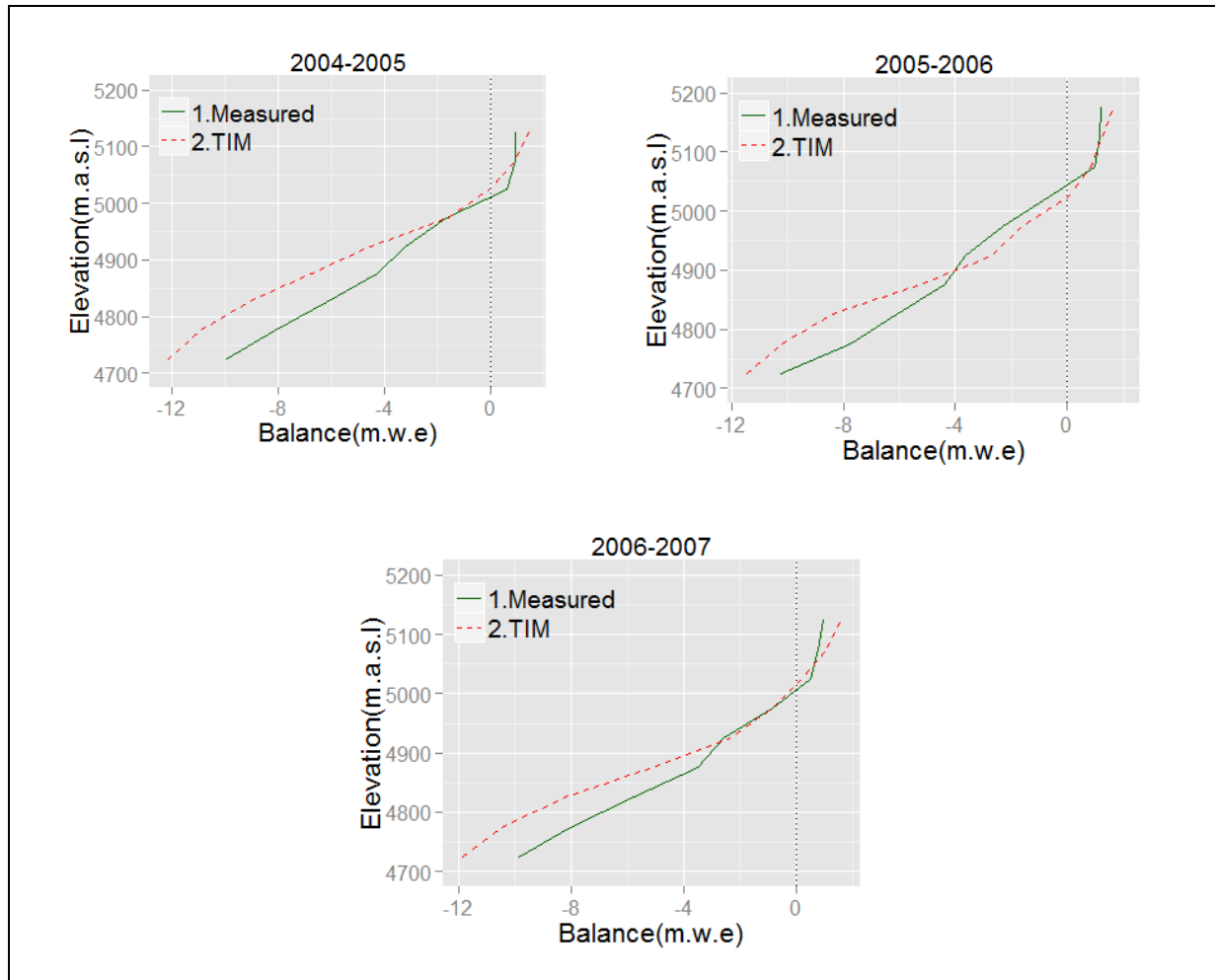


Figure 8.2. Measured and TMI- simulated mass balance profiles for the years of calibration

Finally, for the year 2006-2007, in the ablation area, an overestimation of simulated mass losses of up to 2.4 m.w.e is obtained in 19% of the glacier's area. The results of the simulation show differences with the observations of up to the 2.5 m.w.e in the accumulation zone whereas the UGRH- measured accumulation is constant with 0.97m.w.e above 5075 m.a.s.l. Differences over 2 m.w.e in this zone present 14% of the total glacier's area. The RMSE for simulations is 1.84 m.w.e.

The areal distribution of the simulated- and the UGHR – stage measured glacier's mass gains and losses are shown for the different calibration years in **Figure 8.3**. From these maps, the ELAs (yellow bands in the panels) can be retrieved. One can notice a good agreement between TIM-simulated and measured ELAs, with slight differences of up to only 29 m.

8. Temperature Index Modelling in Tropical Glaciers

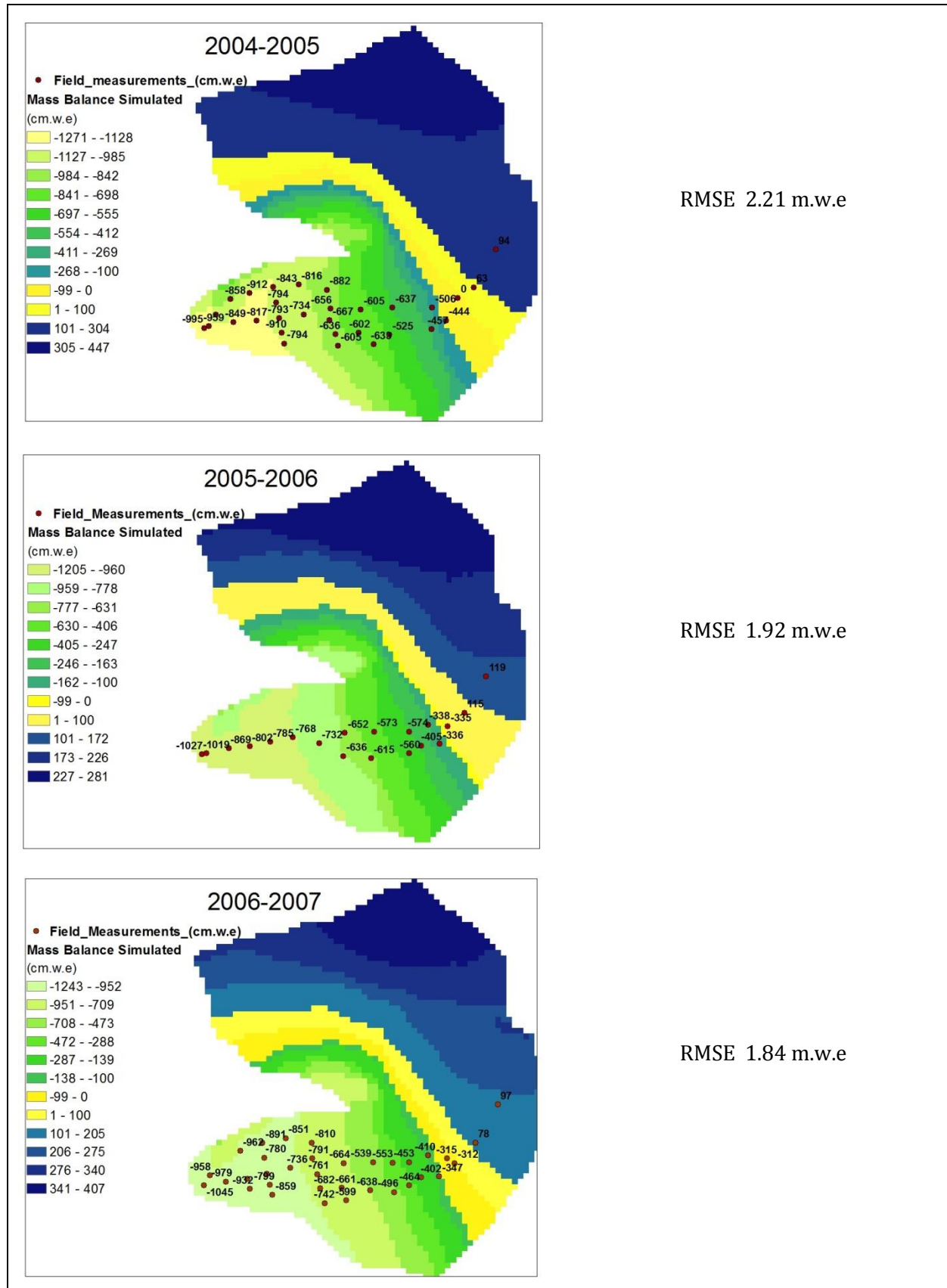


Figure 8.3. TMI- simulated and measured mass balances for the different years of calibration

8.2.3.2 Parameters' sensitivity

8.2.3.2.1 Degree-day Melt Factor

A range of 4-26 mm.w.e °C⁻¹ d⁻¹ for DDF_{ice} and of 0.5-20 mm.w.e °C⁻¹ d⁻¹ for DDF_{snow} was applied to find TMI- model's sensitivity to these two parameters. These ranges were selected according to the degree-day factors ranges found by other authors at other sites, as discussed previously.

The results of the current TMI- simulations show that the degree-day factors exhibit certain trends, depending on the season and, consequently, the use of different seasonal degree-day factors was advocated in the present study. These different degree-day factor ranges were applied in SO, the beginning of the rainy season; NDJFM, the core of the rainy season; and APJJA, the dry season. These periods generally delimit days with similar characteristics of various climate variables, such as precipitation and, thus, the albedo, longwave flux and turbulent fluxes, and, so, daily mass balance averages.

Figure 8.4 shows the response plots of the $DDFs$ 'combinations for each season. In agreement with the problem stated by Hock (1998) related to the ambiguity of selecting a specific (optimal) set of DDF - parameters, the three plots show also that many combinations of $DDFs$ are able to well simulate the discharge. For this reason some additional optimal DDF - selection criteria were used. Thus, the final selection of the best DDF - combination took into account not only the best results for the discharge simulation, but also the least difference between simulated and observed total volume of discharge, accuracy in the ELAs, and coherence with the specific mass balance reported by WGMS (2015) and UGRH (Gallaire *et al.*, 2007). During the simulations, it was found, interestingly, that the simulated mass balances were closer to the observed ones when the deviations of the total discharge volumes were also low.

In addition, it was noticed in the simulations that the $DDFs$ have seasonal trends, similar to those found for other climatic parameters and concordant to the accumulation and ablation regime of the glacier. The DDF_{snow} between the beginning and core of the wet have relatively less differences than the DDF_{snow} of the dry season. In the beginning of the rainy season under normal conditions, the snowfall in the study area is less intense, and accumulation starts but with low intensity, in the core of the wet season the maximum accumulation is generated, while in the dry season no accumulation occurs. Therefore, optimal DDF_{snow} retrieved from the first response plot of **Figure 8.4** is slightly higher (=5.4 mm.w.e °C⁻¹ d⁻¹) than that obtained for the core of the rainy season (=4.8 mm.w.e °C⁻¹ d⁻¹) (second plot) and almost double of that (=2.8 mm.w.e °C⁻¹ d⁻¹) of the dry season (third plot), amount of snowfall in the wet season leads to larger DDF_{snow} . However as accumulation increase, a slight reduction of DDF_{snow} occurs in NDMJJA. In the second (wet) season, a lot of fluctuations can be ascertained from the corresponding panel, as the steady increments of solid and liquid precipitation, as well as the small increments in temperature, generate more melting, especially, from the iced area, which is reflected by an increase of the optimal DDF_{ice} (=16 mm.w.e °C⁻¹ d⁻¹), compared with that of the first season (=9 mm.w.e °C⁻¹ d⁻¹). Thus, larger amounts of snow and deposition allow the snow to maintain itself, but at the same time, more energy input in the ablation area generates maximum $DDFs$ on ice in the core of the wet season.

The dry season characterized by less energy input, especially in the accumulation area (see **Figure 7.12**), less precipitation, but also a slight drop of temperature, leads, logically, to a

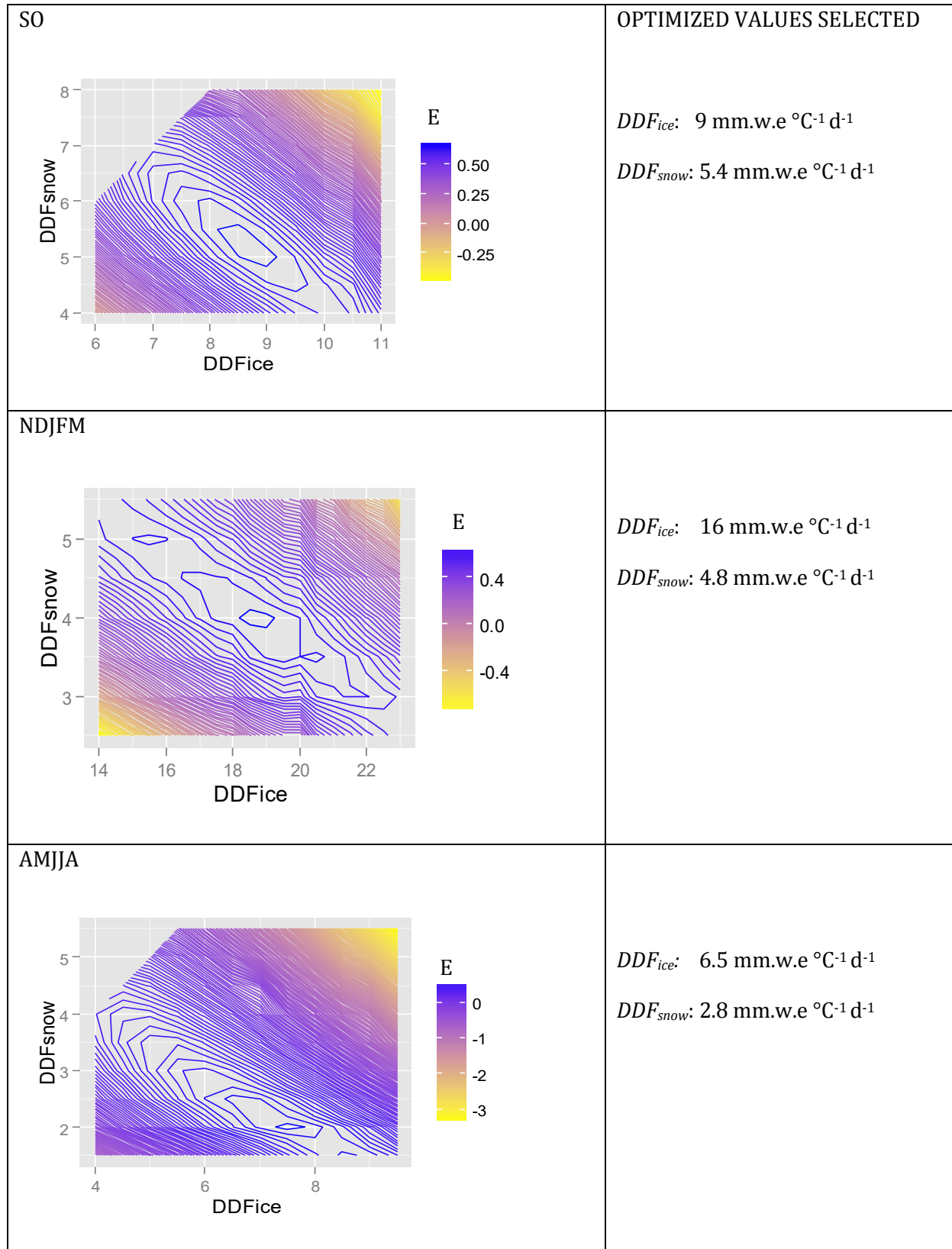


Figure 8.4. Degree-Day Factor sensitivity plots in terms of the Nash-Sutcliffe parameter E for the three seasons considered, with optimal values for ice and snow as indicated

reduction of the optimal values of both DDF_{ice} ($=6.5 \text{ mm.w.e } ^\circ\text{C}^{-1} \text{ d}^{-1}$) and DDF_{snow} ($=2.8 \text{ mm.w.e } ^\circ\text{C}^{-1} \text{ d}^{-1}$). From the panels of **Figure 8.4** one may concluded that the variability of DDF_{ice} across the seasons is bigger than that of DDF_{snow} , reflecting the larger contribution of ice- than snow-melting to discharge. Finally, it may be noted that the $DDFs$ of the simulation area are in the range of those found in the literature (Hock, 2003; Blard *et al.*, 2011).

Results of a calculation of the correlations between the daily mean of various climate variables and the two DDF are listed in the lower part of **Table 8.3** and reveal certain similarities in their behavior and explain the reasons behind the dynamics of the Degree-Day Factors for the simulation of discharge and mass balance in this case.

The DDF of ice shows similar seasonal trends with daily mean precipitation (averaged in the season) ($r=0.81$), relative humidity ($r=0.72$), daily mean longwave emitted by the atmosphere ($r=0.85$) and the surface ($r=0.81$). In regard to temperature, certain correspondence in the daily mean temperature is observed ($r=0.42$). The lower correlation with temperature is caused by the pattern of this variable in the core of the rainy season from 2004-2005, which differs from the other years. The temperature which is usually slightly higher in the core season in comparison to the dry season, did not follow this pattern for this year. In general, the DDF_{ice} mean daily temperature has a similar variation than the seasonal mean temperature. The correlation of DDF_{ice} with seasonal net radiation is good ($r=0.68$). This can be the reason that the temperature degree-day factors found in this research could deliver such satisfactory outcomes of simulating discharge. A certain correlation exists between DDF_{ice} and seasonal shortwave incoming and reflected with

Table 8.3. Correlation of daily means of energy fluxes and degree-day factors for various seasons

Year	Period	DDF_{ice}	DDF_{snow}	T	P	RH	W	S_{inc}^{\downarrow}	S_{ref}^{\uparrow}	L_{inc}^{\uparrow}	L_{sufc}^{\uparrow}	Q_N	Q_{HS}	Q_{HL}
				$^\circ\text{C}$	mmd^{-1}	%	ms^{-1}	Wm^{-2}						
2004-2005	SO	9	5.4	1.36	3.36	76.3	2.98	224	167	286	303	40	4.3	-7.8
2004-2005	NDJFM	16	4.8	2.26	5.60	79.8	2.13	230	140	299	312	76	10	-11.3
2004-2005	AMJJA	6	2.8	2.07	0.78	62.8	1.08	206	136	250	294	29	9.1	-6.4
2005-2006	SO	9	5.4	1.80	2.74	74.3	2.72	241	165	279	305	58	7.8	-10.5
2005-2006	NDJFM	16	4.8	2.09	6.68	78.0	2.11	238	156	298	319	67	5.4	-8.5
2005-2006	AMJJA	6	2.8	1.62	1.45	69.5	1.83	186	138	268	301	16	11.9	-9.6
2006-2007	SO	9	5.4	1.98	1.68	73.6	1.12	234	152	284	304	63	2.9	-1.8
2006-2007	NDJFM	16	4.8	2.13	6.92	80.2	2.12	215	162	301	312	44	10	-9.8
2006-2007	AMJJA	6	2.8	1.83	1.74	74.7	1.07	203	150	270	306	20	2.1	-1.5
2007	SO	9	5.4	1.35	2.81	74.4	1.02	234	188	286	301	33	2.1	-3.1

Correlations (Kendall method)														
DDF_{ice}				0.42	0.81	0.72	0.34	0.34	0.25	0.85	0.81	0.68	-0.04	-0.38
DDF_{snow}				-0.25	0.12	0.04	0.34	0.68	0.68	0.17	0.12	0.34	-0.04	-0.12

correlation coefficients of $r=0.34$ and $r=0.25$, respectively. No correlation between DDF_{ice} and sensible heat and latent heat flux are found.

The $DDF(s)$ of snow behaves similar to the daily mean (averaged in the season) of incoming and reflected shortwave radiation ($r=0.68$) for both and to a less extent with the longwave radiation emitted in the atmosphere ($r=0.17$). DDF_{snow} had also some correlation of ($r=0.34$) with the seasonal net radiation. These findings show a certain correlation of seasonal $DDFs$ with the seasonal daily means of net radiation, shortwave radiation and with longwave radiation emitted by the atmosphere.

Besides, certain statistical association and the correlation of daily means of temperature with certain energy fluxes found in Chapter 5, shows certain correspondence with the explanations given by Ohmura (2001) about the physical basis which explains the accuracy of this method in calculating melting. These physical bases are not indifferent to outer tropical glaciers due to the importance of longwave radiation (incoming) as a contributor to determine seasonal variation in the tropical glacier (Sicart *et al.*, 2011) and found in the last chapter.

8.2.3.2.2 Storage Constants (Mean Residence Times)

The storage constants define the residence times of three different reservoirs in the glacier, representing snow, ice and firn. These storage constants are calibration parameters of the model and are computed based on a cyclic variation of the driving input R_i (sum of meltwater and rain) to the “reservoir” generating a cyclic variation of output runoff Q_i , with peak values delayed by the residence time relative to the time of the input peak (see Eq. 7.31). After input shutoff, the runoff declines exponentially with time. It is clear that the storage constants could change with time of the melting, depending on some aspects, like the concentration of solutes which could generate long contacts with the bed or the type of surface in the routing process. Thus, both a low and fast routing process may be produced even in the same reservoir (Cuffey and Paterson, 2010).

For this study, a large range of storage constants were tested, specifically, for k_{firn} : 50-2500 hours; for k_{snow} 20-510 hours; and for k_{ice} 1-300 hours.

Figure 8.5 shows the TMI- model’s response curves in terms of the Nash-Sutcliffe coefficient E as a function of k_{firn} and k_{snow} , and k_{ice} and k_{snow} for the three seasons defined. The three seasonal plots indicate seasonal trends when combining the pairs of variables, with the best selected values (best adjustment of the model to the observations) represented by the white lines as the average of the season in the years (2004-2007).

As the storage constants represent the residence time for three different (firn, snow and ice) reservoirs, it is rational to think that their different physical characteristics in each season would lead to different water flow velocities in each medium. For instance, the k_{firn} storage constant is the parameter with the largest resident times between the seasons which may be due to the fact that is influenced by the snow coverage across the seasons. k_{ice} exhibits more rapid response than the other two, and therefore less sensitive compared to the other two constants k_{firn} and k_{snow} .

The k - constants for firn and snow are more variable and sensitive than that of ice in the model

8. Temperature Index Modelling in Tropical Glaciers

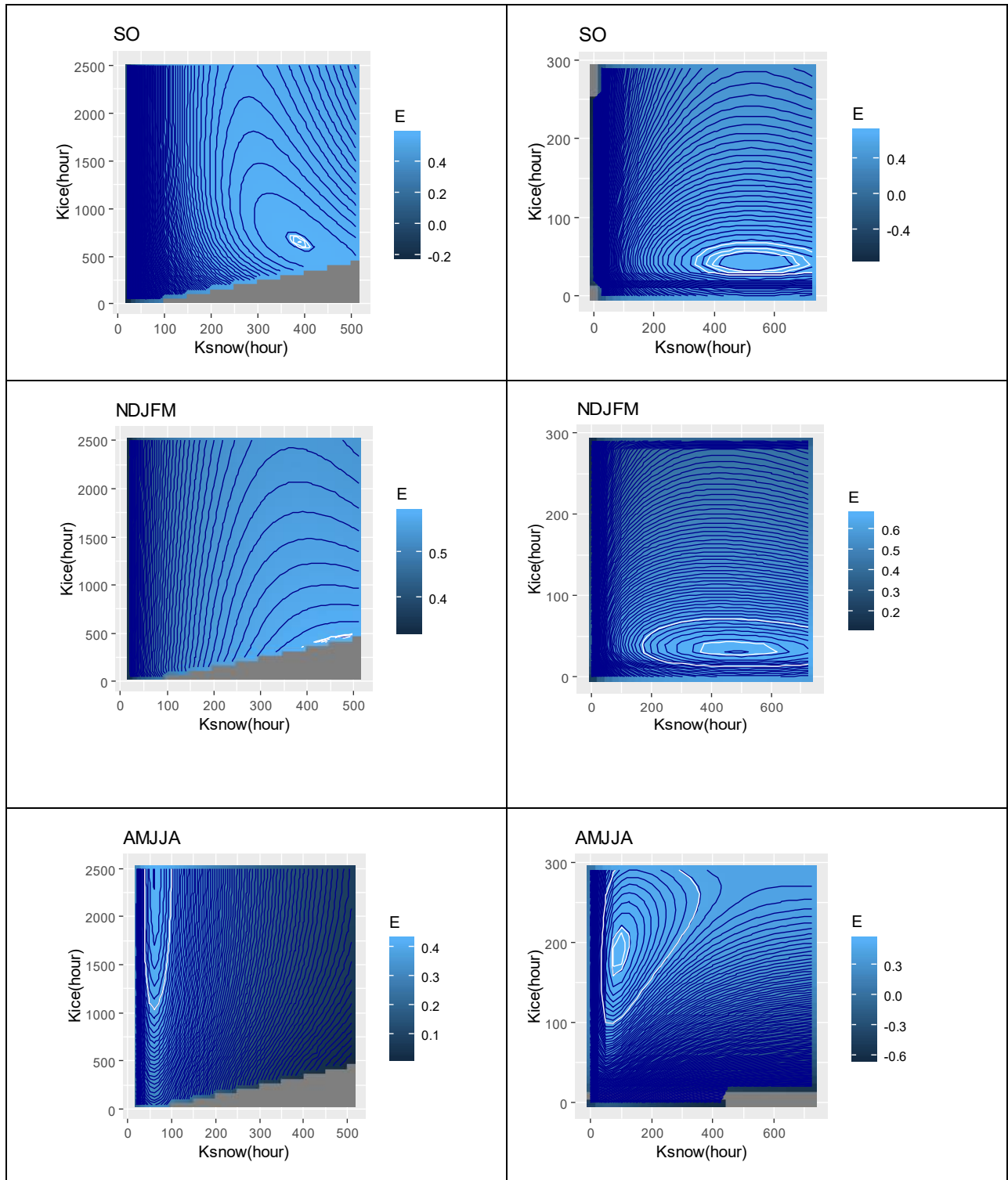


Figure 8.5. TMI-sensitivity of three storage constants (snow, ice and firn) in each season

calibration. Therefore, the best combination of these parameters was first calibrated for each season. The finally optimized optimal k_{firn} – values of 700, 400-500 and 1100 hour and k_{snow} – values of 390, 390 and 60 hour for the three seasons SO, NDJFM and AMJJA, respectively, appear to be reasonable to reflect the melting cycle, with the maximum melting due to maximal temperatures and precipitation occurring in months NDJFM, when the lowest k_{firn} (400-500 hour) and the highest k_{snow} (390 hour) are obtained. This may be due to the fact that in this core

wet season period more snow and probably some bare areas of firn, incrementing the velocity of firn melting, are encountered.

For the minimal discharge (dry) period (AMJJA), high k_{firn} - values above 1100 hour result in the best calibration performance, but with that most conservative value still giving acceptable results for E . Such high k_{firn} - resident times reflect the longer period after the earlier snow accumulation (wet) periods of the glacier, as accumulated snow over firn prevents the latter to melt and new firn even starts to form.

The k_{snow} resident time exhibits less variability between the beginning and the core of the rainy seasons. However, a much smaller k_{snow} - value (60 hour) is found for the dry season this indicates less resident time of the snow, owing most likely to the fact that snow is becoming firn and accumulation is reduced to minimum in this season.

Compared to the other storage constants, those of ice (k_{ice}) are relatively small for the beginning and the core of the rainy seasons (30-80 hour), but increases by about a factor of two for the dry season, when the decrease of liquid precipitation and a slight drop the temperature could increase the time during which the ice melts.

Table 8.4 presents a summary of the storage constants used for different tropical glaciers, including those found in the present research above. Although no other author works with seasonal storage constants, storage and release of water are important factors determining the seasonal runoff pattern. A comparison between the storage constants is therefore difficult. In addition, the sizes of the studied basins are also different and the storage constants are influenced by this factor as well. Nevertheless, certain coherence can be seen between the storage constants for the different glaciers. For instance, for the Zongo glacier, whose area is smaller than that of Artesoncocha, the storage constants are also lower. On the contrary, for the basin of Paron - which includes the Artesoncocha lake - much larger k_{ice} - values (250-500) than those determined here from the lakes' outlet discharge (50-200, depending on the season) were found, reflecting the larger residence time of ice before its meltwater affects the discharge of the Paron basin as a whole.

In general, higher residence time of snow in the beginning and core of the wet season and lower ones in the dry season are typical for the accumulation regime of glaciers in the outer tropics. The lower residence time for ice in the two wet seasons compared to the dry period represent quite well the ablation regimen of the glacier. The larger residence time of firn that occurs in the dry season reflects the natural process of its formation after the accumulation period.

Table 8.4. Reservoir storage constants for various tropical glaciers compared with the seasonal ones determined by the TMI- model in the present study.

Basin/Glacier	Area (km ²)	k_{firn} (hr)	k_{snow} (hr)	k_{ice} (hr)	Reference
Zongo	1.96	350	30	16	(Sicart <i>et al.</i> , 2011)
Paron	38.6			250-500	(Suarez <i>et al.</i> , 2008)
Artesoncocha	7				
SO		700	390	50-80	Current research
NDJFM		400	390	30-70	Current research
AMJJA		1100	60	80-200	Current research

8.2.3.2.3 Threshold Temperature Rain/Snow T_0

The threshold temperature rain/snow T_0 is another sensitive parameter in the model calibration. T_0 determines the fate of the two surfaces, ice and snow and, thus, the distinction between the different degree-day factors. The simulations show that for most seasons the optimal threshold temperature ranges between 2.5°C and 3.5°C, with the latter value obtained especially for the dry season (see **Figure 8.6**). Reduction of the threshold temperature below 2.5°C has a major impact on the calibration quality (in terms of E), especially, in the core of the rainy season (NDJFM) and to a lesser extent in the dry period (AMJJA). Low variability is found at the beginning of the rainy season, the transition period (SO). On the other hand, threshold temperatures above 4°C do not improve the calibration anymore and are, furthermore, unrealistic.

The result above that the threshold temperature T_0 is a sensible parameter in the present glacier simulations, especially, in the core of the rainy season as well as in the dry season, indicates that small changes of the mean daily temperature can strongly affect the glacier dynamics in terms of a change of the altitude where the threshold temperature takes place and, thus, the snow line altitude. These findings corroborate the ideas of Gurgiser *et al.* (2013) and Favier *et al.* (2004) who found a high sensitivity of the mass balance to the temperature and the snow/precipitation phase in the Shallap Glacier, Peru, as both control the snow line in the ablation area. In fact, the threshold temperature found by Gurgiser *et al.* (2013) ranges between 1.1°C and 2.5°C, i.e. is lower than the optimal ones found in the present study above. These differences may depend on certain local atmospheric conditions related, especially to relative humidity, vapor pressure and wind speed. Also, anomalies produced by ENSO can produce changes in the threshold temperatures, for example, by an unusual dryness to be expected during an El Niño event, as it occurred in 2004-2005 and 2005-2006. According to Jennings *et al.* (2018), precipitations events at low relative humidities are more likely to fall as snow at higher T_0 . Indeed, from observational data, the warmest threshold temperatures are seen in mountain dry regions above 4000 m.a.s.l. in the north hemisphere, e.g. 3.8°C in the Rocky Mountain and 4.5°C in the Tibetan Plateau.

8.2.3.1 Validation of discharge

Validation of the calibrated TMI- model is made for the years 2001-2003 for which discharge data at the outlet of Artesoncocha basin was available. The model's performance in terms of the Nash- Sutcliffe Coefficient (E) and the $RMSE$ is presented in **Table 8.5** for each of the three hydrological years. One can notice a satisfactory performance of the TMI-Model using daily data and seasonal degree-day factors, with E - values varying between 0.7 and 0.82 and inversely related $RMSE$ ranging between 0.183-0.139 m³s⁻¹.

Table 8.5. TMI- simulated Nash Sutcliffe Coefficients E and $RMSE$ for the validation period

Year	E	$RMSE$ (m ³ s ⁻¹)	Adjustment (Molnar,2011)
2001-2002	0.82	0.139	Excellent
2002-2003	0.80	0.136	Excellent
2003-2004	0.7	0.183	Very Good

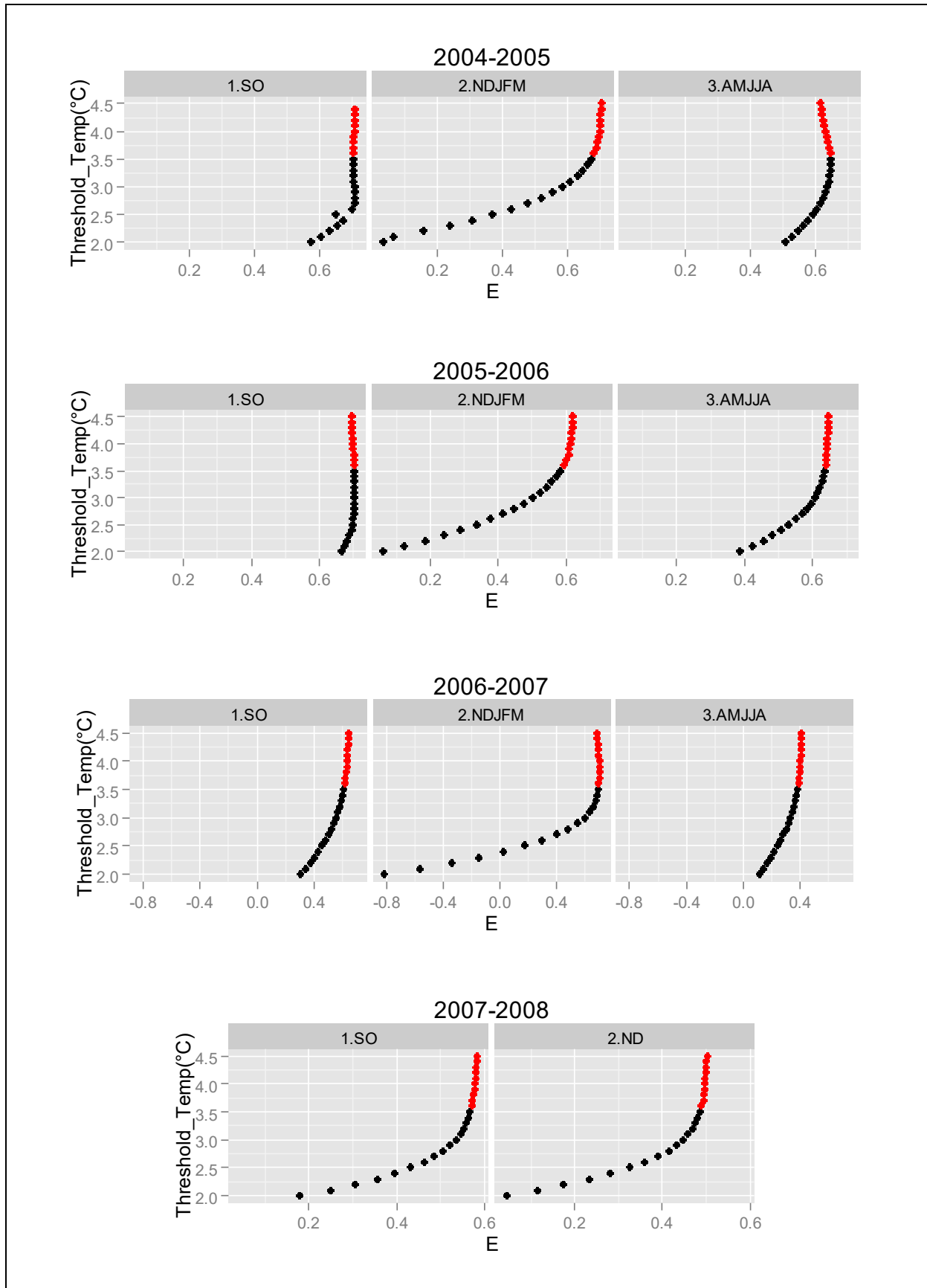


Figure 8.6. Threshold temperature snow/rain T_0 - sensitivity in terms of E . Red points show values of T_0 above 3.5°C

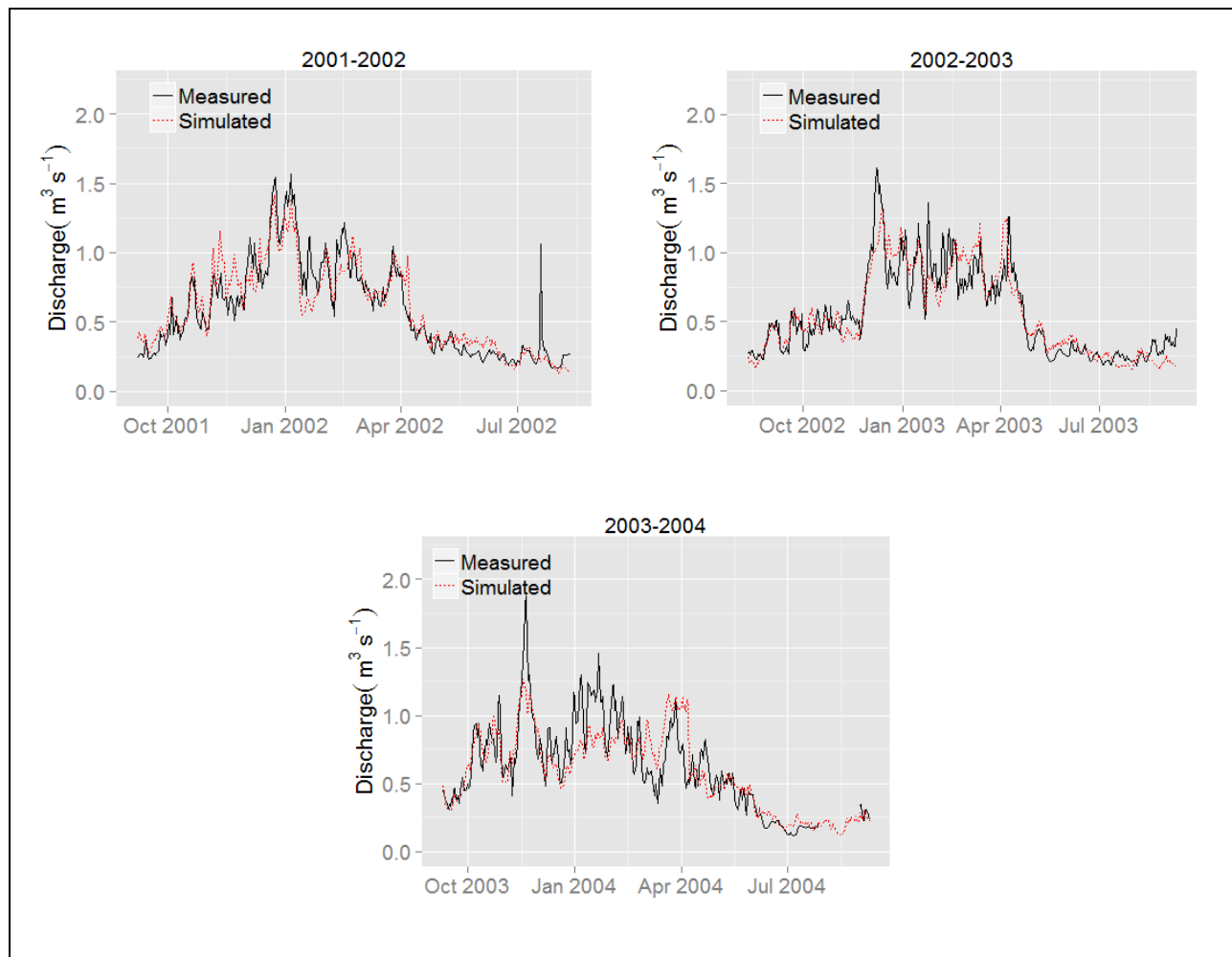


Figure 8.7. TMI-simulated and measured discharge for the validation period

However, the simulated and measured hydrographs shown in **Figure 8.7** indicate some shortcomings of the model's validation performance for certain peak discharges in the rainy season, especially in the year 2003-2004. In the year 2001-2002, there is a peak in the observed discharge in the dry season which could be a measurement error, because such high peaks are not common in this season.

8.2.3.2 Mass balance profiles, ELAs and total mass balance for the validation period

Figure 8.8 shows that the mass loss in the ablation zone is much larger for year 2003-2004 than in the two previous years, especially, in the lower parts of the glacier below 4800 m.a.s.l. For year 2002-2003, the simulation results in a slight recovery of the specific mass balance of the glacier compared with that of the previous year, as the ELA drops underneath 5000 m.a.s.l. in that year, being above that altitude in the two other years. However, the mass balance is still negative according to the data provided by the UGRH and shown in **Table 8.6**.

Table 8.6 summarizes the UGRH- estimated and TMI-simulated specific mass balances and the ELAs for the validation period 2001-2004 as well as for the calibration period 2004-2008, discussed earlier. For the validation years 2001-2003, discharge data is available, but no monthly mass balance measurements. For the subsequent validation year 2003-2004, some official reports by the Peru national authorities list annual mass balance data.

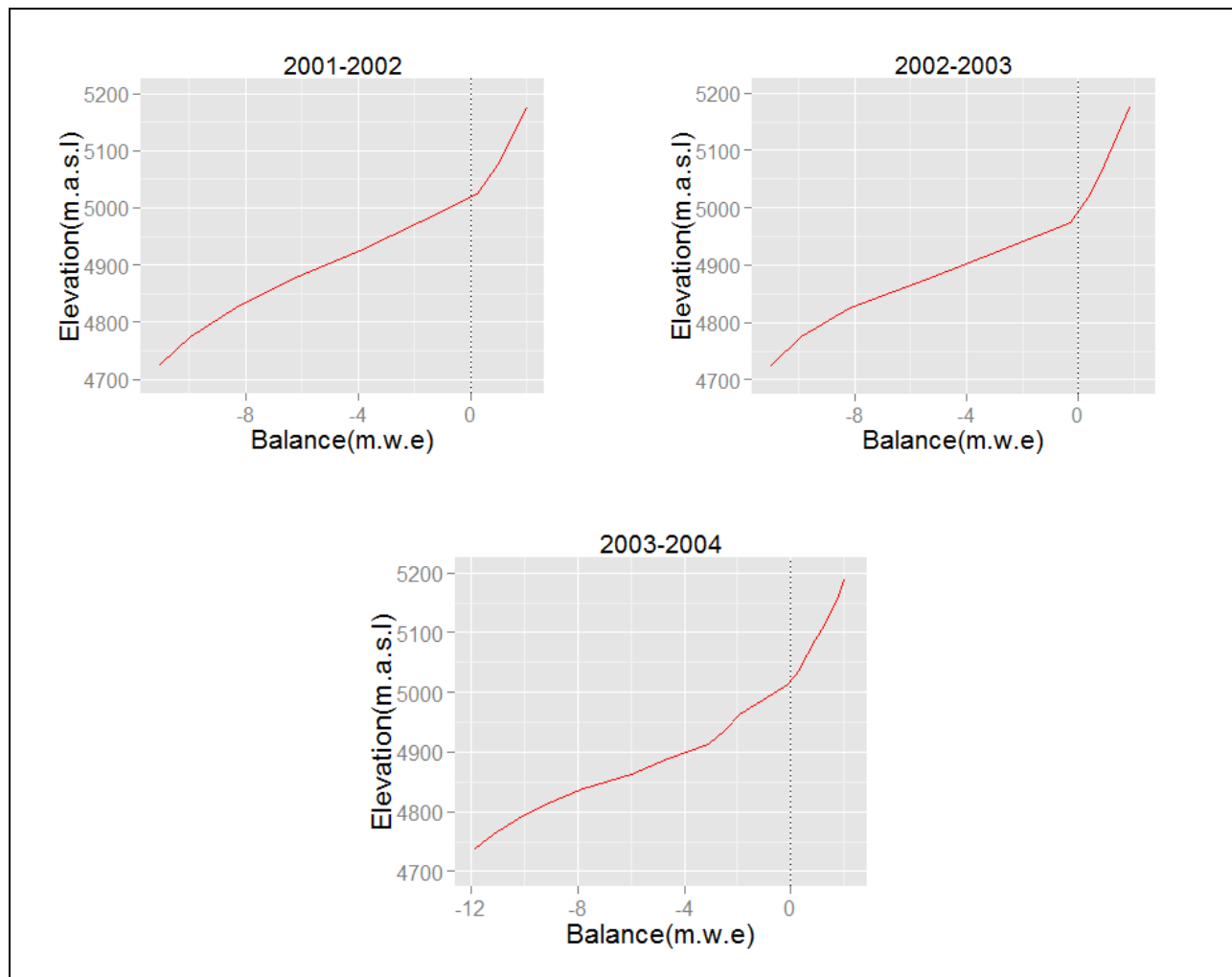


Figure 8.8. TMI-simulated mass balance profiles of the validation period

Table 8.6. Simulated and measured mass balance, ELA, snow line and AAR (accumulation area ratio) for the whole simulation time (validation and calibration periods)

Year	UGRH -mass balance (WGMS, 2015) (m.w.e)	Simulated mass balance (m.w.e)	ELA (UGRH) (WGMS, 2015) (m.a.s.l.)	ELA (simulated) (m.a.s.l.)	Snow line (Rabatel <i>et al.</i> , 2012) (m.a.s.l.)	AAR (%)
2001-2002 ^v		-1.543		5011	4887	56,0
2002-2003 ^v		-1.356	5119	4994	4857	58.9
2003-2004 ^v	-1.48	-1.497	5049	5010	4937	56.8
2004-2005 ^c	-1.55	-1.795	5015	5029	4925	53.8
2005-2006 ^c	-1.67	-1.657	5050	5021	4860	55.1
2006-2007 ^c	-1.52	-1.276	4986	5009	4830	56.9
2007-2008 ^c	0.47					

^v : validation years; ^c : calibration years

Table 8.6 indicates that both measured and simulated mass balances of the Artesonraju glacier are negative over the whole simulation period 2001-2008, with only minor differences between the two. The same holds for the measured and simulated ELAs which oscillate between 4986 m.a.s.l. and 5119 for the first period and between 4994 and 5029 m.a.s.l. for the second one. Despite the fact that the TMI-model's spatial grid resolution is 30 m, the differences between

measured and simulated values are only marginal. However, because of that grid resolution, the simulated ELA represents actually a narrow stripe of a few meters' uncertainty.

The annual trends in the mass balances presented by the WGMS (2015) correspond to those simulated with the temperature index. However, the recovery of the mass balance (lower losses) showed for the years 2004-2005 to 2005-2006 present contrary results in UGRH simulations, the latter shows major mass losses for the same years .

Although there is a decrease in loss in from the year 2005-2006 to 2006-2007, the ELA does not show a corresponding recovery. This may be due to the initial conditions of the start of simulations which were taken from the ELA from the previous year, as informed by WGMS (2015), and not from continuous simulations. However, for the simulation years 2001-2003, in which there was not official estimations of mass balances, and the initial conditions for the water equivalent were taken from the results of previous year of simulation, there are perfect correspondences between the losses of mass and the movement of the ELA.

A recent study that uses the snow line from satellite images as an indicator for the ELA in the tropical glacier of Artesonraju (Rabatel *et al.*, 2012) shows that the snow line at the end of the hydrological year (in the dry season) represent the ELA behaviour quite well in tropical glacier and can be even used as an estimator of the ELA. Thus, this is a comparison of the snow line presented in graphs in such study and the one showed in **Table 8.6**. The snow line presents similar trends of mass loss and gains for the hydrological years 2001-2003.

The results of TMI- model for the seasonal mass balance profiles shown in **Figure 8.9** indicate that the specific mass balance gradient is larger in the ablation zone (2-5 m.w.e./100m) than in the accumulation zone (0.2-1.5 m.w.e./100m) which agrees with observations of other authors (Kaser and Georges, 1999; Sicart *et al.*, 2011; Gurgiser *et al.*, 2013). This high mass-balance gradient is mainly due to frequent changes of the snow cover throughout the long ablation season (Rabatel *et al.*, 2012).

Figure 8.9 shows also the average contribution of the mass balance in each simulated period. The maximum losses and gains are presented in the core of the rainy season, while the melting and accumulation process in the dry period as well as at the beginning of the rainy season are lower.

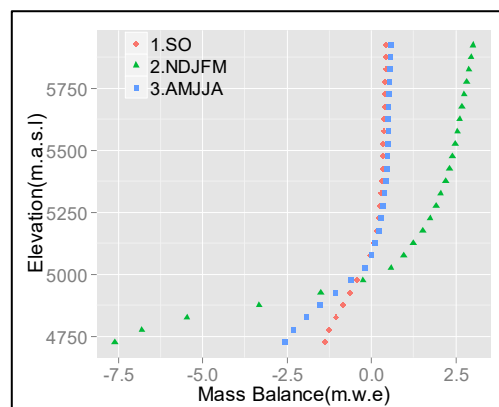


Figure 8.9. Seasonal mass balance profiles

This behavior corresponds to the typical seasonal process of accumulation and ablation in the tropical glacier of Artesonraju, showing that the DDF proposed in this research can certainly reproduce the seasonality in the tropical glaciers, despite of the low seasonality of the temperature.

8.2.3.3 Uncertainties in the simulation

Certain uncertainties described for EBM in section 7.4.2.5 apply also for the simulation with TIM. For instance, the limited quality of climate data and their inherent measurement errors transferred to simulations, especially for the records of daily temperature and precipitation.

Gaps in the measured daily temperature that were filled with multiple regression methods 01.01.2001 and 24.04.2002 (see Chapter 6) are also a source of uncertainty. Predicting long periods of data gaps, as the one in 2001/2002 (see **Figures 6.1**), was a difficult task. However the results in the simulation for those years with TIM results in excellent simulations of discharge.

Another source of uncertainty may be due to the few measurements existing in the accumulation zone of the glacier, which affects also the simulations with EBM. Normally, these zones are abrupt and dangerous in the high mountain of the Cordillera Blanca, making access for measurements difficult (Kaser and Georges, 1999). The net and the instrumentation of the measurements are also costly and cover generally just some parts of the glaciers (Francou *et al.*, 2013). Therefore, the initial conditions, especially for the accumulations, are still difficult to estimate. The estimations of the initial surface conditions in the current TIM simulations were made in ArcGIS with geospatial interpolation based on Kriging analysis which introduces additional errors in the estimations of initial mass, propagating through the model simulations.

8.2.4 Concluding remarks

The temperature index models (TIM) are tools that allow estimating mass balance and discharge in glaciers in a sufficient manner. Its practical use and the few data requirements make this kind of glacier models interesting for areas, where measured climatic variables like energy fluxes are scant and gauges stations nets relatively new, such is often the case in tropical glaciers. In addition, the application of TIM is very suitable for estimations of temperature changes in future climate scenarios.

Despite their simplicity, good performance and low input data requirements, there are not many applications of TIM to tropical glaciers. However, more research is required to determine which of the degree-day factors best represent the glaciers' dynamics and its spatial and seasonal variability. In addition, it is important to assess the possible manner to apply TIM to optimize the results and the seasonal simulation of discharge and mass balances of tropical glaciers.

This is one of the few studies which demonstrates that, with the use of seasonal degree-day melt factors in tropical glaciers, it is possible to use temperature index models in tropical areas. Although the study is based on a small sample of years, this research opens the options to model glaciers using only two variables and, thus, overcome the problem of lack of information in time series of climatic variables required to use more sophisticated models. The practicality of index temperature models makes them attractive to model future scenarios of glacier discharge and

mass balance in climate change scenarios and, hence, the importance of deepening on the knowledge of this issue. The study is limited by the lack of information required for validation, especially the discharge of the Artesoncocha Lake. However, the current simulation shows reasonable results with respect to the possibility of using the temperature index models for the calculation of mass balance and to estimate the decrease of the water resources. This aspect is very important for watersheds, such as the Cordillera Blanca, where an important contribution of surface water (30-45%) comes from these ecosystems (Mark and Seltzer, 2003). Nonetheless, the model could underestimate detailed estimates of flooding and extreme peaks.

The seasonal $DDFs$ and the discharge constants were validated in a period of time of similar extent as the simulated and satisfactory results were obtained regarding the discharge and the specific annual mass balances. However, further research is required to determine whether these $DDFs$ and storage constants for the different stations can be transferable to other glaciers in the tropics.

This feasibility of using temperature index is not accidental since certain studies showed the relationship of temperature with components of the energy balance equation. In the present simulation, signs of certain correlation of DDF_{ice} with the seasonality of longwave radiation fluxes and DDF_{snow} with the seasonality of shortwave fluxes and, thus, both with net radiation were also found. The similar trends that present these variables with each one of the degree-day factors could be the reason that allows obtaining reasonable results with the use of seasonal $DDFs$.

This research provides an insight into the seasonality of storage constants for different media in tropical glaciers which have not been discussed until now and it shows reasonable results in terms of its behaviour.

The simulation confirms, as it was done in the simulation with energy fluxes and presented in previous studies that the temperature that determines the solid state of precipitation and the amount of precipitation is a very important factor in the glacier dynamics of tropical glaciers. The threshold temperature is very important in the temperature index models because it determines the allocation of $DDFs$ for each surface. The threshold temperature was similar to those found in the simulation with energy fluxes presented in Section 7.2.4. It is expected that changes in the altitude, in which this threshold temperature occurs, could be produced by steady increments in mean temperature. Besides, threshold temperatures can change to temporal and local conditions of humidity, wind speed and atmospheric pressure, and these aspects merit more investigations

The results of the mass balances indicate that during the period from 2001 to 2007, continued mass losses occur. This negative trend could lead to an inevitable shrinking of the glacier.

Another important contribution of the present research is the estimation of the storage constant for each season of the year and for each component of the glacier surface, i.e. snow, ice and firn. The novel results prove to be concordant with the seasonal behavior of accumulation and ablation of each of these components in tropical glaciers. Moreover, the storage constants are corroborated, not only for the validation period of TIM, but also for use in the EBM- simulations carried out in Chapter 7.

9 Comparison of Energy Balance Model (EBM) - and Temperature Index Model (TIM) - Simulation Results

In this chapter the main results obtained with the Energy Balance Model (EBM) (Chapter 7) and the Temperature Index Model (TIM) (Chapter 8) are compared. This comparison should be seen in the light of the limitations for building the two models instead of being an evaluation of the ability of each model's performance alone.

Physically basic models, such as the EBM, represent the processes involved in the glacier dynamics in a better manner than those obtained with empirical models, like TIM, so that their simulation results are expected to be also better. However, as the physically based models require a huge amount of input variables, a lack of a few of these may already hinder the possibility to reproduce the important phenomena describing the complex glacier dynamics with sufficient accuracy. This is exactly what has been observed in this research as will be worked out in the following sub-sections.

9.1 Comparison of Simulated Discharge

Table 9.1 shows that the yearly Nash-Sutcliffe coefficients E of the EBM- discharge simulations are consistently lower than those of the TIM for all, but the last year (2007). This difference is particularly pronounced for years 2005-2006 and 2006-2007 and is mainly due to poor representation of peak discharges, mainly between 13.11.2005 and 3.12.2005 (see **Figure 9.1**), by the EBM, in particular. This period within the rainy season had unusually high temperatures ($>1^{\circ}\text{C}$ above the seasonal average) which have a strong influence on albedo, which could not be well represented by the (constant) seasonal albedo used in the EBM. The same occurs in shorter periods in year 2006-2007, for instance, between January 14-27, February 1-9 and August 20-28 (see **Figure 9.1**). The temperature index model (TMI), on the other hand, is better able to handle these big changes of the seasonal temperature in the discharge simulation. This means, in order to improve the EBM- simulation accuracy, working on parameterization of daily albedo changes on tropical glaciers should become a focus of research.

Table 9.1. Comparison of Nash-Sutcliffe Coefficient (E) of EBM- and TIM- discharge simulations

Year	E (EBM)	Adjustment	E (TIM)	Adjustment
2004-2005	0.86	Very Good	0.89	Excellent
2005-2006	0.56	Good	0.78	Very Good
2006-2007	0.60	Good	0.76	Very Good
2007 SOND	0.77	Very Good	0.75	Very Good

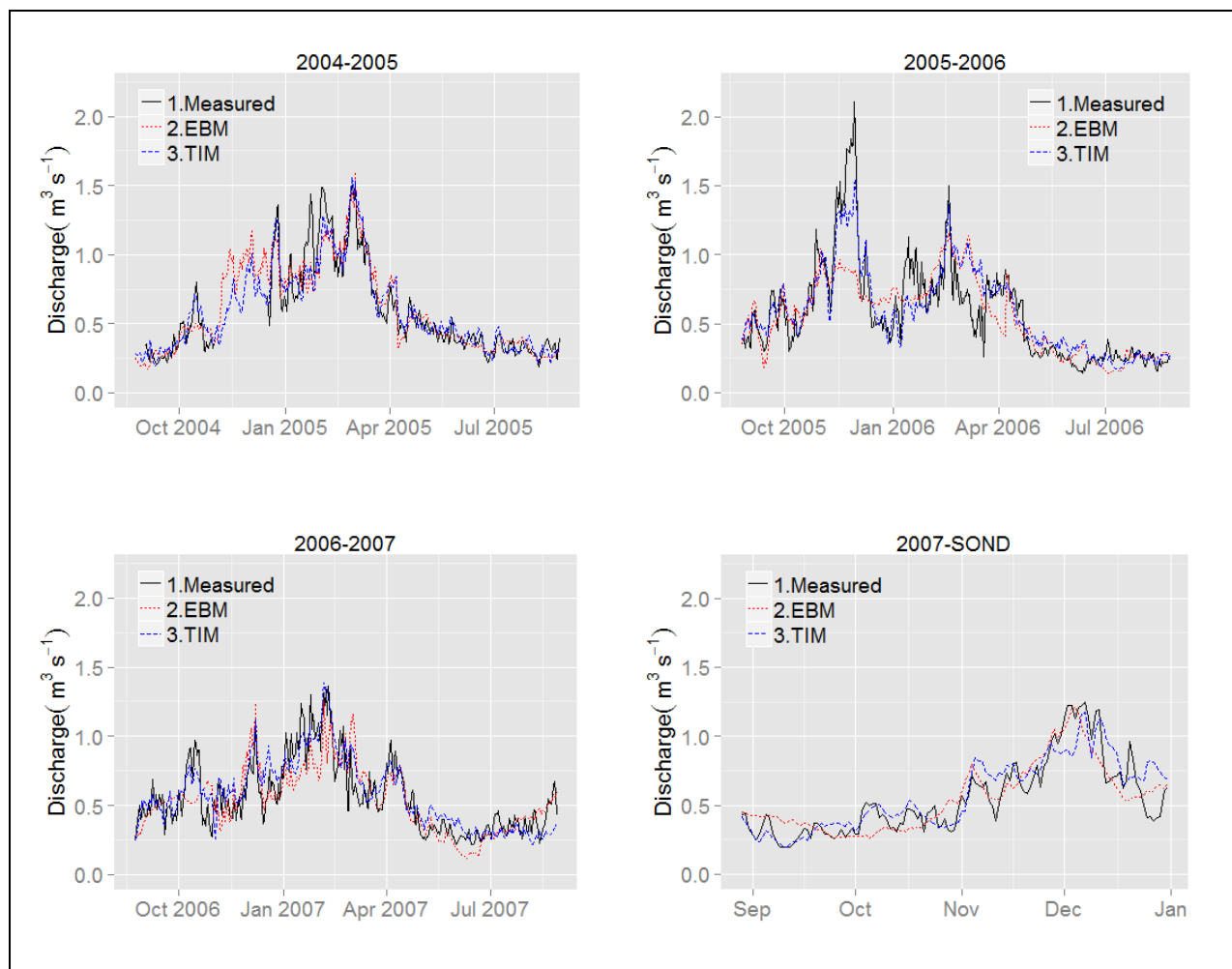


Figure 9.1. Daily measured-, EBM- and TIM- simulated discharge for the different years

9.2 Comparison of Mass Balance Profiles and ELAs

The mass balance profiles of **Figure 9.2** indicate a better agreement of the TIM- simulated profiles with the UGRH-measured ones than those of the EBM, especially, for the years 2004-2005 between 4800 and the 5050 m.a.s.l. In that year TIM overestimates the UGRH- observed mass balance loss less than EBM.

For the year 2005-2006, between 4900 and 5100 m.a.s.l., on the other hand, both models show similar mass losses, with a slight underestimation of less than 1 m.w.e. However, both EMB and TIM overestimate mass losses, especially between 4700 and 4799 m.a.s.l.

For the year 2006-2007, the performances of both EBM and TIM are also pretty similar between 4850 and 5000 m.a.s.l., however, with an overestimation of mass losses in the lower part of the glacier between 4700 and 4850 m.a.s.l. that is particularly pronounced for TIM. In fact, taking the three simulated years together, TIM and, even more so, EBM, simulate larger mass balance losses than measured by UGHR in the glacier's altitude range 4700-4800 m.a.s.l. which accounts for 9.7% of the total glacier's area.

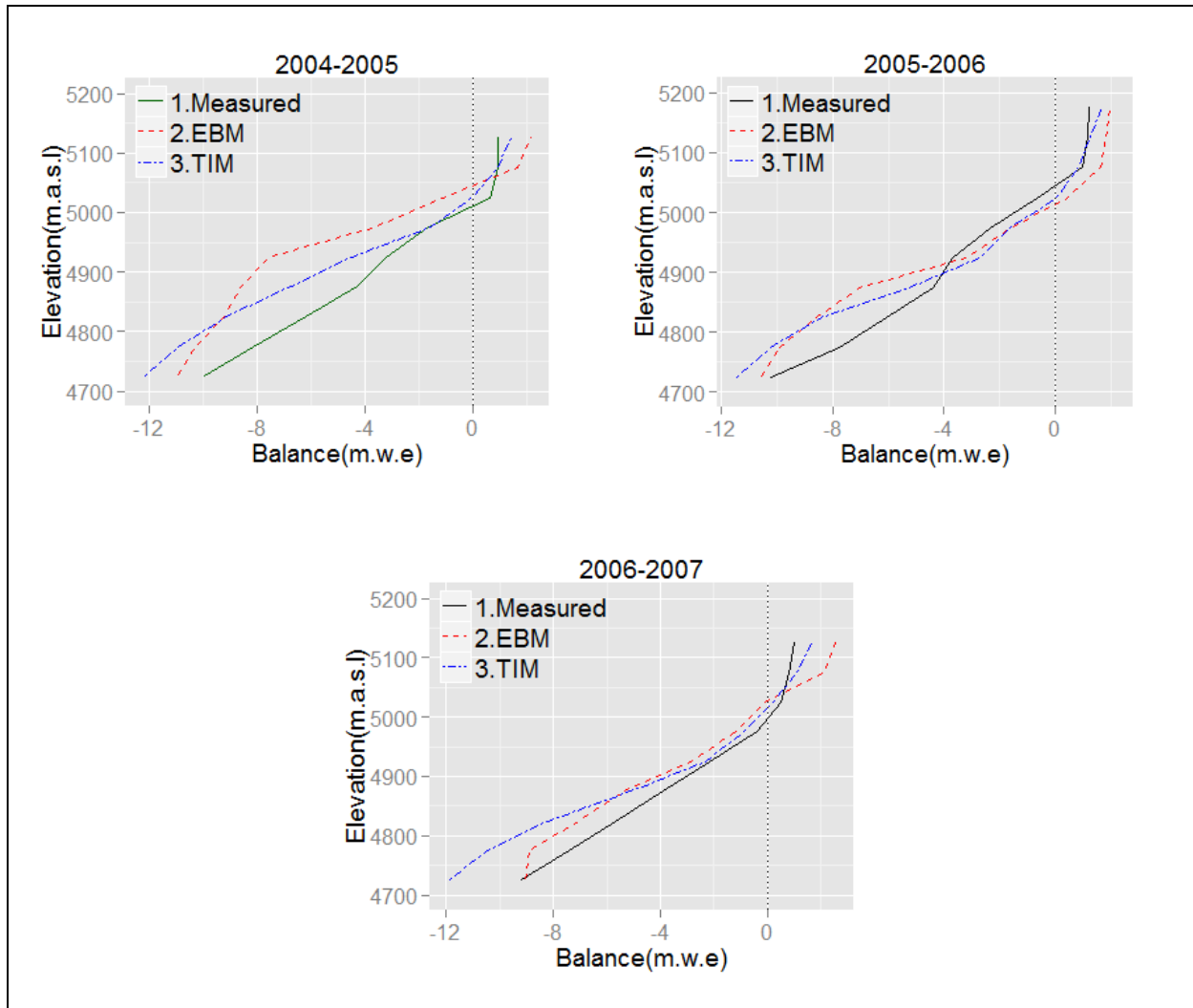


Figure 9.2. Measured-, EBM-, and TIM- simulated mass balance profiles for the different years

As for the ELAs, which are defined by the elevations of the intersection of the simulated mass-balance profiles with the zero-mass-balance ordinate lines in the three panels of **Figure 9.2**, their differences are less than 50 m among the various profiles for the different years. Generally, for both models the ELAs vary between 5000 and 5050 m.a.s.l. in the three years.

For both EBM and TIM exists an area on the glacier surface for which their performance is more accurate. As this area comprises the elevation range 4800-5100 m.a.s.l., and one area with less accurate results between 4700 and 4799 m.a.s.l. in the tongue of the glacier, these results suggest that in the case of the TIM simulations, the application of more DDFs, also per zones within the ablation area, should be tested in further research, in other to reduce this systemic error.

Figure 9.3 shows barplots of the EBM-, TIM- simulated as well as UGRH- measured average total mass balances for the three years investigated. For all years, but particularly for year 2006-2007, differences in the simulated- and measured mass balances are obtained, especially for EBM. This could be a consequence of the uncertainty of the daily energy fluxes (generated by the autocorrelation models (see chapter 6)) used in EBM. Again, similar to the mass-balance profiles above, the TIM- simulated total mass-balances agree much better with the UGRH- reported ones.

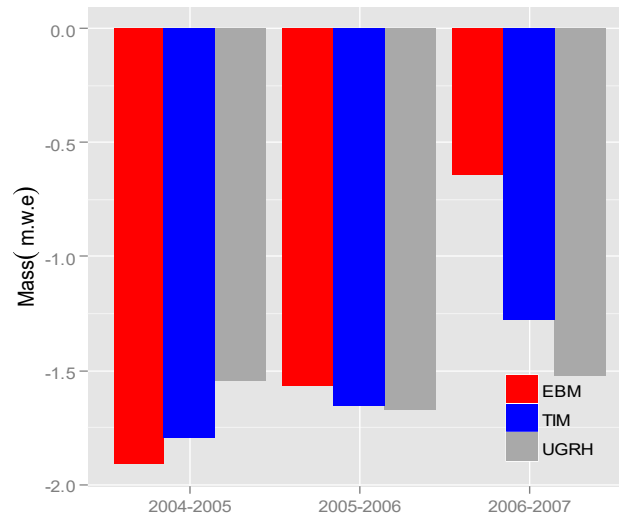


Figure 9.3. Yearly EMB-, and TIM- mass balance and calculated with measured data by UGRH

9.3 Comparison of EBM- and TIM- Calibration Parameters

9.3.1 Energy fluxes and DDFs

The present research complements the conclusions of Ohmura (2001) about the rationality behind temperature index models (TIM). This author attributes the high correlation of temperature with longwave radiation as the main factor to explain the good performance of TIMs. This is clear for mid-latitude glaciers. However, in the case of the outer tropical Artesonraju glacier studied here, a high correlation of Lw_{inc} and Lw_{surf} with relative humidity R_h , and of the temperature with net energy Q_N , and somewhat less, with Sw_{inc} were found (see Chapter 5). It is these correlations of certain energy fluxes with variables related to temperature which contribute to the success of TIMs for glacier modelling in tropical environments.

Furthermore, a correlation of the seasonal degree day factors $DDFs$ with the seasonality of certain energy fluxes in the glacier Artesonraju was also identified. In fact, the good Kendall correlations between seasonal climatic variables and $DDFs$ explain in part the better simulation results obtained for discharge and glacier's mass balance when using seasonal $DDFs$. Although this analysis incorporates not much data, because the simulated period is relatively short, it contributes to an understanding of the good performance of TIM in tropical environments. For instance, the DDF_{ice} which dominates the melting process (of ice) in the ablation area is highly correlated with Lw_{inc} and Lw_{surf} as well as with Q_N , all of which are seasonally strongly varying parameters and so determine considerably the seasonal dynamics of the glacier. Some correlation of DDF_{ice} with Sw_{inc} and Sw_{ref} is also found.

As for DDF_{snow} , which dominates the glacier's accumulation area, it has a strong correlation with Sw_{ref} and Sw_{inc} and less so with Lw_{inc} and at Lw_{surf} . On the other hand, negative correlations of latent heat with DDF_{ice} , and less so, with DDF_{snow} are found. Finally, important correlations of DDF_{ice} with seasonal relative humidity, temperature and precipitation are also detected.

But beyond these results, the most important point is the fact that the seasonal *DDFs* can certainly represent complex interactions of various climatic variables, especially, energy fluxes on the glaciers surface, which change from season to season. In addition, the TIM has the advantage to reproduce anomalies of temperature that occur, for instance, in the wake of El Niño/La Niña events, as explained in Section 9.1. This is very important in the present study case of Andean glaciers whose dynamics are strongly influenced by this climate phenomenon.

9.3.2 Seasonal storage constants (mean residence times)

Seasonal storage constants for firn, ice and snow are calibration parameters in both (EBM and TIM) models and were tested simultaneously, considering that these parameters are a sole characteristic of the glaciers surface and, therefore, should not depend on which model is used. Thus, similar seasonal storage constants were applied in both models.

The optimal storage constants found in the sensitivity analysis of the two models are listed in **Table 9.2**. One can notice from the table that for some seasonal periods, for instance, the dry AMJJA period, differences in the optimal ice- and snow- storage constants, but not in those for firn, arise for the EBM- and TIM- model. Such differences may be due to the inherent parameterization uncertainty in both models, especially, in the 4700-4800 m.a.s.l. elevation range and in the upper part of the accumulation zone above 5400 m.a.s.l, where flow from firn melting does not play much of a role anymore.

Table 9.2. EBM- and TIM- optimized seasonal storage constants for firn, ice and snow

Period	Storage constant (hr)	EBM	TIM
SO	k_{firn}	700-800	700
	k_{snow}	390-400	390
	k_{ice}	50-250	50-80
NDJFM	k_{firn}	500-800	400-500
	k_{snow}	390-450	390
	k_{ice}	30-120	30-170
AMJJA	k_{firn}	1100	1100
	k_{snow}	150-200	60
	k_{ice}	250-300	80-200

9.3.3 Threshold temperature *rain/snow* T_0

Figure 9.4 shows the EBM- and TIM- simulated threshold temperatures *rain/snow* T_0 sensitivity (in terms of the Nash-Sutcliffe coefficient E) for each season of the three years analyzed. One can notice that the EBM- calibrations are more sensitive to changes in this parameter than those of TIM. This is not surprising, as the parameterization and calculation of certain energy fluxes which are cell-distributed in EBM, such as SW_{ref} and LW_{inc} , LW_{surf} and Q_{HL} , depend on the snow/ice characteristics of the surface areas. On the other hand, the sectors between snow-covered and snow-free areas taken in TIM are much larger, so that this model is less sensitive to small spatial variations here. Interestingly, both model calibrations attain their optimal E for T_0 - temperatures ranging between 2.5°C and 3.5°C, although major differences between the two models are found in year 2006-2007.

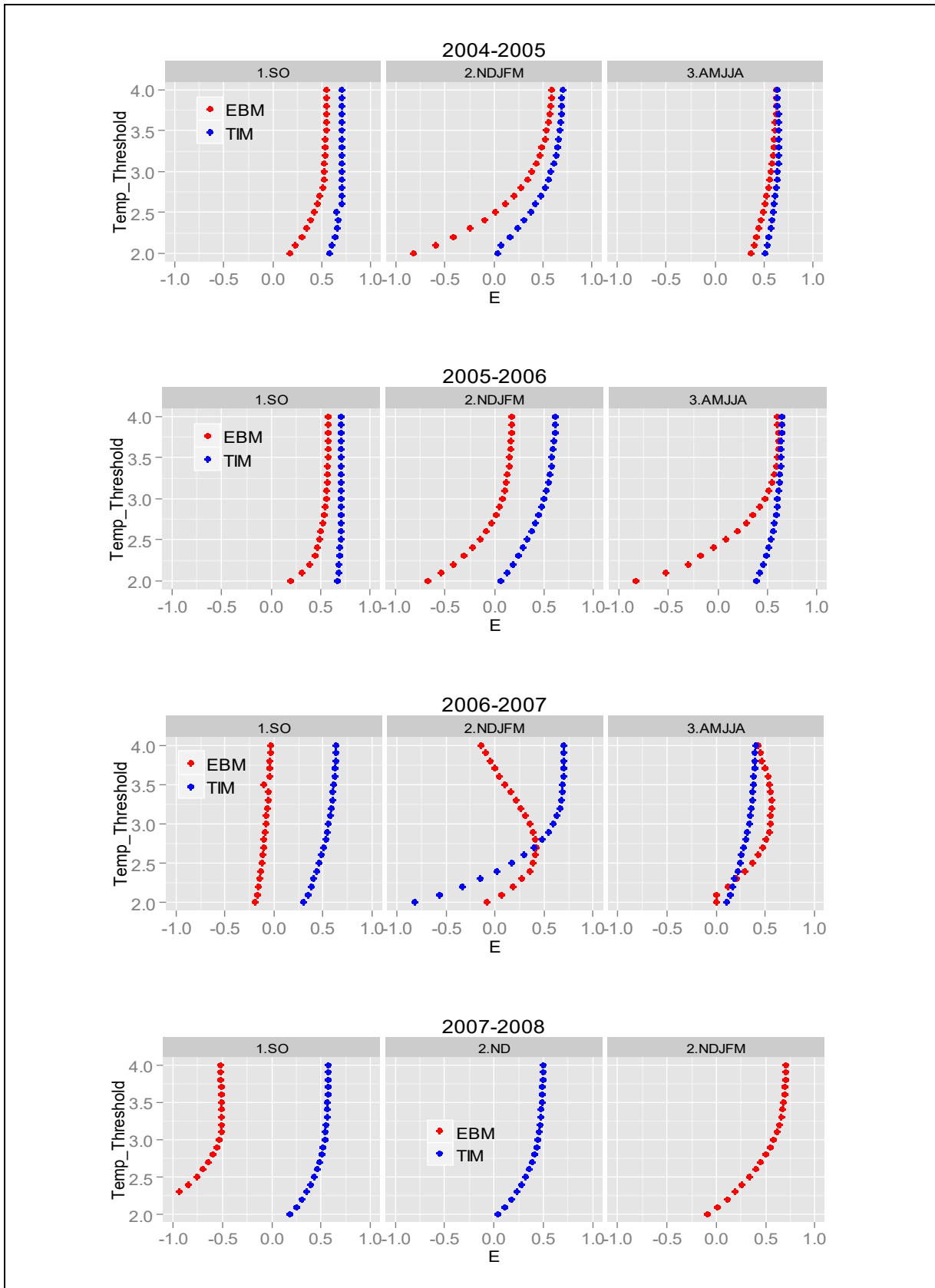


Figure 9.4. EBM- and TIM- simulated seasonal threshold temperature snow/rain T_0 sensitivities in terms of E for the different years

9.4 Concluding Remarks

From the comparison of the various EBM- and TMI- simulation results above it can be clearly concluded that those for discharge and mass balances are better for the latter than for the former model. However, this does not necessarily mean that the EBM-model is generally inferior to the TMI, but its limited performance is most likely due to the sometimes low quality of the data available which precludes the possibility of using the most accurate parameterization in that model. For instance, the use of daily albedos for tropical glaciers, instead of the seasonal albedos employed here in EBM, is expected to improve the performance of this model.

In spite of these restrictions, the present research has been able to highlight the general conditions determining the dynamics of a tropical glacier and, in particular, to understand better the interaction between energy fluxes and the main parameters influencing changes of the glacier's mass balance.

Finally, regarding the success of the TIM model, this is mainly due to the use of seasonal *DDFs* in the model, and for each glacier surface, not done heretofore in glacier modelling. This seasonal approach is so a promising tool for simulating longer time series and therefore to estimate future changes in a glacier, for instance, by using climate predictions from downscaled global climate models (GCM) or, even better, regional climate models (RCM). These kinds of models can overcome the problem of a lack of long-term field measurements of various climatic variables, for instance, energy fluxes and should, so, allow making long-term predictions of the future fate of tropical glaciers.

References

- Alpert, P. (1986) 'Mesoscale indexing of the distribution of orographic precipitation over high mountains', *J. Clim. Appl. Meteorol.*, 25, pp 532-545
- Ambach, W. (1988) 'Interpretation of the Positive-Degree-Days Factor by Heat Balance Characteristics - West Greenland', *Nordic Hydrology*, 19(4), pp. 217-224. doi: 10.2166/nh.1988.014.
- Ames, A. and Francou, B. (1995) 'Cordillera Blanca: glaciares en la historia', *Bulletin Institute Francais des Etudes Andines*, 24(1), pp. 37-64.
- Arnaud, Y., Muller, F., Vuille, M., and Ribstein, P. (2001) 'El Niño-Southern Oscillation (ENSO) influence on a Sajama volcano glacier (Bolivia) from 1963 to 1998 as seen from Landsat data and aerial photography', *Journal of Geophysical Research*, 106, p. 17773. doi: 10.1029/2001JD900198.
- Arnold, J. G., Moriasi, D. N., Gassman, P. W., Abbaspour, K. C., White, M. J., Srinivasan, R., Santhi, C., Harmel, R. D., Van Griensven, A., Liew, M. W., Kannan, N., and Jha, M. K. (2005) Swat: Model Use, Calibration, And Validation, *Transactions of the ASABE*, 55(4), pp. 1491-1508. Available at: <http://swatmodel.tamu.edu> (Accessed: 5 November 2018).
- August H., Auer, Jr. (2010) 'The Rain versus Snow Threshold Temperatures', *Weatherwise*, 27(2), p. 67.
- Autoridad Nacional del Agua (2014) 'Inventario de Glaciares del Perú', *Inventario Nacional de Glaciares y Lagunas*, p. 56. doi: <http://www.ana.gob.pe/media/981508/glaciares.pdf>.
- Baker, D., Escher-Vetter, H., Moser, H., Oerter, H., and Reinwarth, O. (1982) 'A glacier discharge model based on results from field studies of energy balance, water storage and flow', *IAHS Publ*, 138(138), pp. 103-112.
- Baraer, M., Mark, B. G., Mckenzie, J. M., Condom, T., Bury, J., Huh, K. I., Portocarrero, C., Gómez, J., and Rathay, S. (2012) 'Glacier recession and water resources in Peru's Cordillera Blanca', *Journal of Glaciology*, 58(207), pp. 134-150. doi: 10.3189/2012JoG11J186.
- Bejranonda, W. (2015) The prediction of seasonal and inter-annual climate variations and their impacts on the water resources in the eastern seaboard of Thailand. PhD thesis, University of Kassel, Germany.
- Blard, P.H., Wagnon, P., Lavé, J., Soruco, A., Sicart, J.E. and Francou, B. (2011) 'Degree-day melt models for paleoclimate reconstruction from tropical glaciers: calibration from mass balance and meteorological data of the Zongo glacier (Bolivia)', *Climate of the Past Discussions*, 7(3), pp. 2119-2158. doi: 10.5194/cpd-7-2119-2011.
- Braithwaite, R. J. (1995) 'Positive degree-day factors for ablation on the Greenland Ice-sheet studied by energy balance modelling', *Journal of Glaciology*, 41(137), pp. 153-160. doi: 10.3189/1995JoG41-137-153-160.

- Braithwaite, R. J. (2011) 'Degree-days', in *Encyclopedia of Earth Sciences Series*. Springer, pp. 196–199. doi: 10.1007/978-90-481-2642-2_104.
- Braithwaite, R. J. and Olesen, O. B. (1989) 'Calculation of Glacier Ablation from Air Temperature, West Greenland', in Springer, Dordrecht, pp. 219–233. doi: 10.1007/978-94-015-7823-3_15.
- Brockwell, P. and Davis, R. (1991) *Time Series and Forecasting Methods*. Second edition, Springer, New York, NY.
- Cabrera, J. (2011) 'Calibracion en Modelos Ecológicos', Universidad Nacional de Colombia.
- Caceres, B. (2010) 'Actualización del inventario de tres casquetes glaciares del Ecuador'. Master Thesis, Univ. Nice, France, 84p.,2010.
- Ceballos, J. L., Euscátegui, C., Ramírez, J., Cañon, M., Huggel, C., Haeberli, W. and Machguth, H. (2006) 'Fast shrinkage of tropical glaciers in Colombia', in *Annals of Glaciology*, pp. 194–201. doi: 10.3189/172756406781812429.
- Chavimochic Project (2018) CHAVIMOCHIC. Available at: <http://www.chavimochic.gob.pe/descripcion> (Accessed: 10 November 2018).
- Chevallier, P., Pouyaud, B., Suarez, W. and Condom, T. (2011) 'Climate change threats to environment in the tropical Andes: glaciers and water resources', *Regional Environmental Change*, 11(S1), pp. 179–187. doi: 10.1007/s10113-010-0177-6.
- Cleveland, R. B., Cleveland, W. S., McRae, J. E. and Terpenning, I. (1990) 'STL: A seasonal-trend decomposition procedure based on loess', *Journal of Official Statistics*, pp. 3–73. doi: citeulike-article-id:1435502.
- Condom, T., Escobar, M., Purkey, D., Pouget, J. C., Suarez, W., Ramos, C., Apaestegui, J., Tacsí, A. and Gomez, J. (2012) 'Simulating the implications of glaciers' retreat for water management: A case study in the Rio Santa basin, Peru', *Water International*, 37(4), pp. 442–459. doi: 10.1080/02508060.2012.706773.
- Cuffey, K. M. and Paterson, W. S. B. (2010) *The physics of glaciers*. 4th edition, Butterworth-Heinemann, Oxford, UK.
- Dai, A. (2008) 'Temperature and pressure dependence of the rain-snow phase transition over land and ocean', *Geophysical Research Letters*, 35(12), pp. 1–7. doi: 10.1029/2008GL033295.
- Davies, B. (2015) 'Degree day models: Modelling glacier melting', AntarticGlaciers.org.
- Davis, J. C. (1986) 'Statistics and data analysis in geology'. Wiley. Available at: https://books.google.de/books/about/Statistics_and_Data_Analysis_in_Geology.html?id=jexrOI9ORXUC&redir_esc=y (Accessed: 29 October 2018).
- Eeckman, J., Chevallier, P., Boone, A., Neppel, L., De Rouw, A., Delclaux, F., Koirala, D. (2017) 'Providing a non-deterministic representation of spatial variability of precipitation in the Everest region'. *Hydrol. Earth Syst. Sci.* 21, 4879–4893. <https://doi.org/10.5194/hess-21-4879-2017>

- Escher-Vetter (1980) 'Der Strahlungshaushalt des Vernagtferners als Basis der Energiehaushalt Berechnung zur Bestimmung der Schmelzwasserproduktion eines Alpengletschers'. Edited by Aus den Arbeiten der Kommission für Glaziologie der Bayerischen Akademie der Wissenschaften im Rahmen des Sonderforschungsbereiches 81 der Techn. Universität München - Teilprojekt A 1. Wissenschaftliche Mitteilung Meteorologisches Institut Universität München 39 (1980), 1-115.
- Favier, V., Wagnon, P., Chazarin, J. P., Maisincho, L. and Coudrain, A. (2004) 'One-year measurements of surface heat budget on the ablation zone of Antizana Glacier 15, Ecuadorian Andes', *Journal of Geophysical Research Atmospheres*, 109(18), pp. 1–15. doi: 10.1029/2003JD004359.
- Favier, V., Wagnon, P. and Ribstein, P. (2004)b 'Glaciers of the outer and inner tropics: A different behaviour but a common response to climatic forcing', *Geophysical Research Letters*, 31(16), pp. 1–5. doi: 10.1029/2004GL020654.
- Feiccabrino, J., Graff, W., Lundberg, A., Sandström, N. and Gustafsson, D. (2015) 'Meteorological Knowledge Useful for the Improvement of Snow Rain Separation in Surface Based Models', *Hydrology*, 2(4), pp. 266–288. doi: 10.3390/hydrology2040266.
- Fischer, L; Purves, Ross S; Huggel, Christian; Noetzli, Jeannette; Haeberli, Wilfried (2012). 'On the influence of topographic, geological and cryospheric factors on rock avalanches and rockfalls in high-mountain areas'. *Natural Hazards and Earth System Science*, 12(1):241-254.
- Francou, B., Ramirez, E., Cáceres, B. and Mendoza, J. (2000) 'Glacier Evolution in the Tropical Andes Century: during the Last Decades of the 20 Century: Chalcataya, Bolivia, and Antizana, Ecuador', *A Journal of the human Environment*, 29(7), pp. 1–7.
- Francou, B. (2003) 'Tropical climate change recorded by a glacier in the central Andes during the last decades of the twentieth century: Chacaltaya, Bolivia, 16°S', *Journal of Geophysical Research*, 108(D5), p. 4154. doi: 10.1029/2002JD002959.
- Francou, B., Vuille, M., Favier, V. and Cáceres, B. (2004) 'New evidence for an ENSO impact on low-latitude glaciers: Antizana 15, Andes of Ecuador, 0°28'S', *Journal of Geophysical Research Atmospheres*, 109(18), pp. 1–17. doi: 10.1029/2003JD004484.
- Francou, B., Ribstein, P., Wagnon, P., Ramirez, E. and Pouyaud, B. (2005) 'Glaciers of the Tropical Andes: Indicators of Global Climate Variability', in *Global Change and Mountain Regions Advances in Global Change Research Volume 23*. Springer, Dordrecht, pp. 197–204. doi: 10.1007/1-4020-3508-X_20.
- Francou, B., Rabatel, A., Soruco, A., and Ginot, P. (2013) 'Glaciares de los Andes Tropicales víctimas del Cambio Climático', *Secretaría General Comunidad Andina, Proyecto de Adaptación al Impacto del Retroceso Acelerado de los Glaciares en Los Andes Tropicales –PRAA*, Institute de recherche pour le développement IRD, pp. 101.
- Fuchs, M. (2005) Energy Balance. *Encyclopedia of Soils in the Environment . Reference Module in Earth Systems and Environmental Sciences*, pp. 438-441

- Fuchs, P., Asaoka, Y., and Kazama, S. (2013). 'Estimation of glacier melt in the tropical Zongo with an enhanced temperature-index model'. *Journal of Japan Society of Civil Engineers, Ser. B1 (Hydraulic Engineering)*, 69. I_187-I_192. doi: 10.2208/jscejhe.69.I_187.
- Gallaire, R., Condom, T., Gómez, J., Cochachin, A. and Zapata, M. (2007) 'Informe Cuatrienal de Resultados Científicos'. INRENA, GREATICE, IRD.
- Garreaud, R. D. and Aceituno, P. (2001) 'Interannual rainfall variability over the South American Altiplano', *Journal of Climate*, 14(12), pp. 2779–2789. doi: 10.1175/1520-0442(2001)014<2779:IRVOTS>2.0.CO;2.
- GGWS (2019) El Niño and La Niña Years and Intensities Based on Oceanic Niño Index (ONI), actualized Jan Null, CCM, Updated through Jul-Aug-Sep 2019, <https://ggweather.com/enso/oni.htm>, (Accessed: 30 October 2019)
- Gurgiser, W., and Marzeion, B. (2013) 'Modeling energy and mass balance of Shallap Glacier, Peru', *The Cryosphere*, 7(6), pp. 1787–1802. doi: 10.5194/tc-7-1787-2013.
- Hartmann, D. L., (1994) *Global Physical Climatology*. Academic Press, 411 pp.
- He, Z. H., Parajka, J., Tian, F. Q. and Blöschl, G. (2014) 'Estimating degree-day factors from MODIS for snowmelt runoff modeling', *Hydrology and Earth System Sciences*, 18(12), pp. 4773–4789. doi: 10.5194/hess-18-4773-2014.
- Hirsch, R. M., Slack, J. R. and Smith, R. A. (1982) 'Techniques of trend analysis for monthly water quality data', *Water Resources Research*, 18(1), pp. 107–121. doi: 10.1029/WR018i001p00107.
- Hock, R. (1998) 'Modelling of glacier melt and discharge', PhD thesis. Geographisches Institut ETH Zürich. No. 12430 MODELLING. doi: 10.3929/ethz-a-001891975.
- Hock, R. (1999) 'A distributed temperature-index ice- and snowmelt model including potential direct solar radiation'. *Journal of Glaciology*, 45(149), 101-111. doi:10.3189/S0022143000003087
- Hock, R. (2003) 'Temperature index melt modelling in mountain areas', *Journal of Hydrology*, 282(1–4), pp. 104–115. doi: 10.1016/S0022-1694(03)00257-9.
- Hock, R. (2005) 'Glacier melt: A review of processes and their modelling', *Progress in Physical Geography*, 29(3), pp. 362–391. doi: 10.1191/0309133305pp453ra.
- Hock, R. and Holmgren, B. (2005) 'A distributed surface energy-balance model for complex topography and its application to Storglaciären, Sweden', *Journal of Glaciology*. Cambridge University Press, 51(172), pp. 25–36. doi: 10.3189/172756505781829566.
- Hock, R. (2010a) 'Glacier Mass Balance. Summer school in Glaciology Fairbanks/ McCarthy. 7-17 June 2010', Summer school in Glaciology - Fairbanks/McCarthy, (June), pp. 1–10. doi: 10.1007/978-94-007-6311-1_6.
- Hock, R. (2010b) 'Glacier Meteorology Energy Balance', *Energy*, (June), pp. 1–10.

- Hock, R. and Tijm-Reijmer, C. (2012) A mass-balance, glacier runoff and multi-layer snow model DEBAM and DETIM distributed energy balance and distributed enhanced temperature index model user's manual. Available at: <http://www2.gi.alaska.edu/~regine/modelmanual.pdf> (Accessed: 30 October 2018).
- IACS (2011) Glossary of Glacier Mass, International Hydrological Programme of the United Nations Educational, Scientific and Cultural Organization (UNESCO), 86, p. 114. Available at: unesdoc.unesco.org/images/0019/001925/192525e.pdf.
- INAIGEM (2016) 'Reconocimiento de peligros naturales en la laguna nueva "Artesoncocha alta"', Ministerio del Medio Ambiente Perú.
- IPCC (2014) Cambio climático 2014: Informe de síntesis. Contribución de los Grupos de trabajo I, II y III al Quinto Informe de Evaluación del Grupo Intergubernamental de Expertos sobre el Cambio Climático [Equipo principal de redacción, R.K. Pachauri y L.A. Meyer (eds.)]. IPCC, Ginebra, Suiza, 157 págs.
- IPCC (2008) Cambio climático 2007: Informe de síntesis de Expertos sobre el Cambio Climático. Ginebra: doi: 10.1256/004316502320517344.
- Jakubauskas, M. E., Legates, D. R. and Kastens, J. H. (2002) 'Crop identification using harmonic analysis of time-series AVHRR NDVI data', *Computers and Electronics in Agriculture*. Elsevier, 37(1-3), pp. 127-139. doi: 10.1016/S0168-1699(02)00116-3.
- Jennings, K.S., Winchell, T.S., Livneh, B. and Molotch, N. (2018) 'Spatial variation of the rain-snow temperature threshold across the Northern Hemisphere'. *Nat Commun* 9, 1148 (2018). <https://doi.org/10.1038/s41467-018-03629-7>.
- Jordan, E., Ungerechts, L., Cáceres, B., Peñafiel, A. and Francou, B. (2005) 'Estimation by photogrammetry of the glacier recession on the Cotopaxi Volcano (Ecuador) between 1956 and 1997', *Hydrological Sciences Journal*, 50(6), pp. 949-962. doi: 10.1016/j.diff.2010.12.003.
- Juen, I. (2006) 'Glacier mass balance and runoff in the tropical Cordillera Blanca, Perú.', Dissertation, University of Innsbruck Austria. pp. 3-195. doi: 10.13140/RG.2.1.4885.5520.
- Karmeshu, N. (2015) 'Trend Detection in Annual Temperature & Precipitation using the Mann Kendall Test - A Case Study to Assess Climate Change on Select States in the Northeastern United States', *Mausam*, 66(1), pp. 1-6. doi: 10.1260/0957456021499207.
- Kaser, G. and Georges, C. (1997) 'Changes of the equilibrium line altitude in the tropical Cordillera Blanca (Perú) between 1930 and 1950 and their spatial variations', *Annals of Glaciology*, 24, pp. 344-349.
- Kaser, G. and Georges, C. (1999) 'On the Mass Balance of Low Latitude Glaciers with Particular Consideration of the Peruvian Cordillera Blanca', *Geografiska Annaler, Series A: Physical Geography*, 81(4), pp. 643-651. doi: 10.1111/1468-0459.00092.
- Kaser, G. and Osmaston, H. A. (2002) *Tropical Glaciers*, *Eos, Transactions American Geophysical Union*. Cambridge University Press, 83(35), p. 389. doi: 10.1029/2002E0000287.

- Kaser, G., Juen, I., Georges, C., Gómez, J. and Tamayo, W. (2003) 'The impact of glaciers on the runoff and the reconstruction of mass balance history from hydrological data in the tropical Cordillera Blanca, Perú', *Journal of Hydrology*, 282(1–4), pp. 130–144. doi: 10.1016/S0022-1694(03)00259-2.
- Khavse, R., Deshmukh, R., Manikandan, N., Chaudhary, J L., Kaushik, D., Gandhi, I., Viswadhylaya, K. and Raipur, C. G. (2015) 'Statistical Analysis of Temperature and Rainfall Trend in Raipur District of Chhattisgarh', *Current World Environment*, 10(1), pp. 305–312.
- Kiehl, J. T. and Trenberth, K. E., (1997) 'Earth's Annual Global Mean Energy Budget' *Bull. Amer. Meteor. Soc.*, 78, 197-208.
- Koch, M. (2014) 'Development of a set of interpolation and autoregression techniques in the R©-environment to impute missing data in hydrological and climate time series', developed internally at Kassel University and used by courtesy of M. Koch, University of Kassel, Germany.
- Konzelmann, T., Roderik, S.W, Gruell, W., Bintaja, R., Henneken, E., and Abe-Ouchi, A. (1994) 'Parameterization of global and longwave incoming radiation for the Greenland Ice Sheet', *Global and Planetary Change*, Volume 9, Issues 1–2, pp. 143-164. doi.org/10.1016/0921-8181(94)90013-2
- Lang, H. and Braun, L. (1990) 'On the information content of air temperature in the context of snow melt estimation', *IAHS*, 190(190), pp. 347–354.
- Lejeune, Y., Wagnon, P., Bouilloud, L., Chevallier, P., Etchevers, P., Martin, E., Sicart, J.E., Habets, F., (2007) 'Melting of a snow cover in a tropical mountain environment in Bolivia: processes and modelling'. *Journal of Hydrometeorology* 8, 922–938.
- Lliboutry, L. (1971) *The physics of glaciers*, Geoforum. Edited by M. . Butterwoth-Heinemann, Oxford, UK. doi: 10.1016/0016-7185(71)90086-8.
- Lozano, M. and Koch, M. (2014) 'Modeling Surface Mass Balance and Glacier Water Discharge in the Tropical Glacierized Basin of Artesoncocha in La Cordillera Blanca , Peru', *11th International Conference on Hydrosience and Engineering*. ICHE -Hamburg University.
- Mark, B. and Seltzer, G. (2003) 'Tropical glacier meltwater contribution to stream discharge: A case study in the Cordillera Blanca, Peru', *Journal of Glaciology*, 49(165), pp. 271–281. doi: 10.3189/172756503781830746.
- Martinec, J. (1960) 'The degree day factor for snowmelt runoff forecasting', *General Assembly for Helsinki. Commission on Surface Water*, 51.
- Maussion, F., Gurgiser, W., Großhauser, M., Kaser, G. and Marzeion, B. (2015) 'ENSO influence on surface energy and mass balance at Shallap Glacier, Cordillera Blanca, Peru', *Cryosphere*, 9(4), pp. 1663–1683. doi: 10.5194/tc-9-1663-2015.
- Min Raj Lamsal (2012) 'A Brief Introduction of Physics of Glaciers and Avalanches', *The Himalayan Physics*, 3(3), pp. 60–63. doi: 10.1002/bio.803.

Molnar, P. (2011). 'Calibration'. Watershed Modelling, SS 2011. Institute of Environmental Engineering, Chair of Hydrology and Water Resources Management, ETH Zürich. Switzerland.

Mölg, T., Cullen, N. J., Hardy, D. R., Kaser, G. and Klok, L. (2008) 'Mass balance of a slope glacier on Kilimanjaro and its sensitivity to climate', *International Journal of Climatology*, 28(7), pp. 881–892. doi: 10.1002/joc.1589.

Oerlemans, J. (2005) 'Extracting a Climate Signal from 169 Glacier Records', *Science*, 308(5722), pp. 675–677. doi: 10.1126/science.1107046.

Ohmura, A. (2001) 'Physical Basis for the Temperature-Based Melt-Index Method', *Journal of Applied Meteorology*, 40(4), pp. 753–761. doi: 10.1175/1520-0450(2001)040<0753:PBFTTB>2.0.CO;2.

Oke, T. R. (1987) Boundary layer climates, *Earth-Science Reviews*. doi: 10.1016/0012-8252(90)90005-G.

Perry, L. B., Seimon, A. and Kelly, G. M. (2014) 'Precipitation delivery in the tropical high Andes of southern Peru: new findings and paleoclimatic implications', *International Journal of Climatology*. Wiley-Blackwell, 34(1), pp. 197–215. doi: 10.1002/joc.3679.

Pierrehumbert, R. (2005) 'Tropical Glacier Retreat, Real Climate'. Available at: <http://www.realclimate.org/index.php/archives/2005/05/tropical-glacier-retreat/>

Plüss, C. and Ohmura, A. (1997) 'Longwave Radiation on Snow-Covered Mountainous Surfaces', *Journal of Applied Meteorology*, 36(6), pp. 818–824. doi: 10.1175/1520-0450-36.6.818.

Puertas, O., Carvajal, Y. and Quintero, M. (2011) 'Estudio De Tendencias De La Precipitación Mensual En La Cuenca Alta-Media Del Río Cauca, Colombia.', *Dyna*, 78(169), pp. 112–120. Available at: http://repository.upenn.edu/mes_capstones/47.

Qiang, Fu (2003). 'Radiation (Solar)'. In Holton, James R. (ed.). *Encyclopedia of atmospheric sciences*. 5. Amsterdam: Academic Press. pp. 1859–1863. ISBN 978-0-12-227095-6. OCLC 249246073.

Rabatel, A., Bermejo, A., Loarte, E., Soruco, A., Gomez, J., Leonardini, G., Vincent, C. and Sicart, J. E. (2012) 'Can the snowline be used as an indicator of the equilibrium line and mass balance for glaciers in the outer tropics?', *Journal of Glaciology*, 58(212), pp. 1027–1036. doi: 10.3189/2012JG12J027.

Rabatel, A., Francou, B., Soruco, A., Gomez, J., Cáceres, B., Ceballos, J. L., Basantes, R., Vuille, M., Sicart, J. E., Huggel, C., Scheel, M., Lejeune, Y., Arnaud, Y., Collet, M., Condom, T., Consoli, G., Favier, V., Jomelli, V., Galarraga, R., Ginot, P., Maisincho, L., Mendoza, J., Ménégoz, M., Ramirez, E., Ribstein, P., Suarez, W., Villacis, M. and Wagnon, P. (2013) 'Current state of glaciers in the tropical Andes: A multi-century perspective on glacier evolution and climate change', *Cryosphere*, 7(1), pp. 81–102. doi: 10.5194/tc-7-81-2013.

Rabatel, A., Ceballos, J., Micheletti, N., Jordan, E., Braitmeier, M., González, J., Mölg, N., Ménégoz, M., Huggel, C., and Zemp, M. (2017): Toward an imminent extinction of Colombian glaciers?,

Geografiska Annaler: Series A, Physical Geography. ISSN: 0435-3676 (Print) 1468-0459 (Online)
Journal homepage: <http://www.tandfonline.com/loi/tgaa20>

Racoviteanu, A., Manley, W., Arnaud, Y., and Williams, M. (2007) 'Evaluating digital elevation models for glaciologic applications: An example from Nevado Coropuna, Peruvian Andes'. *Global and Planetary Change*. 59. 110-125. [10.1016/j.gloplacha.2006.11.036](https://doi.org/10.1016/j.gloplacha.2006.11.036).

Rayner, J. N. (1971) *An introduction to spectral analysis. Monographs in spatial and environmental systems analysis*. ISBN-13: 978-0850860269. Pion p. 174.

Ribstein, P., Tiriau, E., Francou, B. and Saravia, R. (1995) 'Tropical Climate and Glacier Hydrology - a Case-Study in Bolivia', *Journal of Hydrology*, 165(1-4), pp. 221-234.

Ronchail, J. and Gallaire, R. (2006) 'ENSO and rainfall along the Zongo valley (Bolivia) from the Altiplano to the Amazon basin', *International Journal of Climatology*, 26(9), pp. 1223-1236. doi: [10.1002/joc.1296](https://doi.org/10.1002/joc.1296).

Salzmann, N., Huggel, C., Rohrer, M., Silverio, W., Mark, B. G., Burns, P. and Portocarrero, C. (2013) 'Glacier changes and climate trends derived from multiple sources in the data scarce Cordillera Vilcanota region, southern Peruvian Andes', *The Cryosphere*, 7(1), pp. 103-118. doi: [10.5194/tc-7-103-2013](https://doi.org/10.5194/tc-7-103-2013).

Saunders, I. R. and Bailey, W. G. (1997) 'Longwave Radiation Modeling In Mountainous Environments', *Physical Geography*, 18(1), pp. 37-52. doi: [10.1080/02723646.1997.10642605](https://doi.org/10.1080/02723646.1997.10642605).

Schaner, N., Voisin, N., Nijssen, B. and Lettenmaier, D. (2012). 'The contribution of glacier melt to streamflow'. *Environmental Research Letters*. 7. [10.1088/1748-9326/7/3/034029](https://doi.org/10.1088/1748-9326/7/3/034029).

Schoolmeester, T., Johansen, K.S., Alfthan, B., Baker, E., Hesping, M. and Verbist, K. (2018) 'Atlas de Glaciares y Aguas Andinos. El impacto del retroceso de los glaciares sobre los recursos hídricos'. UNESCO and GRID-Arendal.

Shapiro, S. S. and Wilk, M. B. (1965). 'An analysis of variance test for normality (complete samples)'. *Biometrika* 52 (3-4): 591-611. doi:[10.1093/biomet/52.3-4.591](https://doi.org/10.1093/biomet/52.3-4.591).

Sicart, J. E., Ribstein, P., Wagnon, P and Brunstein, D. (2001) 'Clear sky albedo measurements on a sloping glacier surface: A case study in Bolivian Andes', *Journal of Geophysical Research*, 106, 31, 729-31,737. doi: [10.1029/2000JD000153](https://doi.org/10.1029/2000JD000153)

Sicart, J. E., Hock, R. and Six, D. (2008) 'Glacier melt, air temperature, and energy balance in different climates: The Bolivian Tropics, the French Alps, and northern Sweden', *Journal of Geophysical Research Atmospheres*, 113(24), pp. 1-11. doi: [10.1029/2008JD010406](https://doi.org/10.1029/2008JD010406).

Sicart, J. E., Hock, R., Ribstein, P., Litt, M., Ramirez, E. (2011) 'Analysis of seasonal variations in mass balance and meltwater discharge of the tropical Zongo Glacier by application of a distributed energy balance model', *Journal of Geophysical Research Atmospheres*, 116(13), pp. 1-18. doi: [10.1029/2010JD015105](https://doi.org/10.1029/2010JD015105).

- Singh, P., Kumar, N. and Arora, M. (2000) 'Degree-day factors for snow and ice for Dokriani Glacier, Garhwal Himalayas', *Journal of Hydrology*, 235(1-2), pp. 1-11. doi: 10.1016/S0022-1694(00)00249-3.
- Soruco, A., Vincent, C., Francou, B. and Gonzalez, J. F. (2009) 'Glacier decline between 1963 and 2006 in the Cordillera Real, Bolivia', *Geophysical Research Letters*, 36(3), pp. 2-7. doi: 10.1029/2008GL036238.
- Soruco, A., Vincent, C., Francou, B. and Rabatel, A. (2014) 'Comparación de métodos para estimar el balance de masa del Glaciar de Zongo, Bolivia (16o S , 68o O)', *Geoacta*, 39(1), pp. 154-164.
- Suarez, W., Chevallier, P., Pouyaud, B. and Lopez, P. (2008) 'Modelling the water balance in the glacierized Parón Lake basin (White Cordillera, Peru)', *Hydrological Sciences Journal*, 53(1), pp. 266-277. doi: 10.1623/hysj.53.1.266.
- Sugathan, N., Biju, V. and Renuka, G. (2014) ' Influence of soil moisture content on surface albedo and soil thermal parameters at a tropical station', *Journal Earth Syst Sci* 123: 1115. <https://doi.org/10.1007/s12040-014-0452-x>
- Swinbank, W. C. (1963) 'Long-wave radiation from clear skies', *Quarterly Journal of the Royal Meteorological Society*, 89(381), pp. 339-348. doi: 10.1002/qj.49708938105.
- Thompson, L., Mosley-Thompson, E., Brecher, H., Davis, M., León, B., Les, D., Lin, P., Mashiotta, T., Mountain, K. (2006). "Inaugural Article: Abrupt tropical climate change: Past and present". *Proceedings of the National Academy of Sciences*. 103 (28): 10536. Bibcode:2006PNAS..10310536T. doi:10.1073/pnas.0603900103. PMC 1484420. PMID 16815970.
- Unidad de Glaciología y Recursos Hídricos (UGRH) (2010) *Inventario de glaciares, Cordillera Blanca, Peru*, Autoridad Nacional del Agua, Huaraz, pp. 81
- Valéry, A., Andréassian, A., and Perrin, P. (2010) 'Regionalization of precipitation and air temperature over high-altitude catchments - learning from outliers'. *Hydrological Sciences Journal - Journal des Sciences Hydrologiques*, 55:6, 928-940, DOI 10.1080/02626667.2010.504676
- Veettil, B. K., Leandro Bayer Maier, É., Bremer, U. F. and de Souza, S. F. (2014) 'Combined influence of PDO and ENSO on northern Andean glaciers: a case study on the Cotopaxi ice-covered volcano, Ecuador', *Climate Dynamics*, 43(12), pp. 3439-3448. doi: 10.1007/s00382-014-2114-8.
- Vergara, W., Deeb, A., Leino, I., Kitoh, A. and Escobar, M. (2011) 'Assessment of the Impacts of Climate Change on Mountain Hydrology', *The World Bank*. doi: 10.1596/978-0-8213-8662-0
- Villacís, M., Cadier, E., Pouyard, B., Caceres, B., Nuñez, J., Galárraga, R., and Francou, B. (2010) 'Relaciones Hidrológicas entre el glaciar y los páramos de los Andes tropicales del Ecuador: su papel en la disponibilidad de recursos hídricos', *IV Simposio Internacional sobre cambios globales*. Universidad Mayor de San Andrés. <http://wecdocs.unep.org>.

- VSP (no date) 'Seasonal Kendall Test for Monotonic Trend'. Available at: http://vsp.pnnl.gov/help/Vsample/Design_Trend_Seasonal_Kendall.htm (Accessed: 27 November 2018).
- Vuille, M., Bradley, R. S. and Keimig, F. (2000) 'Interannual climate variability in the Central Andes and its relation to tropical Pacific and Atlantic forcing', *Journal of Geophysical Research: Atmospheres*, 105(D10), pp. 12447–12460. doi: 10.1029/2000JD900134.
- Vuille, M., Francou, B., Wagnon, P., Juen, I., Kaser, G., Mark, B. G. and Bradley, R. S. (2008) 'Climate change and tropical Andean glaciers: Past, present and future', *Earth-Science Reviews*, 89(3–4), pp. 79–96. doi: 10.1016/j.earscirev.2008.04.002.
- Vuille, M., Kaser, G. and Juen, I. (2008b) 'Glacier mass balance variability in the Cordillera Blanca, Peru and its relationship with climate and the large-scale circulation', *Global and Planetary Change*, 62(1–2), pp. 14–28. doi: 10.1016/j.gloplacha.2007.11.003.
- Wagnon, P., Ribstein, P., Francou, B. and Pouyaud, B. (1999) 'Annual cycle of energy balance of Zongo Glacier, Cordillera Rreal, Bolivia', *Journal of Geophysical Research*, 104(D4), pp. 3907–3923.
- Wagnon, P., Ribstein, P., Francou, B. and Sicart, J E. (2001) 'Anomalous heat and mass budget of Glaciar Zongo , Bolivia , during the 1997 / 98 El Ni • o year', *October*, 47(156), pp. 21–28.
- Wagnon, P., Lafaysse, M., Lejeune, Y., Maisincho, L., Rojas, M. and Chazarin, J. P. (2009) 'Understanding and modeling the physical processes that govern the melting of snow cover in a tropical mountain environment in Ecuador', *Journal of Geophysical Research Atmospheres*, 114(19), pp. 1–14. doi: 10.1029/2009JD012292.
- Wayne, D. (1990). 'Kolmogorov–Smirnov one-sample test'. *Applied Nonparametric Statistics* (2nd ed.). Boston: PWS-Kent. pp. 319–330. ISBN 978-0-534-91976-4.
- WGMS (2015) 'Global Glacier Change Bulletin No. 1 (2012-2013)', in Zemp, M., Gärtner-Roer, I., Nussbaumer, S. U., Hüsler, F., Machguth, H., Mölg, N., Paul, F., and Hoelzle, M. (eds. . (ed.). IUGG(IACS)/ UNEP/UNESCO/WMO, World Glacier Monitoring Service, Zurich, Switzerland, p. 230.
- Winkler, M., Juen, I., Mölg, T., Wagnon, P., Gómez, J. and Kaser, G. (2009) 'Measured and modelled sublimation on the tropical Glaciar Artesonraju, Perú', *Cryosphere*, 3(1), pp. 21–30. doi: 10.5194/tc-3-21-2009.
- Ye, H., Cohen, J. and Rawlins, M. (2013) 'Discrimination of Solid from Liquid Precipitation over Northern Eurasia Using Surface Atmospheric Conditions*', *Journal of Hydrometeorology*, 14(4), pp. 1345–1355. doi: 10.1175/JHM-D-12-0164.1.
- Zakšek, K., Oštir, K. and Kokalj, Ž. (2011) 'Sky-view factor as a relief visualization technique', *Remote Sensing*, 3(2), pp. 398–415. doi: 10.3390/rs3020398.